Wave Overtopping and Toe Scouring at Sea Defences with Permeable Shingle Foreshores: A Physical Model Study

A thesis Submitted to the

University of Warwick

for the degree of

Doctor of Philosophy

by

Md Salauddin

School of Engineering

January 2020

Declaration

This thesis is submitted to the University of Warwick in support of my application for the degree of Doctor of Philosophy. I hereby declare that it has been composed by myself and has not been submitted in any previous application for any degree.

January 2020

Md Salauddin

Contributions to Knowledge

Journal Articles

1. Salauddin, M., Pearson, J. M., 2019. Wave overtopping and toe scouring at plain vertical wall with a shingle foreshore: A Physical model study. Ocean Engineering, 171(1): pp. 286-299. DOI: https://doi.org/10.1016/j.oceaneng.2018.11.011
2. Salauddin, M., Pearson, J. M., 2019. Experimental study on toe scouring at sloping walls with gravel foreshores. Journal of Marine Science and Engineering, 7(7), 198. DOI: https://doi.org/10.3390/jmse7070198
3. Salauddin, M., Pearson, J. M., 2020. Laboratory investigation of overtopping at a sloping structure with permeable shingle foreshore. Ocean Engineering, 197 (1): pp. 1-13. DOI: https://doi.org/10.1016/j.oceaneng.2019.106866

Peer Reviewed Conference Papers

1. Salauddin, M., Pearson, J. M., 2018. Overtopping of vertical structures: new prediction methods to account for shingle beaches. In: Peer Reviewed Proceedings of the 7th International Conference on the Application of Physical Modelling in Coastal and Port Engineering and Science (Coastlab18), Santander, Spain.
2. Salauddin, M., Pearson, J. M., 2018. Distribution of wave by wave overtopping volumes at vertical seawalls. In: Peer Reviewed Proceedings of the 3rd International Conference on the Protection against Overtopping, HR Wallingford, Lake District, UK.
3. Salauddin, M., Pearson, J. M., 2018. A laboratory study on wave overtopping at vertical seawalls with a shingle foreshore. In: Peer Reviewed Proceedings of the 36th International Conference on Coastal Engineering (ICCE), ASCE, Baltimore, USA.
4. Salauddin, M., Pearson, J. M., 2018. A review on the design guidance for the application of vertical seawalls on shingle foreshores. In: Peer Reviewed Proceedings of the 4th International Conference on Advances in Civil Engineering (ICACE), Bangladesh.

5. Salauddin, M., Abolfathi, S, O'Sullivan, J., Pearson, J. M., 2020. Distribution of wave by wave overtopping volumes at sloping walls with a permeable gravel foreshore. (Accepted for oral presentation in 37th International Conference on Coastal Engineering, ICCE-2020, ASCE, Sydney).

Scholarships and Awards

— Chancellor's International Scholarship, full funding (tuition fees and living expenses) for PhD study, University of Warwick (Oct. 2016 – Mar. 2020).

— Open Access Funding, Library, University of Warwick (Dec. 2019)

— Conference Travel Grant, University of Warwick (Aug. 2018)

— Research Consumable Grant, School of Engineering, University of Warwick (2017).

Abstract

Wave overtopping and toe scouring are considered two primary coastal processes at the wave/structure interface of sea defence structures. It is therefore important to have reliable prediction methods for these coastal processes at coastal infrastructures. The existing prediction formulae currently available are principally based on fitting to experimental measurements, (e.g. empirical formulae) reported in the overtopping manual. However, to date, most parametric studies regarding these aspects (e.g. wave overtopping cited in the scientific literature) have tended to focus on structures having impermeable foreshores, with investigations on permeable beaches (e.g. shingle beaches) being less well-studied. Accordingly, there is a distinct knowledge gap on these coastal processes at sea defences (e.g. vertical seawall and sloping structure with permeable gravel slopes) due to limited field and laboratory research on these types of sea defences.

The purpose of this study was to investigate wave overtopping and toe scouring characteristics at sea defences (e.g. a vertical seawall and a 1 in 2 sloping structure) on permeable shingle foreshores. The small-scale laboratory study was conducted in two phases. Phase I focused on the overtopping and scouring processes at the plain vertical seawall, and Phase II investigated the overtopping and scouring characteristics at a smooth 1 in 2 sloping structure. Each Phase consisted of undertaking wave flume experimental investigations based on three configurations, namely a plain vertical wall or a sloping structure with permeable shingle foreshores of two different particle sizes (d_{50} of 13 mm and 24 mm) together with an impermeable foreshore representing the control condition.

The physical model experiments were undertaken in a two-dimensional wave channel at the University of Warwick, UK by adapting the well-established guidelines of EurOtop (2018), Powell (1990) and Wolters et al. (2009) for typical two-dimensional experimental investigations. An impermeable sloping foreshore with a uniform slope of 1 in 20 was constructed in front of the model structure. Two constant deep-water wave steepnesses ($s_{m-1,0} = 0.02$

and 0.06) were tested with six different toe water depths. Each test comprised of 1,000 pseudo-random wave sequences. Permeable (gravel) foreshores, with slopes of 1 in 20 then simulated using crushed anthracite (specific gravity of 1.40 T/m^3) following Powel (1990). For the 1 in 50 geometrical scaling, model anthracite d_{50} values of 2.10 mm and 4.20 mm represented prototype gravels with d_{50} values of 13 mm and 24 mm, respectively.

Detailed measurements were taken to parameterize the mean overtopping rate, mean sediment rate, individual overtopping volume, probability of overtopping and scour depths on a plain vertical seawall and a 1 in 2 sloping structure, for both impermeable and permeable shingle beach configurations. The resulting overtopping and scouring characteristics at the structures were then compared with existing empirical formulations from the literature to identify differences in the permeable and impermeable foreshore characteristics.

For both structural configurations (e.g. vertical wall and sloping structure) the measured baseline overtopping characteristics corresponding to the impermeable foreshore (control condition) showed an overall good agreement with the existing empirical prediction formulae for the tested wave conditions covered within this study. Within the experimental limitations of this study, it was found that the measured mean overtopping rate was reduced significantly for the case of permeable foreshores when compared to the predictions reported for the impermeable slope. However, when comparing the wave by wave overtopping volumes, no significant differences were observed.

The relationship of the scour depth with toe water depth, Iribarren number, and wall slope were investigated from the test results of this work and through a comparison with available datasets in the literature. For both plain vertical wall as well as sloping structure, the results of this study showed that the relative toe scour depth at the structure on a shingle beach, was influenced by the relative toe water depth and Iribarren number. Within the experimental limitations, the maximum toe scour depths were observed for the experiments under spilling and plunging wave attack.

Before conducting this study, limited prediction guidance was available to predict the mean overtopping discharges and mean sediment rates at sea defences on permeable shingle foreshores. Therefore, for the prediction of overtopping characteristics at sea defences (e.g. vertical walls and sloping structures) on permeable gravel foreshores, revised predictions tools are suggested. The outcomes of this study are intended for practitioners and researchers in predicting wave overtopping characteristics at sea defence structures with permeable gravel foreshores.

Keywords: Overtopping discharge, Scour depth, Sediment discharge, Shingle foreshore, Sloping structure, Vertical seawall, and Wave by wave overtopping volume.

Acknowledgements

I thank and remember my Almighty Allah for providing me the motivation, strength, and ability to complete my doctoral research thesis from one of the esteemed higher education institutes in the world.

Firstly, I would like to express my deepest regards and gratitude to my supervisor Dr. Jonathan Pearson for his valuable guidance, advice, and assistance throughout the period of my PhD study. Without his continuous support and encouragement in every single step of my PhD study, this thesis would not have been possible.

Next, I would like to place my cordial appreciations to the staff of the Warwick Water Group, University of Warwick for their kind support during my PhD study. I am particularly grateful to Dr. Soroush Abolfathi for his continuous academic, technical and personal support throughout my PhD study. My sincere thanks go to Mr. Ian Baylis for his kind assistance and support in carrying out the laboratory experiments. I thank and remember my colleague Mr. Shudi Dong of Warwick Water for his great co-operation and technical support throughout the project.

I would also like to extend my thanks to my panel members, Professor Toby Mottram and Dr. Xueyu Geng for their constructive comments and suggestions in carrying out my PhD research. Also, my cordial appreciations go to Dr. Peter Gammon and Kerrie Hatton for their continuous administrative supports and advice throughout the study.

I am deeply grateful to Professor Jentsje Van der Meer of IHE-Delft, the Netherlands, who encouraged me in conducting cutting-edge research on extreme wave hazards at sea defences. I would also like to thank Professor Tom Bruce of the University of Edinburgh for his valuable advice in carrying out the analysis of wave by wave overtopping volumes.

In addition, I thank the Doctoral College of the University of Warwick for funding my PhD research under the Chancellor's International Scholarship scheme. I sincerely appreciate the financial support of the School of Engineering of the University of Warwick in carrying out the laboratory experiments through the research consumables grant.

I sincerely thank the administration of the Chittagong University of Engineering and Technology, Bangladesh, for providing me a higher study leave in order to pursue my PhD study at the University of Warwick.

I want to thank my friends and colleagues who directly or indirectly supported me during the course of my study. I am especially grateful to Dr. Anup Barai of Warwick Manufacturing Group for his continuous advice and support throughout my PhD study.

Last but not least, I am profoundly grateful to my family members for their continuous support and encouragement throughout my life. I would like to thank particularly my wife Mrs Sumaiya Arifin for her outstanding support, accompany, care and inspiration during my PhD journey.

Table of Contents

List of Figures

Chapter 1

Chapter 2

Chapter 3

Chapter 5

Chapter 6

Appendices

List of Tables

Appendices

List of Abbreviations

Abbreviation	Explanation
CLASH	Crest Level Assessment of Coastal Structures by full scale monitoring and Hazard Analysis on permissible wave overtopping
IPCC	Intergovernmental Panel on Climate Change
JONSWAP	Joint North Sea Wave Project
RMSE	Root Mean Square Error
SI	Scatter Index
SPH	Smooth Particle Hydrodynamics
SWL	Still Water Level
VOWS	Violent Overtopping of Waves at Seawalls

Notation

Symbol	Meaning	Unit
a	Scale parameter in Weibull distribution	[-]
b	Shape parameter in Weibull distribution	[-]
d_b	Submergence depth of the berm	[m]
d_{50}	Mean sediment size	[mm]
g	Gravitational acceleration	[m/s^2]
h	Water depth near wave paddle	[m]
h_b	Water depth at breaking	[m]
h_t	Water depth at toe of the structure	[m]
h_*	Impulsiveness parameter	[-]
H	Individual wave height	[m]
H_{0max}	Maximum wave height at structure toe	[m]
H_m	Mean wave height	[m]
H_{m0}	Significant wave height determined from spectra analysis	[m]
H_s	Significant wave height determined from time series analysis (= $H_{1/3}$)	[m]
I_r	Iribarren number or breaker parameter (= $\zeta_{m-1,0}$)	[-]
L_0	Local wave length based on linear theory	[m]
L_m	Mean wave length based on linear theory ($gT_m^2/2\pi$)	[m]
$L_{m-1,0}$	Spectral wave length based on linear theory ($gT_{m-1,0}^2/2\pi$)	[m]
L_p	Peak wave length based on linear theory ($gT_p^2/2\pi$)	[m]
N_{ow}	Number of overtopping waves	[-]
N_{test}	Number of experimental data	[-]
N_w	Number of incident waves	[-]
P_{ov}	Probability of overtopping per wave (N_{ow}/N_w)	[-]
P_{ow}	Percentage of overtopping waves (N_{ow}/N_w)*100	[%]
P_v	Probability of exceedance of overtopping volume	[-]
q	Mean overtopping discharge per m width	[m^3/s per m]

R_c	Crest freeboard	[m]
$R_{u2\%}$	Run-up level exceeded by 2% of incident waves	[m]
s_{max}	Maximum scour depth	[m]
s_t	Toe scour depth	[m]
s_{tmax}	Maximum toe scour depth	[m]
$s_{m-1,0}$	Wave steepness based on spectral period, $T_{m-1,0}$	[-]
s_{om}	Wave steepness based on average wave period, T_m	[-]
s_{op}	Wave steepness based on spectral peak period, T_p	[-]
T_m	Average wave period calculated from time series analysis	[s]
$T_{m-1,0}$	Average spectral wave period defined from spectral analysis by m_{-1}/m_0	[s]
T_p	Spectral peak wave period	[s]
u_{cr}	Critical horizontal velocity	[m/s per m]
u_{max}	Maximum orbital velocity at bottom of node	[m/s per m]
u_{*cr}	Critical shear velocity	[m/s per m]
u_{*max}	Maximum shear velocity	[m/s per m]
V	Volume of overtopping wave per m width	[m^3 per m]
V_{bar}	Mean overtopping volume per m width	[m^3 per m]
V_{max}	Maximum individual overtopping volume	[m^3 per m]
w	Sediment fall velocity	[m/s per m]
α	Slope of the structure	[radians]
γ	Peak enhancement factor of JONSWAP spectrum	[-]
γ_f	Roughness factor on a slope	[-]
λ	Geometric Model scale	[-]
π	3.1416	[-]
θ	Seabed slope	[radians]
ρ	Fluid density	[T/m^3]
Γ	Mathematical gamma function	[-]

CHAPTER 1

Introduction

1.1 Synopsis

This chapter introduces the reader to the research work undertaken within this study. First, Section 1.2 describes the motivation of this experimental study by discussing the background of the research, and followed by an introduction to the research problem. Next, the research objectives of this study are presented in Section 1.3. Lastly, this chapter ends with an outline of this thesis in Section 1.4.

1.2 Motivation

Coastal zone refers to the interface between land and ocean, where both natural and man-made hard or soft defence structures protect the hinterland areas against coastal flooding. Since the past decades, conventional coastal engineering solutions have resulted in hard structures, such as seawalls, dykes, and embankments. Apart from the hard-engineering approaches, nature-based protection approaches, such as shingle beaches and barriers, have been implemented as efficient coastal protection approach due to their natural capability to mitigate wave-induced energy (McCall et al., 2014). Nonetheless, coastal hazards, such as impairment of coastal infrastructure and coastal flooding, may occur at shingle beaches and barriers stemming from wave overtopping, over-washing, erosion, and barrier breaching processes (EurOtop, 2018; McCall et al., 2015). Beach material contained within overtopping waves can be particularly hazardous to personnel.

The performance of the coastal structures such as vertical or near vertical seawalls and harbour breakwaters can be classified in many ways, using complex functions of wave and geometric parameters. For instance, many man-made coastal structures have been designed to limit overtopping, whereby predictions derived from general empirical formulas are fitted to laboratory measurements. Whilst these structures may be efficient in mitigating wave overtopping, they may be subject to impulsive wave

breaking, hence giving sudden and violent overtopping flows and scouring at toe, the interactions of which are somewhat difficult to describe with any degree of certainty.

Wave overtopping or over-washing has substantially affected the functional efficiency of breakwater, which has been considered as one of the key hydraulic responses of breakwater (Franco et al., 1994). The design for tolerable overtopping of waves has been viewed as a prime concern in designing any sea defence structure (EurOtop, 2018). The impacts and consequences of wave-induced overtopping are illustrated briefly in EurOtop (2018). The wave overtopping can causes damages to sea defence structures, along with potential flooding and breaching. It can be hazardous to personnel (e.g., pedestrians, passengers travelling in a vehicle or cyclists) occupying behind the defence structure. It can also cause damages to property, operation, and infrastructure being protected, resulting in economic and environmental loss. Additionally, it can result in inconvenient low-depth inundation

Figure 1.1 showcases several instances of wave overtopping phenomena over sea defence observed across the United Kingdom (UK), which demonstrate the catastrophic power of wave-induced overtopping events. Figure 1.1(a) portrays the wave overtopping onto a moving train, in which the railway line is located adjacent to the seawall. As observed from Figure 1.1 (a), the overtopped water may hit the windows of the moving train, thus causing the train to move slowly. In some cases, overtopping of sediments may be noted where beach materials contain within the overtopping waves.

Figures 1.1(b) and (c) illustrate the violent wave overtopping events over the seawalls at two locations within the UK. Such violent wave overtopping incidents can cause significant damages to the sea defence structure. As depicted above, it can be hazardous to both personal and properties residing behind the structure.

Figure 1.1(d) describes coastal flooding induced by extreme wave overtopping events at Exmouth Seafront, UK in 2018, as reported by the BBC (2018). It caused breaching to the flood defence and damages to the hinterland properties, including homes and business areas (see BBC, 2018).

a. b.

c. d.

Figure 1.1 Instances of wave overtopping – a) overtopping onto a moving train in UK (EurOtop, 2018), b) overtopping at seawalls in Isle of Man, UK (IOMTODAY, 2018), c) voilent overtopping at seawalls in Dover, UK (EurOtop, 2018), and d) flooding due to wave overtopping at Exmouth Seafront, UK (BBC, 2018)

Thus far, the previous segments have emphasised on the wave overtopping processes at sea defence. Turning next to scouring at sea defence, similar to overtopping characteristics, toe scouring at a coastal structure is also one of the most important coastal processes at the wave/structure interface, which may trigger substantial damages and failure of the coastal structure. Over the years, researchers have reported that failure of coastal structures, such as seawalls in the UK, has very often occurred due to scouring at the toe of the structure (see Fowler, 1992; Powell, 1987; Sutherland et al., 2003). Figure 1.2 displays the undermining of the toe of the seawall caused due to the scouring phenomenon at Corton, UK.

Figure 1.2 Undermining of the toe of the seawall due to scouring phenomenon, Corton, UK (Source: Whitehouse, 2006)

Overall, it has been widely accepted that wave overtopping and toe scouring are the two key coastal processes at the wave/structure interface of sea defence. This is at a time when the combined influence of climate change and global sea level rise, as estimated by the Intergovernmental Panel on Climate Change (IPCC) (see Church et al., 2013) at 4 mm/year for the 21st century in several regions, have set a long-standing threat of coastal hazards on the sea defence across nearshore regions. This phenomenon can eventually trigger

extreme wave overtopping events with relatively short return period (Chini et al., 2013). It is, therefore, integral to have better knowledge on the key coastal processes, such as overtopping and toe scouring at the coastal infrastructures.

Since past few years, many parametric experimental studies have been conducted to clarify the phenomenon of wave overtopping on coastal structures with fixed impermeable beaches. Based on these predominantly small-scale laboratory measurements, several empirical formulas have been prescribed to predict overtopping at the mentioned structures (EurOtop, 2018). Nonetheless, with the use of a fixed impermeable bed in front of a model coastal structure, toe scouring phenomenon cannot be observed during the experimental attempts. With the introduction of mobile beds within the laboratory, it would be possible to observe scouring at the toe of the model structures, along with overtopping measurements, thus indicating more realistic simulation of real-life situations.

Another aspect is that despite the vast coastal morphodynamics investigations have been carried out across sandy beaches, only a few studies have probed into gravel beaches (De San Román-Blanco et al., 2006). In predicting the cross-shore profile change for a gravel beach, several empirical models are available in the literature, such as empirical models prescribed by Bradbury and Powell (1992); Lorang (2002); Van der Meer (1992), as well as Van Hijum and Pilarczyk (1982). Apart from these, Gentile and Giasi (2003) described a methodological approach for the remodelling of shingle beaches, which has been then applied to assess the re-naturalisation process of a gravel beach called Torre del Porto located in the South-East of Italy (see Altomare and Gentile, 2011; 2013). Apart from the empirical models, recent physical model studies have been undertaken to investigate the dynamic response of gravel barriers and beaches under the combined actions of tides, waves, and storm. For instance, vast laboratory studies on gravel barriers and beaches have been undertaken in the BARDEX project (see Williams et al., 2012a). The numerical simulations of gravel beaches using the XBeach model were validated with the gathered laboratory datasets, together with field studies on gravel beaches (see McCall et al., 2015; Williams et al., 2012b).

A paucity of parametric studies devoted to breaching, overtopping, and overwash processes of gravel beaches and barriers had been noted (see Bradbury, 2000; Matias et al., 2012; Obhrai et al., 2008; Pearson, 2010). As mentioned above, the vast majority of overtopping data applied in EurOtop (2018) were derived from small-scale measurements with impermeable foreshore slopes. To date, a handful of parametric studies have looked into the characteristics of wave overtopping and toe scouring at sea defence with permeable foreshores. Upon applying the existing prediction methods to sea defence with permeable gravel slopes, knowledge is required on the influence of permeable foreshore on wave overtopping and scouring behaviour.

Evidently, a clear knowledge gap is present on these coastal processes at sea defence, such as vertical seawall and sloping structure with permeable gravel slopes, due to limited field and laboratory studies on such sea defence. That being mentioned, this study is aimed at extending the existing empirical predictions of wave overtopping and scouring at vertical seawalls and smooth sloping structures for the case of permeable gravel foreshores. The extension depicted in this study blankets a comprehensive laboratory study on these coastal characteristics at plain vertical wall and a 1 in 2 smooth sloping structure, undertaken on both impermeable and permeable foreshore slopes.

1.3 Research Objectives

The overall aim of this experimental research is to investigate the wave overtopping and toe scouring characteristics at sea defence, such as vertical seawalls and sloping structures, with permeable shingle foreshore slopes.

In arriving at the prediction guidance for permeable shingle foreshores, the key coastal processes, including wave overtopping and toe scouring, at sea defence with shingle beaches had been investigated in this present study, based on an extensive two-dimensional small-scale wave flume test. The performance of these coastal processes was examined for two forms of sea defence, which are shingle beach in front of a plain vertical wall, and shingle beach in front of a sloping wall. The experimental work on overtopping features had been also performed at sea defence with the application of impermeable bed (control condition) to identify differences in permeable and

impermeable foreshore characteristics.

Based on the narrative elaborated in this chapter and the research gaps detected within the context of overtopping and toe scouring characteristics at sea defence with permeable slopes, the following outlines the specific research objectives of this study:

— To investigate wave overtopping characteristics (mean overtopping rate, wave by wave overtopping volumes, and probability of overtopping waves) at plain vertical walls with permeable and impermeable foreshores.
— To inspect scour depths at the toe of plain vertical wall on permeable shingle beach, subjected to breaking and non-breaking waves.
— To examine wave-induced overtopping characteristics at 1 in 2 smooth impermeable sloping structures with permeable and impermeable slopes.
— To study toe scouring features of sloping structures with permeable foreshore configurations.

1.4 Thesis Outline

This thesis is structured as follows:

— This particular chapter (Chapter 1) presents the overall introduction of this research work, including a description of the motivation of the research and the research objectives.
— Chapter 2 discusses in detail the theoretical background of the principal coastal processes, including overtopping and scouring at the wave structure interface of sea defence. After that, a brief description of key design parameters, typically applied to predict coastal processes, is presented. This chapter also reports the available prediction techniques to estimate the wave overtopping and toe scouring characteristics at two typical sea defences, namely vertical seawalls, and sloping structures.
— Chapter 3 describes the research methodology employed in this experimental study. It particularly demonstrates the laboratory set up, scaling of bed materials, measurement techniques, wave conditions, test matrices, and the procedures involved in carrying out the small-scale two-dimensional wave flume experimental works. Next, it presents the

calibration of measured wave conditions. Lastly, it discusses the accuracy of the overtopping measurement system for both tested structural configurations in this study; plain vertical wall and sloping structure.

— Chapter 4 presents the outcomes retrieved from the physical model experiments on plain vertical wall, along with permeable and impermeable foreshores, in order to assess the wave overtopping and toe scouring characteristics within the tested conditions. It also compares the test results of this study with the present empirical prediction methods, which are then used to propose prediction guidance for the implications of a permeable foreshore in front of a plain vertical seawall.

— Chapter 5 demonstrates the wave overtopping and toe scouring features derived from laboratory experiments at sloping structures, along with permeable and impermeable bed configurations. Preliminary prediction guidance is also proposed in this chapter to estimate the mean overtopping rate at a 1 in 2 sloping structure with permeable shingle foreshore.

— Chapter 6 presents the resulting distribution of wave by wave overtopping volumes for the conditions stipulated in this study. It elaborates the estimation of Weibull shape parameter b values from the distribution of measured wave by wave overtopping volumes, following an investigation on the correlation between Weibull b values and a set of key parameters.

— The final chapter (Chapter 7) summarises the primary outcomes derived from this study and provides several recommendations for further investigations within this topic area.

CHAPTER 2

Literature Review

2.1 Synopsis

This chapter introduces the background of key parameters and the principal processes of wave structure interface at coastal defences, along with several existing prediction methods to estimate those coastal processes. First, Section 2.2 defines and reviews several key design parameters and principal processes of wave structure interface at sea defences. Next, the two principal sea defence structures are defined in Section 2.3. Then, the methods that predict wave overtopping at vertical walls and sloping structures are reported. In Section 2.5, scientific work pertaining to estimation of toe scouring at coastal structures is discussed. A summary ends this chapter.

2.2 Definition of Key Parameters and Principal Processes

2.2.1 Wave Height

In a wave, the wave height (H) is defined as the vertical distance between the highest (wave crest) and the lowest water surface elevation (wave trough), see Figure 2.1. The most applicable form of wave height is the significant wave height (H_s) that can be determined via visual observations or from time series analysis of a wave record or from the wave spectra analysis (Holthuijsen, 2007). For instance, practitioners and engineers in the coastal engineering domain calculate H_s either from time-series analysis or spectral analysis. The H_s derived from time-series analysis of a wave record is denoted by $H_{1/3}$, calculated by taking an average of the highest one-third of the waves.

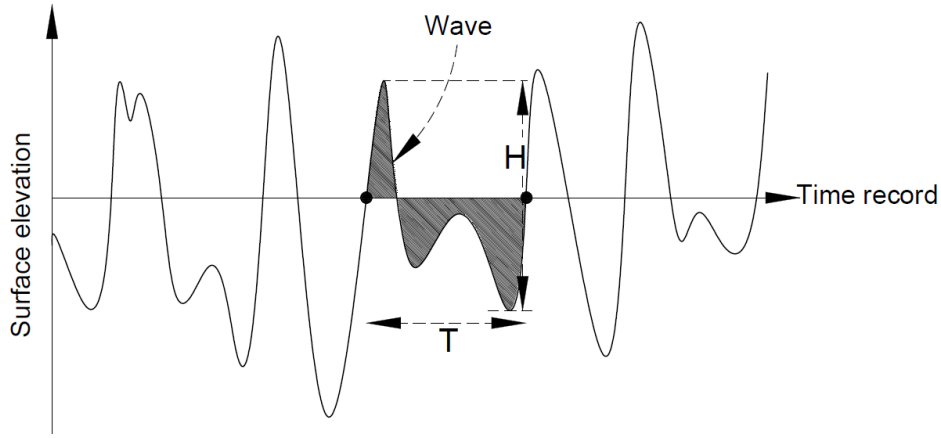

Figure 2.1 Definition sketch of a wave from time record of the sea surface elevation (Adapted from Holthuijsen, 2007)

Another definition of the H_s, which refers to the spectral significant wave height (H_{m0}) that is calculated from the spectral analysis, is also frequently applied in coastal engineering. For instance, the H_{m0} at the toe of the structure is applied to predict wave overtopping (EurOtop, 2018). Figure 2.2 illustrates an example of a wave spectrum for irregular waves. In relatively deep water, there is no variation between H_{m0} and significant wave height from time series analysis ($H_{1/3}$) (EurOtop, 2018). At relatively deep water, H_{m0} from a wave spectrum can be calculated by using Equation 2.1:

$$H_{m0} \approx 4\sqrt{m_0} \tag{2.1}$$

where, m_0 is the zeroth order moment of the variance energy density spectrum (Holthuijsen, 2007).

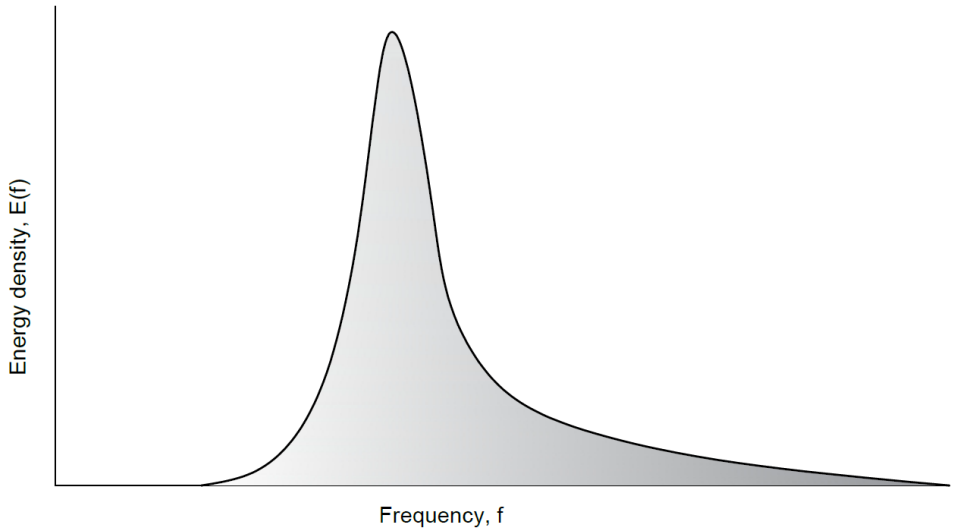

Figure 2.2 Example of a wave spectrum for irregular waves (Adapted from Holthuijsen, 2007)

2.2.2 Wave Period

The wave period, T, is defined as the time interval between the start and the end of a wave (see Figure 2.1). Peak wave period, T_p (peak of the spectrum), mean wave period, T_m, derived from wave record, and significant wave period, $T_{1/3}$ (mean of the highest 1/3 of waves) are commonly used in coastal engineering. Another definition of wave period is the average wave period calculated from spectral analysis, $T_{m-1,0}$ ($= m_{-1}/m_0$), which is frequently employed to predict wave overtopping and wave run-up. It is believed that the spectral wave period, $T_{m-1,0}$, gives additional weight to the longer wave periods in a wave spectrum, when compared to the average wave period (EurOtop, 2018).

The ratio of peak period, T_p, and the mean period, T_m, usually vary between 1.1 and 1.25 (CIRIA et al., 2007; EurOtop, 2018). For a single peaked spectrum in relatively deep water, it is believed that the spectral peak wave period, T_p, is usually 1.1 times of the average wave period derived from spectral analysis, $T_{m-1,0}$ (CIRIA et al., 2007; EurOtop, 2018).

2.2.3 Wave Steepness and Iribarren Number

The ratio of wave height to wave length, which is known as wave steepness "s" (Equation 2.2), helps to define both the wave characteristics and the

breaking process. The various forms of wave steepness are presented in Equations 2.3 – 2.5. Generally, for the wind sea state wave steepness varies from $s_{m-1,0} = 0.04$ to $s_{m-1,0} = 0.06$, while $s_{m-1,0} = 0.01$ for swell wave conditions (EurOtop, 2018).

$$s = \frac{H}{L} \tag{2.2}$$

Wave steepness based on peak wave period,

$$s_{op} = \frac{H_{m0}}{L_p} = \frac{H_{m0}}{gT_p^2/2\pi} \tag{2.3}$$

Wave steepness based on mean wave period,

$$s_m = \frac{H_{m0}}{L_m} = \frac{H_{m0}}{gT_m^2/2\pi} \tag{2.4}$$

Wave steepness based on average wave period derived from spectral analysis,

$$s_{m-1,0} = \frac{H_{m0}}{L_{m-1.0}} = \frac{H_{m0}}{gT_{m-1,0}^2/2\pi} \tag{2.5}$$

The Iribarren number (I_r) or breaker parameter or surf-similarity parameter ($\zeta_{m-1,0}$) is the combination of structure slope and wave steepness (see Equation 2.6) that describes a certain type of wave breaking. The type of wave breaking as a function of Iribarren number is presented in Table 2.1 (EurOtop, 2018). Figure 2.3 portrays the classification of wave breaking on a slope.

$$I_r = \frac{\tan\propto}{\sqrt{\frac{H_{m0}}{L_{m-1,0}}}} \tag{2.6}$$

where, α is the slope of the structure, H_{m0} denotes the spectral significant wave height and $L_{m-1,0}$ presents the deep water wave length.

Table 2.1 The type of wave breaking as a function of Iribarren number

Type of breaking	Spilling	Plunging	Collapsing	Surging
Iribarren number	$I_r < 0.2$	$0.2 < I_r < 2\text{-}3$	$I_r \pm 2\text{-}3$	$I_r > 2\text{-}3$

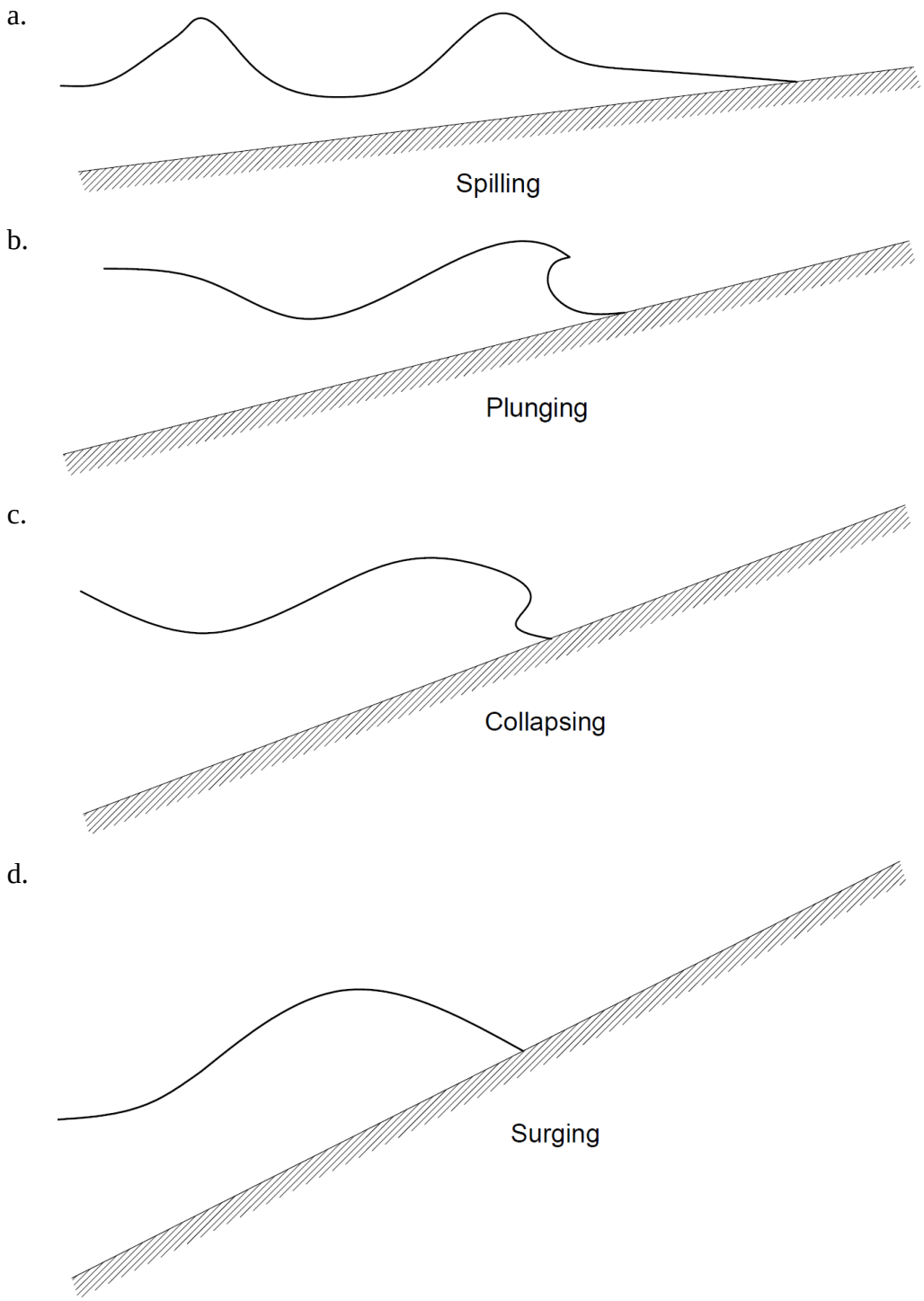

Figure 2.3 Types of wave breaking on a slope – a) Spilling, b) Plunging, c) Collapsing, and d) Surging waves (Adapted from EurOtop, 2018)

2.2.4 Wave Energy Spectrum

The two primary forms of wave energy spectrum widely applied in coastal engineering are Pierson-Moskowitz and JONSWAP spectra. The Pierson-Moskowitz spectrum represents the distribution of wave energy with frequency for a completely developed sea state that signifies the correlation between wind speed and wave growth (Pierson and Moskowitz, 1964). The empirical expression of the Pierson-Moskowitz spectrum is given in Equation 2.7 in terms of original frequency, as prescribed by Holthuijsen (2007).

$$E_{PM}(f) = \propto_{\mathrm{P}} \mathrm{g}^2(2\pi)^{-4} f^{-5} \exp\left[-\frac{5}{4}(\frac{f}{f_m})^{-4}\right] \tag{2.7}$$

where, f_m denotes the peak frequency of the spectrum, g is the gravitational acceleration, U stands for wind speed, α_P is known as Phillips constant equals to 0.0081, and β = 0.74.

Hasselmann et al., (1973) improved the Pierson-Moskowitz spectrum under a project entitled JONSWAP (Joint North Sea Wave Observation Project) by adding a multiplying factor (peak enhancement factor γ) to it (see Equation 2.8). The JONSWAP spectrum represents a young sea state, where the waves continue to grow and signifies that the energy spectrum is not fully developed. The sharpness of peak in JONSWAP spectrum is determined by the value of peak enhancement factor (γ). The parameterised JONSWAP spectrum with peak enhancement factor γ = 3.3 has been widely used as a design energy spectrum by coastal engineers (Holthuijsen, 2007).

$$E_J(f) = \propto_{\mathrm{P}} \mathrm{g}^2(2\pi)^{-4} f^{-5} \exp\left[-\frac{5}{4}(\frac{f}{f_m})^{-4}\right] \gamma^{exp\left[-\frac{1}{2\sigma^2}\left(\frac{f}{f_m}\right)^2\right]} \tag{2.8}$$

$$\sigma = \begin{cases} \sigma_a & f \leq f_m \\ \sigma_b & f = f_m \end{cases}$$

where, γ is the peak enhancement factor, σ_a is the left side width of the spectrum and σ_b is the right side width of the JONSWAP spectrum.

2.2.5 Crest Freeboard

The crest freeboard (R_c) refers to the vertical distance between the top of the structure and the still water level (see Figure 2.4). The ratio of crest height to the significant wave height is called relative crest freeboard (= R_c/H_{m0}).

2.2.6 Wave Overtopping

Wave overtopping at a coastal structure principally happens when the wave run-up levels of the largest waves are greater than the crest height of the structure (TAW, 2002). The crest freeboard (R_c) is defined as the variation in elevation between the crest height and the still water level line (see Figure 2.4).

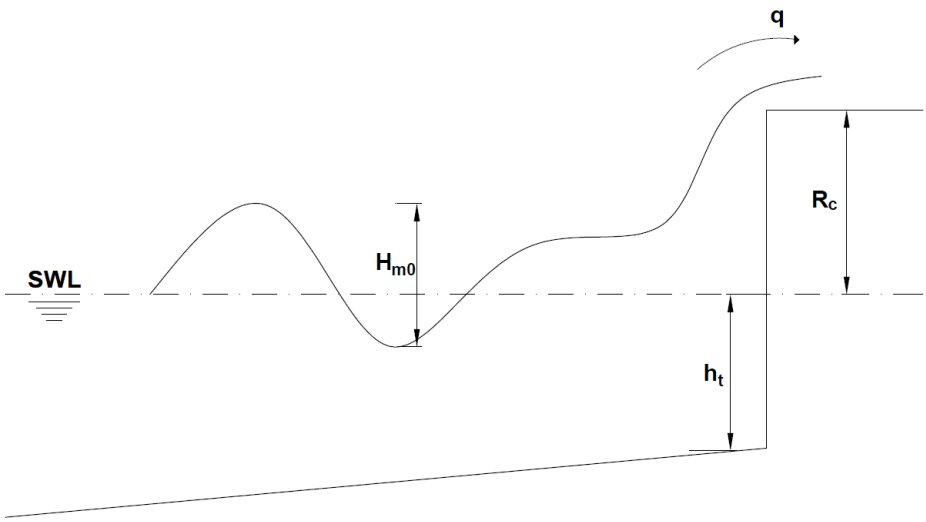

Figure 2.4 Definition sketch of wave overtopping parameters on a plain vertical wall

2.2.7 Toe Scouring

Toe scouring is defined as the formation of a scour hole at the toe of a structure, which may lead to undermining and even failure of the structure due to redistribution of sediment close to the structure toe subjected to wave action over time (Müller et al., 2008; Pearson, 2010). Figure 2.5 displays a schematic cross-section of the toe scouring at seawalls.

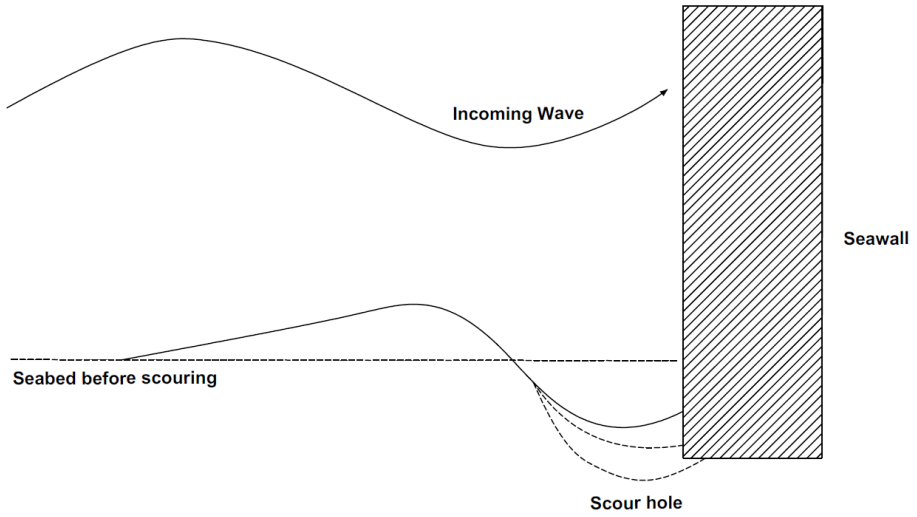

Figure 2.5 Definition sketch of toe scouring process at seawalls (Adapted from Zhu et al., 2010)

2.3 Types of sea defence structures

Sea defence structures are usually applied along the coast to provide protection to the hinterland areas against coastal flooding. Wave overtopping is believed as one of major concern for such sea defence structures. Sloping sea dikes and embankment seawalls; rubble mound structures; and, vertical and steep walls are the three principal categories of sea defence structures (EurOtop, 2018). This study investigated two types of sea defence structures; vertical walls and smooth sloping seawalls, therefore, only these defences are discussed in the following.

2.3.1 Vertical Walls

Many coastal flooding or erosion defence structures, such as urban seawalls and harbour breakwaters around the world especially in the United Kingdom, are formed by vertical or battered walls (Allsop, 2000; 2009; Allsop and Bray, 1994). Vertical walls protect hinterland areas from heavy wave action by reflecting it back. Such structure is typically formed of stone or concrete blocks, massive concrete piles or sheet steel piles (EurOtop, 2018). Figure 2.6 shows instances of vertical structures.

In relatively deep water, waves approaching structures are smaller, when compared to local water depth and reflected back, usually without breaking, in which the conditions are termed ‘pulsating’ or ‘non-impulsive’ (Figure 2.7). If the waves are larger than the water depth, they can break onto the structure, whereby this condition is termed as ‘impulsive’ (see Figure 2.8) (Bruce et al., 2010; Pearson et al., 2002). Under impulsive wave conditions, wave induced forces can be very high in magnitude and short in duration, thus breaking violently against seawall with 10-40 times higher wave loads than non-impulsive conditions. Despite the short duration, damage or failure of a vertical seawall can occur due to high impact loads (Allsop et al., 1996; Oumeraci, 1994). The wave overtopping phenomenon subjected to impulsive conditions is termed as a ‘violent’ overtopping.

a.

b.

Figure 2.6 Vertical structures: a) Modern caisson breakwater, and b) Stone blockwork seawall (Source: EurOtop, 2018)

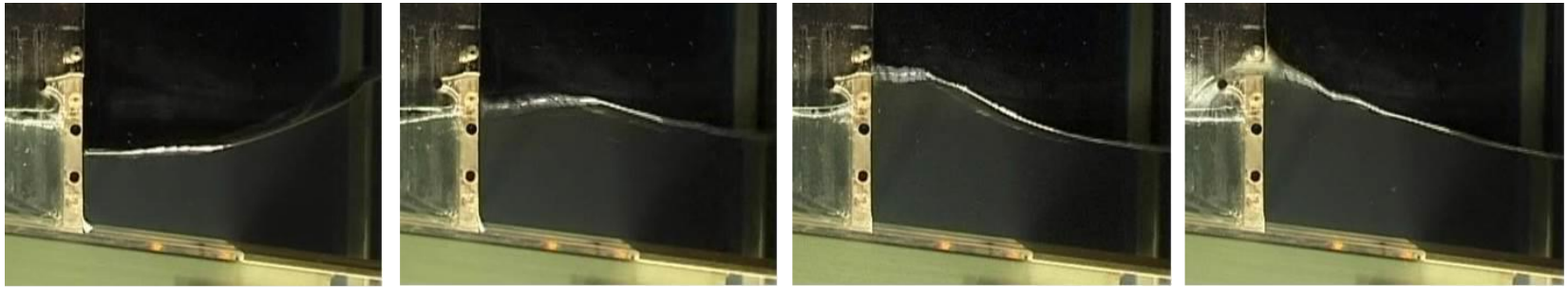

Figure 2.7 Non-impulsive wave overtopping at a plain vertical wall subjected to non-impulsive wave attack (Source: EurOtop, 2018)

Figure 2.8 Impulsive (violent) wave overtopping at a plain vertical wall subjected to impulsive wave attack (Source: EurOtop, 2018)

2.3.2 Sloping Structures

Sloping sea dikes and embankment seawalls are common forms of sea defences that are typically applied along the coasts to protect the land behind from coastal flooding. Such structures are commonly noticed along the coasts of Germany, the Netherlands, Denmark, and the United Kingdom. The structures are impermeable, and are made of fine sand or clay. On the seaward side of such defences, a revetment is usually applied using asphalt, concrete slabs, or concrete blockwork to protect against erosion induced by wave action. Figure 2.9 illustrates the sloping structures.

a.

b.

Figure 2.9 Sloping structures: a) Coastal dikes, NL (EurOtop, 2018), and b) Sloping seawall, UK (Geograph, 2012)

2.4 Prediction of Wave Overtopping

Mean overtopping discharge and individual maximum overtopping volume are the two key direct flow parameters that describe wave overtopping hazards (EurOtop, 2018). In predicting the overtopping characteristics at sea defences, three prediction methods are widely used by designers, namely empirical methods, numerical modelling, and physical modelling. It is noteworthy to highlight that in this work, the measured overtopping characteristics from small-scale physical model study were compared with the predicted values using empirical formulae derived from the literature.

2.4.1 Empirical Methods

Many parametric experimental studies have investigated the phenomenon of wave overtopping on coastal structures with fixed impermeable beaches based on laboratory measurements, wherein several empirical formulae have been proposed for the prediction of overtopping at the studied structures. This work probed into wave overtopping on plain vertical walls and smooth sloping structures, thus only empirical methods for the assessment of wave overtopping at these two coastal defences are discussed here. One should note that all the empirical overtopping equations presented in this study are based on the probabilistic design approach, unless otherwise stated.

2.4.1.1 Mean Overtopping Discharge

Mean overtopping discharge (q) in terms of per linear metre of width of the structure (l/m/s) is often used to describe the wave overtopping phenomenon. The literature depicts a general exponential equation (see Equation 2.9) to describe q on many coastal structures, such as vertical and sloping structures, armoured rubble mound breakwaters, and coastal dikes (EurOtop, 2018; Franco et al., 1994; Owen, 1980).

$$\frac{q}{\sqrt{\mathrm{g}H_{m0}^{3}}} = a\exp\left(-b\frac{R_c}{H_{m0}}\right) \tag{2.9}$$

WhereH_{m0} represents the significant wave height based on spectral analysis, a signifies the scale parameter, b denotes the shape factor, R_c/H_{m0} stands for the relative crest freeboard, and $q/\sqrt{(\mathrm{g}H_{m0}\text{^}3}$) is defined as the relative wave overtopping discharge (EurOtop, 2018).

Vertical Walls

A significant amount of experimental investigations has assessed the derivation of empirical prediction methods to estimate the mean overtopping discharge at plain vertical walls. In fact, many empirical formulae are found in the literature to estimate the wave overtopping at such coastal structures. For instance, in 2007, EurOtop manual described two empirical formulae (Equations 2.10 and 2.11) to predict the mean overtopping discharge (q) at plain vertical walls, subjected to non-impulsive and impulsive wave conditions.

For non-impulsive conditions ($h_* > 0.3$),

$$\frac{q}{\sqrt{gH_{m0}^3}} = 0.04 \exp\left(-2.6 \frac{R_c}{H_{m0}}\right) \qquad \text{for } 0.1 < \frac{R_c}{H_{m0}} < 3.5 \qquad (2.10)$$

For impulsive conditions ($h_* \leq 0.2$),

$$\frac{q}{{h_*}^2 \sqrt{g{h_t}^3}} = 1.5 * 10^{-4} * \left(h_* \frac{R_c}{H_{m0}}\right)^{-3.1} \qquad \text{for } 0.03 < h_* \frac{R_c}{H_{m0}} < 1.0 \qquad (2.11)$$

In which, $h_* = 1.35 \frac{h_t}{H_{m0}} \frac{2\pi h_t}{gT_{m-1,0}^2}$

Bruce and Van der Meer (2008), who reworked on the formulae proposed by EurOtop (2007) to assess overtopping at vertical structures, prescribed a new formula for impulsive conditions to allow both formulae for non-impulsive and impulsive conditions to be plotted on the same axes (see Equation 2.12).

For impulsive conditions,

$$\frac{q}{\sqrt{gH_{m0}^3}} = \mathrm{a} \sqrt{\frac{H_{mo}}{h_t}} \frac{1}{s_{m-1.0}} \left(\frac{R_c}{H_{m0}}\right)^{-3} \qquad (2.12)$$

In an intensive experimental study, Victor and Troch (2012) reported that the empirical formula prescribed in EurOtop manual (2007) failed to predict the wave overtopping at smooth impermeable steep sloping structures with small relative freeboards. They suggested a new set of empirical formulae to better predict the overtopping at such structures subjected to non-impacting waves (see Equations 2.13 and 2.14 for steep slopping structures to vertical walls ($0 \leq \cot\alpha \leq 1.43$).

$$\frac{q}{\sqrt{gH_{m0}^3}} = (0.033\cot\alpha + 0.062)\exp\left[(1.08\cot\alpha - 3.45)\frac{R_c}{H_{m0}}\right] \tag{2.13}$$

valid for $0 \leq \frac{R_c}{H_{m0}} \leq 0.8$

$$\frac{q}{\sqrt{gH_{m0}^3}} = 0.2\exp\left[(1.57\cot\alpha - 4.88)\frac{R_c}{H_{m0}}\right] \text{ for } 0.8 \leq \frac{R_c}{H_{m0}} \leq 2.0 \tag{2.14}$$

where, α is the slope angle of the structure.

Van der Meer and Bruce (2014) proposed a decision chart that provides various empirical equations in light of varying conditions. They suggested that distinguishing vertical walls with sloping foreshore from those without sloping foreshore in deep water is essential to gain better prediction methods for vertical structures. With the use of UG10 dataset from Victor and Troch (2012) and CLASH (2004) database, Van der Meer and Bruce (2014) demonstrated a modified version of EurOtop (2007) formulae to estimate wave overtopping for steep slopes up to vertical walls in deep water (non-breaking waves) (see Equation 2.15 for vertical walls with sloping foreshore). They also proposed a new set of formulae to predict wave overtopping at plain vertical walls under impulsive conditions (see Equations 2.16 and 2.17 for sloping foreshore).

— For non-impulsive conditions ($h_t^2/(H_{m0}L_{m-1,0}) > 0.23$),

$$\frac{q}{\sqrt{gH_{m0}^3}} = 0.05\exp\left(-2.78\frac{R_c}{H_{m0}}\right) \tag{2.15}$$

— For impulsive conditions, $(h_t^2/(H_{m0}L_{m-1,0}) \leq 0.23)$,

$$\frac{q}{\sqrt{gH_{m0}^3}} = 0.011\left(\frac{H_{mo}}{hs_{m-1.0}}\right)^{0.5} \exp\left(-2.2\frac{R_c}{H_{m0}}\right) \quad \text{for } 0 < \frac{R_c}{H_{m0}} < 1.35 \qquad (2.16)$$

and

$$\frac{q}{\sqrt{gH_{m0}^3}} = 0.0014\left(\frac{H_{mo}}{hs_{m-1.0}}\right)^{0.5} \left(\frac{R_c}{H_{mo}}\right)^{-3} \quad \text{for } \frac{R_c}{H_{m0}} \geq 1.35 \qquad (2.17)$$

Troch et al., (2014) asserted that for vertical walls, the formulae proposed by Victor and Troch (2012) (see Equations 2.13 and 2.14) gave better prediction than that prescribed by Van der Meer and Bruce (2014) (see Equation 2.15) for very small and zero freeboards ($0 \leq R_c/H_{m0} \leq 0.27$), as well as for large crest heights ($R_c/H_{m0} > 0.8$).

Recently, EurOtop (2018) updated its version of EurOtop manual (2007), along with the proposal of using new empirical equations to estimate the mean overtopping rate at plain vertical walls with and without foreshore (see Equations 2.15 - 2.17 that consider foreshore slope). The empirical formulae prescribed in EurOtop (2018) to estimate mean overtopping discharge at plain vertical walls are those provided by Van der Meer and Bruce (2014). The graphical representation of the empirical prediction methods to estimate mean overtopping rate at vertical walls for non-impulsive conditions is presented in Figure 2.10, while Figure 2.11 for those with impulsive conditions.

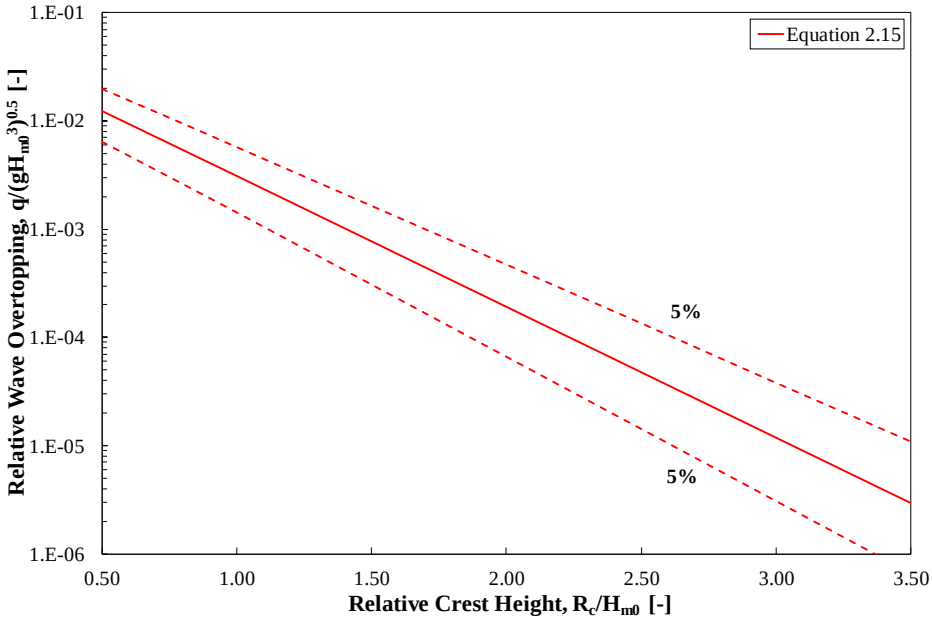

Figure 2.10 Empirical prediction of mean overtopping rate at vertical walls under non-impulsive conditions

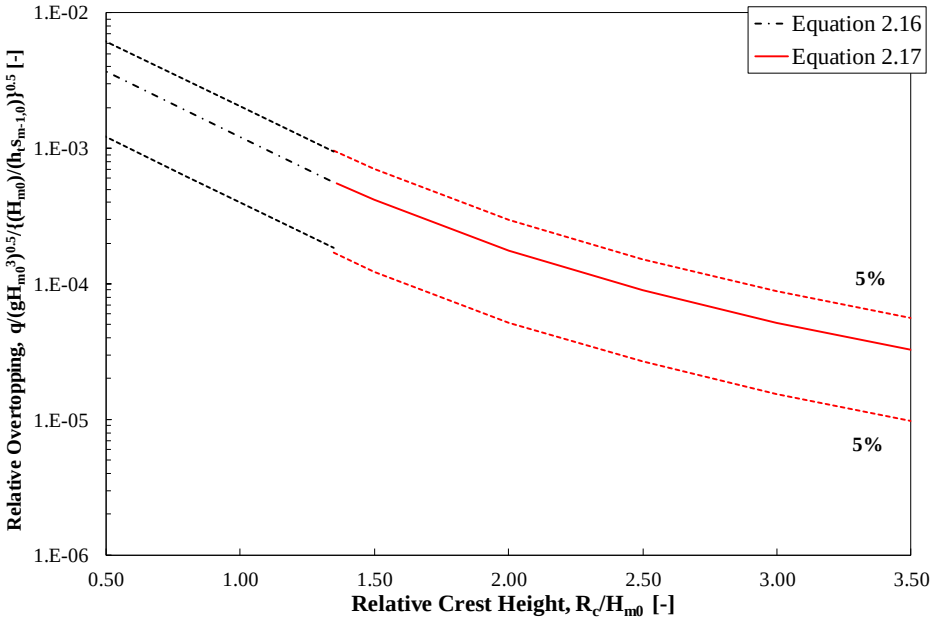

Figure 2.11 Empirical prediction of mean overtopping rate at vertical walls under impulsive wave conditions

Smooth Sloping Structures

In its initial overtopping manual, EurOtop (2007) recommended the following empirical relationships (see Equations 2.18-2.19) based on the mean value approach for the probabilistic estimation of mean overtopping rates at sloping structures.

— for breaking waves ($\xi_{m-1,0} < \sim 2$)

$$\frac{q}{\sqrt{gH_{m0}^3}} = \frac{0.067}{\sqrt{\tan\alpha}} \cdot \xi_{m-1,0} \cdot \exp\left(-4.75 \frac{R_c}{\xi_{m-1,0} \cdot H_{m0} \cdot \gamma_f}\right) \quad (2.18)$$

— and for non-breaking waves ($\xi_{m-1,0} > \sim 2$) maximum value of

$$\frac{q}{\sqrt{gH_{m0}^3}} = 0.2 \cdot \exp\left(-2.6 \frac{R_c}{H_{m0}\, \gamma_f}\right) \quad (2.19)$$

where, γ_f is the influence factor of roughness elements on a slope [-] and $\xi_{m-1,0}$ denotes the breaker parameter to distinguish breaking from non-breaking waves. Equation 2.18 signifies the estimation of overtopping for plunging or breaking waves ($\xi_{m-1,0} < \sim 2$), while Equation 2.19 denotes the maximum overtopping induced by non-breaking or surging waves ($\xi_{m-1,0} > \sim 2$).

Goda (2009) established a set of empirical formulations to predict the mean of overtopping discharges at sloping structures by analysing the selected CLASH datasets. As a result, the new formulas provided better prediction, when compared to those estimated by EurOtop (2007) (see Equations 2.20-2.24).

$$\frac{q}{\sqrt{gH_{m0}^3}} = \exp\left(-A - B \frac{R_c}{H_{m0}}\right) \quad (2.20)$$

where,

$$A = A_0 \tanh\left[(0.956 + 4.44\tan\theta).\left(\frac{h_t}{H_{m0}} + 1.242 - 2.032\tan^{0.25}\theta\right)\right] \quad (2.21)$$

$$B = B_0 \tanh\left[(0.822 - 2.22\tan\theta) \times \left(\frac{h_t}{H_{m0}} + 0.578 + 2.22\tan\theta\right)\right] \quad (2.22)$$

$$A_0 = 3.4 - 0.734\cot\propto + 0.239\cot^2\propto - 0.016\cot^3\propto \quad (2.23)$$

$$B_0 = 2.3 - 0.5\cot\propto + 0.15\cot^2\propto - 0.011\cot^3\propto \quad (2.24)$$

valid for $0 \leq \cot\propto \leq 7$

where, θ refers to seabed slope, α is structure slope, while h_t represents toe water depth.

In year 2014, Etemad-Shahidi and Jafari suggested new formulas (see Equations 2.25-2.26) to predict the mean of overtopping rates at smooth impermeable sloping structures by using the decision tree approach, along with nonlinear regression model. The revised formulas outperformed the existing empirical predictions in estimating the overtopping at sloping structures (Etemad-Shahidi and Jafari, 2014).

$$\frac{q}{\sqrt{gH_{m0}^3}} = 0.032 \cdot \exp\left[-2.6\left(\frac{R_c}{H_{m0}}\right)^{1.6} \cdot (\xi_{m-1,0})^{-1.26}\right] \quad (2.25)$$

valid for $\frac{R_c}{H_{m0}} \leq 1.62$

$$\frac{q}{\sqrt{gH_{m0}^3}} = 0.032 \cdot \exp\left[-5.63\left(\xi_{m-1,0}\right)^{-1.26} - 3.283\left(\frac{R_c}{H_{m0}} - 1.62\right)^{0.83}\right] \quad (2.26)$$

valid for $\frac{R_c}{H_{m0}} > 1.62$

Van der Meer and Bruce (2014) prescribed a new set of formulas (see Equations 2.27-2.28) to predict the average overtopping rates at sloping structures both for breaking and non-breaking waves. The application of Goda's (2009) formula was limited to slopes steeper than 1 in 2. They added that Goda's (2009) formula had overestimated the wave overtopping at gentle slopes with very low and zero crest freeboards.

The formulas proposed by Van der Meer and Bruce (2014) were incorporated into the updated overtopping manual (EurOtop, 2018). In order to estimate the mean for overtopping discharges at smooth slopping structures under breaking and non-breaking wave conditions, EurOtop (2018) recommended the following empirical expressions (see Equations 2.27 and 2.28):

— for breaking waves ($\xi_{m-1,0} < \sim 2$)

$$\frac{q}{\sqrt{gH_{m0}^3}} = \frac{0.023}{\sqrt{\tan\alpha}} \cdot \xi_{m-1,0} \cdot \exp\left[-\left(2.7\frac{R_c}{\xi_{m-1,0} \cdot H_{m0} \cdot \gamma_f}\right)^{1.3}\right] \quad (2.27)$$

— and for non-breaking waves ($\xi_{m-1,0} > \sim 2$) maximum value of

$$\frac{q}{\sqrt{gH_{m0}^3}} = 0.09 \cdot \exp\left[-\left(1.5\frac{R_c}{H_{m0}\,\gamma_f}\right)^{1.3}\right] \quad (2.28)$$

Figure 2.12 illustrates a graphical representation of the prediction method prescribed by EurOtop (2018) to estimate the overtopping rates at smooth sloping structures under non-breaking waves. In the said figure, the predicted values of dimensionless mean overtopping rates using Equation 2.28 were plotted against the dimensionless freeboard, thus enabling the comparison between empirical prediction and measurements from laboratory tests.

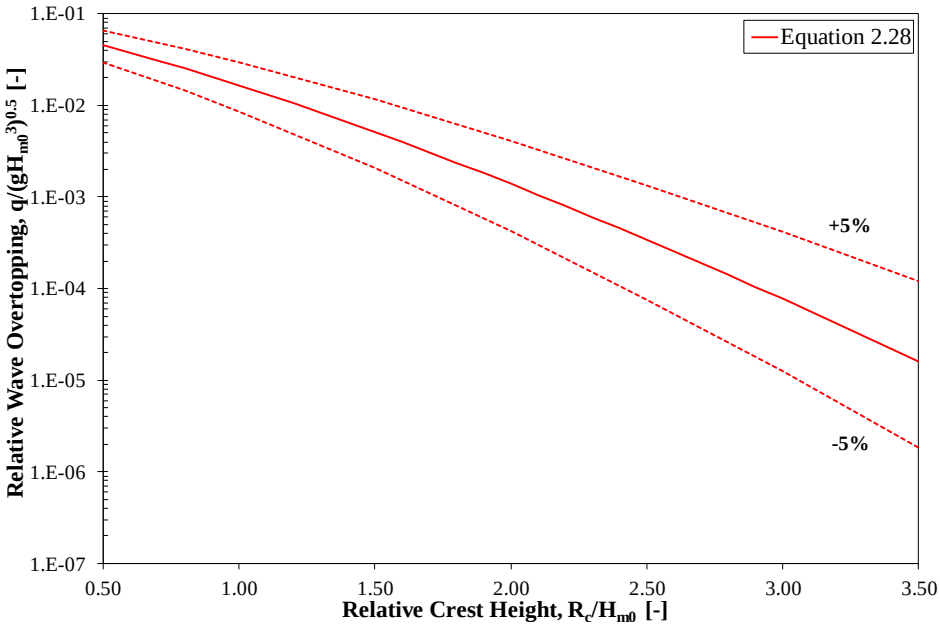

Figure 2.12 Empirical prediction of mean overtopping rate at sloping structures for non-breaking waves

2.4.1.2 Overtopping Volumes

Wave overtopping refers to a dynamic and irregular process stemming from the random nature of waves, whereby the amount of overtopped water in an overtopping event can vary significantly from the mean of overtopping (Van

der Meer and Janssen 1994). Although it is impossible to describe the wave overtopping process wholly by applying the mean of wave overtopping rate (q), this 'dynamic and irregular process' can be described satisfactorily by using the overtopping wave volume distribution (EurOtop, 2018). In assessing the tolerable wave overtopping levels and in predicting the probable overtopping hazards on individuals or property, the wave-by-wave overtopping volumes (distribution of volumes and maximum individual volumes) are often used, instead of the average overtopping discharge.

This section discusses the formulas for empirical predictions to estimate the distribution of individual overtopping volume and the maximum individual overtopping volume at a plain vertical structure under perpendicular wave attack.

Distribution of Individual Overtopping Volume

A substantial number of studies have described the distribution of individual overtopping volume in a sequence of incident waves. In 1994, Van der Meer and Janssen described the distribution of individual overtopping volume by using the two-parameter Weibull distribution (see Equation 2.29).

$$P_v = 1 - exp\left[-\left(\frac{V}{a}\right)^b\right] \tag{2.29}$$

where, V refers to the overtopping volume per wave, P_v denotes the probability that an individual overtopping volume will not exceed V, while a and b are scale and shape parameters, respectively, for Weibull distribution. The dimensional scale factor, a, has units of overtopping discharge per unit length that normalises the Weibull distribution. The shape parameter, b, is non-dimensional and it defines the extreme tail of Weibull distribution.

Maximum Individual Overtopping Volume

For both non-impulsive and impulsive conditions, the maximum individual overtopping volume (V_{max}) at a plain vertical structure can be estimated by determining the number of overtopped waves (N_{ow}) in a sequence, as shown in the following Equation (EurOtop, 2018).

Maximum individual overtopping volume (V_{max}),

$$V_{max} = a(ln\, N_{ow})^{1/b} \tag{2.30}$$

where, N_{ow} refers to the number of overtopping waves.

To estimate the scale factor, a, EurOtop (2018) proposed the following empirical relationship(Equation 2.31), along with an empirical correlation between $\Gamma(1 + 1/b)$ and shape factor, b.

$$a = \left(\frac{1}{\Gamma\left(1+\frac{1}{b}\right)}\right)\left(\frac{qT_m}{P_{ov}}\right) \tag{2.31}$$

where, Γ signifies the gamma function, and P_{ov} refers to the probability of overtopping waves (N_{ow}/N_w).

For the distribution of wave-by-wave volumes at a plain vertical wall, the b parameter can be predicted by employing the empirical expressions suggested by EurOtop (2018) (see Equations 2.32-2.33).

— For non-impulsive conditions, b

$$b = \begin{cases} 0.66 & \text{for } s_{m-1,0} = 0.02 \\ 0.88 & \text{for } s_{m-1,0} = 0.04 \end{cases} \qquad (h_t^2/(H_{m0}L_{m-1,0}) > 0.23 \tag{2.32}$$

— For impulsive conditions, b

$$b = 0.85 \qquad (h_t^2/(H_{m0}L_{m-1,0}) \leq 0.23 \tag{2.33}$$

In order to determine the Weibull shape factor b at smooth sloping structures, Zanuttigh et al., (2013) prescribed a new prediction formula (see Equation 2.34) by presenting a correlation between b and relative discharge ($q/(gH_{m0}T_{m-1,0})$).

$$b = 0.73 + 55\left(\frac{q}{gH_{m0}T_{m-1,0}}\right)^{0.8} \tag{2.34}$$

<u>2.4.1.3 Proportion of overtopping waves</u>

The proportion of overtopping waves or the probability of overtopping waves (P_{ov}) at a coastal structure can be predicted by using the empirical prediction methods suggested by EurOtop (2018). In estimating the maximum individual wave overtopping volume, the estimation of probability of overtopping waves (P_{ov}) is required.

For a known relative crest freeboard (R_c/H_{m0}), EurOtop (2018) proposed the following empirical formulas (see Equations 2.35 and 2.36) to evaluate the proportion of overtopping waves (P_{ov}) at a plain vertical wall under perpendicular wave attack, subjected to non-impulsive and impulsive wave conditions.

— For non-impulsive conditions ($h_t^2/(H_{m0}L_{m-1,0}) > 0.23$), P_{ov}

$$P_{ov} = \frac{N_{ow}}{N_w} = exp\left[-1.21\left(\frac{R_c}{H_{m0}}\right)^2\right] \tag{2.35}$$

— For impulsive conditions ($h_t^2/(H_{m0}L_{m-1,0}) \leq 0.23$), P_{ov}

$$P_{ov} = \frac{N_{ow}}{N_w} = 0.024\left[\frac{{h_t}^2}{(H_{m0}L_{m-1,0})}\left(\frac{R_c}{H_{m0}}\right)\right]^{-1} \tag{2.36}$$

with minimum predicted using Equation 2.35.

In estimating the probability of overtopping waves (P_{ov}) at smooth sloping structures, Van der Meer and Janssen (1994) gave the following expression (Equation 2.37) by considering a Rayleigh distribution of the wave run-up heights, along with the use of 2% run-up height ($R_{u2\%}$).

$$P_{ov} = \exp\left[-\left(\sqrt{-\,ln0.02}\,\frac{R_c}{R_{u2\%}}\right)^2\right] \tag{2.37}$$

For a relatively gentle slope with a breaker parameter below $\xi_{m-1,0} \leq 4.0$, the following basic formula (see Equation 2.38) can be applied to predict the run-up heights at smooth sloping structures (TAW, 2002).

$$\frac{R_{u2\%}}{H_{m0}} = 1.65\,\xi_{m-1,0} \tag{2.38}$$

Equations 2.37 and 2.38 proposed by Van der Meer and Janseen (1994) and TAW (2002), respectively, were incorporated in the overtopping manual; EurOtop (2007; 2018). It is noteworthy to highlight that these formulations are based on the measurement of run-up level that is usually calculated at a point on a straight slope, while the overtopping is measured on or behind the crest of the structure (EurOtop, 2018). Therefore, EurOtop (2018) has warned that these formulations always overestimate the number of overtopping waves.

Instead of using 2% run-up height ($R_{u2\%}$), Victor et al., (2012) proposed an empirical expression (see Equation 2.39) to estimate the probability of overtopping at smooth impermeable slopes by using a known relative freeboard and slope, subjected to non-breaking wave attack.

$$P_{ov} = \exp\left[-\left((1.4 - 0.30\cot\propto)\frac{R_c}{H_{m0}}\right)^2\right] \tag{2.39}$$

2.4.2 Numerical Methods

Numerical models are often employed by coastal engineers to simulate wave overtopping at coastal structures by employing them to solve complex flow equations within a numerical domain (EurOtop, 2018). In recent years, many studies have implemented the numerical models in designing coastal structures.

The major advantages of numerical models are that they can be applied to simulate structural geometries, do not result in scale effects, to gather the required measurements for complicated phenomena to be assessed by using physical models (Altomare et al., 2015). Besides, Altomare et al., (2015), and Altomare and Gentile (2013) asserted that numerical models demand fewer number of simulations, when compared to physical models, thus the possibility to have a cost-effective modelling approach by reducing time, resources, and money. In recent years, many numerical investigations have been devoted to the application of smoothed particle hydrodynamics (SPH) model, which evaluates varying hydrodynamic coastal processes (see Abolfathi et al., 2018; Shao, 2010). Shao (2010) described the application of incompressible SPH flow model by simulating breaking wave run-up and overtopping at a breakwater armoured with porous materials. The researcher asserted that in the field of coastal hydrodynamics, the incompressible SPH flow model may serve as a good numerical modelling scheme.

Nonetheless, for the application of numerical models, many researchers have warned about their high computational time, sophisticated computer system, and representation of physics. For instance, EurOtop (2018) reported that the existing numerical models are incapable of reproducing all the required physical processes in a computationally effective method.

2.4.3 Physical Modelling

In order to assess hydraulic and structural performances of a coastal structure; theoretical, empirical, and numerical methods are generally applied with some simplifications of the real world (Wolters et al., 2009). Due to its simplifications from the prototype situation, many uncertainties may lurk in the application of these methods to design coastal structures. Physical model tests are usually used to reproduce a physical system in assuring the correct representation of physical processes without making simplified assumptions (Hughes, 1993; Wolters et al., 2009). In a nutshell, a physical model is commonly defined as the scale representation of a prototype system in the laboratory (Hughes, 1993).

In determining the mean wave overtopping rate and individual overtopping wave-by-wave volumes, as well as in establishing the empirical formulae to estimate wave overtopping at coastal structures, the physical model tests are applied as a reliable technique (EurOtop, 2018). One of the main benefits of a physical model is that it can reproduce a prototype condition in a controlled environment without simplifying assumptions that are normally applied to a numerical or analytical method (Hughes, 1993; Wolters et al., 2009). Another advantage of physical models is that conducting experiments and data collection with the use of a small-scale physical model is more cost-effective and feasible, in comparison to field study (Hughes, 1993).

Having considered the positive effects of physical modelling, several negative issues, including scale and model effects, must be weighed in to ascertain its proper application in estimating wave overtopping. Scale effects in models are induced due to inappropriate reproduction of a physical system (EurOtop, 2018; Wolters et al., 2009). Laboratory effects may occur in physical modelling due to the boundary conditions of the designed model or due to the inappropriate simulation of prototype forcing conditions (Hughes, 1993; Wolters et al., 2009). Another negative aspect of physical modelling is that at times, it is expensive due to the requirement of high resources and computational time. For instance, Altomare et al., (2015) asserted that with the use of physical tests, it is possible to retrieve the required data, but ‘it can be very time consuming and expensive’.

2.5 Prediction of Toe Scouring

2.5.1 Time development of scour depth

The development of a scour depth has a strong correlation with storm duration or number of waves (Sutherland et al., 2003). The time required to generate a considerable amount of scour is defined as a time scale (Sumer and Fredsøe, 2002), as illustrated in the following Figure.

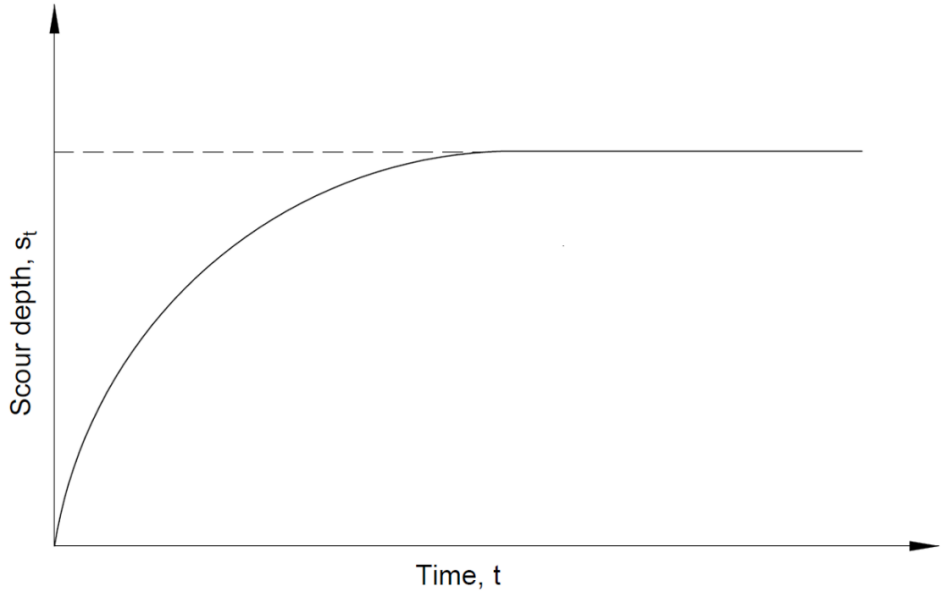

Figure 2.13 Development of scour depth over time (Adapted from Sumer and Fredsøe, 2002)

2.5.2 Relationship between scour depth and relative toe water depth

The literature depicts a strong correlation between toe scour depth and relative water depth at the structure. Müller et al., (2008) demonstrated a trend line by describing the development of non-dimensional toe scour depth (S_t/H_s) with respect to breaker type (h_b/L_m) for vertical seawalls on a sandy beach (see Figure 2.15). Here, H_s is defined as the highest one-third of wave heights = $H_{1/3}$, h_t refers to toe water depth, h_b signifies water depth at breaking, and L_m stands for deep-water wave length based on mean wave period, T_m. A similar trend of scour hole depths was also observed in plain vertical wall tests with shingle beach profiles (Pearson, 2010) (see Figure 2.15).

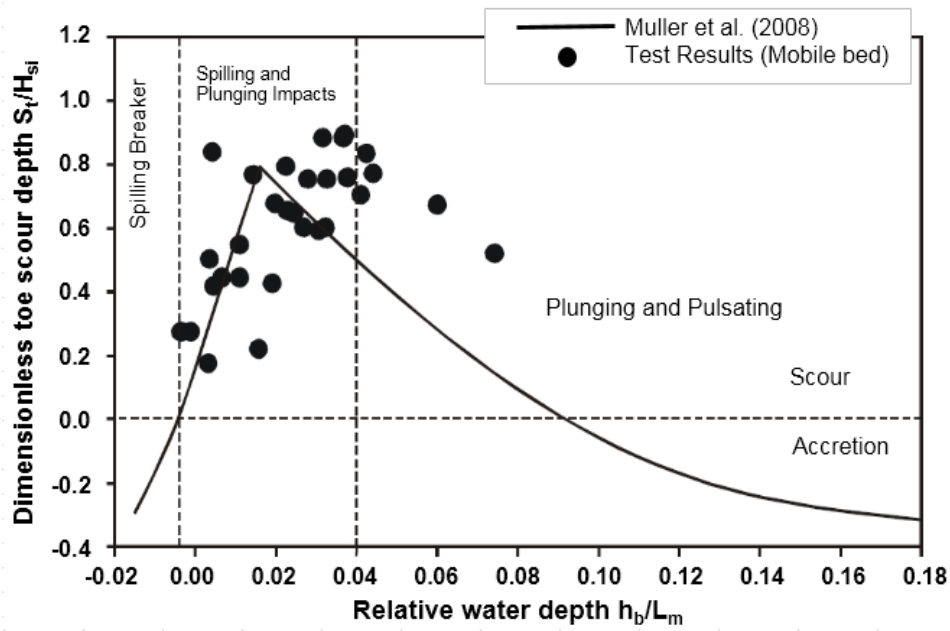

Figure 2.14 Non-dimensional toe scour depth at a vertical wall on a shingle beach as a function of breaker type (Adapted from Pearson ,2010)

2.5.3 Empirical prediction of toe scouring on sandy beach

Many studies reported that the failure of coastal structures, such as seawalls in the UK, very often occurred due to scour at the toe of the structure (Sutherland et al., 2003). In order to better comprehend this phenomenon as well as to provide prediction guidance, many experimental and field studies have placed focus on toe scouring at coastal structures with sandy foreshores (see Fowler, 1992; Kraus and Smith, 1994; Pearce et al., 2006; Sutherland et al., 2006a; Tsai et al., 2009; Xie, 1981, 1985). Both laboratory and field studies have examined toe scouring at vertical structures using sandy beach profiles (see Müller et al., 2008; Sutherland et al., 2006b; Whitehouse, 2006). Apart from experimental studies, several numerical studies have been performed recently to understand the scouring patterns at coastal structures (see Jayaratne et al., 2016; Jayaratne et al., 2014, 2015; Tahersima et al., 2011; Tofany et al., 2014).

In 2003, Sutherland et al., reported empirical design formulae to estimate toe scouring depth at seawalls and at the trunk of breakwaters for both breaking and non-breaking wave conditions. For example, for the suspended sediment

transport mode, Xie (1981) suggested the following two criteria (see Equation 2.40) to determine two scour patterns in front of a vertical structure. The author proposed an empirical relationship to design maximum scour depth in front of a vertical structure on a fine sand bed (see Equation 2.41). It is also essential to note that the tests were mainly performed under normally incident regular wave attack.

$$\frac{u_{max}-u_{cr}}{w} \geq 16.5 \text{ or } \frac{u_{*max}-u_{*cr}}{w} \geq 1.12 \tag{2.40}$$

Maximum scour depth,

$$\frac{S_{max}}{H_s} = \frac{0.4}{(\sinh 2\pi \frac{h}{L})^{1.35}} \qquad \text{for relatively fine sand} \tag{2.41}$$

where, u_{max} denotes the maximum orbital velocity at the bottom of the node, u_{cr} presents the critical velocity, u_{*max} refers to the maximum shear velocity at the bottom of the node, w signifies the sediment fall velocity, and h is the water depth.

Hughes and Fowler (1991) proposed the following empirical design relationship (see Equation 2.42) to predict maximum scour depth at vertical walls, subjected to non-breaking for normal incident of irregular wave attack.

$$\frac{S_{max}}{T_p(u_{rms})_m} = \frac{0.05}{(\sinh 2\pi \frac{h}{L})^{0.35}} \tag{2.42}$$

where, s_{max} refers to the peak scour depth at a distance $L/4$ from the wall, L denotes the wave length, and $(u_{rms})_m$ presents the peak rms velocity.

Based on an experimental study that looked into scouring at vertical walls on a 1:15 sandy bed under random wave attack, Fowler (1992) prescribed an empirical formula (see Equation 2.43) to predict the maximum scour depth in front of a vertical seawall by illustrating the correlation between non-dimensional scour depth and relative toe water depth.

$$\frac{S_{max}}{H_0} = \sqrt{\frac{22.72h_w}{L0} + .25} \tag{2.43}$$

In 1998, Whitehouse provided a contour plot to approximate toe scour depths at a plain vertical seawall with a sandy bed by plotting the non-dimensional

scour depths (S_{3000}/H_s) in light of non-dimensional water depth and wave steepness (see Figure 2.15). It is noteworthy to highlight that the study was limited to only one sediment size, d_{50} = 0.20 mm.

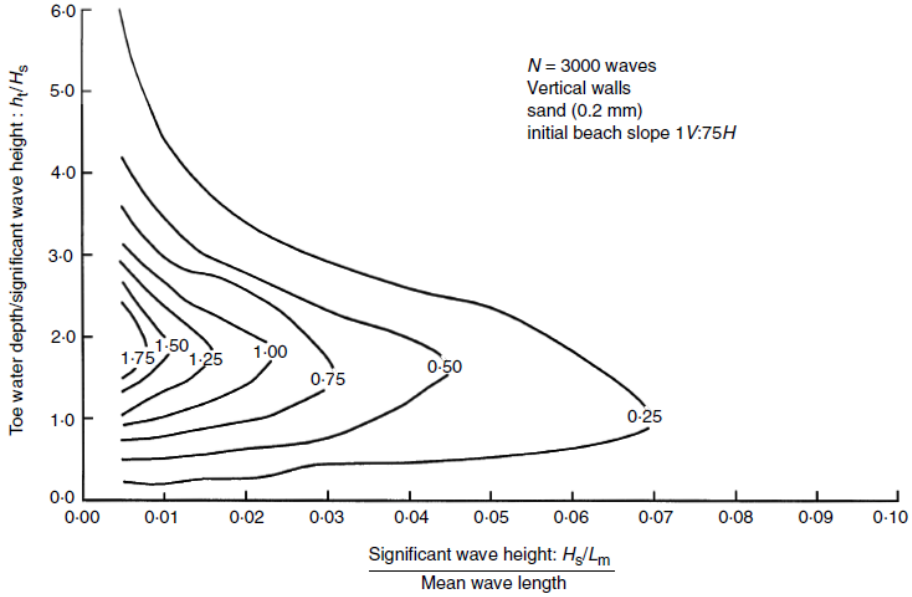

Figure 2.15 Scour development in front of a vertical seawall on a sandy bed, where the contour line represents (S_{3000}/H_s) (Source: Whitehouse, 1998)

For sloping structures under non-breaking wave attacks, Sumer and Fredsøe (2002) suggested the following empirical formula (see Equation 2.44) by expressing the scour depth as a function of breakwater slope.

$$\frac{S}{H} = \frac{f(\propto)}{\left[\sinh\left(\frac{2\pi h}{L}\right)\right]^{1.35}} \tag{2.44}$$

where,

$$f(\propto) = 0.3 - 1.77\exp\left(-\frac{\propto}{15}\right) \qquad \text{for } 30° \leq \alpha \geq 90° \tag{2.45}$$

in which, α refers to the slope of the wall in degrees.

In order to enhance the understanding of toe scouring phenomenon at seawalls, Sutherland et al., (2006a) performed an experimental study on a 1 in 2 sloping wall with a 1 in 75 foreshore, and on a vertical wall with foreshore slopes of 1 in 30 and 1 in 75. The researchers asserted that the empirical expression (see Equation 2.43) provided by Fowler (1992) resulted in overestimation of scour depth at relatively low water depth, while the prediction formula (see Equation 2.44) prescribed by Sumer and Fredsøe

(2002) overestimated scour depth at relatively high water depth (Sutherland et al., 2008; Wallis et al., 2009). Additionally, the authors claimed that toe scouring is independent of the slope of the structure and further claimed that scour depths at sloping walls do not differ from those reported at vertical walls. These authors then proposed a new empirical expression to predict maximum toe scour depth for seawalls on a sandy beach (see Equation 2.46). For a known beach slope, the authors suggested another empirical equation to predict toe scour depth at vertical walls with sandy beaches (see Equation 2.47).

$$\frac{S_{tmax}}{H_s} = 4.5\mathrm{e}^{-8\pi(h_t/L_m+0.01)}\left(1-\mathrm{e}^{-6\pi(h_t/L_m+0.01)}\right) \tag{2.46}$$

valid for $-0.013 \leq h_t/L_m \leq 0.18$

$$\frac{S_t}{H_s} = 6.8(0.207\ln(\alpha)+1.51)\mathrm{e}^{-5.85k_m h_t}(1-\mathrm{e}^{-3k_m h_t}) - 0.137 \tag{2.47}$$

valid for $-0.04 \leq h_t/L_m \leq 0.12$

where, S_{tmax} represents the maximum toe scour depth, S_t denotes the toe scour depth, H_s is defined as the highest one-third of wave heights = $H_{1/3}$, α signifies the beach slope, h_t indicates the toe water depth, and L_m stands for the deep-water wave length based on mean wave period, T_m.

2.5.4 Empirical prediction of toe scouring on shingle beach

Only a handful of studies have assessed toe scouring at sea defences with permeable shingle beach configurations. For instance, to date, limited knowledge is available on scour depth at a sloping wall with permeable shingle foreshore slope. With prototype sedmiment diamaters of $5 < d_{50} < 30$ mm, and a model scale of 1:17, Powell and Lowe (1994) devised a non-dimensional scour plot to predict toe scouring depth at a vertical wall on permeable shingle beach under normal incident of irregular wave attack (see Figure 2.16).

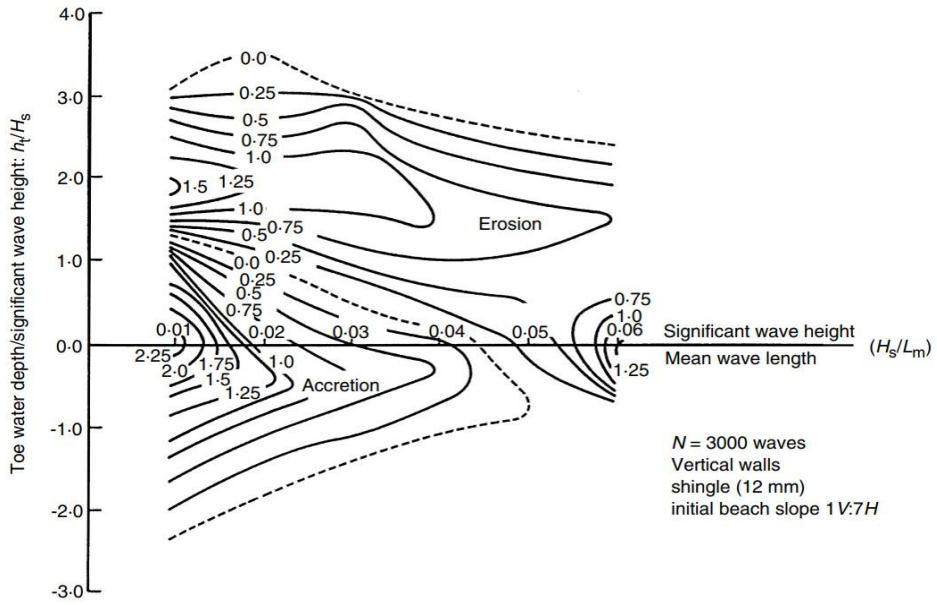

Figure 2.16 Scour development in front of a vertical seawall on a shingle bed, with contour line represented by (S_{3000}/H_s) (Source: Powell and Lowe, 1994)

Jayaratne et al., (2015) performed a laboratory study on scouring at vertical seawall with a sandy slope and two gravel slopes. The gravel slopes at d_{50} = 2.20 mm with a density of 2904 kg/m^3 and 2.50 mm with a density of 2805 kg/m^3 had been tested. Based on the best-fitting analysis, they suggested an empirical model (see Equation 2.48) to estimate the scour depth at gravel slope of d_{50} = 2.20 mm using the maximum wave height at the toe of the slope, submergence of the berm, and local wave length. To date, these empirical models, together with new data, have not been validated with other datasets.

$$\frac{S}{L_0} = -0.0322\frac{d_b}{H_{0max}} + 0.0174 \qquad \text{for gravel } d_{50} = 2.20 \text{ mm} \qquad (2.48)$$

where, L_0 refers to the local wave length, d_b denotes the submergence depth of the berm, and H_{0max} signifies the maximum wave height at the toe of the foreshore slope.

2.6 Summary

Overall, the researchers certainly agree on the significance of the reliable prediction of coastal processes, for instance, wave-induced overtopping and toe scouring at the wave structure interactions of sea defences. Over the years, many studies have focused on these key coastal processes. A review of the existing overtopping prediction methods showed that most parametric studies on the investigation of wave overtopping at structures have largely been undertaken on fixed impermeable beach foreshore, with investigations on permeable shingle beaches in scarcity. A paucity of experimental studies was also noted in toe scouring processes on permeable shingle beaches. As a consequence, little knowledge is available in the literature on the performance of these processes at coastal structures with permeable shingle foreshores. This knowledge gap has been addressed in this present study, by reporting the outcomes and analyses of an extensive small-scale two-dimensional wave flume investigation of two structural configurations (e.g. a plain vertical wall and a smooth 1 in 2 sloping wall), along with three foreshore configurations: two particle sizes, as well as an impermeable foreshore that represents the control condition. The research methodology of this experimental study is elaborated in the following chapter.

CHAPTER 3

Research Methodology

3.1 Synopsis

The previous chapter reported the scientific literature on the investigations of the key coastal processes e.g. wave overtopping and toe scouring at vertical walls as well as at sloping structures. The aim of this chapter is to present an overview of the experimental set-up followed in this study to carry out the two-dimensional small-scale wave flume tests. The research methodology adopted in this research is discussed in this chapter presenting all the steps forward to achieve the research objectives. First, section 3.2 discusses the laboratory set-up of this study in details by reporting the characteristics of two-dimensional wave flume along with the beach materials used to recreate permeable foreshore slopes. The features of model sea defence structures are also presented in section 3.2 followed by the description of the measurement devices. Section 3.3 interprets the incident wave conditions followed in this experimental work. The experimental program and testing procedure are noted briefly in section 3.4. The calibration of incident wave conditions is reported in section 3.5. The final section of this chapter discusses the accuracy of the tested overtopping measurement system.

3.2 Laboratory Description

The laboratory set up for this experimental work has been performed by adapting the guidelines of EurOtop (2018) and Wolters et al. (2009) for typical two-dimensional wave flume investigations. Physical model experiments were undertaken in a two-dimensional wave flume within the school of engineering at the University of Warwick. The wave channel has a length of 22 m, a width of 0.60 m and an operating depth of 0.40 m - 0.70 m. The sidewalls and bottom of the wave flume are built of glass. The flume is equipped with an absorbing piston type wavemaker to generate regular as well as random waves. A side view of the wave flume is presented in Figure 3.1.

A geometric scale 1:5 to 1:50 is usually applied for small scale experiments in a two-dimensional wave flume to represent the prototype situation and to model a random sea state in the flume (EurOtop, 2018). A length scale of 1:50 was applied in this study to generate random sea wave conditions within the wave flume.

Figure 3.1 – Photograph of the wave flume

3.2.1 Beach Materials

To represent a shingle bed within the laboratory, crushed anthracite has been satisfactorily used as a model beach material by researchers over the years, e.g. Powell (1990), Coates and Dodd (1994). To perform the experiments on permeable foreshores, two different shingle sediments were used and reproduced by crushed anthracite with a quoted specific gravity of 1.40, with the adaption of the well-known method of Powell (1990).

The scaling of mobile shingle beaches was applied, by adapting the well-established methodology of Powel (1990). For the selection of model beach sediment in laboratory investigations, Powel (1990) described that model sediment should satisfy the following three criteria:

— In physical model tests, permeability should be accurately reproduced to reach the real beach slope.

— The correct reproduction of the relative magnitudes of the onshore and offshore movement to evaluate whether the erosion or accretion will occur at the beach.

— To identify the minimum wave velocity for initiating the motion of the beach, the threshold of movement should be correctly scaled in the experiments.

To fulfil these requirements, Powell (1990) proposed the methodology of Yalin (1963), Komar and Miller (1973) and Dean (1973) for the beach permeability, threshold of movement and, onshore and offshore movement criteria respectively. In summary, Powell (1990) reported the following formulations (Equations 3.1 – 3.4) to scale the model bed material.

— For accurate representation of permeability

$$\lambda_{\mathrm{D}} = \left(\frac{\lambda\, K_{\mathrm{p}}}{K}\right)\left(\frac{Re_{\mathrm{p}}}{\lambda^{\frac{1}{2}}\,\lambda_{\mathrm{D}}}\right) \tag{3.1}$$

— For accurate representation of onshore/offshore movement

$$\lambda_{\Delta} = \frac{\lambda\,\lambda_{\mathrm{CD}}}{\lambda_{\mathrm{D}}} \tag{3.2}$$

where,

$$\lambda_{\mathrm{CD}} = \left(\frac{C_{\mathrm{D_P}}}{C_D}\right)\left(\frac{Re_{\mathrm{p}}}{\lambda^{\frac{1}{2}}\,\lambda_{\mathrm{D}}}\right) \tag{3.3}$$

— For accurate threshold of motion

$$\lambda_{\Delta}{\lambda_{\mathrm{D}}}^{3/4} = \lambda^{3/4} \tag{3.4}$$

where, λ is the model scale, K_{p} and Re_{p} are the permeability and Reynolds number of the prototype situation, λ_{Δ} , Δ is $(\rho_{\mathrm{s}} - \rho_{\mathrm{f}})/\rho_{\mathrm{f}}$, ρ_{f} and ρ_{s} are the specific gravities of the fluid and sediment respectively, C_{D} is the drag coefficient and $C_{D\mathrm{p}}$ is the prototype drag coefficient. For known prototype values of K_{p} and Re_{p}, there are four equations to solve for four unknowns λ, λ_{D}, λ_{Δ} and λ_{CD}. As also mentioned by Powell (1990) that these four formulations can only be solved with the assumption of prototype condition,

which makes $\lambda = \lambda_D = \lambda_\Delta = \lambda_{CD}$ and subsequently three variables remain as unknown.

Another aspect is that the correct replication of all three criteria is practically unreachable since the model bed materials have only two characteristics (size and specific gravity of the sediments). In 1990, Powell found that the filtered anthracite materials with a quoted specific gravity of 1.39 justify most of the requirements by reproducing the correct magnitudes of onshore/offshore movement and threshold of motion. Later, this methodology was adapted by Coates and Dodd (1994) to scale down a narrow gravel bed d_{50} of 15 mm with a prototype density of 2.65 (T/m^3). These researchers concluded that at a 1:50 scaling filtered anthracite sediment d_{50} of 2.50 mm with a density of 1.40 (T/m^3) satisfy the most of the requirements to reproduce an assumed prototype gravel bed d_{50} of 15 mm.

In this work, the mobile gravel beds were reproduced with the use of the crushed anthracite by adapting the methodology of Powell (1990). Two different assumed prototype gravel slopes d_{50} of 13 mm and 24 mm with a prototype specific gravity of 2.65 (T/m^3) were reproduced with the use of two different sizes of model sediments, see Figure 3.2. At a model length scale of 1:50, for assumed gravel beds d_{50} of 13 mm and 24 mm with a prototype specific gravity of 2.65 (T/m^3), the required sediment properties are listed in Table 3.1 with the application of expressions as suggested by Powell (1990) (Equations 31. –3.4).

a.

b.

Figure 3.2 Photographs of model beach sediments - a) d_{50} of 2.10 mm, and b) d_{50} of 4.20 mm

Table 3.1 Properties of model bed materials

Prototype d_{50} [mm]	Model Scale	Model d_{50} [mm]	Sp. Gravity of sediment ρ_s [T/m^3] for threshold of motion	Sp. Gravity of sediment ρ_s [T/m^3] for onshore or offshore movement
13	1:50	2.1	1.42	1.39
24	1:50	4.2	1.45	1.37

As observed in Table 3.1, the model sediment should have a specific gravity around 1.40 to satisfy the requirements of the correct magnitudes of onshore/offshore movement and threshold of motion. Hence, the filtered anthracite with a quoted specific gravity of 1.40 has been used in this study, which is also commercially available in various sizes. In Figure 3.3, the grain size distribution curve of each gravel sediment is presented.

a.

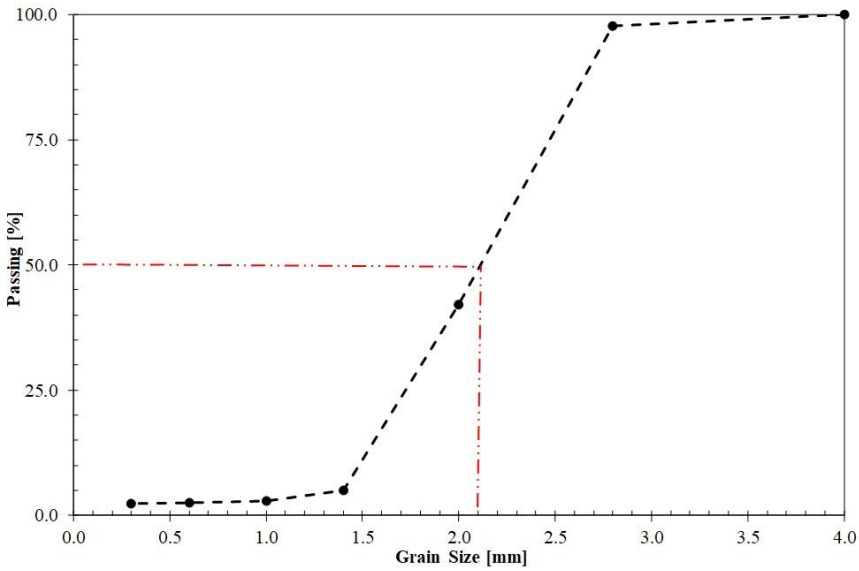

b.

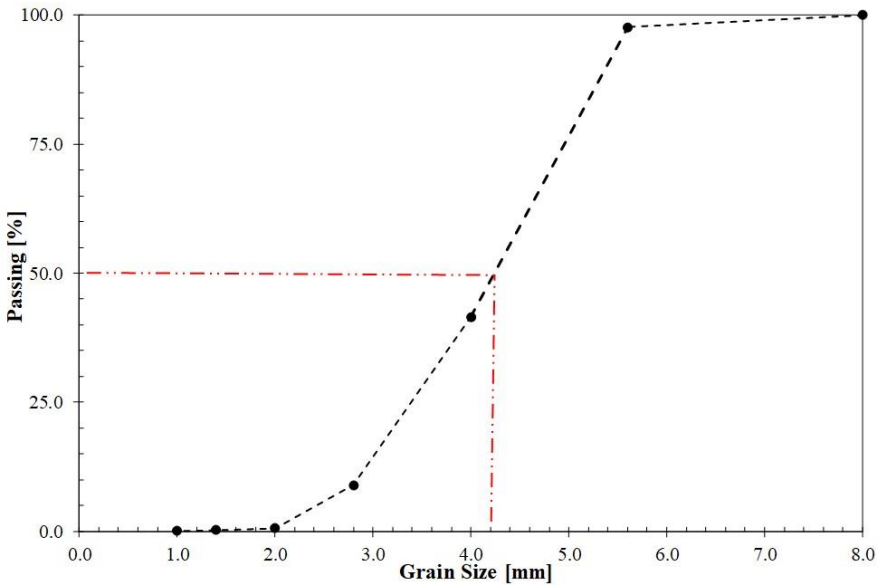

Figure 3.3 The grading curves of model beach sediments - a) d_{50} of 2.10 mm, and b) d_{50} of 4.20 mm

3.2.2 Model Structure

In this work, the experimental investigation on wave overtopping and toe scouring were conducted at two distinct coastal structures; a plain vertical seawall and a smooth 1 in 2 sloping wall. For both vertical seawall and sloping wall, a sloping foreshore with a uniform slope of 1:20 was constructed in front of the structure to generate depth limited waves. A smooth impermeable slope was constructed to perform the experiments with a solid beach. A permeable shingle beach was made of scaled anthracite to conduct the experiments for the shingle beach configurations. The schematic of the

test set-up for the plain vertical wall is presented in Figure 3.4 and for the sloping wall is shown in Figure 3.5.

For the experiments on shingle foreshores, there was an impermeable glass foreshore below a permeable shingle bed of thickness of 200 mm. Due to the existence of impermeable substrate below the permeable layer, there is a possibility that the flow below the foreshore can be influenced by the impermeable substrate below the permeable layer. To reduce any uncertainty which may arise from the permeable layer on top of the impermeable substrate, the thickness of the permeable shingle foreshore was made with a reasonable thick layer of sediments (200 mm in depth). For the tested conditions, it was observed that the shingle foreshore was thick enough to allow the bed level changes, indicating that there is a limited influence of the impermeable substrate below the designed permeable layer for the test set-up followed within study.

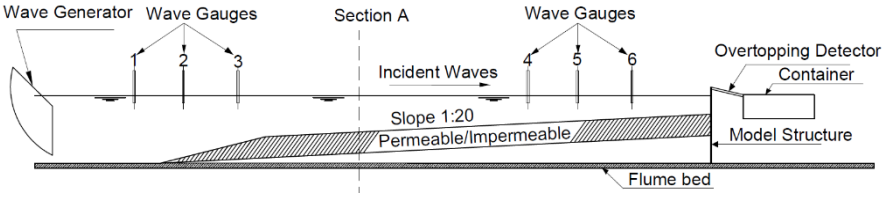

a.

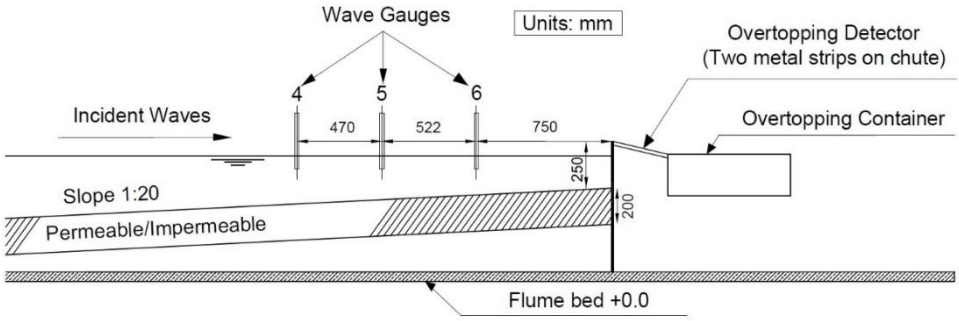

b.

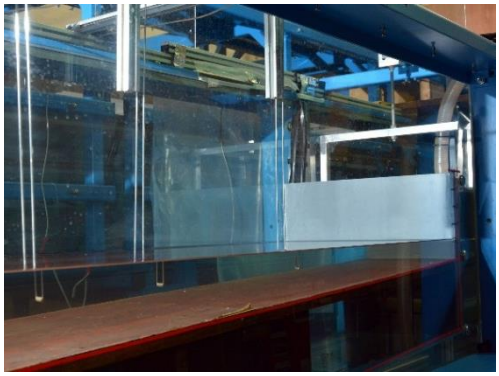

c.

d.

Figure 3.4 Test set –up for plain vertical wall: a. Cross-section along the length of wave channel, b. The overtopping measurement techniques and location of wave gauges (A-A'), c. Photograph of impermeable bed configuration, and d. Photograph of shingle bed (d_{50} = 13 mm) configuration

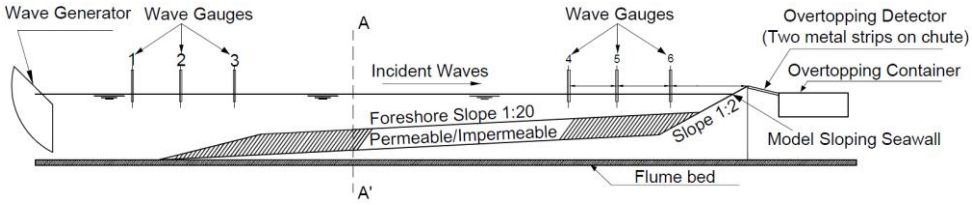

a.

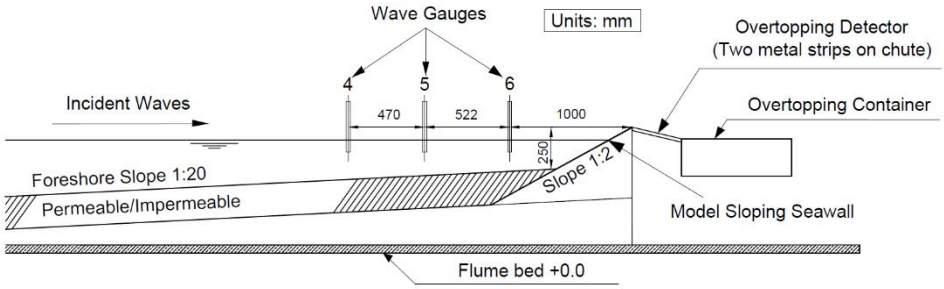

b.

c.

Figure 3.5 Test set –up for sloping structure: a. Cross-section along the length of wave channel, b. The overtopping measurement techniques and location of wave gauges (A-A'), and c. Photograph of shingle bed (d_{50} = 13 mm) configuration

3.2.3 Measurement of wave conditions

The wave heights and periods were calculated by measuring free water surface elevations at the different points during the experiments. The gauges were set at a frequency of 128 Hz to sample the water surface elevation for a test run. To separate the incident and reflected condition, a 3-point method was applied to determine the wave conditions at the structure as well as at deep water (near wave paddle), see Mansard and Funk (1980). To determine the deep water wave conditions, one set of three wave gauges (number 1, 2 and 3) were positioned near wave paddle at relatively deep water, see Fig. 3.4 and 3.5. The water surface elevations at the structure were measured by placing another set of three wave gauges (number 4, 5 and 6 in Fig. 3.4 and 3.5) close to the structure. The probe spacing between wave gauges was calculated as following the approach prescribed by Mansard and Funk (1980).

The distance between the structure and nearest wave gauge (number 6 in Figure 3.4 and 3.5) was found using the methodology described by Klopman and Van der Meer (1999) which enables to avoid the effects of a reflective structure on incident significant wave heights. The wave gauge in front of the vertical seawall was positioned at 750 mm (0.25 times of wave length associated with peak frequency and local water depth) from the face of the structure, see Figure 3.4. For the experiments with sloping structure, the closet wave gauge (number 6, Fig. 3.5) was set at 1000 mm from the face of the wall. As reported by Klopman and Van der Meer (1999), for the vertical walls there is limited influence of the structure on the incident significant wave heights thus it is possible to place the multi-gauge wave measurement method adjacent to the structure. This is because vertical structure is almost near to a perfectly reflective wall thus as per linear wave theory no evanescent wave modes are present only the incident and reflected waves exist (Klopman and Van der Meer, 1999).

To compensate the reflected waves originating from the structure, the wave paddle was equipped with an active absorption system during the overtopping and scouring tests. However, due to the presence of high reflection induced by structure, there may be existence of uncertainties in the determination of incident inshore wave characteristics. Thus, to reduce probable uncertainties

in the measurement of inshore wave characteristics, the incident wave conditions were calibrated by repeating the test sequence without the presence of structure, which enables the effects of wave-structure induced reflection to be evaluated.

3.2.4 Measurement of overtopping

To collect and measure the overtopping discharges, an overtopping measuring container was placed on the rear side of the structure, connected with an overtopping chute from the crest of structure. For the tested conditions on the shingle beach, a perforated sheet made of stainless steel was positioned on the upper side of container to collect the overtopped sediment particles. The diameter of the hole of the perforated sheet was smaller than the diameter of model shingle beach which enables the overtopped sediments to be separated from the water. A suction pump was attached with the measuring container to empty it after or during a test run.

The collection container was suspended from a load-cell that allows the measurement of overtopping mass as a form of change in voltage for each overtopping event, during the experimental test sequence. The voltage across the loadcell was set to increase with the increase of overtopped water volume in the container for an overtopping event. In this study, a single point loadcell with a quoted capacity of 100 kg was used. The logging system of the loadcell allows to record a maximum of 10v. It is note that the maximum capacity of the overtopping container was limited to 30 litres, hence, the prior to testing the logging system of the loadcell was calibrated as such the generated voltage of the loadcell cannot exceed the maximum capacity of the overtopping container. The calibration of used load-cell is described in Appendix A1.

Even though the tested loadcell showed a strong linear relationship between the voltage and overtopping mass, however, the output loadcell voltage had some noise in the data, see Fig A.2 in Appendix A1. Due to the existence of the noise in the output voltage, the accurate prediction of an overtopping event from the loadcell data would be difficult, especially for an experiment

with a lot of overtopping events. Hence, an overtopping detector was used to detect an overtopping event alongside the load-cell.

The overtopping detector was made with the use of two parallel metal strips of metal tape setting across the overtopping chute i.e. along the crest of structure. A wire was connected to the metal strips, and attached to a battery to make a simple circuit, e.g. the circuit diagram in Figure 3.6. During an overtopping event, water overtops the crest of structure and goes through the metal strips, which is configured to show a voltage spike, as the overtopped water passes the strips. Thus, allowing identification of every wave-by-wave overtopping volume during each test.

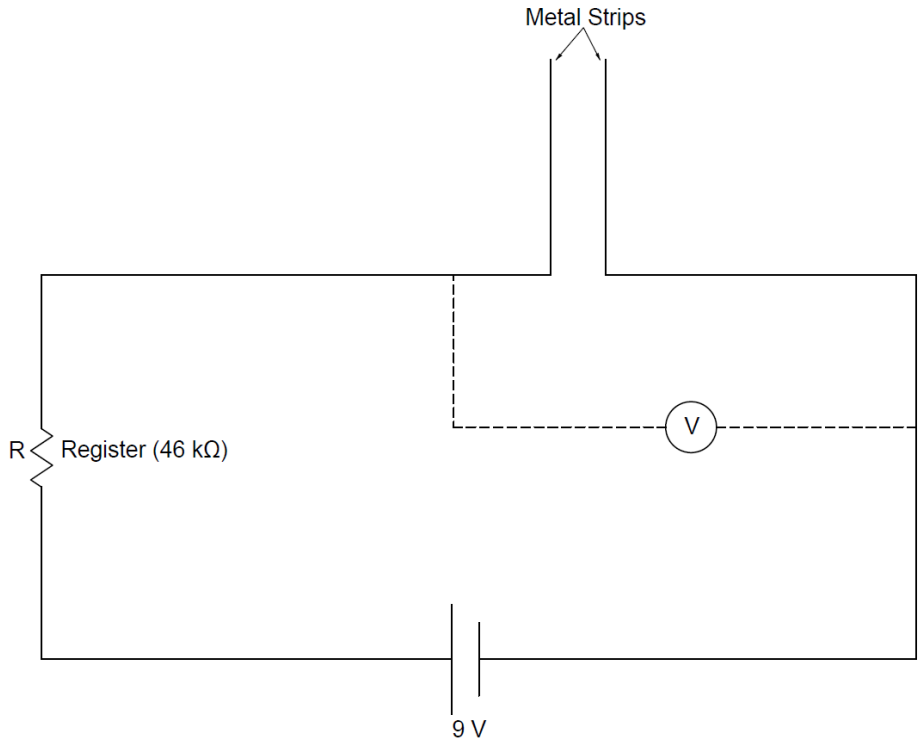

Figure 3.6 Sample circuit diagram of overtopping detector

The load-cell and overtopping detector were connected with a data logger to process and store all the output signals at a desired frequency of 20 Hz. At the end of the experiment, collected data were passed through an algorithm to determine the total overtopping volume and the wave by wave overtopping volumes for an experiment, which enables to filter the sample outputs by removing the noise from the raw data. During an experiment with a large number of overtopping waves, some small overtopping events might have

been undetected by the detector. Since mean overtopping volume is calculated based on the difference between initial and final voltage of load-cell, hence, it has no influence on the calculation of average overtopping volume within this study. Furthermore, the Weibull b value for an overtopping sequence is generally calculated using the relatively large wave by wave volumes, therefore, small overtopping volumes will not have any significant influence on the distribution of wave by wave volumes.

3.2.5 Measurement of scouring

Measurements of toe scouring and wave overtopping were conducted simultaneously for tests on plain vertical seawalls with a shingle foreshore. Due to the simultaneous measurements of overtopping and toe scouring, all the tests were performed with 1000 random waves and the scour depth was also calculated for 1000 wave cycles. Prior to the start of each experiment, the shingle bed was reshaped to the initial profile which was uniform 1:20 permeable foreshore slope in front of the vertical wall.

A depth point gauge was used to measure the scour depths at the end of the test. For each experiment, scour depth at toe (S_t) and maximum scour depth (S_{max}) were measured after a test run. For selected conditions, scour depths were also measured at several locations along the shingle bed to determine the bed profile of shingle beach after wave attack. This was performed using the depth point gauges at defined locations as well as a digital camera from a fixed position and subsequent analysis was applied.

3.3 Wave Conditions

In general, for a wind sea state wave steepness in deep water varies from s_{op} = 0.04 to s_{op} = 0.06 and for swell wave conditions it is usually s_{op} = 0.01 (EurOtop, 2018). To generate both wind sea state and swell sea conditions, two constant wave steepnesses (s_{op}= 0.02 and 0.05) in relatively deep water were tested in this study.

The JONSWAP energy spectrum is usually applied as the design spectrum by coastal engineers (Holthuijsen, 2007) and employed in experimental studies by researchers for enabling comparison of gathered data. The mean values of shape parameters for the JONSWAP energy spectrum, are $\gamma = 3.3$,

$\sigma_a = 0.07$ and $\sigma_b = 0.09$ (Holthuijsen, 2007; Wolters et al., 2009). To generate a realistic irregular wave field, a parameterized JONSWAP wave spectrum with a peak enhancement factor, $\gamma = 3.3$ ($\sigma_a = 0.07$ and $\sigma_b = 0.09$) was applied. Each experiment consisted of approximately 1000 random waves as suggested by EurOtop (2018) and Wolters et al. (2009). This enabled the acquisition of the measured overtopping characteristics which were statistically independent of the storm duration (number of waves) for the experiment run.

At a 1:50 scaling, the incident significant wave heights (H_{m0}) were tested from 0.05 m to 0.16 m and corresponding wave periods were in the range of 0.80 s to 2.26 s. The incident wave conditions at the toe of the structure is presented in Table 3.2.

Table 3.2 Incident wave conditions at the toe of the structure

	T_p [sec]									
s_{op} [-] / H_{m0} [m]	0.05	0.055	0.06	0.07	0.08	0.09	0.10	0.12	0.14	0.16
0.02	1.27	1.33	1.39	1.50	1.60	1.70	1.79	1.96	2.12	2.26
0.05	0.80	0.84	0.88	0.95	1.01	1.07	1.13	1.24	1.34	1.43

3.4 Test Program and Procedure

For both structural configuration i.e. plain vertical seawall and sloping wall, a matrix of around 180 test conditions (wave steepnesses, crest freeboards, water depths, shingle sizes) were covered in this study, Table 3.3 and 3.4. Six depths within the water column at the toe of the structure, were tested to examine the wave overtopping and toe scouring at vertical walls on shingle beaches. In addition, tests were conducted with negative toe water depths (water depth below beach level) to investigate the toe scouring at a coastal structure with a shingle foreshore.

Prior to start of each experiment, the shingle foreshore was reshaped to the initial beach profile which was smooth 1 in 20 slope in front of the structure. Afterwards, the wave gauges were calibrated and positioned at designed location before running waves in the flume. For the measurements on

scouring, the initial bed profile was measured along the length of the flume using depth gauges.

As following the test conditions described in Table 3.3 and 3.4, the small-scale experiments were conducted for a certain storm duration to cover at least 1000 random waves. For the experiments with extreme wave overtopping, the overtopping container was emptied during experiments using a suction pipe connected to the tank. For the tested conditions on shingle foreshore, the overtopped sediment materials were collected from the container and dried in order to determine the volume of overtopped sediment. The wave induced toe scour depth and maximum scour depth were measured after a test run with the use of depth gauge. To investigate the bed level changes due to an irregular wave attack, the scour depths were also measured at several locations using point depth gauges along the bed profile after running an experiment.

Table 3.3 Summary of test conditions for the plain vertical seawall

Structural configuration	Bed configuration	Toe water depth, h_t [m]	Crest Freeboard, R_c [m]	Wave Height, H_{m0} [m]	Wave steepness, s_{op} [-]	Wave Period, $T_{m-1,0}$ [s]
Vertical wall	Impermeable/ shingle bed d_{50} of 13 mm / shingle bed d_{50} of 24 mm	0.060	0.190	0.05-0.16	0.02	1.27-2.26
					0.05	0.80-1.43
	Impermeable/ shingle bed d_{50} of 13 mm / shingle bed d_{50} of 24 mm	0.075	0.245	0.05-0.16	0.02	1.27-2.26
					0.05	0.80-1.43
	Impermeable/ shingle bed d_{50} of 13 mm / shingle bed d_{50} of 24 mm	0.100	0.150	0.05-0.16	0.02	1.27-2.26
					0.05	0.80-1.43
	Impermeable/ shingle bed d_{50} of 13 mm / shingle bed d_{50} of 24 mm	0.150	0.100	0.05-0.16	0.02	1.27-2.26
					0.05	0.80-1.43
	Impermeable/ shingle bed d_{50} of 13 mm / shingle bed d_{50} of 24 mm	0.180	0.140	0.05-0.16	0.02	1.27-2.26
					0.05	0.80-1.43
	Impermeable/ shingle bed d_{50} of 13 mm / shingle bed d_{50} of 24 mm	0.200	0.050	0.05-0.16	0.02	1.27-2.26
					0.05	0.80-1.43
	Shingle bed d_{50} of 13 mm / shingle bed d_{50} of 24 mm	-0.050		0.05-0.16	0.02	1.27-2.26
					0.05	0.80-1.43
	Shingle bed d_{50} of 13 mm / shingle bed d_{50} of 24 mm	-0.030		0.05-0.16	0.02	1.27-2.26
					0.05	0.80-1.43

Table 3.4 Summary of test conditions for 1 in 2 sloping structure

Structural configuration	Bed configuration	Toe water depth, h_t [m]	Crest Freeboard, R_c [m]	Wave Height, H_{m0} [m]	Wave steepness, s_{op} [-]	Wave Period, $T_{m-1,0}$ [s]
Sloping Structure	Impermeable/ shingle bed d_{50} of 13 mm / shingle bed d_{50} of 24 mm	0.060	0.190	0.05-0.16	0.02	1.27-2.26
					0.05	0.80-1.43
	Impermeable/ shingle bed d_{50} of 13 mm / shingle bed d_{50} of 24 mm	0.075	0.245	0.05-0.16	0.02	1.27-2.26
					0.05	0.80-1.43
	Impermeable/ shingle bed d_{50} of 13 mm / shingle bed d_{50} of 24 mm	0.100	0.150	0.05-0.16	0.02	1.27-2.26
					0.05	0.80-1.43
	Impermeable/ shingle bed d_{50} of 13 mm / shingle bed d_{50} of 24 mm	0.150	0.100	0.05-0.16	0.02	1.27-2.26
					0.05	0.80-1.43
	Impermeable/ shingle bed d_{50} of 13 mm / shingle bed d_{50} of 24 mm	0.180	0.140	0.05-0.16	0.02	1.27-2.26
					0.05	0.80-1.43
	Impermeable/ shingle bed d_{50} of 13 mm / shingle bed d_{50} of 24 mm	0.200	0.050	0.05-0.16	0.02	1.27-2.26
					0.05	0.80-1.43
	Shingle bed d_{50} of 13 mm / shingle bed d_{50} of 24 mm	-0.050		0.05-0.16	0.02	1.27-2.26
					0.05	0.80-1.43
	Shingle bed d_{50} of 13 mm / shingle bed d_{50} of 24 mm	-0.030		0.05-0.16	0.02	1.27-2.26
					0.05	0.80-1.43

3.5 Calibration of incident wave conditions

Although the paddle was equipped with an active absorption system to compensate the reflected waves originating from the structure, due to the presence of reflections induced by structure, uncertainties may arise in the determination of incident inshore wave characteristics. For the tested conditions, the reflection coefficient varied from 0.25 to 0.45 at a relatively deep water, near the structure the observed values were in the range from 0.37 up to 0.79. This is the reason why the experiments were also carried out without the structure in place to mitigate the structure induced reflection in the measurements.

To calibrate the inshore wave characteristics, the measurements were also carried out by repeating the experiments without the existence of the structure in the flume (bare flume). It is to note that during calibration tests, the position of wave gauges was exactly as same as real experiments, as shown in Figure 3.4 and 3.5. In the following sub-sections, the measured wave heights and periods derived from the calibration tests are presented and discussed.

3.5.1 Measured wave heights

The significant wave heights at the shallow coastal water usually vary from those observed at the deep oceanic water due to the presence of complex phenomenon such as wave breaking, shoaling, etc. in the nearshore region. The incident wave heights at the toe of the structure as well as at a relatively deep water (near wave paddle) were determined for the tested conditions. The correlation between the H_{m0}at deep water and nearshore region (close to the structure) is illustrated in Figure 3.7 for two different experimental case. As expected, it can be seen from the illustrations that the measured values of wave heights at the structure varies noticeably from those observed at the deep water. For example, it can be noticed from Figure 3.7 (a) that for the same input conditions (h = 0.67 m, h_t = 0.18 m and input wave periods) the measured wave heights at the deep water are reasonably higher compare to those reported at nearshore region.

a.

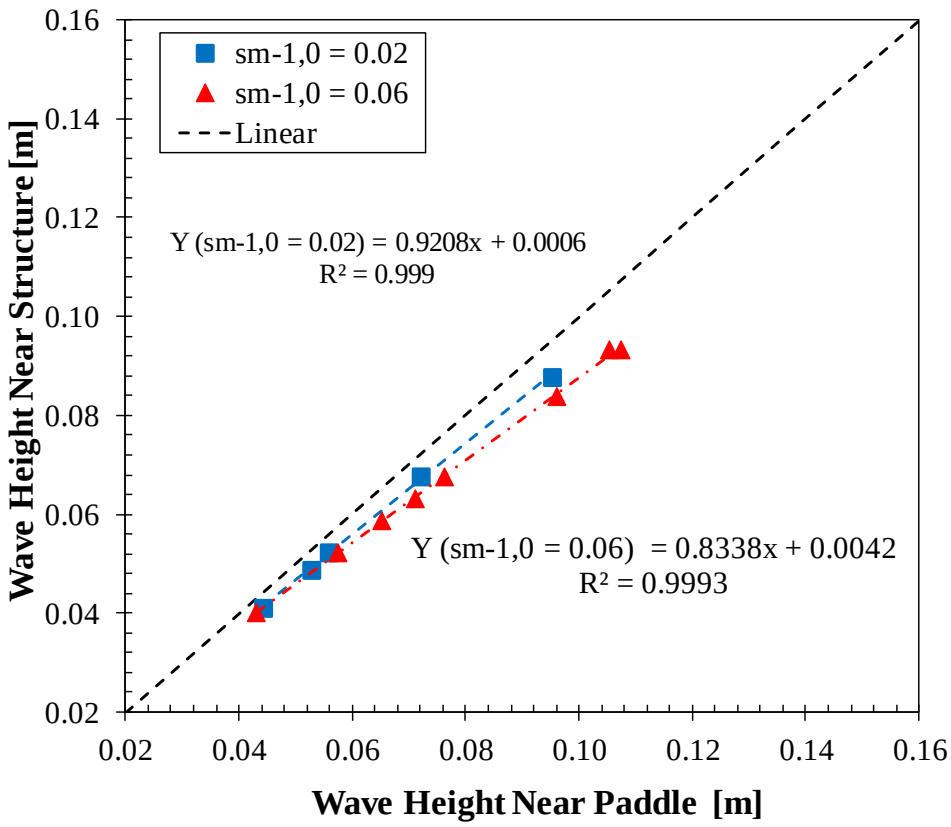

b.

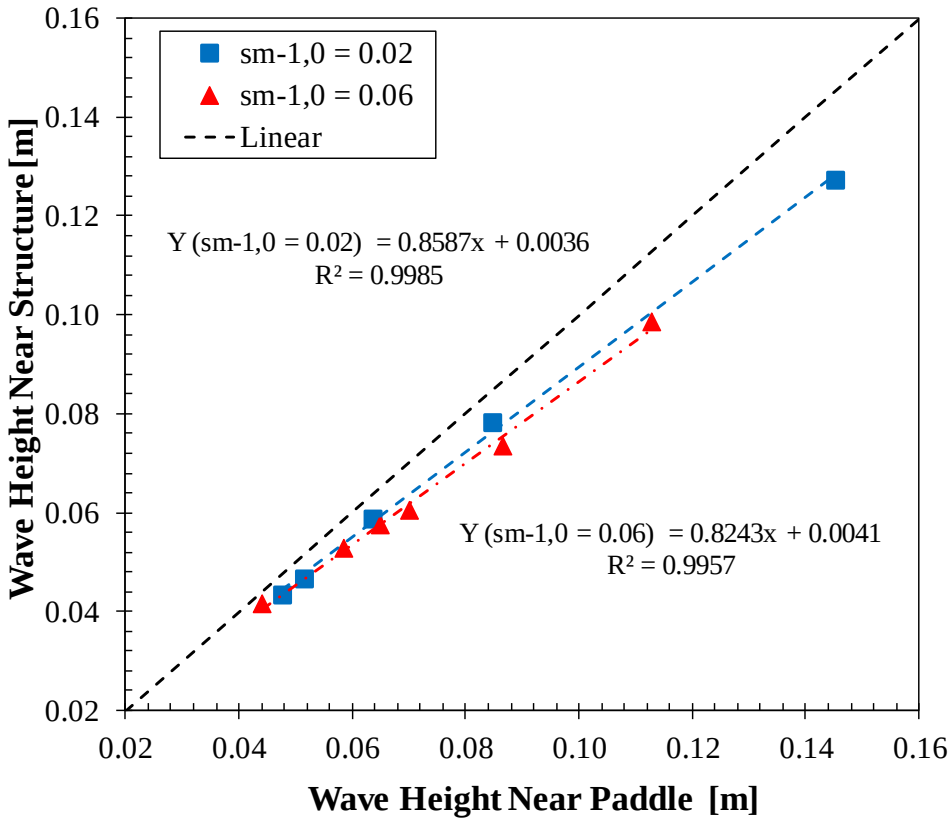

Figure 3.7 The correlation between wave height at deep water and at structure – a) h = 0.67 m and h_t = 0.18 m, and b) h = 0.65 m and h_t = 0.16 m

In the estimation of wave overtopping at breakwaters, the spectral significant wave height (H_{m0}) at the toe of the structure is usually used. On the other hand, the offshore significant wave height calculated from the time series analysis ($H_{1/3}$) is very often applied to predict scour depth at the structure. In this study, both forms of significant wave height that means H_{m0} as well as $H_{1/3}$ have been calculated for the tested conditions. There is no remarkable variation between H_{m0} and $H_{1/3}$ at a relatively deep water, however, at shallow water the significant wave heights calculated from wave spectra analysis (H_{m0}) may differ from those determined from time series analysis ($H_{1/3}$) due to wave breaking phenomenon at depth limited conditions (EurOtop, 2018).

For the tested conditions covered within this study, the variation between H_{m0} and $H_{1/3}$ for each individual wave condition was observed. In Figure 3.8 and Figure 3.9, the observed relationship between measured H_{m0} and $H_{1/3}$ at both deep water (near wave paddle) and shallow water (near the structure) is presented for two different tested water depths. In both cases, it can be clearly seen from the graphs (Figure 3.8 and Figure 3.9) is that there is no significant variation between the measured values of H_{m0} and $H_{1/3}$ for the measurements at deep water conditions. For example, if we look at the data points corresponding to deep water condition in Figure 3.8(a), it is noticeable that both forms of significant wave height give almost the same value. However, for the same input wave parameters, a noticeable variation between H_{m0} and $H_{1/3}$ can be observed for the shallow water depth, see Figure 3.9(b). Similar characteristics of H_{m0} and $H_{1/3}$ were also reported by Salauddin and Van der Meer (2016) for rubble mound armoured breakwaters with 1 in 30 foreshore slope.

a.

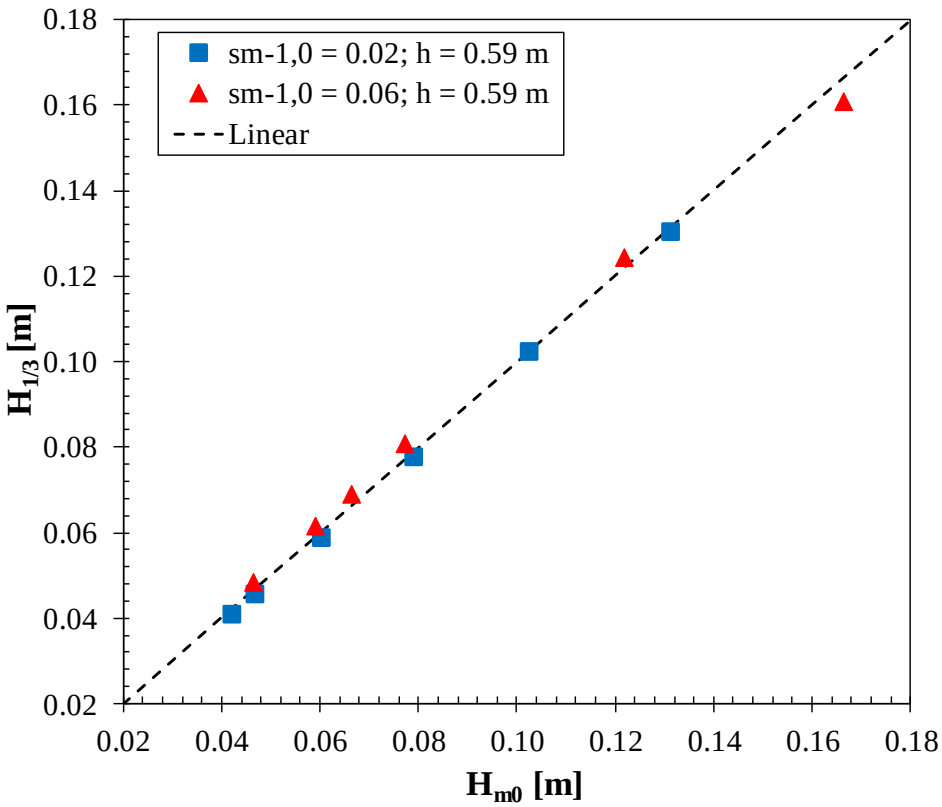

b.

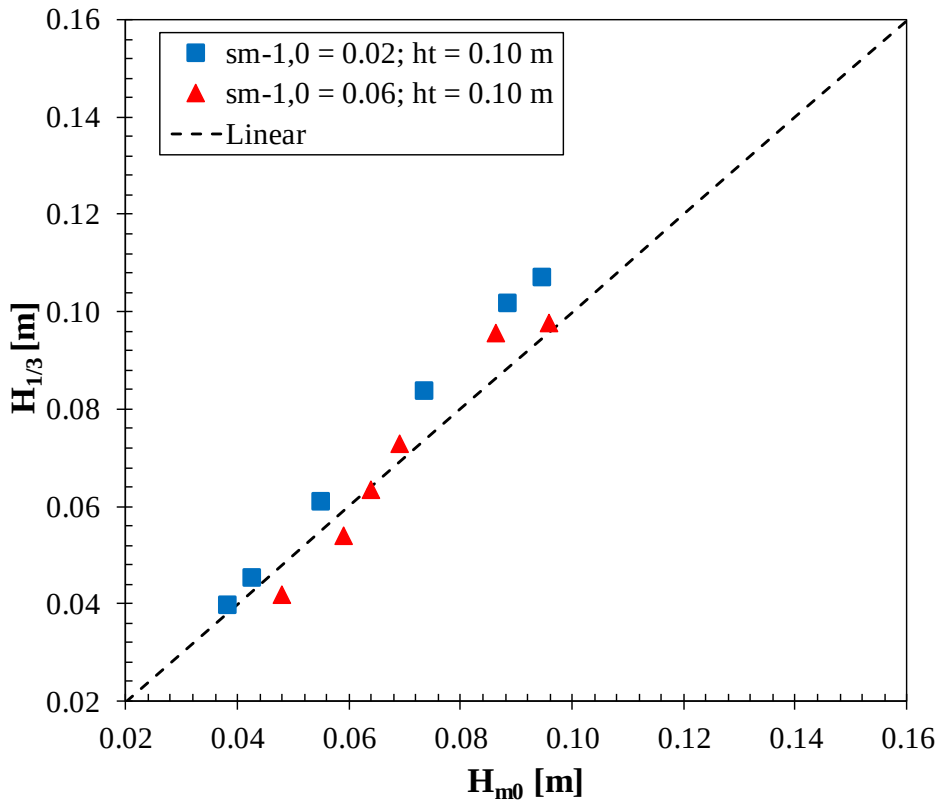

Figure 3.8 The correlation between H_{m0} and $H_{1/3}$ - a) deep water, h = 0.59 m, and b) shallow water, h_t = 0.10 m

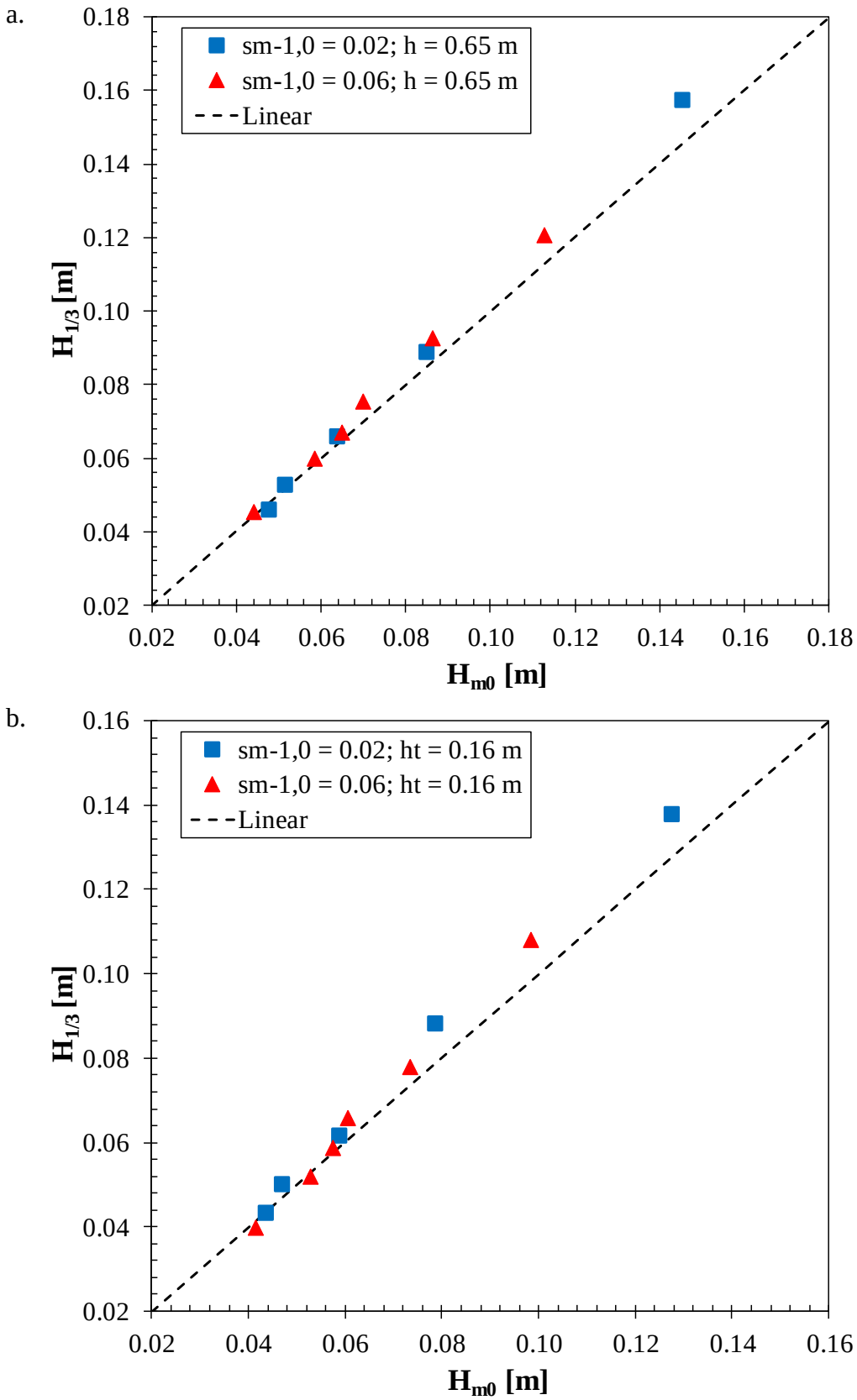

Figure 3.9 The correlation between H_{m0} and $H_{1/3}$ - a) deep water, h = 0.65 m, and b) shallow water, h_t = 0.16 m

3.5.2 Measured wave periods

As described in previous chapter (section 2.2.2) that the three definitions of wave periods are usually employed by the coastal engineers which are T_p, T_m and $T_{m-1,0}$. In this work, all these three forms of wave periods were determined from the gathered dataset for each tested wave condition.

For a certain water depth, the correlation between T_p and $T_{m-1,0}$ at a relatively deep water and near the structure is presented in Figure 3.10. One of the conclusions from the graphs is that the measured peak periods (T_p) were slightly higher than the mean spectral wave periods ($T_{m-1,0}$) for most of the cases as expected. There is, however, the opposite trend of wave periods was observed for few cases at shallow water because of wave breaking phenomenon e.g. tests with relatively short periods, as reported in Figure 3.10.

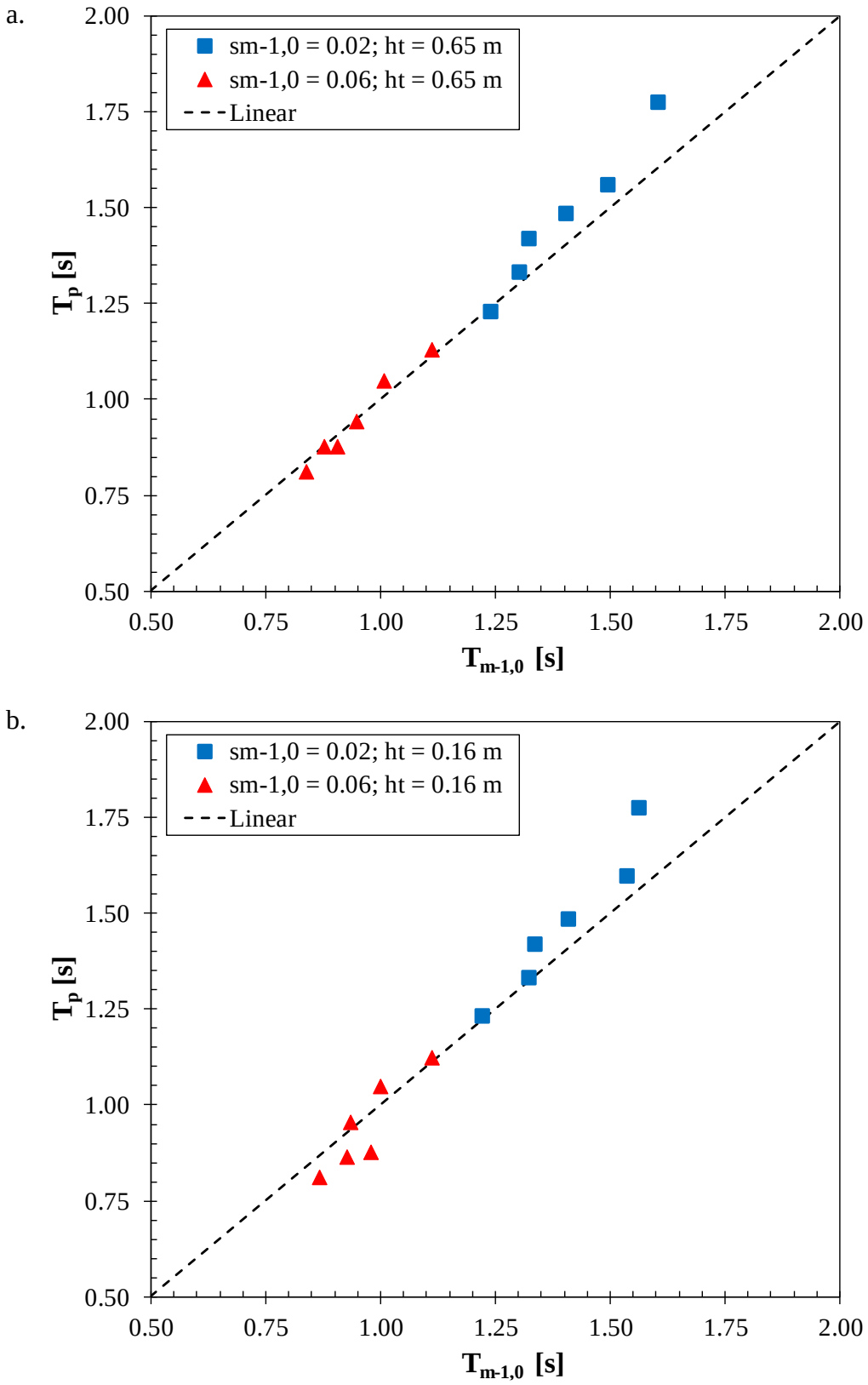

Figure 3.10 The correlation between T_p and $T_{m-1,0}$ - a) deep water, h = 0.65 m, and b) shallow water, h_t = 0.16 m

Further, the variation of measured wave period from the deep water to shallow water was also investigated. Figure 3.11 illustrates a relationship between the measured wave periods close to the structure and at a relatively deep water (near wave paddle) for a tested water depth. It can be concluded from the graph that there is no remarkable variation between the measured incident wave periods at deep water and at the toe of the structure for all three forms of wave periods.

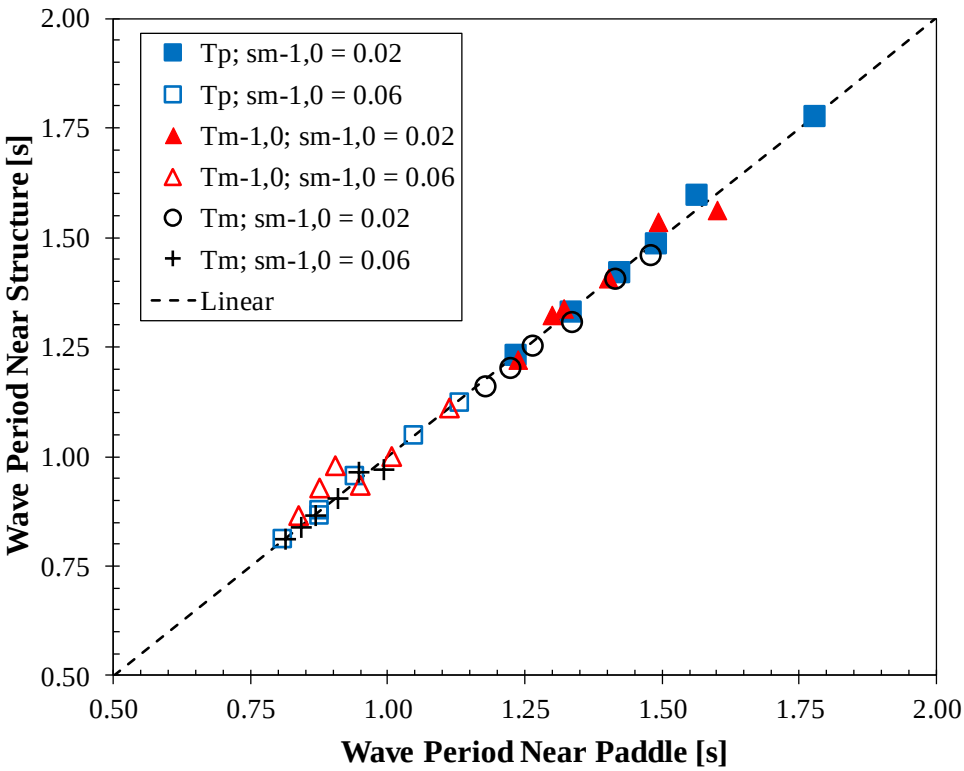

Figure 3.11 Variation of measured wave periods at deep water and shallow water

CHAPTER 4

Results Analysis and Discussion – Plain Vertical Wall

4.1 Synopsis

In the previous chapter, research methodology adopted in this study has been presented. The present chapter presents the results of the analyses of gathered dataset on the wave overtopping and toe scouring at plain vertical walls with permeable foreshores. Section 4.2 examines the distribution of measured wave heights for the conditions covered within this study. The next section discusses the measured wave overtopping characteristics at vertical walls with both impermeable and permeable beds. Then, the resulting scouring characteristics at vertical walls with permeable shingle foreshores are reported. Afterwards, a preliminary prediction guidance to estimate the overtopping at a plain vertical wall on a shingle foreshore is proposed, based on the test results and a comparison with the available prediction methods. The chapter ends with presenting and discussing some of the key findings of this study within the context explained in this chapter.

4.2 Distribution of Measured Wave heights

In general, the incident wave heights at a relatively deep water follow the Rayleigh distribution (EurOtop, 2018). To investigate the resulting distribution of measured wave heights at plain vertical walls for the tested conditions within this study, the distribution of wave heights at a relatively deep water (near wave paddle) are plotted and compared with the Rayleigh distribution in Figure 4.1, for six different tested conditions including both swell ($s_{m-1,0}$ = 0.02) and storm ($s_{m-1,0}$ = 0.06) wave conditions. In graphs, H is the individual wave height, H_m is the mean wave height and the dashed line is the estimated Rayleigh distribution for a tested condition.

a.

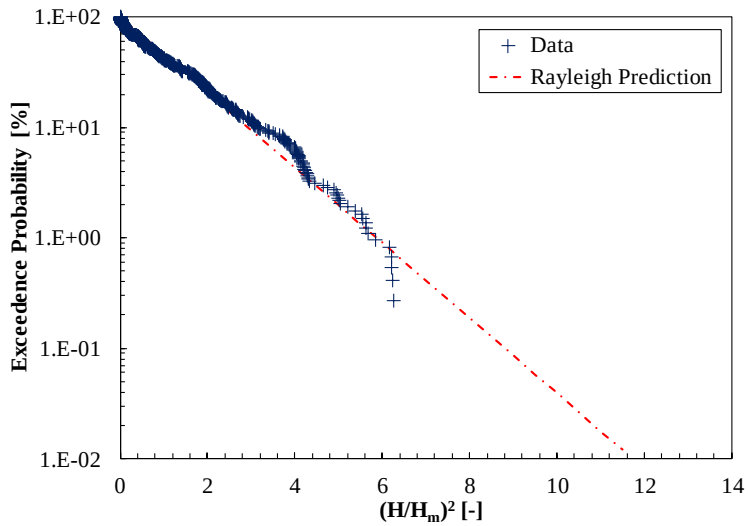
Data
Rayleigh Prediction
Exceedence Probability [%]
1.E+02
1.E+01
1.E+00
1.E-01
1.E-02
0
2
4
6
8
10
12
14
(H/Hm)² [-]

b.

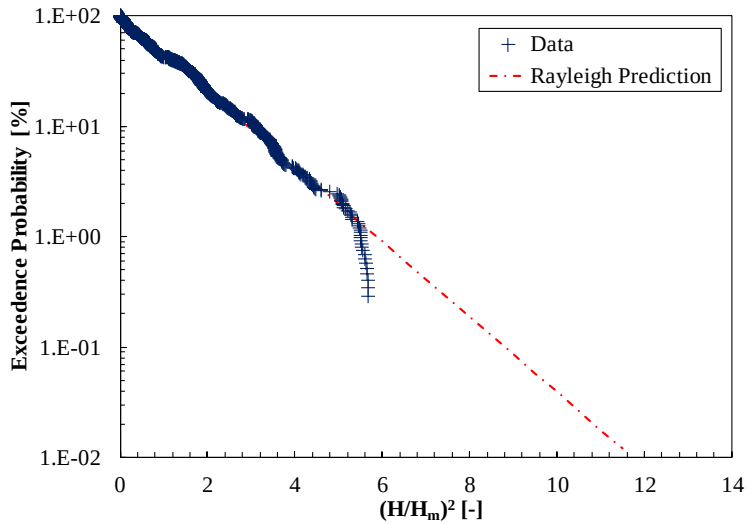
Data
Rayleigh Prediction
Exceedence Probability [%]
1.E+02
1.E+01
1.E+00
1.E-01
1.E-02
0
2
4
6
8
10
12
14
(H/Hm)² [-]

c.

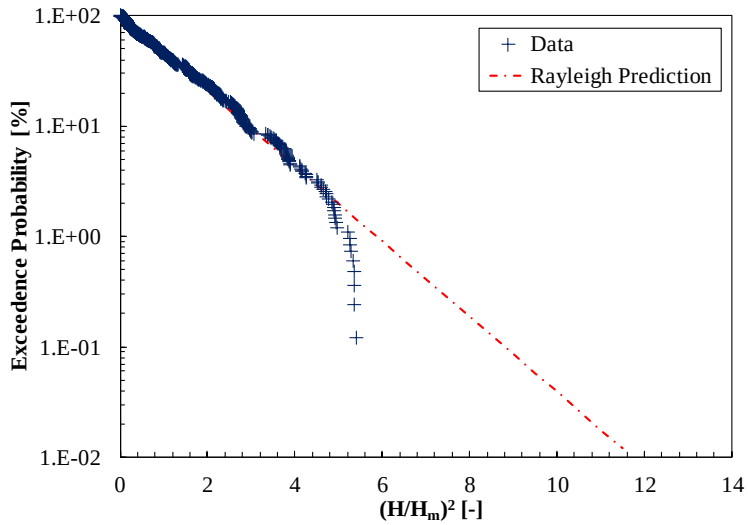
Data
Rayleigh Prediction
Exceedence Probability [%]
1.E+02
1.E+01
1.E+00
1.E-01
1.E-02
0
2
4
6
8
10
12
14
(H/Hm)² [-]

d.

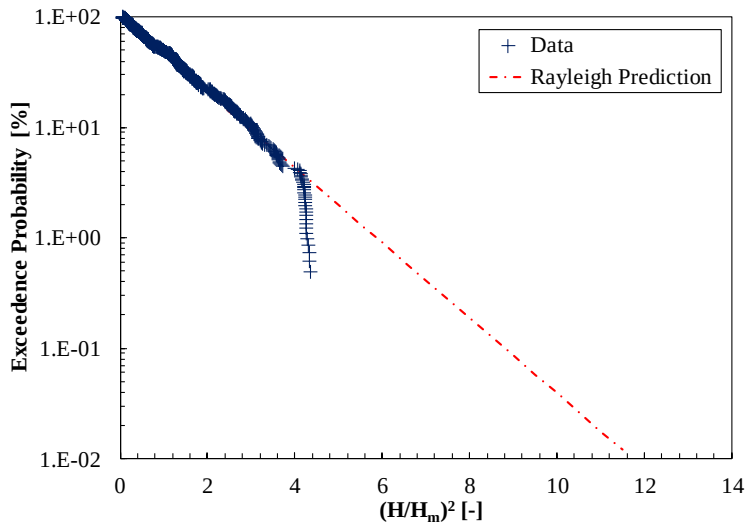

e.

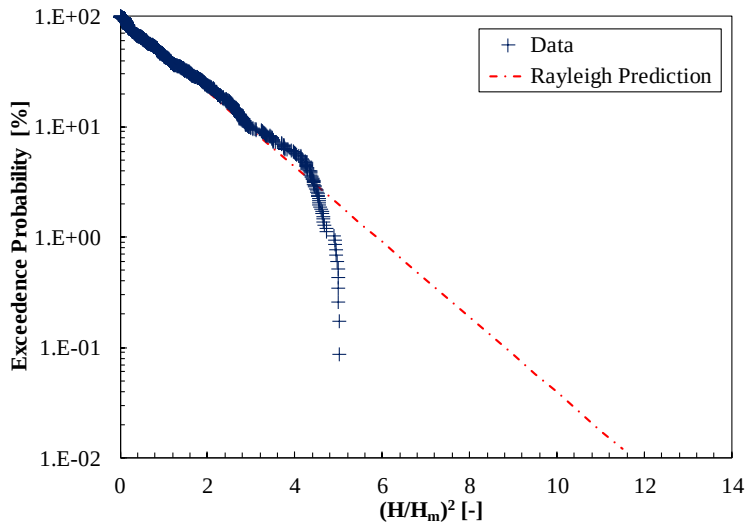

f.

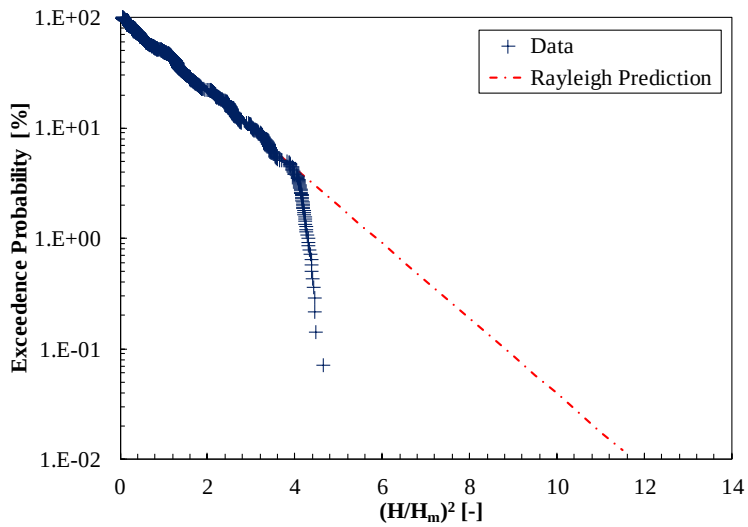

Figure 4.1 Comparison of the distribution of wave heights with the Rayleigh predictions (vertical wall) - a) $s_{m-1,0}$ = 0.02, H_{m0} = 0.06 m, h_t = 0.16 m b) $s_{m-1,0}$ = 0.06, H_{m0} = 0.056 m, h_t = 0.19 m c) $s_{m-1,0}$ = 0.02, H_{m0} = 0.070 m, h_t = 0.10 m d) $s_{m-1,0}$ = 0.06, H_{m0} = 0.010 m, h_t = 0.18 m e) $s_{m-1,0}$ = 0.02, H_{m0} = 0.074 m, h_t = 0.06 m, and f) $s_{m-1,0}$ = 0.06, H_{m0} = 0.010 m, h_t = 0.16 m.

It is certainly noticeable from graphs that the measured wave heights overall follow the predicted Rayleigh distribution for both low ($s_{m-1,0}$ = 0.02) and high wave steepness ($s_{m-1,0}$ = 0.06). Nevertheless, the test results demonstrate that the wave heights for relatively high waves were measured slightly lower compared to those predicted by Rayleigh distribution. For example, if we consider the resulting distribution of measured wave heights as presented in Figure 4.1(b), it can be noticed that the data overall follow the general trend of the predicted Rayleigh distribution with in some cases for the larger waves being lower than the estimated line. These characteristics of the larger waves in a wave sequence may be occurred due to the presence of wave breaking phenomenon near the wave paddle under depth-limited conditions.

4.3 Wave Overtopping

The wave overtopping investigations were benchmarked with an impermeable foreshore in front of the vertical seawall, subjected to both non-impulsive and impulsive conditions. In the following sections, the resulting overtopping characteristics at vertical walls with both impermeable and permeable foreshores are presented.

4.3.1 Mean overtopping discharge

4.3.1.1 Impulsive wave conditions

The mean overtopping rate for a plain vertical wall on an impermeable foreshore (reference case), are compared with the empirical predictions prescribed by EurOtop (2018), see Figure 4.2 for impulsive wave attack. In Figure 4.2, the dashed lines represent the prediction lines (Equations 2.16 – 2.17) of EurOtop (2018) considering an impermeable bed in front of the vertical wall, subjected to the impulsive wave attack. Figure 4.2 shows that the results of this study showed an overall good agreement with the empirical predictions for the impulsive conditions covered within this study.

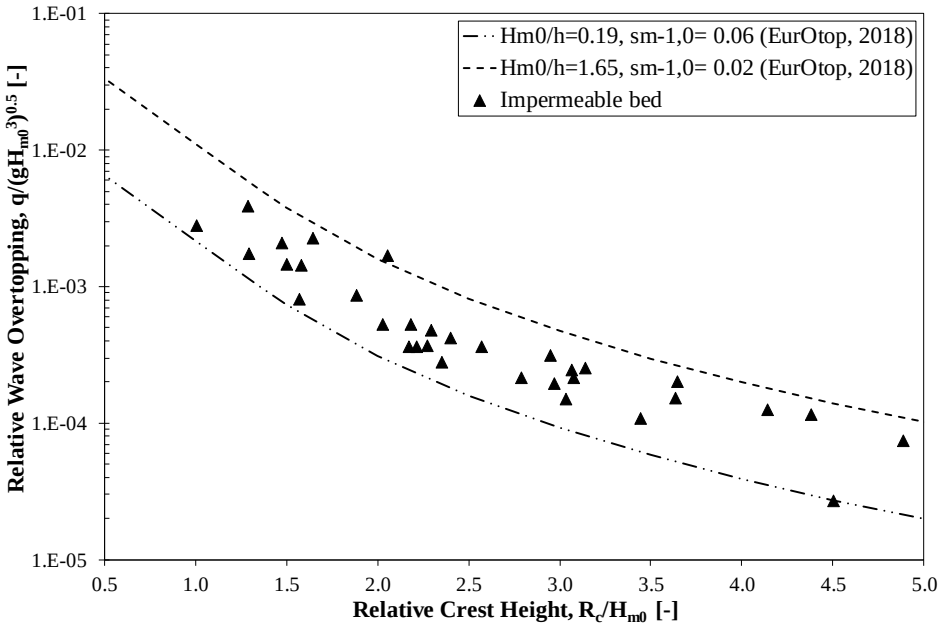

Figure 4.2 Mean overtopping discharge at a plain vertical wall on an impermeable foreshore, subjected to impulsive conditions

In Figure 4.3, the resulting mean overtopping discharges at a plain vertical wall on shingle beds are compared with the empirical formulae (Equations 2.16 – 2.17) proposed by EurOtop (2018) as well as with overtopping characteristics observed in reference case (solid bed) under impulsive wave attack. For the impulsive conditions tested on the shingle beaches, a noticeable reduction on the mean overtopping rate is observed compared to the test results on an impermeable bed. When comparing the two beach foreshore configurations, it was observed that the larger shingle bed of d_{50} of 24 mm, gave a greater overall reduction in overtopping discharge, as indicated by the dashed trend lines.

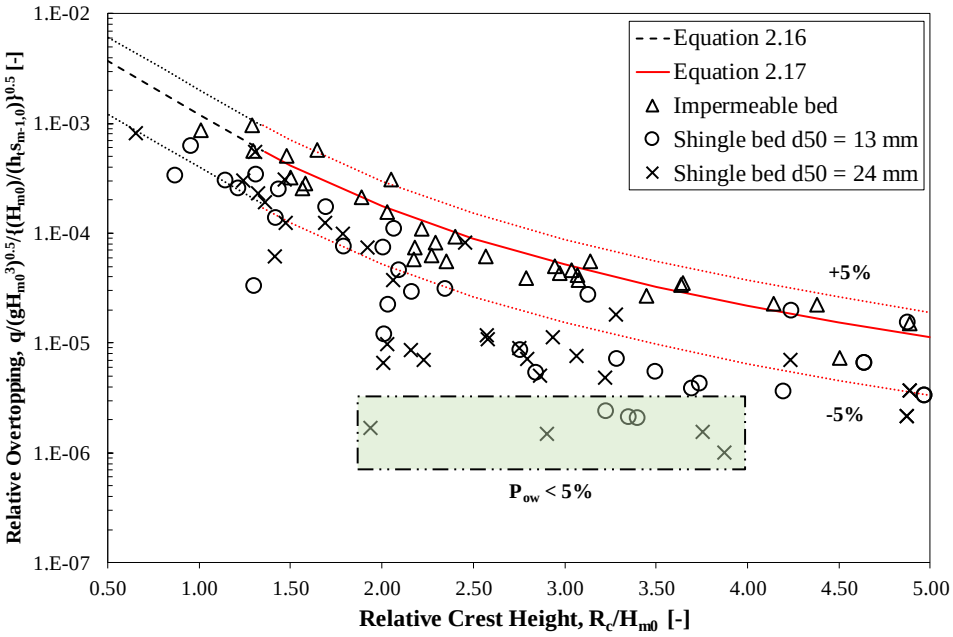

Figure 4.3 Mean overtopping discharge at plain vertical walls with both permeable and impermeable foreshores, subjected to impulsive conditions

It is noticeable from Figure 4.3 is that experiments with shingle foreshores give more scatter compared to the impermeable bed configurations, subjected to impulsive wave attack. The higher scatter values of relative overtopping discharge are observed for the data points corresponding to low overtopping waves (less than 5%), see Figure 4.3. These are often associated with a very few number of overtopped waves, leading to an uncertainty in the measurement of wave overtopping. Similar scatter characteristics of wave overtopping for experiments with less than 5% overtopping waves (P_{ow}), were also reported by Zanuttigh et al., 2013 in the determination of wave by wave overtopping characteristics for smooth slopes and rubble mound breakwaters.

Furthermore, a 'best-fit' analysis was performed on the measured overtopping data to observe the reduction factor by introducing mobile beds and to propose the empirical overtopping discharge formula for the estimation of mean overtopping at vertical seawalls on a shingle foreshore, see Figure 4.4. Following the approach suggested by EurOtop (2018), for the higher freeboards with impulsive overtopping, average overtopping discharges at vertical walls on the mobile beds are described by a power law function.

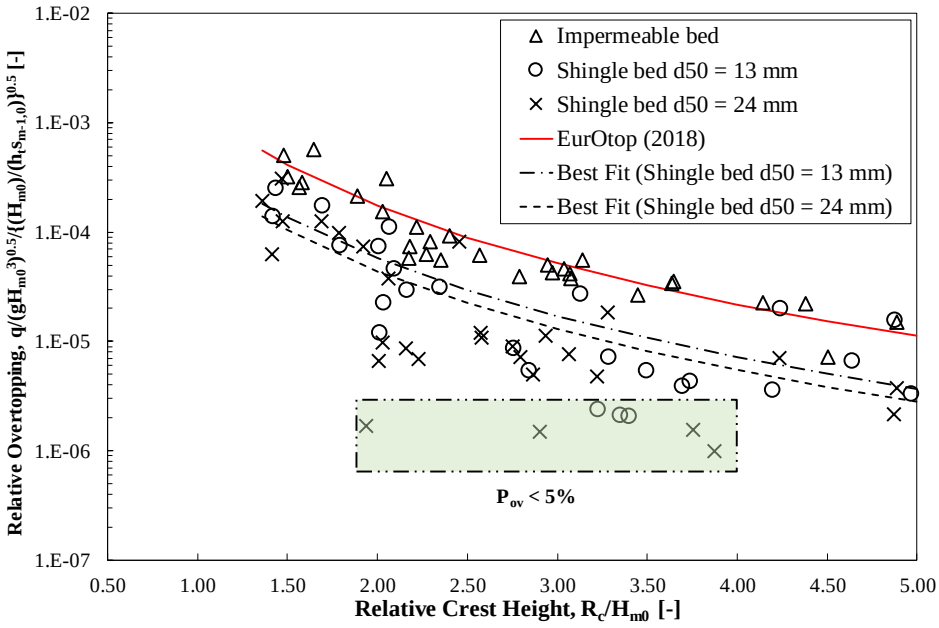

Figure 4.4 Best-fit analysis on the resulting mean overtopping discharge at plain vertical walls under impulsive wave conditions

Based on the 'best-fit' analysis on the tested conditions, the overtopping rate is reduced by an around factor of 3 for shingle bed of d_{50} of 13 mm (Equation 4.1) and approximate factor of 4 for shingle bed of d_{50} of 24 mm (Equation 4.2), when compared to the empirical prediction of EurOtop (2018) for solid impermeable bed (Equation 2.17). It should be noted that for lower relative freeboards (R_c/H_{m0}<1.35) less data was collected for impulsive conditions, thus it is not possible to give a defined trend through the best-fit analysis.

The best-fit trend line for shingle bed of d_{50} = 13 mm (Impulsive conditions),

$$\frac{q}{\sqrt{gH_{m0}^3}} = 0.00046\,\left(\frac{H_{mo}}{h_t s_{m-1.0}}\right)^{0.5}\left(\frac{R_c}{H_{mo}}\right)^{-3.0} \qquad 1.35 \leq \frac{R_c}{H_{m0}} \leq 5.0 \qquad (4.1)$$

with a corresponding least square regression, R^2 = 0.63

The best-fit trend line for shingle bed of d_{50} = 24 mm (Impulsive conditions),

$$\frac{q}{\sqrt{gH_{m0}^3}} = 0.00035\,\left(\frac{H_{mo}}{h_t s_{m-1.0}}\right)^{0.5}\left(\frac{R_c}{H_{mo}}\right)^{-3.0} \qquad 1.35 \leq \frac{R_c}{H_{m0}} \leq 5.0 \qquad (4.2)$$

with a corresponding least square regression, R^2 = 0.54

Alongside the R^2 best-fitted analysis, the root mean square error (rmse) analysis has been carried out in this study, to observe the reliability of the best-fitted equations. This has been performed by adopting the method of Owen (1980) and Victor et al. 2012, with the use of measured and predicted values of mean overtopping discharge, see Equation 4.3.

$$\text{rmse} = \sqrt{\frac{1}{N_{test}} \sum_{n=1}^{N_{test}} \left[\log\left(\frac{q_{measured}}{\sqrt{gH_{m0}^3}} \right)_n - \log\left(\frac{q_{predicted}}{\sqrt{gH_{m0}^3}} \right)_n \right]^2} \tag{4.3}$$

in which, N_{test} is defined as the number of experimental results used to derive an equation. The smaller rmse-value means the better prediction formula which fits the specific dataset well. The rmse value demonstrates the standard deviation of the measured values about the predicted mean overtopping rates on a log-log scale.

The 90% reliability interval is expressed in Equation 4.4 by assuming that the logarithms of the measured non-dimensional mean overtopping rates are normally distributed about the logarithms of the predicted values. The upper and lower bound of the 90% prediction interval are expressed in Equation 4.5.

$$\log\left(\frac{q_{measured}}{\sqrt{gH_{m0}^3}} \right)_{90\%} = \log\left(\frac{q_{predicted}}{\sqrt{gH_{m0}^3}} \right)_{90\%} \pm 1.645\, rmse \tag{4.4}$$

$$\Rightarrow \begin{cases} \left(\frac{q_{measured}}{\sqrt{gH_{m0}^3}} \right)_{90\%,upper} = \left(\frac{q_{predicted}}{\sqrt{gH_{m0}^3}} \right) 10^{1.645 rmse} \\ \left(\frac{q_{measured}}{\sqrt{gH_{m0}^3}} \right)_{90\%,lower} = \left(\frac{q_{predicted}}{\sqrt{gH_{m0}^3}} \right) 10^{-1.645 rmse} \end{cases} \tag{4.5}$$

Furthermore, Bias analysis has been also carried out by comparing predicted values of proposed equations with the measurements, see Equation 4.6. It is to note that Bias value indicates the mean of the absolute error resulting from the equations. As such the negative Bias values indicate that the predictions by using the specific equation are under estimated.

$$\text{Bias} = \frac{1}{N_{test}} \sum_{n=1}^{N_{test}} \left[\log\left(\frac{q_{predicted}}{\sqrt{gH_{m0}^3}} \right)_n - \log\left(\frac{q_{measured}}{\sqrt{gH_{m0}^3}} \right)_n \right] \tag{4.6}$$

The error measures of proposed equations (4.1 and 4.2) for the prediction of overtopping rates at vertical walls with permeable foreshores are presented in Table 4.1. Also, the error measures of empirical line of EurOtop (2018) within the context of impermeable slope are shown in Table 4.1. The resulting data points, which correspond to the impermeable bed, show an overall very good agreement (a rmse value of 0.11 and Bias value of 0.028) with the predictive method of EurOtop (2018) as observed in Table 4.1.

Table 4.1

The error measures of proposed equations for the prediction of overtopping rates at vertical walls with permeable foreshores (impulsive conditions)

Error Indicator	Equation 2.17 (Impermeable)	Equation 4.1 (d_{50} of 13 mm)	Equation 4.2 (d_{50} of 24 mm)
rmse	0.11	0.25	0.28
Bias	0.028	0.056	0.118

For the tested impulsive conditions, the rmse value based on the measured and predicted values of average overtopping rates was observed 0.25 and 0.28 for shingle bed of d_{50} = 13 mm (Equation 4.1) and d_{50} = 24 mm (Equation 4.2) respectively. From Table 4.1, it can be also reported that the estimated Bias values for the proposed equations are also reasonable, 0.056 and 0.118 for Equation 4.1 and 4.2 respectively. These error characteristics of the proposed equations indicate overall a good correlation of measured values with the new prediction formulae. It is important to note that the scatter data points which are the experiments with relatively low overtopping (less than 5%) as indicated in Figure 4.4, are not considered in the error analysis of revised equations.

4.3.1.2 Non-impulsive wave conditions

The measured mean overtopping rate at a plain vertical wall with an impermeable bed under non-impulsive conditions are plotted in Figure 4.5. Results are then compared with the empirical prediction of EurOtop (2018), indicating by a dashed line in Figure 4.5. For the tested non-impulsive conditions, the graph demonstrates that the measured data overall follow the trend of the empirical prediction line of EurOtop (2018).

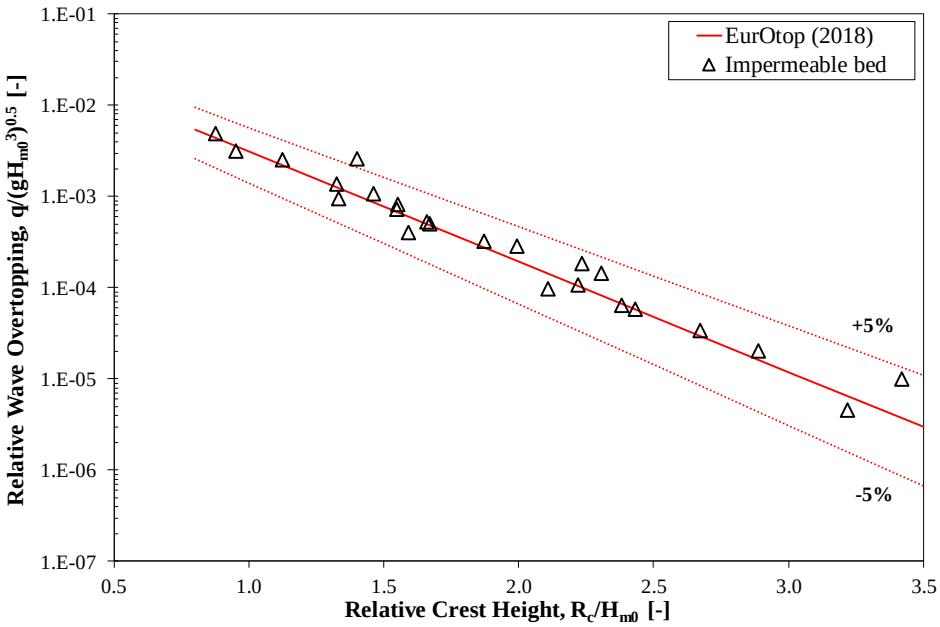

Figure 4.5 Mean overtopping discharge at a plain vertical wall on an impermeable foreshore, subjected to non-impulsive conditions

Figure 4.6 illustrates a comparison between the mean overtopping discharge for the shingle bed and impermeable solid bed configurations, under non-impulsive wave conditions. The empirical expression (Equation 2.15) of new overtopping manual (EurOtop, 2018) is presented by a solid line. The data points corresponding to solid impermeable bed show an overall good agreement with the predictive method of EurOtop (2018), as indicated by dotted lines in Figure 4.6 (R^2 = 0.96). For the non-impulsive test conditions on shingle beaches, the results of this study demonstrate that permeable shingle foreshore provides a reduction in the overtopping discharge at vertical seawalls, compared to an impermeable beach configuration.

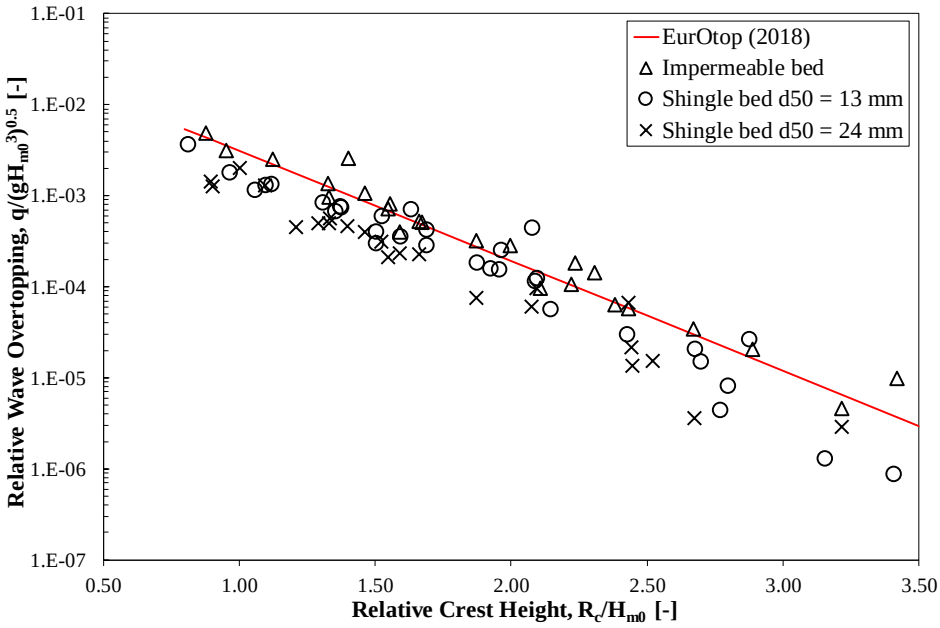

Figure 4.6 Mean overtopping discharge at plain vertical walls for both permeable and impermeable foreshores, subjected to non-impulsive conditions

For relatively high freeboards (R_c/H_{m0} > 3.0), Figure 4.6 shows that under non-impulsive conditions, introduction of larger shingle beach (d_{50} of 24 mm) shortens the overtopping discharge remarkably compared to a solid impermeable beach. However, the data points corresponding to relatively high toe water depths (low freeboards) indicate that there is no remarkable difference between mobile and solid beach configurations compared to those reported for higher relative freeboards. This may be happened because when waves are small compared to water depth, they do not break onto the structure. Thus, the energy dissipation by breaking onto the permeable foreshore is not really happened for non-breaking wave conditions with low freeboards.

Furthermore, a 'best-fit' analysis was carried out on the measured values under non-impulsive conditions for the plain vertical walls with permeable shingle foreshores, see Figure 4.7. When compared to the empirical prediction of EurOtop (2018) for impermeable beach configuration (Equation 2.15), it appears that under non-impulsive conditions mean overtopping discharge is reduced by approximately a factor of 1.5 for shingle bed of d_{50} of 13 mm (Equation 4.7) and about a factor of 2 for shingle bed of d_{50} of 24

mm (Equation 4.8). It should be noted that the scatter data points corresponding to relative freeboards higher than 3.5 are not considered in the 'best-fit' analysis.

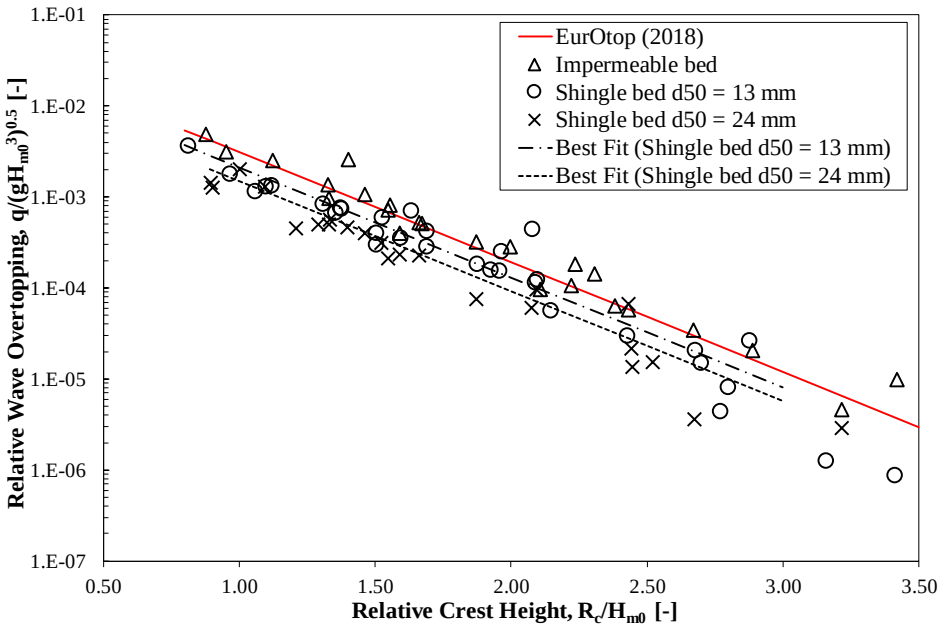

Figure 4.7 Best-fit analysis on the resulting mean overtopping discharge at plain vertical walls under non-impulsive wave conditions

The best-fit trend line for shingle bed of d_{50} = 13 mm (non-impulsive),

$$\frac{q}{\sqrt{gH_{m0}^3}} = 0.033 \exp\left(-2.77 \frac{R_c}{H_{m0}}\right) \tag{4.7}$$

with a corresponding least square regression, $R^2 = 0.92$

The best-fit trend line for shingle bed of d_{50} = 24 mm (non-impulsive),

$$\frac{q}{\sqrt{gH_{m0}^3}} = 0.024 \exp\left(-2.91 \frac{R_c}{H_{m0}}\right) \tag{4.8}$$

with a corresponding least square regression, $R^2 = 0.94$

Furthermore, for the quantitative evaluation of the reliability of the revised equations for shingle foreshores, statistical indicators e.g. rmse and Bias were calculated using the definitions as presented in Equations 4.3-4.6. The error measures of proposed equations (Equation 4.6 and 4.7) for the prediction of overtopping rates at vertical walls with permeable foreshores under non-impulsive wave conditions are reported in Table 4.2. The reliability of the existing empirical formulation (Equation 2.15) of EurOtop (2018) for the prediction of mean overtopping rate considering an impermeable foreshore configuration is also shown in Table 4.2. As expected, it is seen from Table 4.2 that the prediction line of EurOtop (2018) show a strong correlation with the measurements on the impermeable slope by providing relatively lower statistical errors e.g. Bias and rmse values

Table 4.2

The error measures of proposed equations for the prediction of overtopping rates at vertical walls with permeable foreshores (non-impulsive conditions)

Error Indicator	Equation 2.15 (Impermeable)	Equation 4.7 (d_{50} of 13 mm)	Equation 4.8 (d_{50} of 24 mm)
rmse	0.11	0.10	0.11
Bias	-0.023	0.013	-0.004

As seen in Table 4.2, the rmse value was reported only 0.10 and 0.11 for shingle bed of d_{50} = 13 mm and d_{50} = 24 mm respectively, indicates that the predictions with the use of new equations agree well with the measurements. The observed Bias errors for the revised equations were also lower i.e; 0.013 for Equation 4.7 and - 0.004 for Equation 4.8, shows that the average absolute error resulting from the revised equations are also reasonable. Based on the reasonably lower rmse and Bias values of the proposed equations, it can be reported that the revised empirical formulations (Equation 4.7 and 4.8) for shingle foreshores provide a good agreement with the measurements of this study.

4.3.2 Mean overtopped sediment discharge

For the experiments with the mobile shingle beds, alongside the mass of overtopped water, the mass of overtopped sediment was simultaneously measured to determine the average overtopping sediment discharge. The quoted specific gravity of 1.40 was used to determine the volume of overtopped sediments from collected dry weight of sediments.

In Figure 4.8, the measured average overtopping rate of sediment and water at a plain vertical wall on a shingle foreshore is plotted against the relative freeboard of the structure, subjected to impulsive wave conditions. It is to note that the overtopping of sediment was not observed for the tested conditions on non-impacting and impacting waves $(h_t^2/(H_{m0}L_{m-1,0}) > 0.03)$. It is noticeable that overall the amount of the overtopped sediment was considerably lower compared to the amount of the overtopped water.

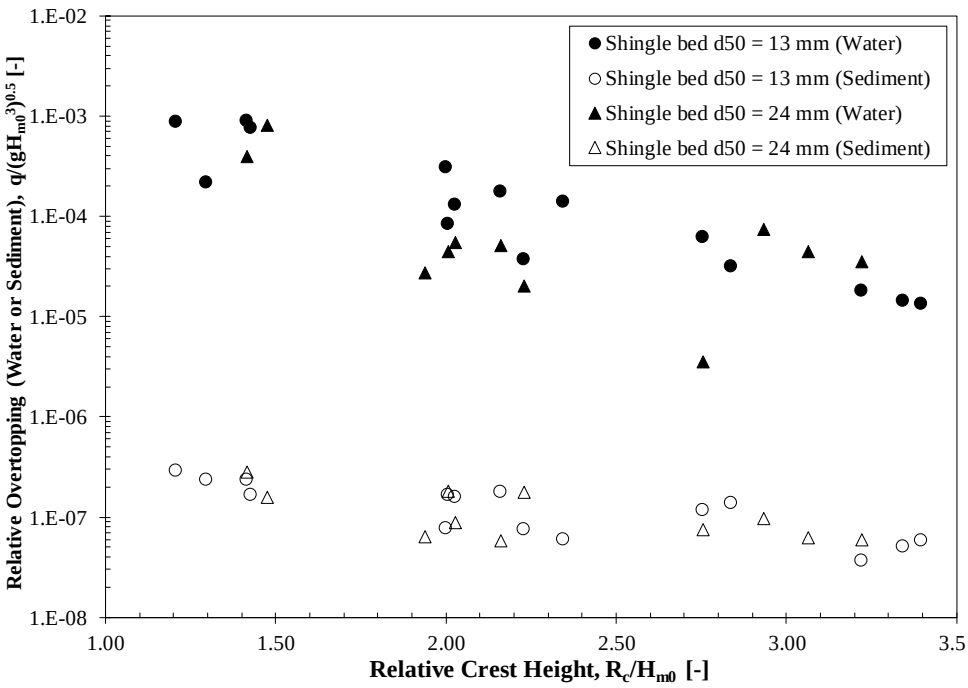

Figure 4.8 Mean overtopping discharge of sediment and water at a plain vertical wall with a shingle foreshore

For the quantitative evaluation of the proportion of overtopped sediment, the ratio of volume of the overtopped sediment to the volume of the overtopped water is plotted against the relative freeboard of the structure in Figure 4.9. Overall, the data points in Figure 4.9 demonstrate that measured volume of sediment passing the crest of the structure was maximum around 0.5% of the volume of overtopped water. For instance, if we look at relative freeboard of 2.01 for shingle bed of 24 mm more closely, it is noticeable that the amount of the overtopped sediment is 0.41% of the overtopped water.

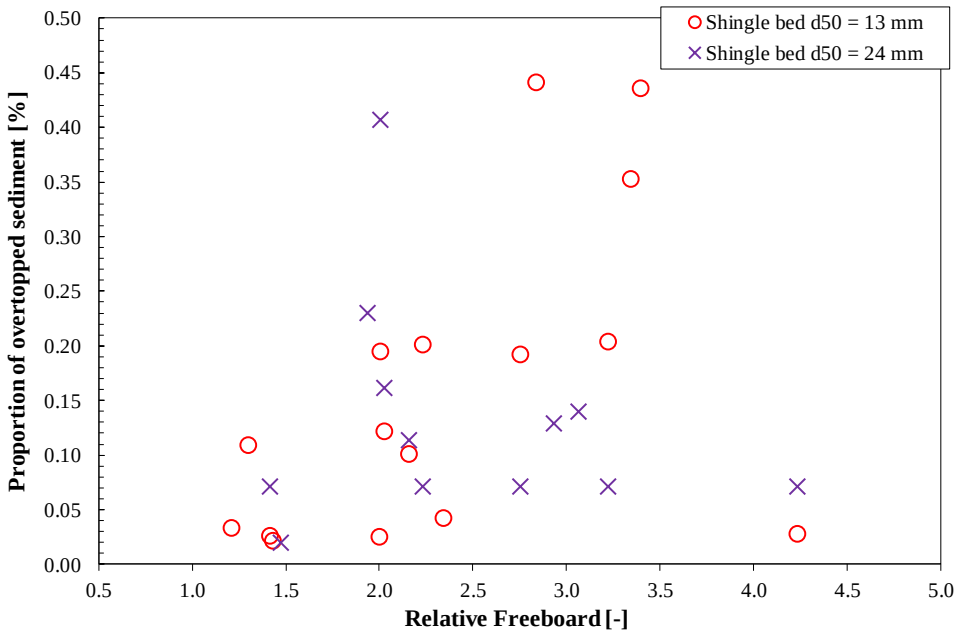

Figure 4.9 Proportion of overtopped sediment at a plain vertical wall with a shingle foreshore

4.3.3 Proportion of overtopping waves (P_{ov})

Figure 4.10 shows the variation of the measured proportion of overtopping waves at vertical walls with relative freeboard of the structure. The results from the benchmark tests (impermeable foreshore) are plotted in Figure 4.10, as the reference case. The percentage of waves overtopping predicted with the use of new empirical formulae (Equations 2.35 - 2.36) and plotted in Figure 4.10 by six different lines showing six values of impulsiveness parameter $(h_t^2/(H_{m0}L_{m-1,0}))$. In Figure 4.10, the solid black line $(h_t^2/(\mathrm{H_{m0}}L_{m-1,0}) = 0.24)$ represents the estimated proportion of overtopping

waves for non-impulsive wave conditions reported by EurOtop (2018) for plain vertical walls.

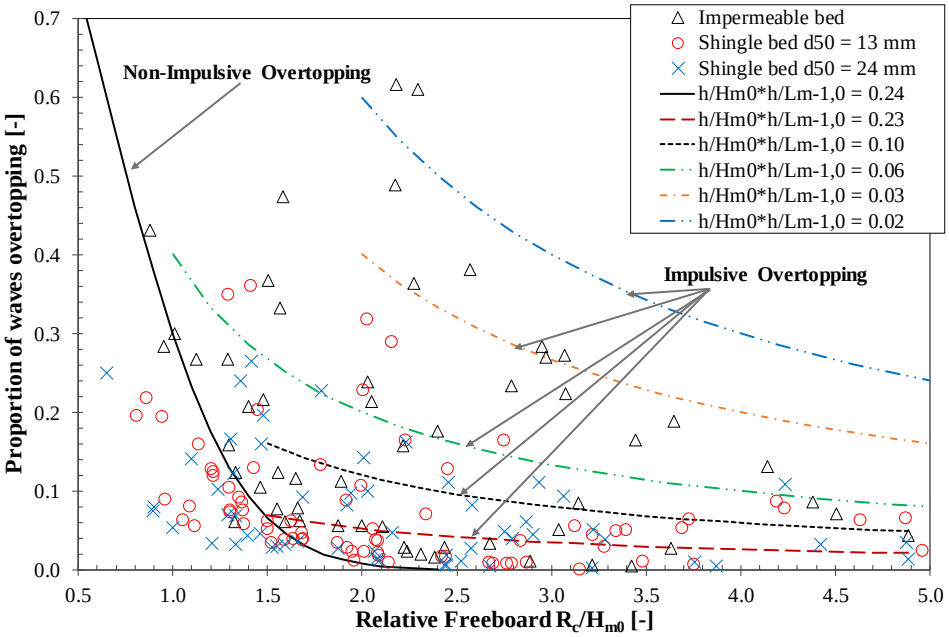

Figure 4.10 Proportion of waves overtopping at plain vertical walls for both solid and shingle beach configurations, with respect to impulsiveness parameter

In Figure 4.10, it is seen that for the impermeable foreshore configuration, the measured data points with respect to different impulsiveness parameter overall follow the trend of that reported by EurOtop (2018), subjected to both impulsive and non-impulsiveness conditions. It can be also reported that the as expected the small values of the impulsiveness parameter provide higher number of overtopping waves.

Furthermore, Figure 4.11 shows a direct comparison between the measured proportion of overtopping waves at vertical walls for both solid and shingle beds with the empirical predictions reported by EurOtop (2018). For the tested conditions on the impermeable foreshore, the measured data points overall show a good agreement with the empirical predictions that described by EurOtop (2018). However, for the shingle foreshore configurations, it is observed that the measured values are somewhat lower than the predicted values of EurOtop (2018).

It is also noticeable from Figure 4.11 that the probability of overtopping decreases with the increase of sediment sizes, indicating that the porosity of the shingle beds has an influence on the proportion of overtopping waves. For instance, the data points corresponding to experiments with shingle beach of d_{50} of 24 mm give larger reduction in overtopping proportions compared to data points of shingle beach of d_{50} of 13 mm.

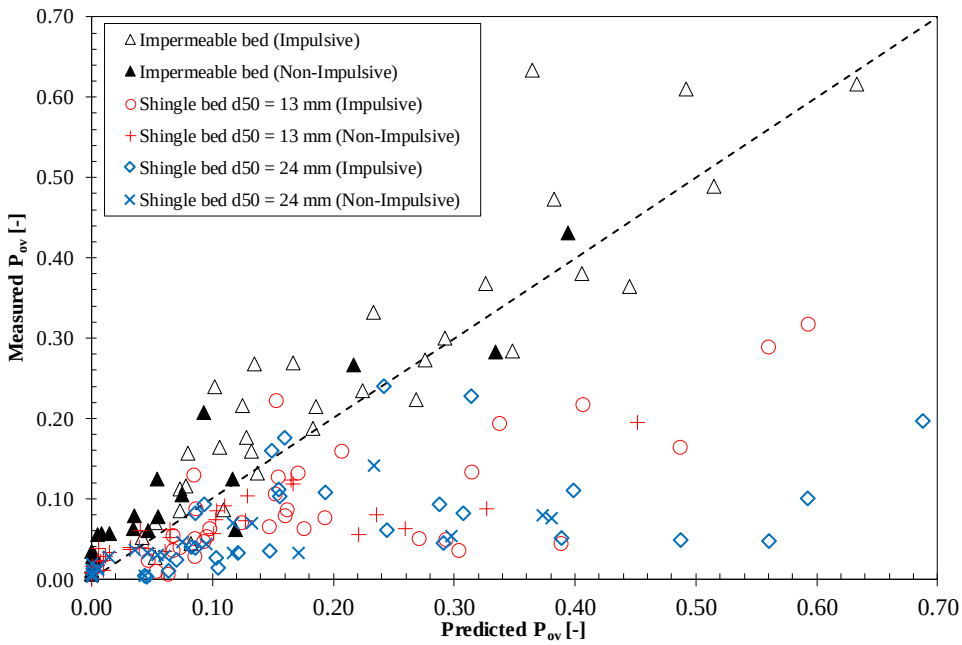

Figure 4.11 A comparison between measured and predicted proportion of overtopping waves at plain vertical walls

4.3.4 Maximum individual overtopping volumes (V_{max})

In Figure 4.12, the measured maximum individual overtopping wave volumes (V_{max}) at plain vertical walls on a solid impermeable bed are compared with those predicted values using empirical prediction (Equation 2.30) proposed by EurOtop (2018). The graph also compares the measured maximum individual overtopping wave volumes at plain vertical walls on the shingle beds with the empirical predictions suggested by EurOtop (2018) for both impulsive and non-impulsive conditions. For both shingle and solid beds, the maximum individual overtopping wave volumes were predicted using the empirical formula (Equation 2.30) for vertical walls given by new overtopping manual EurOtop (2018).

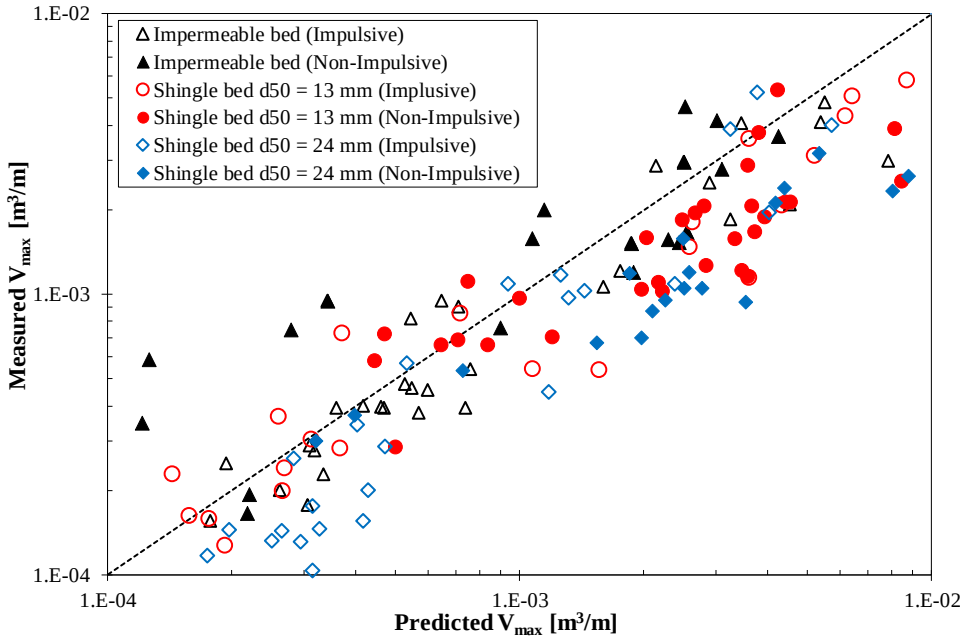

Figure 4.12 Comparison of measured and predicted individual overtopping volumes at plain vertical walls on impermeable and shingle foreshores

Overall, the data points corresponding to impermeable beach demonstrate that measured maximum individual volume, V_{max} correlates reasonably well (within a factor 2) with the predicted maximum individual overtopping wave volumes under both impulsive and non-impulsive wave conditions. In general, the maximum individual wave by wave volumes for permeable foreshores were found somewhat lower than the predicted values by EurOtop (2018). Nevertheless, due to the scatter characteristics of the data points, it can be concluded that there is no significant difference in the estimation of wave by wave overtopping volumes for impermeable and permeable shingle foreshore in front of a plain vertical seawall.

4.4 Toe Scouring

4.4.1 Relationship between development of scour depth and storm duration

For this study, the initial bed profile was 1:20 plain permeable shingle beach. As noted previously, tests were performed for 1000 irregular wave cycles, and simultaneous measurements of overtopping and toe scouring, were measured. To investigate development time for maximum toe scour depth, an initial selection of experiments was also undertaken for 3000 irregular waves, with scour depths measured, after approximately 1000, 2000 and 3000 wave cycles.

In Figure 4.13, the measured scour depths are plotted against the number of waves for the tested shingle foreshore configurations. For both gravel foreshores, it is seen that the maximum scour depth occurred at around 1000 random waves. For example, if we look at Figure 4.13(a) the peak scour depth can be noticed at around 1000 waves overall for all the cases, despite of different wave conditions (wave periods).

Similar characteristics of maximum scour depths were also revealed by Sumer and Fredsøe (2000) for a sloping seawall, in which authors noticed that the peak scour depth occurs between 1000 to 2000 irregular waves at a 1 in 1.2 seawall on a sandy bed. Hence, the calculated scour depth at 1000 waves, was adopted for all the tested conditions, as the maximum scour depth.

a.

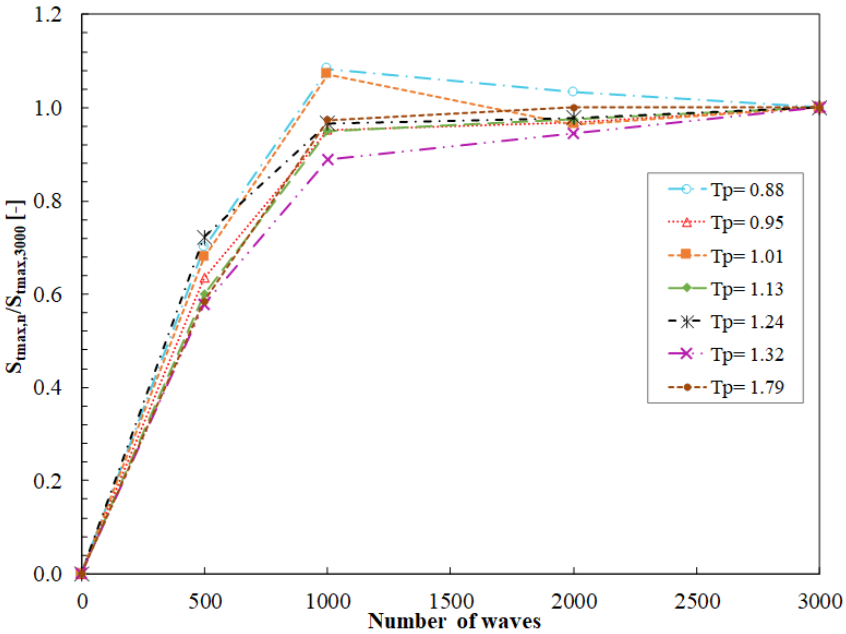

b.

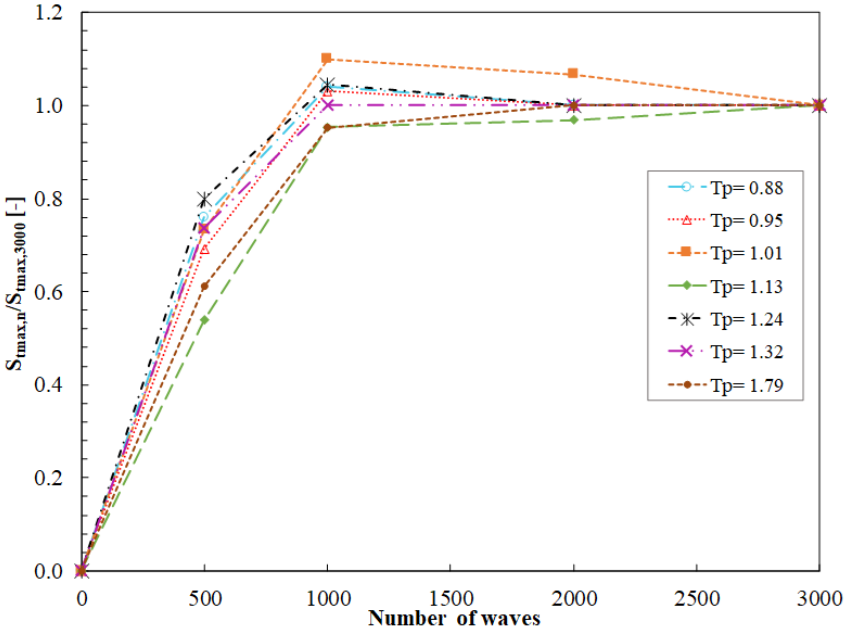

Figure 4.13 Relationship between development of scour depth and storm duration at plain vertical walls - a) d_{50} = 13 mm, and b) d_{50} = 24 mm

4.4.2 Bed level changes for a vertical wall with a shingle foreshore

Figure 4.14 shows the observed bed level changes (final – initial elevation of bed) after 1000 random waves for both swell and storm sea state. In Figure 4.14, negative values of bed level changes represent scour while positive values denote accretion. All the tests were performed with same initial bed profile (1:20 uniform shingle bed) and same wave conditions but with different toe water depths (h_t = 0.18 m, h_t = 0.16 m, h_t = 0.15 m, h_t = 0.10 m, h_t = 0.075 m and h_t = 0.06 m). It should be noted that experiments with nominal wave steepness (s_{op}) of 0.02 and 0.05 were designed to replicate swell sea conditions and storm sea state respectively.

The results of this study demonstrate that for any given relative toe water depth, accretion at the toe of the structure was reported for swell sea state whereas scouring was noted for wind sea state. This can be also related with the two different wave characteristics resulting two distinct physical mechanisms, which dominate the movement or transport of bed materials. In general, swell waves with relatively long wave periods generate accretion at shingle beaches through the onshore sediment transport of beach materials whereas steep storm waves provide scouring through the offshore movement of sediment materials (Sherman, 1991).

Furthermore, it can be also observed from Figure 4.14 that for any given wave conditions, the maximum accretion or scouring occurs for lowest toe water depth. For instance, all the tests in Figure 4.14 (a) were performed with a nominal wave steepness of 0.02 and with significant wave height (H_{m0}) of 0.085 m but with six different toe water depths. The test results showed that maximum accretion (0.081 m) at the structure occurred for lowest toe water depth of 0.06 m, see Figure 4.14 (a).

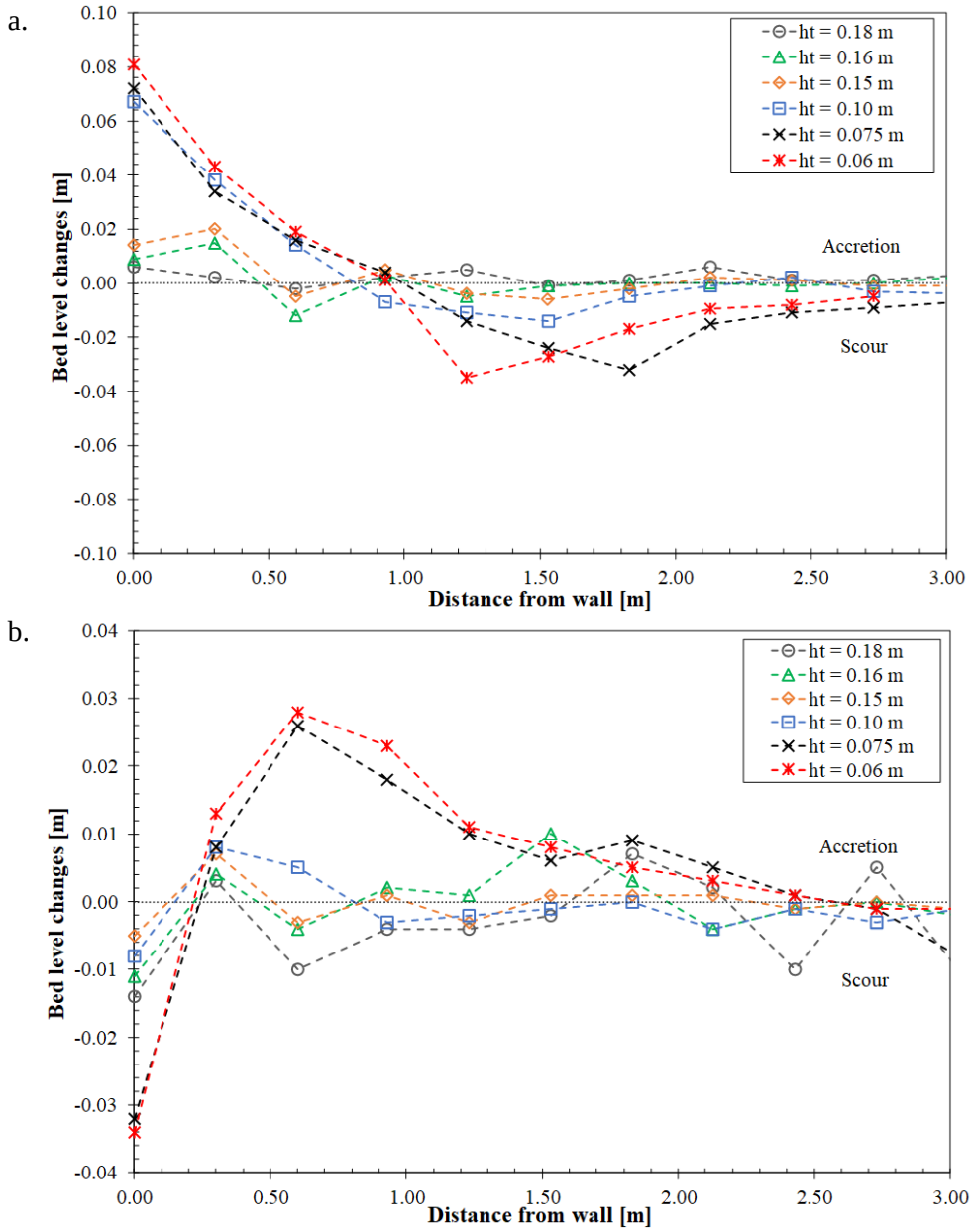

Figure 4.14 Bed level changes after 1000 waves - a) s_{op} = 0.02, H_{m0} = 0.085 m, and b) s_{op} = 0.05, H_{m0} = 0.12 m

4.4.3 Variation of toe scour depth with Iribarren number

The Iribarren number (I_r) or surf similarity parameter is the combination of structure slope and wave steepness (e.g. Equation 2.6), which describes wave breaking types. To observe the relationship of toe scour depth with wave breaking, the measured non-dimensional toe scour depths with respect to Iribarren numbers are presented in Figure 4.15, where $H_{1/3}$ is the significant wave height at deep water and S_t is the scour depth at the toe of the structure. Negative values of non-dimensional toe scour depth represent the accretion at the structure whereas negative relative toe water depths denote the presence of an extended beach above the still water level prior to the start of the experiment.

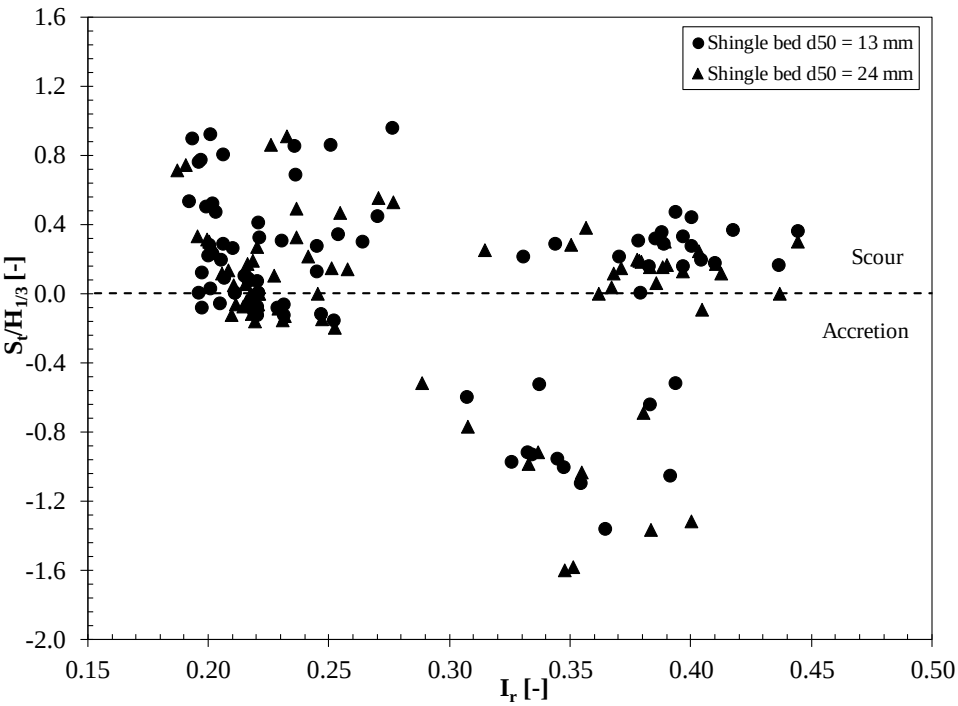

Figure 4.15 Variation of non-dimensional toe scour depth at a plain vertical wall with Iribarren number

The graph demonstrates that there is a considerable variation in toe scour depths for similar values of Iribarren number. For instance, for the experiments with shingle bed of d_{50} of 24 mm, the data points corresponding to Iribarren numbers between 0.35 and 0.40 represent toe scour depths between 1.6 x $H_{1/3}$ and 0.4 x $H_{1/3}$. These scatter characteristics of data points

indicate that for the tested conditions within this study, it is not possible to draw a clear relationship between toe scour depths and Iribarren number only.

4.4.4 Variation of toe scour depth with local wave height

Based on the laboratory measurements, Jayaratne et al. (2015) established an empirical linear relationship between scour depth and local wave height for a known local wave length and submergence of the berm to estimate the scour depth at a vertical wall on a gavel slope d_{50} of 2.20 mm, see Equation 2.48 in Chapter 2. To observe the relationship between scour depth and local wave height for the tested conditions covered within this study, measured dimensionless toe scour depths (S_t/L_m) are plotted against the local wave height ($h_t/H_{1/3}$) at the toe of the vertical wall in Figure 4.16, adopting the approach followed by Jayaratne et al. (2015).

In Figure 4.16, L_m is the mean wave length based on T_m, S_t is the scour depth at the toe of vertical wall, $H_{1/3}$ is the significant wave height and h_t is the toe water depth. It is seen that the test results are scatter, indicating that the scour depths do not vary with the variation of local wave heights for the tested impulsive and non-impulsive conditions covered within study.

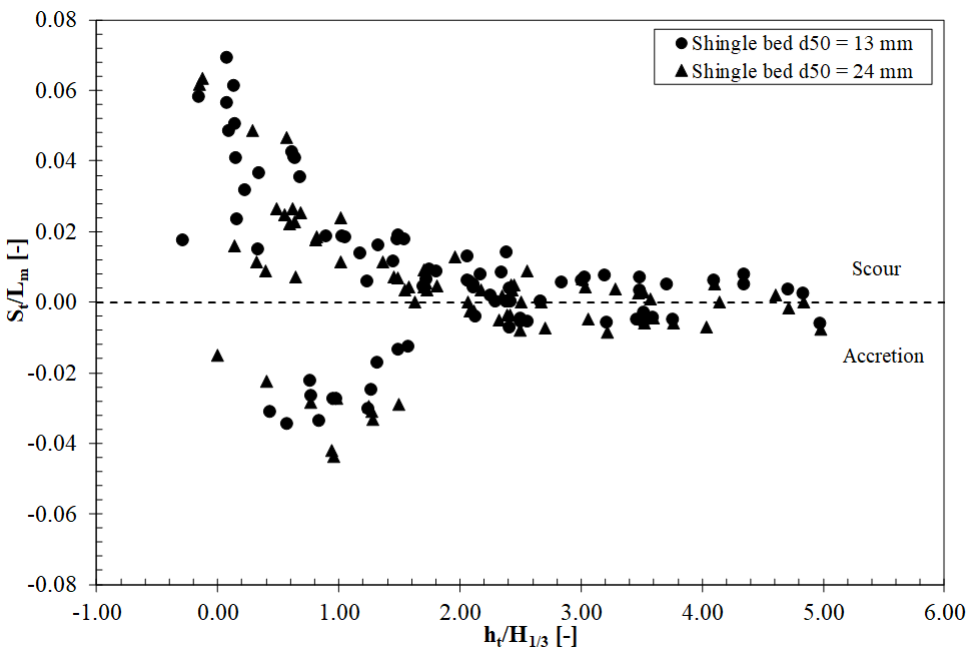

Figure 4.16 Variation of non-dimensional toe scour depth at a plain vertical wall with local wave height

4.4.5 Variation of toe scour depth with relative water depth

The non-dimensional toe scour depth ($S_t/H_{1/3}$) at a plain vertical wall on shingle beds as a function of relative toe water depth is presented in Figure 4.17. Based on experimental and field studies, Sutherland et al. (2006b) and Müller et al. (2008) concluded that maximum toe scour depths at a plain vertical seawall on a sandy bed occurs under plunging wave impacts. Similar trends of the maximum toe scour depths were also observed within this study, as shown in Figure 4.17.

Within experimental limitations, the results show that the greatest toe scour depth (accretion or scouring) occurs for the spilling and plunging waves ($0.005 \leq h_t/L_m \leq 0.04$). For example, maximum accretion is observed around $S_t/H_{1/3}$ =1.60 and maximum erosion is reported $S_t/H_{1/3}$ = 0.95 at relative toe water depth (h_t/L_m) of about 0.025 under spilling and plunging conditions.

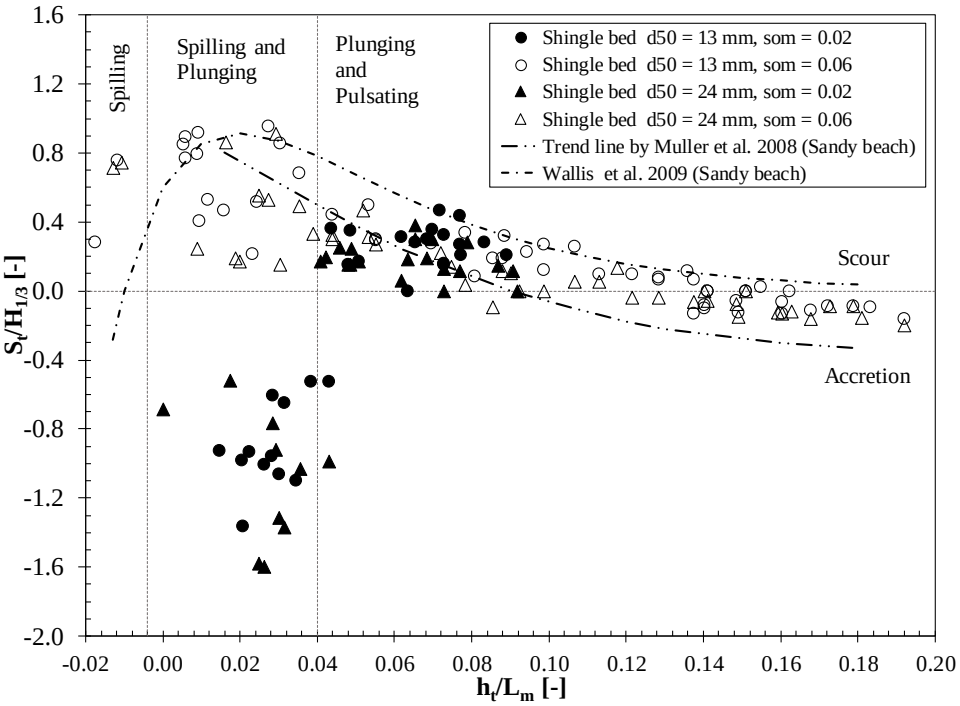

Figure 4.17 Variation of non-dimensional toe scour depth at a plain vertical wall with relative toe water depth

For plunging and pulsating breakers (h_t/L_m > 0.04), the data points demonstrate that the overall non- dimensional toe scour depth continued to

decrease, as the relative toe water depth increased. For relatively high-water depths (h_t/L_m > 0.10), the results show accretion at the toe of the vertical wall on a shingle beach with similar features reported by Müller et al. (2008); Wallis et al. (2009) for a sandy beach.

Overall, the results demonstrate that the accretion at the toe of the structure occurred for waves with low wave steepness (long period), whereas scouring at the structure was observed for high wave steepness, subjected to spilling and plunging conditions. For instance, the data points corresponding to wave steepness of 0.02 under spilling and plunging conditions give accretion at the structure while tests with high wave steepness of 0.06 provide scouring at the toe of the structure for the same relative toe water depth.

This can be also related with reality where accretion at the structure is mostly observed for swell sea state and toe scouring under storm sea conditions. It should be noted that experiments with wave steepness of 0.02 and 0.06 were designed to replicate swell sea conditions and storm sea state respectively.

4.4.6 Variation of toe scour depth with relative water depth and Iribarren number

Figure 4.18 shows the variation of measured scour depths with relative toe water depth and Iribarren number. For the conditions tested within this study, the Iribarren number, I_r was varied from 0.15 to 0.45 and categorised into two ranges as following:

- $0.15 < I_r < 0.30$ and

- $Ir > 0.30$

The data points in Figure 4.18 show that for a certain relative toe water depth, the maximum toe scour depths occur for the larger Iribarren numbers. For example, for shingle foreshore d_{50} of 24 mm, at a relative toe water depth (h_t/L_m) of approximately 0.03, the data point corresponds to Iribarren number of 0.21 ($0.15 < I_r < 0.30$) represent the scour depth equals to 0.15 x $H_{1/3}$ whereas the data point corresponds to higher Iribarren number of 0.36 (I_r > 0.30) denotes the scour depth of - 1.37 x $H_{1/3}$ (accretion at the structure).

Similar characteristics of scour depths with respect to relative water depth and Iribarren numbers, were also reported by Sutherland et al. (2006b) on sandy beaches.

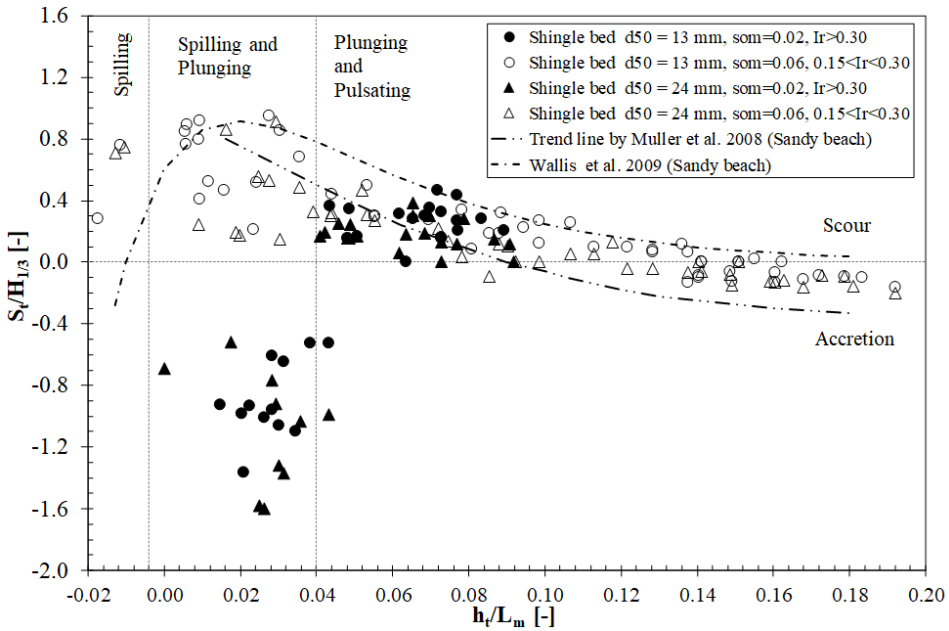

Figure 4.18 Variation of non-dimensional toe scour depth at a plain vertical wall with relative toe water depth and Iribarren number

4.5 Relationship between overtopping and scouring

The resulting difference between toe scouring in swell and storm conditions happened due to the combination of incoming wave characteristics and the interactions between impermeable and shingle foreshores such that different scour depths between impermeable and permeable slope generate different physical characteristics on the wall resulting in difference overtopping. The non-dimensional toe scour depth (S_t / $H_{1/3}$) at a plain vertical wall on shingle beds as a function of Weibull b parameter is presented in Figure 4.18(a) and Figure 4.18(b), for shingle bed d_{50} of 13 mm and 24 mm respectively.

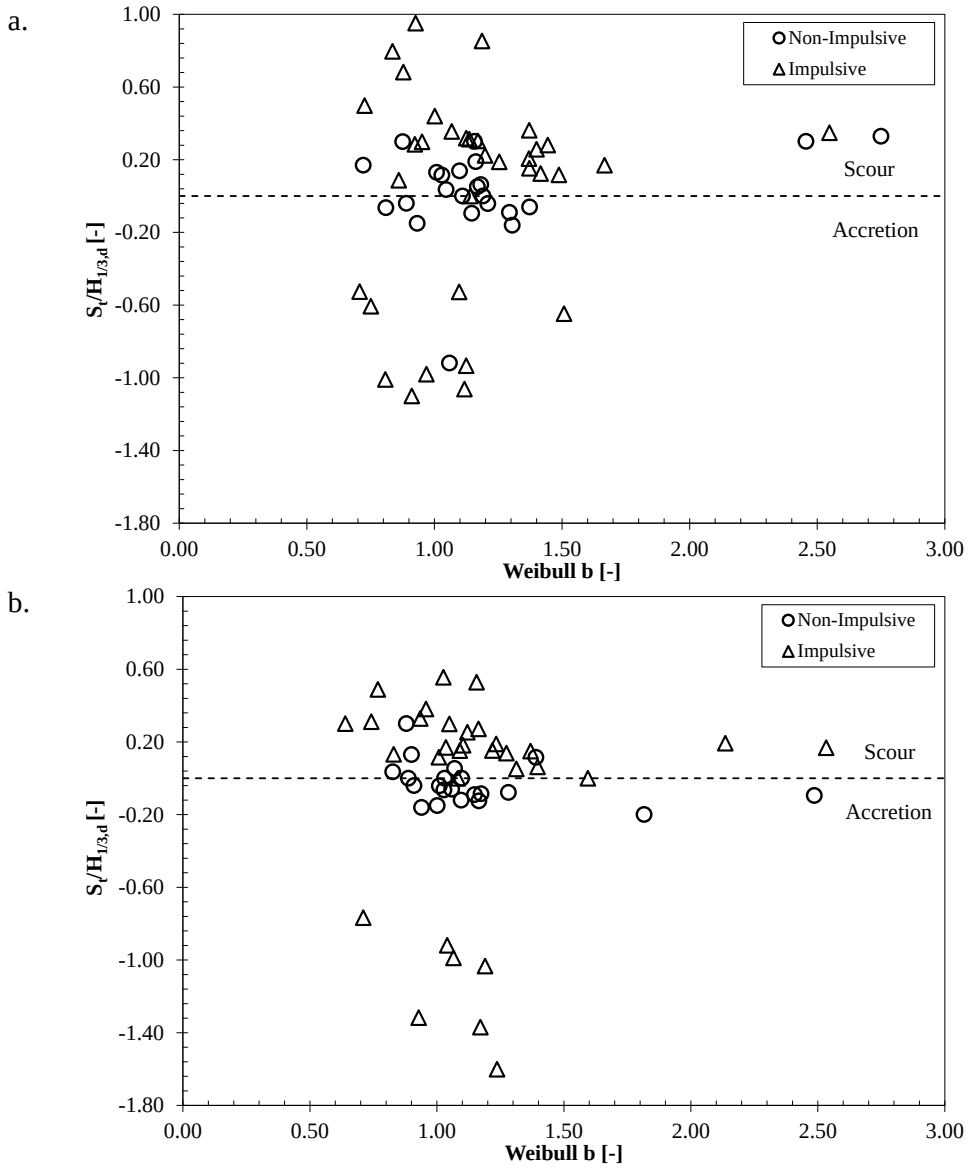

Figure 4.18 Relationship between overtopping and scouring at plain vertical walls with shingle foreshore - a) d_{50} = 13 mm, and b) d_{50} = 24 mm

The results in Figure 4.18 demonstrate that overall greater scour depths were observed for the experiments under impulsive wave conditions, when compared to the non-impulsive conditions. This has been happened due to the two different coastal processes generated from two distinct wave conditions, i.e. non-impulsive and impulsive wave attack. Under non-impulsive wave conditions, waves approaching structures are smaller, when compared to the local water depth and reflected back, usually without breaking, and therefore the resulting scour depths are also smaller. For impulsive conditions, the waves are relatively larger than the water depth, they can break onto the

structure, and generate greater scour depths at the toe of the structure.

The graph also shows that there is a considerable variation in non-dimensional toe scour depths for similar values of Weibull b parameter. These scatter characteristics of data signify that it is not possible to draw a concrete relationship between scour depths and Weibull b parameter for the tested conditions within this study.

4.6 Implications for overtopping prediction methods

The preliminary design guidance for the estimation of mean overtopping discharges at a plain vertical wall under both impulsive and non-impulsive conditions presented in this chapter is an extension to those reported in EurOtop (2018). The new overtopping manual EurOtop (2018) suggested Equation 2.15 for non-impulsive and Equations 2.16- 2.17 for impulsive wave conditions to predict average overtopping rate at vertical structures.

Within experimental limitations, the results of this study demonstrate that for both impulsive and non-impulsive wave conditions the mean overtopping is reduced noticeably with the use of shingle beaches, when compared to an impermeable beach profile. For a permeable shingle 1:20 foreshore slope, the alternative formulae can be applied to predict mean overtopping rate at a plain vertical wall, subjected to impulsive and non-impulsive wave conditions, e.g. Equations 4.1 -4.2 and Equations 4.7-4.8 for impulsive and non-impulsive wave attack respectively. In the absence of any other information to the contrary, a conservative approach is recommended, i.e. an impermeable beach configuration, see prediction formulae (Equations 2.15-2.17) reported by EurOtop (2018).

Overall, the probability of overtopping waves at a plain vertical wall on shingle beds were slightly lower than the impermeable bed configuration (e.g. Figure 4.11). However, as observed in Figure 4.12, it is noticeable from the present research that the maximum individual overtopping wave volumes measured for shingle foreshores do not differ from those measured for impermeable slopes. Due to stochastic nature of wave by wave overtopping, a conservative approach is recommended to estimate the maximum individual

overtopping volumes and proportion of overtopping waves, i.e. empirical predictions reported by EurOtop (2018) considering an impermeable beach profile.

Currently, there is no known design guidance to estimate the mean overtopping sediment rates at a plain vertical seawall, the initial step is to establish whether the waves at the toe of the seawall are likely to be broken wave conditions. For non-impulsive and impulsive waves with conditions in the range, $(h_t^2/(H_{m0}L_{m-1,0}) > 0.03)$, sediment within in the overtopping waves are less likely. Under impulsive conditions, in the range of $h_t^2/(H_{m0}L_{m-1,0}) < 0.03$, it is expected to have up to 0.5% of sediment within the overtopping waves.

4.7 Summary

Detailed measurements have been undertaken to parameterize the mean overtopping rate, mean sediment rate, maximum individual overtopping volume, probability of overtopping and, scour depths on a plain vertical seawall, for both impermeable and mobile shingle beach configurations. The measured distributions of incident wave heights overall follow the trend of that estimated by Rayleigh formulations which indicates that the probable errors in the measurements of wave heights within this study were minimal. As depicted in Chapter 3, the experimental investigation on the accuracy of the overtopping measurement system showed that the measured overtopping volumes don't really differ noticeably from the given values (actual volumes). These results suggest that the overall probable errors in the measurement systems and data analysis are expected to be minimal.

For the tested conditions of reference case (impermeable foreshore), the results of this study provided an overall good agreement with the empirical equations of EurOtop (2018). When impermeable and shingle beaches were compared, it was noticeable that mean overtopping characteristics reduced remarkably for both impulsive and non-impulsive wave conditions. The overtopping of sediment was only observed for the experiments with impulsive wave conditions. The peak wave by wave overtopping volumes and

probability of overtopping waves were somewhat lower than those estimated by empirical formulations.

The resulting overtopping characteristics on permeable shingle foreshores showed a significant reduction on dimensionless mean overtopping discharge, when compared with the impermeable foreshore. While there were no experiments performed on sandy beach, the difference between impermeable and permeable foreshore slope happened due to the variation of wave structure interactions between impermeable and shingle foreshores e.g. the impermeable and permeable generate different physical mechanisms (e.g. wave energy dissipation on permeable slope) on the foreshore resulting in difference in overtopping.

The maximum scour depths were reported at around 1000 random wave cycles for spilling and plunging waves. Within this study, it was noticed that scour depths at a vertical breakwater on a gravel foreshore is strongly correlated with the relative toe water depth and Iribarren number.

CHAPTER 5

Results Analysis and Discussion – Sloping Structure

5.1 Synopsis

This chapter presents and discusses the detailed analysis of experimental study on a sloping seawall with both impermeable and permeable shingle foreshores. The incident wave characteristics observed for the experiments with sloping structure are reported in section 5.2. Afterwards, section 5.3 describes the wave overtopping measurements at sloping walls with both impermeable and permeable foreshore configurations. The test results and analysis of scouring dataset are presented and discussed in section 5.4 of this chapter. The final section reports an overview of the chapter.

5.2 Distribution of Measured Wave Heights

In Figure 5.1, six examples of the distribution of measured incident wave heights at a relatively deep water (near wave paddle) are presented and compared with the deep-water Rayleigh distribution of wave heights for six different tested conditions. The graphs presented in Figures 5.1(a) – (d) were comprised of experiments with relatively higher water depths whereas the test results as shown in Figures 5.1(e) – (f) were tested with comparatively lower water depths.

For relatively larger water depths, it is noticeable from the graphs (Figures 5.1(a) – (d)) that the measured wave heights overall follow the predicted Rayleigh distribution for both swell and storm sea conditions. There is, however, data points that correspond to relatively high waves that were found slightly lower than the prediction which may have occurred due to the occurrence of wave breaking near the wave paddle under depth-limited conditions. For instance, the data points corresponding to the example in Figure 5.1 (d) show that resulting wave heights clearly follow the trend estimated by Rayleigh distribution with only the larger waves being smaller than the prediction.

a.

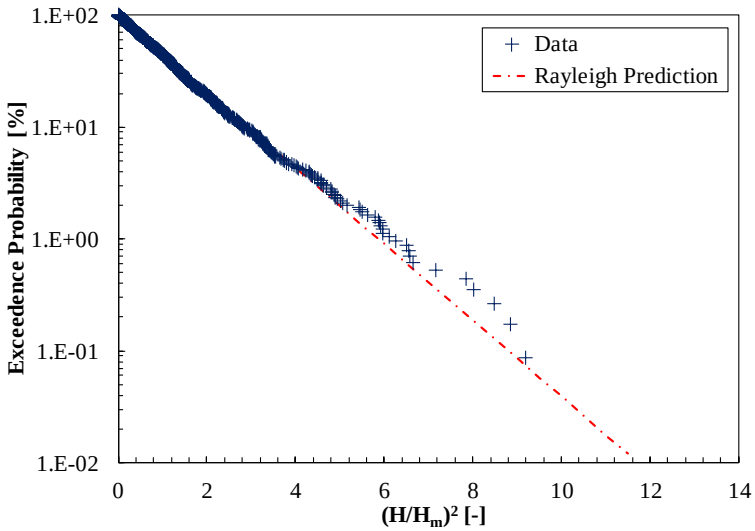
1.E+02
1.E+01
1.E+00
1.E-01
1.E-02
Exceedence Probability [%]
0
2
4
6
8
10
12
14
(H/Hm)² [-]
Data
Rayleigh Prediction

b.

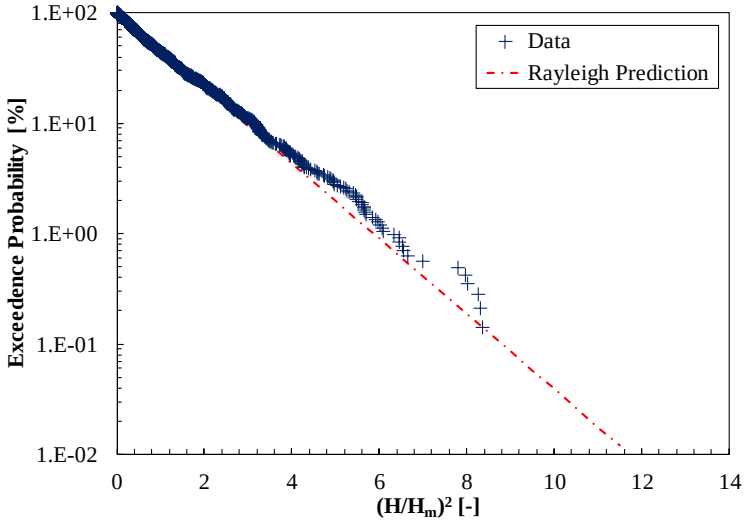
1.E+02
1.E+01
1.E+00
1.E-01
1.E-02
Exceedence Probability [%]
0
2
4
6
8
10
12
14
(H/Hm)² [-]
Data
Rayleigh Prediction

c.

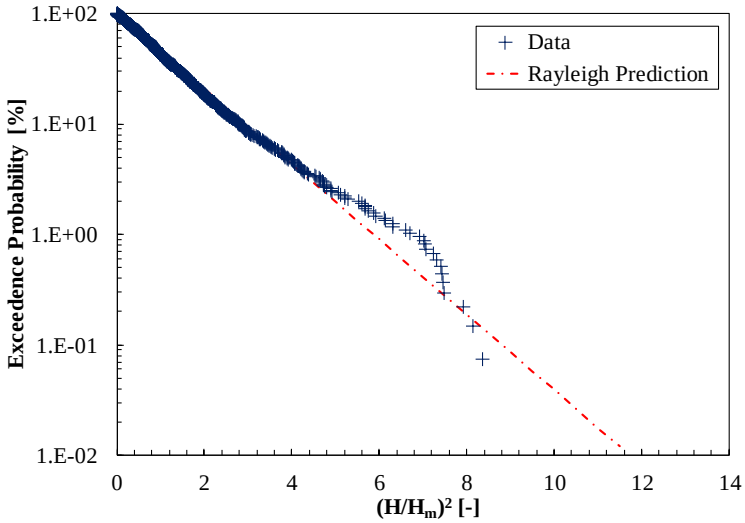
1.E+02
1.E+01
1.E+00
1.E-01
1.E-02
Exceedence Probability [%]
0
2
4
6
8
10
12
14
(H/Hm)² [-]
Data
Rayleigh Prediction

d.

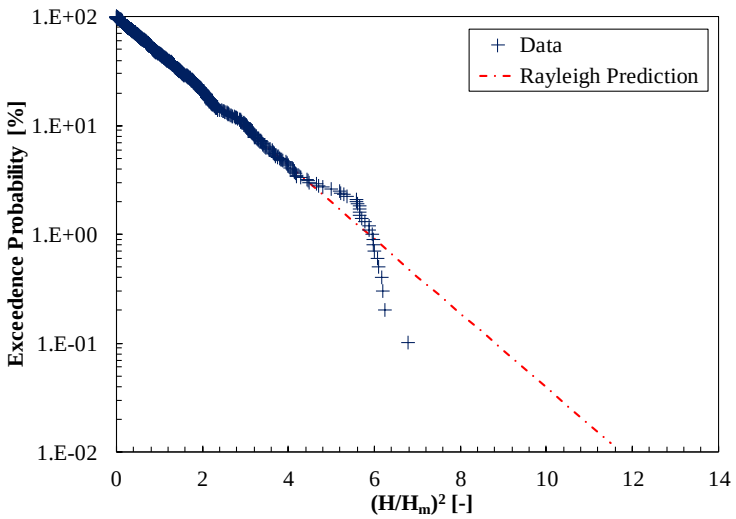

e.

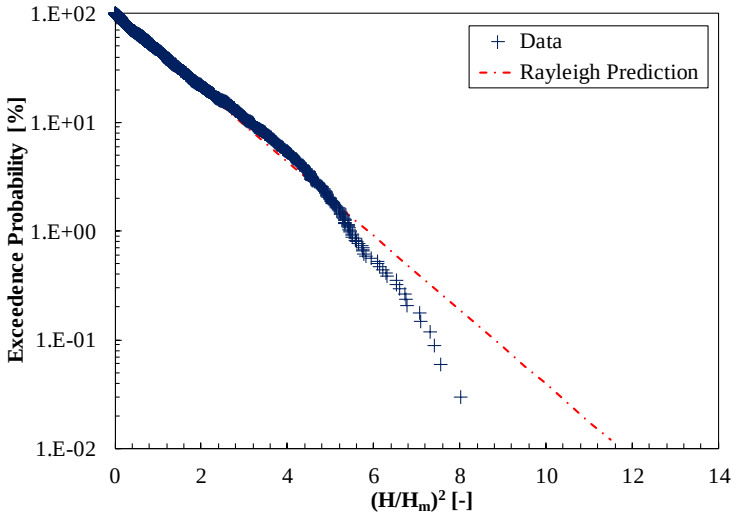

f.

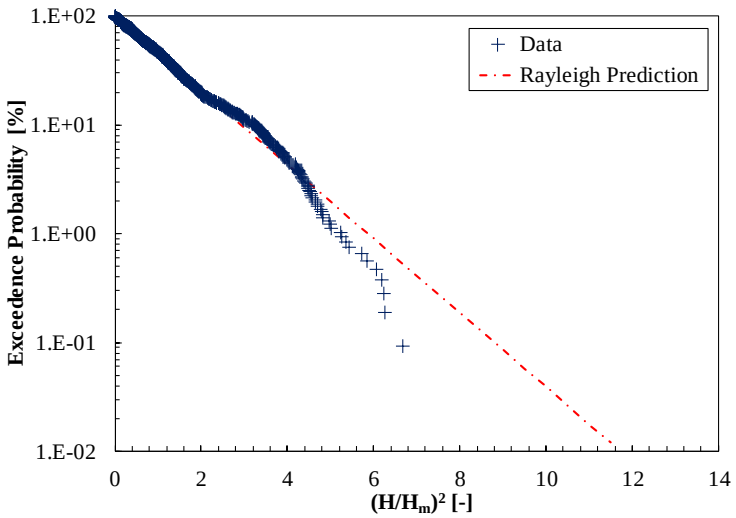

Figure 5.1 Comparison of the distribution of wave heights with the Rayleigh predictions (sloping structure) - a) $s_{m-1,0}$ = 0.02, H_{m0} = 0.06 m, h_t = 0.19 m b) $s_{m-1,0}$ = 0.06, H_{m0} = 0.056 m, h_t = 0.16 m c) $s_{m-1,0}$ = 0.02, H_{m0} = 0.070 m, h_t = 0.16 m d) $s_{m-1,0}$ = 0.06, H_{m0} = 0.078 m, h_t = 0.19 m e) $s_{m-1,0}$ = 0.02, H_{m0} = 0.062 m, h_t = 0.06 m, and f) $s_{m-1,0}$ = 0.06, H_{m0} = 0.010 m, h_t = 0.10 m.

The variation between the measured wave heights and prediction was observed somewhat higher for the experiments with comparatively lower water depths. For example, if we look at Figure 5.1, we can clearly notice that the measured data points correspond to relatively lower water depths (Figures 5.1(e) – (f)) exhibit an overall higher variation from the prediction compared to the higher ones (Figures 5.1(a) – (d)). This variation has been triggered by the presence of wave breaking phenomenon in depth limited conditions.

The slight variation between the distribution of measured wave heights and Rayleigh distribution has been observed only for few conditions (depth limited conditions), due to the limitations of wave paddle stroke. However, from the calibration of overtopping measurement system along with the validation of the measurements with EurOtop (2018), it is evident that this slight variation between the measured and predicted distribution of wave heights can be neglected within this study.

5.3 Wave Overtopping

Investigations on wave overtopping were benchmarked with the measurements of baseline overtopping characteristics at a sloping wall with an impermeable foreshore (control condition). In this section, the measured mean overtopping discharge, mean sediment discharge, proportion of overtopping waves and, maximum individual overtopping volumes on a sloping structure, for both impermeable and permeable gravel bed configurations are presented, and compared with the existing empirical formulations from literature. It is to note that the resulting distributions of wave by wave overtopping volumes at sloping structures are not discussed within this chapter.

5.3.1 Mean overtopping discharge

In Figure 5.2, the measured relative overtopping discharges $q/\sqrt{(gH_{m0}^3)}$ for the impermeable foreshore configuration (reference case) are compared with the predicted values, using the existing empirical predictions for sloping structures. To predict the mean overtopping rates, the empirical predictions of Goda (2009), Etemad-Shahidi and Jafari (2014) and EurOtop (2018) are presented in Figures 5.2(a), 5.2(b) and 5.2(c) respectively.

a.

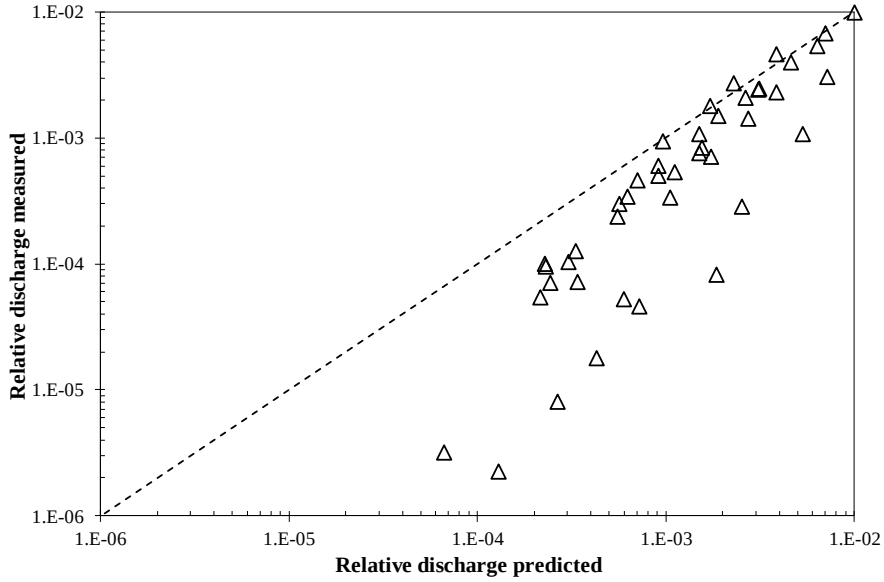
1.E-02
1.E-03
1.E-04
1.E-05
1.E-06
Relative discharge measured
1.E-06
1.E-05
1.E-04
1.E-03
1.E-02
Relative discharge predicted

b.

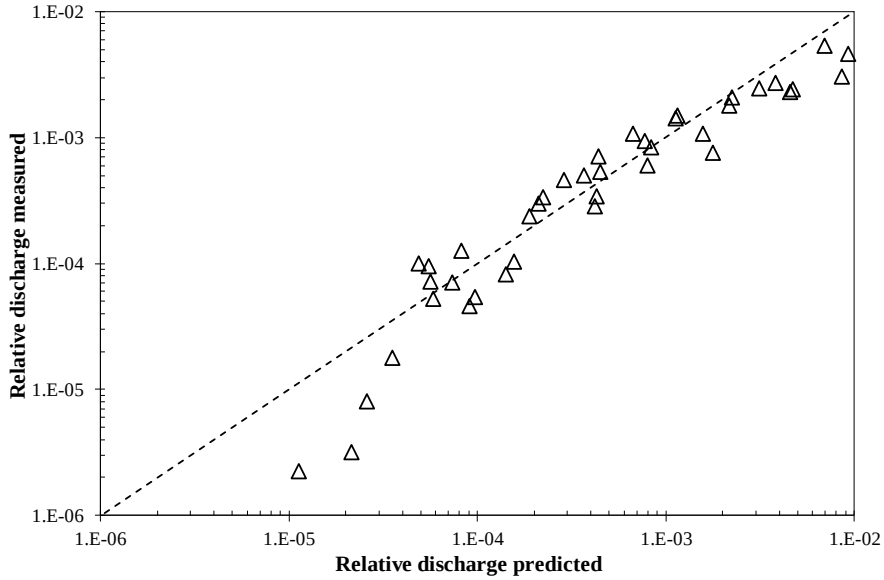
1.E-02
1.E-03
1.E-04
1.E-05
1.E-06
Relative discharge measured
1.E-06
1.E-05
1.E-04
1.E-03
1.E-02
Relative discharge predicted

c.

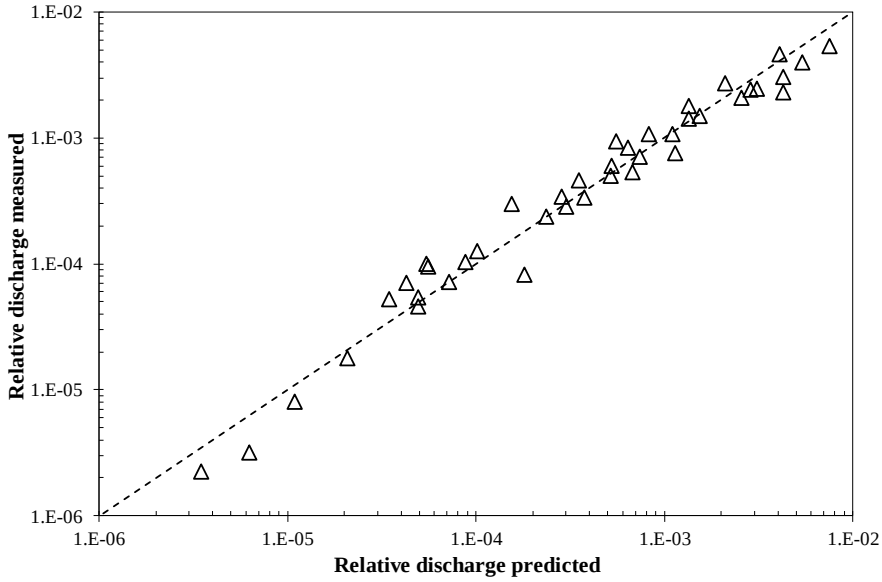

Figure 5.2 Measured relative overtopping discharges at a sloping wall on an impermeable foreshore, compared to the prediction of a) Goda (2009), b) Etemad-Shahidi and Jafari (2014), and c) EurOtop (2018)

It is seen from Figure 5.2(a) that the predictions of the Goda (2009) formulae (Equations 2.20-2.24) overestimate the mean overtopping rates at sloping structures (1 in 2) for the tested conditions covered within this study. Similar characteristics of Goda's formulae for the prediction of mean overtopping rates at sloping structures with gentle slopes (milder than 1 in 2) were also reported by Van der Meer and Bruce (2014).

When comparing the results of the reference case with the empirical formulae of Etemad-Shahidi and Jafari (2014) and EurOtop (2018), it is seen that both the predictions of Etemad-Shahidi and Jafari (2014), Equations 2.25-2.26, and EurOtop (2018), Equation 2.28, overall succeed in providing the estimation of the mean overtopping rate, see Figure 5.2. However, it is also noticeable that the measured values overall showed slightly better agreement with the predicted values of EurOtop (2018) compared to the those observed by Etemad-Shahidi and Jafari (2014).

For the quantitative comparison of the accuracy of the prediction formulae, the statistical error analysis such as root mean square error (rmse) and Bias analysis have been undertaken and reported in Table 5.1. The root mean square error (rmse) analysis and Bias analysis were performed with the use of measured and estimated values of overtopping using empirical formulations, as defined in Equations 4.3-4.6 in Chapter 4.

Table 5.1

The error measures of existing empirical equations for the prediction of overtopping rates at a sloping wall with an impermeable foreshore

Error Indicator	Goda (2019) – Eqns. (2.20-2.24)	Etemad-Shahidi and Jafari (2014) – Eqns. (2.25-2.26)	EurOtop (2018) – Eqn. 2.28
rmse	0.60	0.26	0.12
Bias	0.38	0.09	0.007

As seen in Table 5.1, the prediction formulae of EurOtop (2018) outperforms the predictions of Etemad-Shahidi and Jafari (2014) and Goda (2009) by providing relatively lower rmse and Bias values for the tested impermeable bed configuration.

The measured average overtopping rates for both impermeable (reference case) and gravel bed configurations are plotted in Figure 5.3. The solid line in Figure 5.3 represents the empirical expression of EurOtop (2018) considering an impermeable foreshore (Equation 2.28).

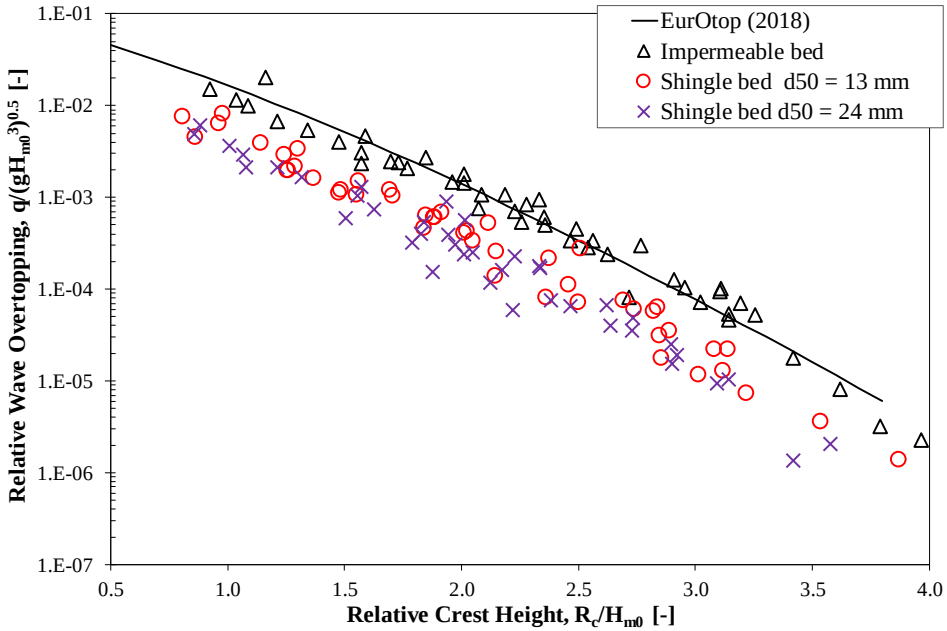

Figure 5.3 Mean overtopping discharge at sloping structures for both impermeable and permeable foreshore configurations

The graph (Figure 5.3) demonstrates that average overtopping discharges are reduced substantially for permeable gravel foreshore configurations compared to those observed for impermeable slope. From Figure 5.3, it is also observed that the shingle foreshore of prototype grain diameter of 24 mm, provide a greater reduction in mean overtopping rate, when the two permeable bed configurations are compared.

Further, a 'best-fit' analysis was performed on the resulting average overtopping discharges to observe the reduction margin with the introduction of gravel foreshores compared to an impermeable slope, see Figure 5.4 and Equations 5.1-5.2. As seen in Figure 5.4, the mean overtopping rate is decreased by an approximate factor of 3.0 for gravel d_{50} of 13 mm (Equation 5.1) and about a factor of 4.0 for d_{50} of 24 mm (Equation 5.2) in comparison to the prediction (Equation 2.18) of EurOtop (2018). It is important to note that best-fit equations have been derived by adapting the formulations of EurOtop (2018), which enables a direct comparison between new equations and existing empirical formulae.

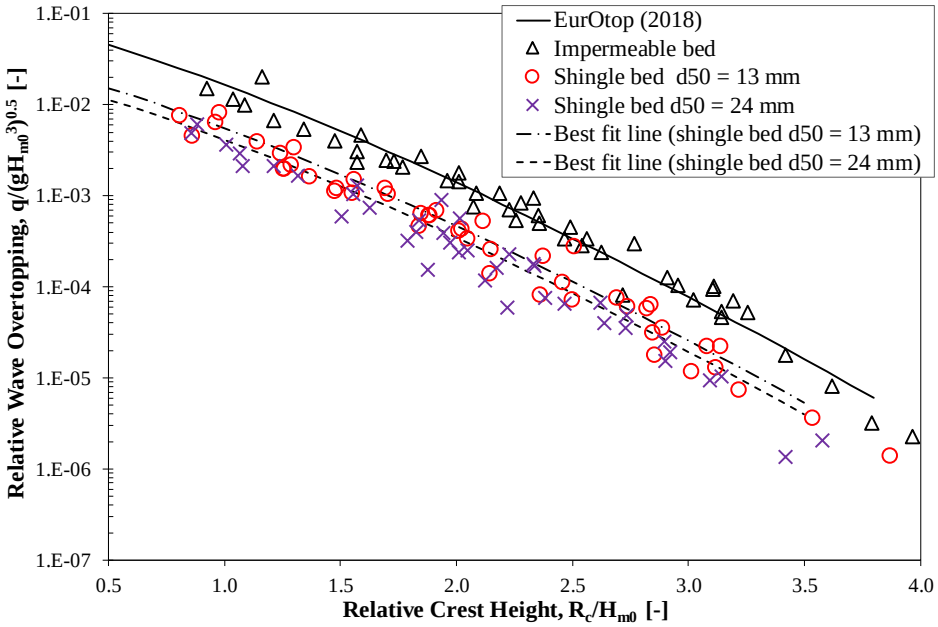

Figure 5.4 Best-fit analysis on the resulting mean overtopping discharge at sloping structures with shingle foreshore configurations

The best-fit trend line for shingle bed of d_{50} = 13 mm,

$$\frac{q}{\sqrt{gH_{m0}^3}} = 0.03 \cdot \exp\left[-\left(1.5\frac{R_c}{H_{m0}}\right)^{1.3}\right] \tag{5.1}$$

The best-fit trend line for shingle bed of d_{50} = 24 mm,

$$\frac{q}{\sqrt{gH_{m0}^3}} = 0.0225 \cdot \exp\left[-\left(1.5\frac{R_c}{H_{m0}}\right)^{1.3}\right] \tag{5.2}$$

Additionally, in Figure 5.5 and Figure 5.6, the test results have been compared with the predicted values using new best-fitted equations (Equations 5.1 - 5.2). For both cases, it can be clearly seen that the measured values of mean overtopping discharge show overall good agreement with the predictions.

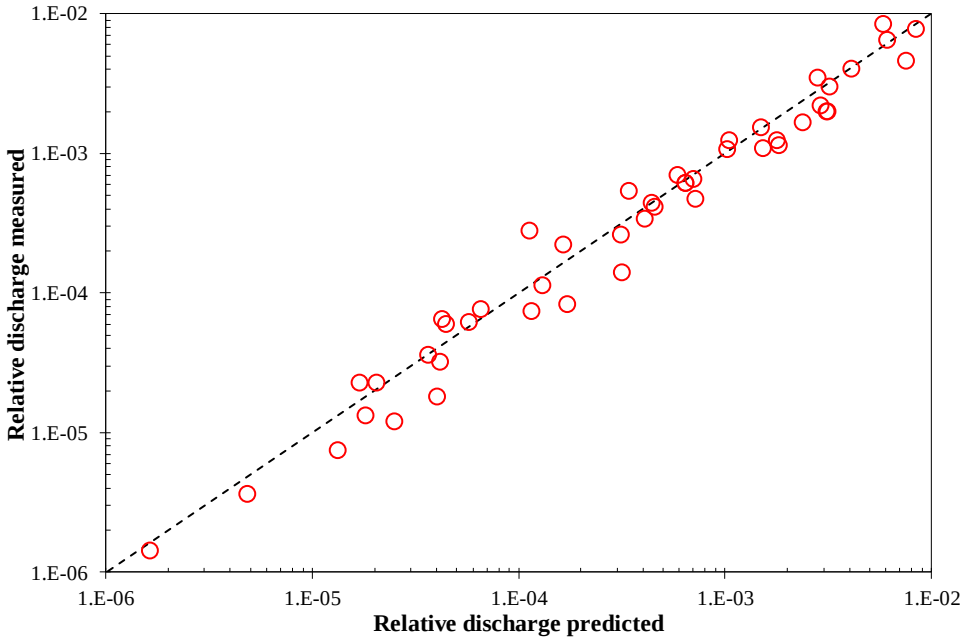

Figure 5.5 Comparison of measured relative discharge versus relative discharge predicted with the new equation - shingle bed d_{50} of 13 mm

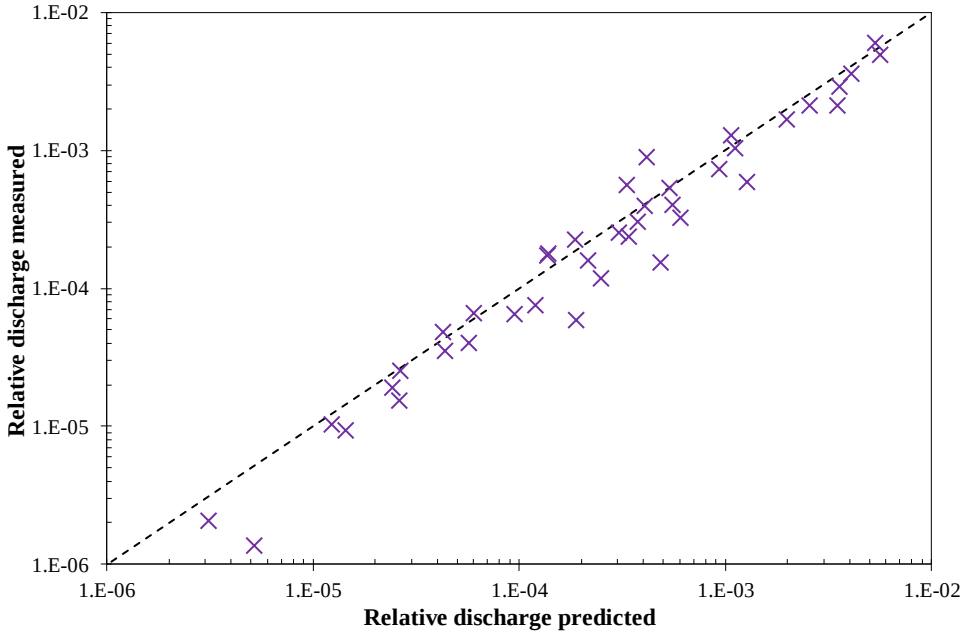

Figure 5.6 Comparison of measured relative discharge versus relative discharge predicted with the new equation - shingle bed d_{50} of 24 mm

To investigate the reliability of the proposed equations, a root mean square error (rmse) analysis was performed with the use of measured and predicted values of overtopping using new equations (Equations 5.1-5.2), as following the approach applied by Owen (1980) and Victor et al. (2012), see Equations 4.3-4.5. In addition to rmse analysis, Bias analysis was also carried out to find the reliability of the derived equations, see Equation 4.6. In Table 5.2, the error measures of the proposed revised equations in the prediction of mean overtopping rate at sloping walls with permeable foreshores are shown.

Table 5.2

The error measures of proposed equations for the prediction of overtopping rates at sloping walls with permeable foreshores

Error Indicator	Equation 5.1 (d_{50} of 13 mm)	Equation 5.2 (d_{50} of 24 mm)
rmse	0.14	0.15
Bias	0.03	0.10

For the conditions tested, the rmse value based on the measured and estimated values of overtopping was only 0.14 and 0.15 for gravel d_{50} of 13 mm (Equation 5.1) and d_{50} of 24 mm (Equation 5.2) respectively, see Table 5.3. Similar to rmse values, the observed Bias values for the new formulations were also smaller i.e; 0.03 for Equation 5.1 and 0.10 for Equation 5.2. These indicate that despite some scatter, in general, the predictions by using the revised expressions (Equations 5.1-5.2) exhibit a promising trend with the actual measurements.

5.3.2 Estimation of roughness factor for the influence of permeable foreshore

Furthermore, in the prediction of overtopping at sloping structures, the effect of various factors such as influence of roughness factor of the armour slope, influence of berm, etc. in the reduction of overtopping is often incorporated by using a 'gamma factor' in the empirical expression, such as roughness factor of the sloping structure in Equation 2.28. To adopt a simple overall coefficient approach for the influence of permeable foreshore in the wave

overtopping, measured mean overtopping rates are compared with various assumed foreshore roughness factors in Figure 5.7, using the empirical formulation of EurOtop (2018).

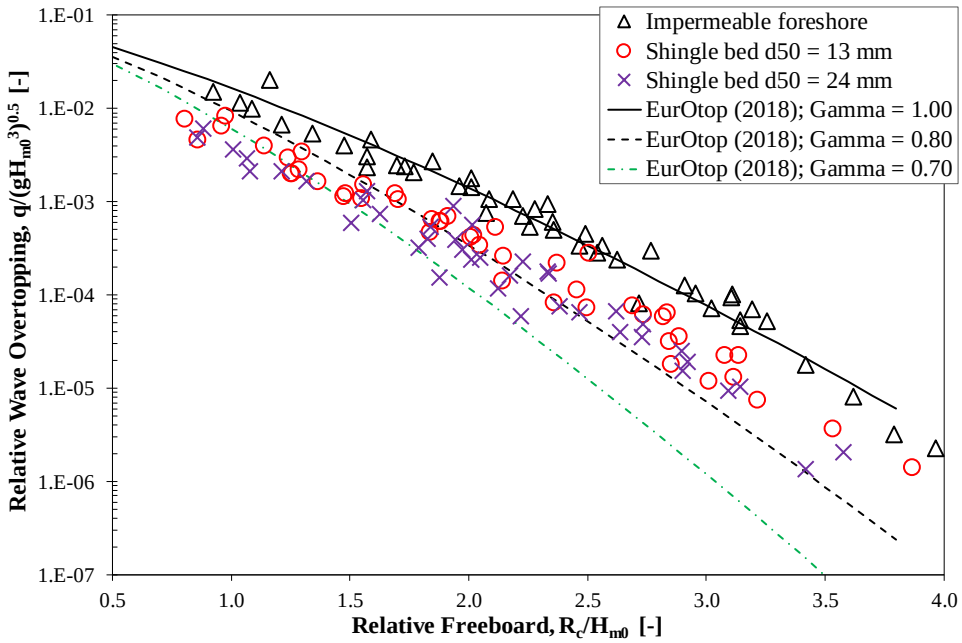

Figure 5.7 Estimation of roughness factor for the influence of permeable foreshore at sloping structure

In Figure 5.7, the solid line represents the prediction of EurOtop (2018) considering a 'gamma factor' equals to 1.0 for the impermeable foreshore using Equation 2.28. Although, it is evident from the graph that test results of permeable foreshores do not perfectly fit with all data, using the "best-fit" empirical lines assuming foreshore roughness factors i.e.; 'gamma factor' of 0.70 (for d_{50} of 24 mm) and 0.80 (for d_{50} of 13 mm) using Equation 2.18. Nevertheless, an approximate trend is observed.

5.3.3 Mean sediment discharge

To determine the average overtopping sediment rate, the mass of sediment collected in the overtopping container was measured (dry weight), together with the mass of the water passing the parapet of the structure. The dry weight was converted to a volume with the use of the quoted specific gravity of 1.40 in order to ensure that the sediment measurements were dimensionally accurate. Figure 5.8 shows the measured mean overtopping characteristics for

the volume of water and the overtopping characteristics of the sediment for the tested shingle foreshore configurations.

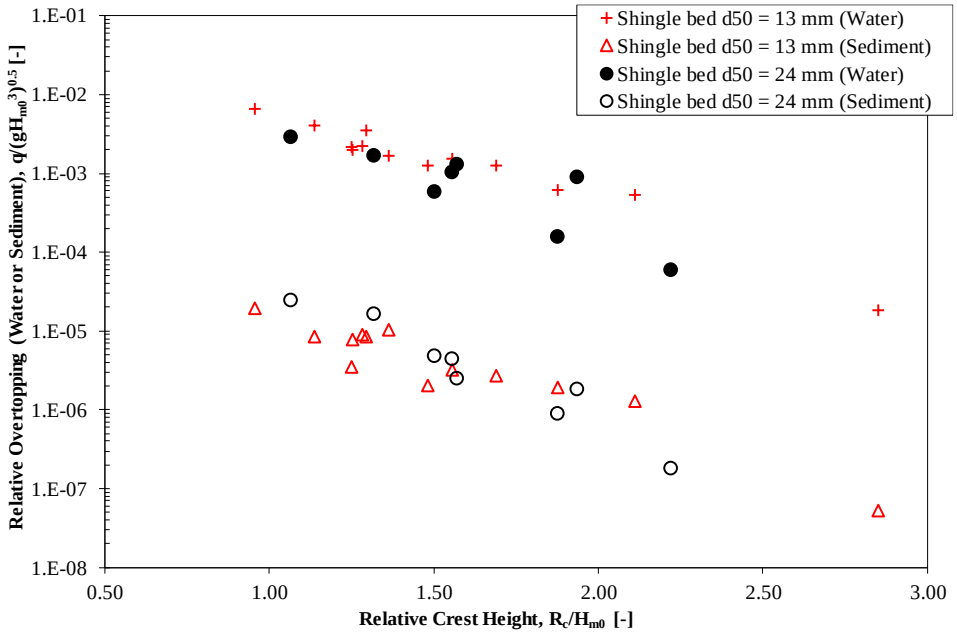

Figure 5.8 Mean overtopping discharge of sediment and water on a sloping structure

In Figure 5.8, the resulting data points demonstrate that the amount of sediment passes the parapet of the structure is significantly lower compared to the amount of overtopped water. Also, it is noticeable from the graph that there is no apparent effect of the size of the shingle foreshore slope on the overtopping of the sediment material at sloping structure.

Further, in Figure 5.9, the proportion of overtopped sediment materials (the ratio of volume of the overtopped sediment to the volume of the overtopped water) is plotted against the relative freeboard of the sloping structure. It is noticeable from Figure 5.9 that the amount of sediment materials passed the parapet of the sloping structure were in the range from 0.20 to 1% of the amount of overtopped water for the tested shingle bed configurations. Sediment material contained within the overtopping waves can be hazardous to personnel, hence, a conservative approach is recommended i.e. it is suggested to expect up to 1% of the sediment material within the overtopping waves.

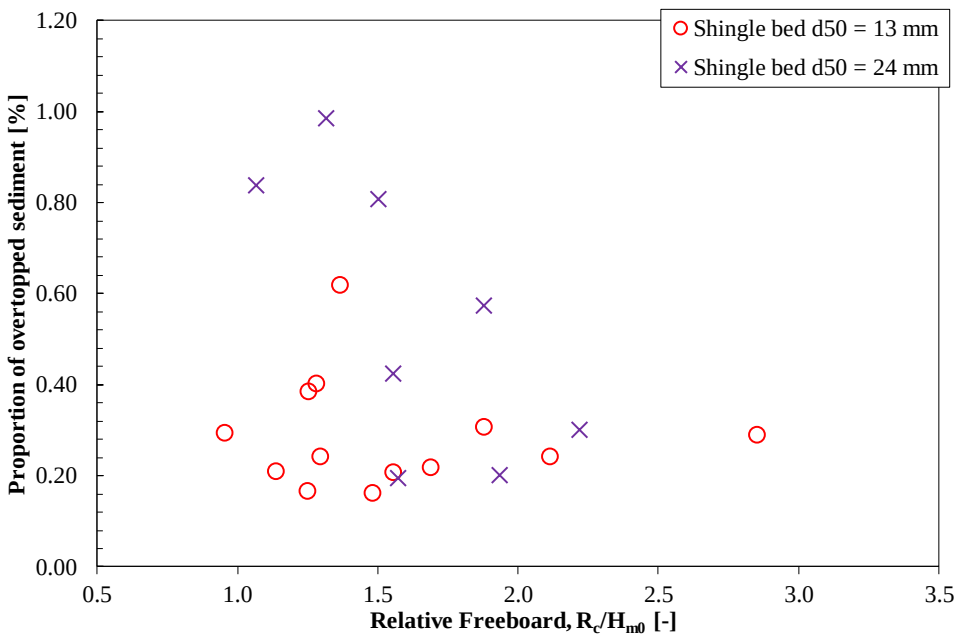

Figure 5.9 Proportion of overtopped sediment at a sloping structure with a shingle foreshore

5.3.4 Proportion of overtopping waves (P_{ov})

In Figure 5.10, the resulting proportion of overtopping waves (P_{ov}) are compared with the predicted values (Equations 2.37-2.38) as reported by EurOtop (2018). For both solid and shingle beach configurations, it is evident that the measured values are lower than the estimated values of EurOtop (2018). As expected, this occurs due to the overestimation of the number of overtopping waves by using the predictions of EurOtop (2018).

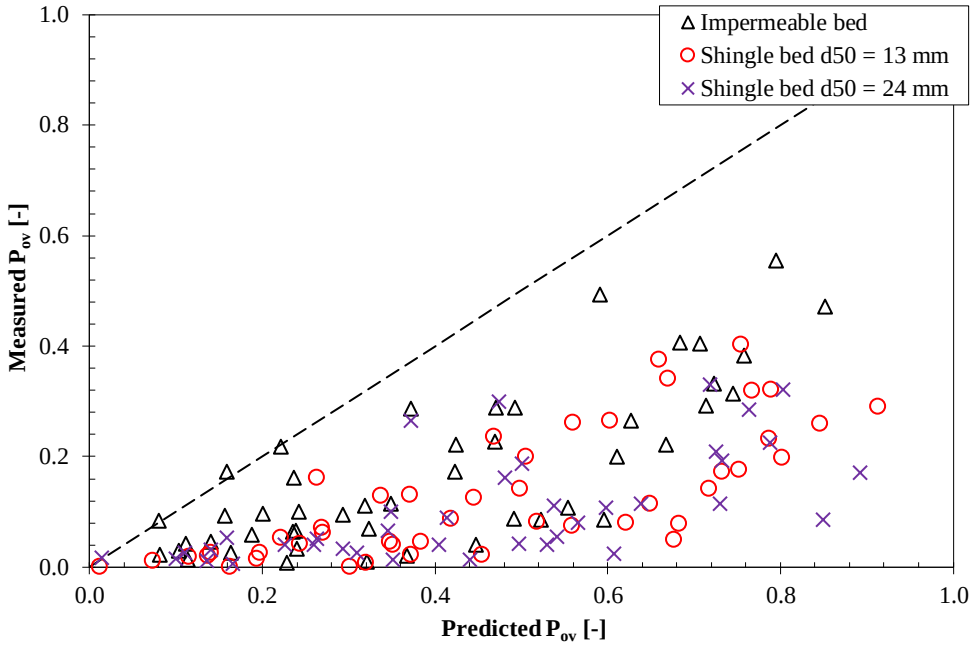

Figure 5.10 A comparison of measured and predicted proportion of overtopping waves at sloping structures

In Figure 5.11, the measured proportion of waves overtopping is plotted as a function of dimensionless freeboard and then compared with the empirical prediction (Equation 2.39) of Victor et al. (2012). The data points correspond to the benchmark tests represent the experiments with the impermeable foreshore. These follow the Victor et al. (2012) prediction to within a factor of 2. It is also noticeable that the measured data points correspond to shingle foreshores are somewhat lower than the empirical values for both tested shingle bed configurations. When comparing the two gravel slopes, it is noticeable that the larger gravel d_{50} of 24 mm, provides a higher overall reduction in the proportion of waves overtopping.

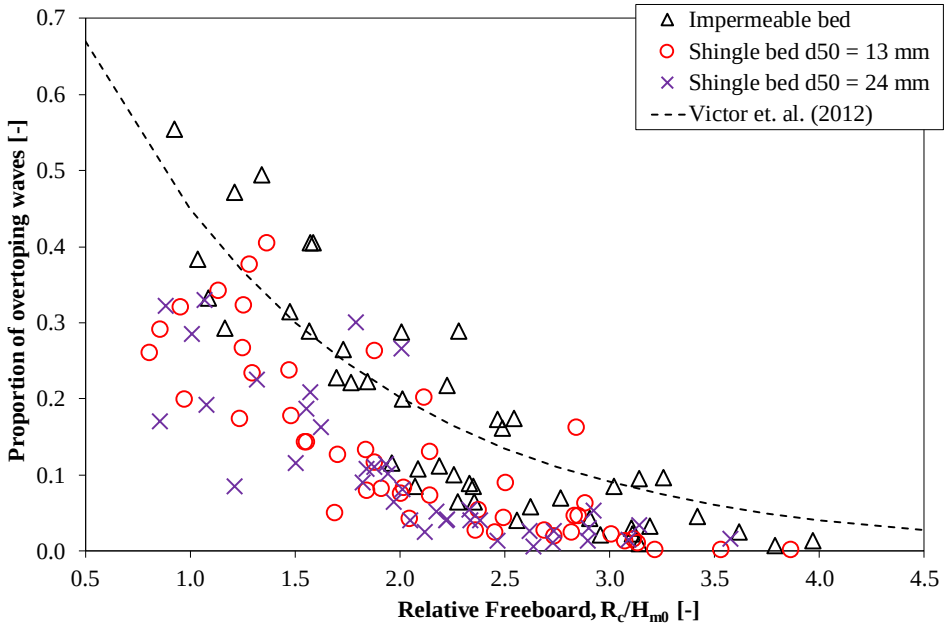

Figure 5.11 Proportion of overtopping waves at sloping structures for both impermeable and permeable foreshore configurations

Figure 5.12 is plotted to quantify the reduction of probability of overtopping waves with the application of permeable foreshore configurations. In Figure 5.12, the reductions are calculated as the ratio of the difference between measured and predicted values of P_{ov} over the predicted values.

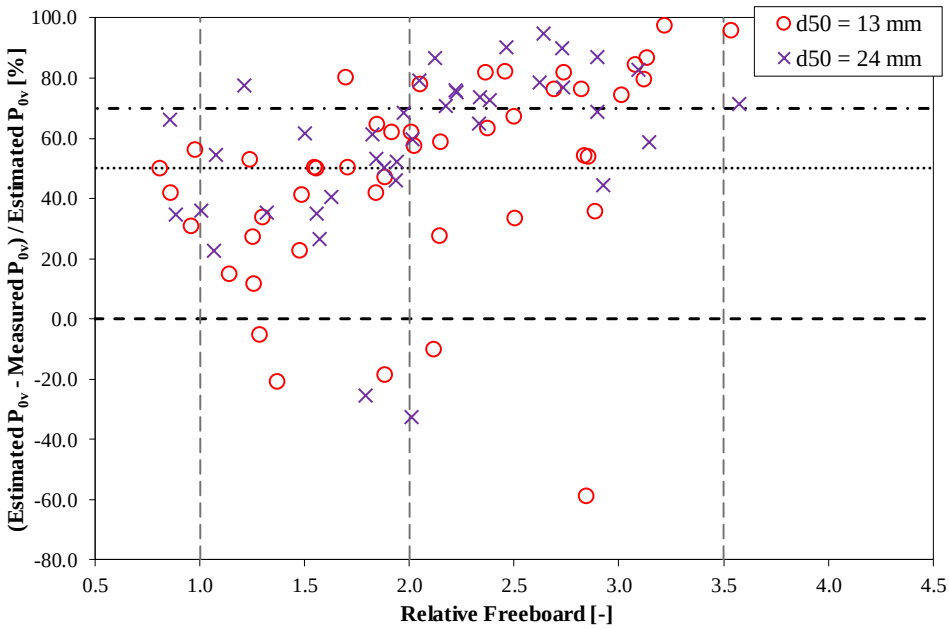

Figure 5.12 Reduction in proportion of overtopping waves at sloping structures for permeable foreshore configurations

It is evident from Figure 5.12 that with the rise of relative freeboard of the structure, the influence of permeable foreshore in the reduction of P_{ov} also increases. For instance, the measured proportion of overtopping waves was reduced by an average of 50% for relative freeboards of 1.0 to 2.0 compared with the predictions, whereas on an average 75% reduction was observed for relative freeboards of 2.0 to 3.5.

5.3.5 Maximum individual overtopping volume (V_{max})

For the tested conditions, Figure 5.13 compares the measured maximum individual overtopping wave volumes at sloping walls with the empirical prediction of Victor et al. (2012) i.e. the number of predicted overtopping waves are based on the formulation (Equation 2.39) of Victor et al. (2012). The resulting data points correspond to both impermeable and shingle beach configurations approximately follow the trend of reported by Victor et al. (2012). It is evident that there is no discernible variation in the prediction of the maximum volumes for impermeable and permeable foreshores at sloping structures. Similar characteristics of overtopping wave volumes were also reported for vertical breakwaters with permeable shingle foreshores as reported in Chapter 4.

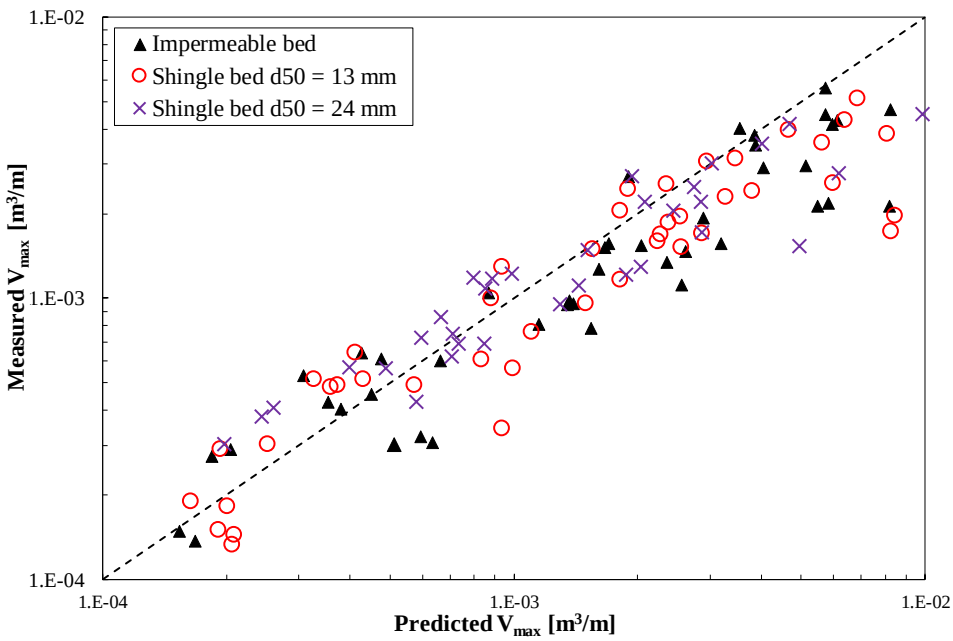

Figure 5.13 A comparison of measured and predicted maximum overtopping volumes at sloping structures

5.4 Toe Scouring

5.4.1 Relationship between development of scour depth and storm duration

In general, the development of a scour depth has a strong correlation with the storm duration or the number of waves, as already mentioned earlier in Chapter 2. In 2000, Sumer and Fredsøe reported that the peak scour depth occurs between 1000 – 2000 irregular waves at a 1 in 1.2 sloping seawall with a sandy foreshore.

To observe the relationship between development of scour hole at the toe of the sloping wall and storm duration for the conditions covered within this study, the measured scour depths are plotted against the number of waves in Figure 5.14. The experiments were performed with approximately 3000 random wave cycles to observe the development of scour depths, where the measurements were conducted at around 1000, 2000 and 3000 waves respectively. Figure 5.14 (a) represents the development of scour hole for the experiments with the shingle bed d_{50} of 13 mm whereas Figure 5.14 (b) demonstrates the development of scour hole for the experiments with the shingle bed d_{50} of 24 mm.

For both shingle bed configurations, it is noticeable that the maximum value of scour depth occurs at approximately 1000 waves, and it reveals similar features as reported in Chapter 4 for vertical walls. This is the reason the measured scour depth at around 1000 waves, was adopted as the maximum scour depth for the tested conditions covered within this study. However, it is to note that the measured scour depths are plotted only in Fig. 5.14 while the underlying shore dynamics and physical mechanisms which are not considered, are not one-dimensional.

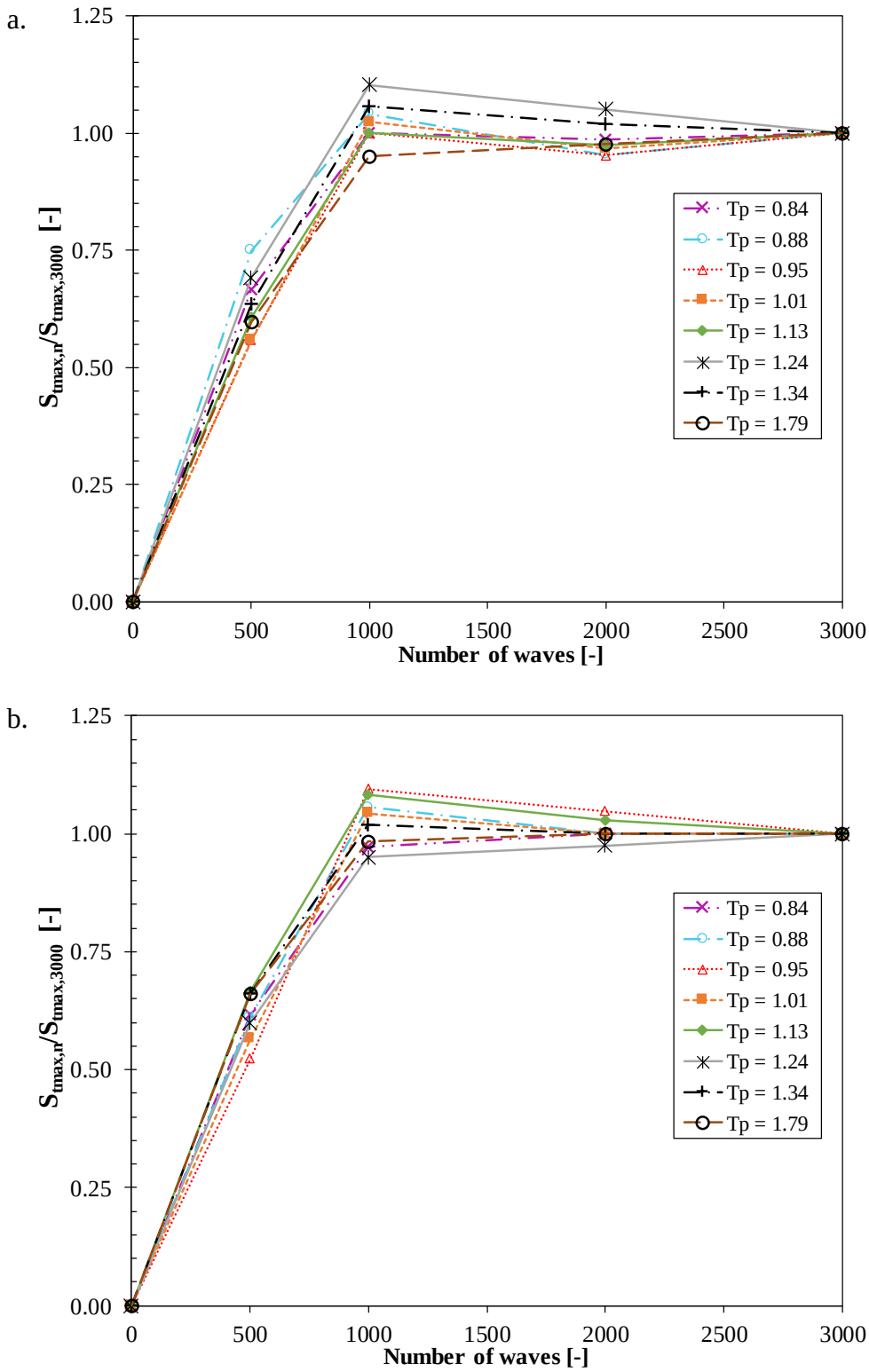

Figure 5.14 Relationship between development of scour depth and storm duration at sloping structures - a) d_{50} = 13 mm, and b) d_{50} = 24 mm

5.4.2 Bed level changes for a sloping wall with a shingle foreshore

The variation of bed level (final elevation – initial elevation of foreshore) due to the random wave attack was inspected for the tested conditions within this study. In Figure 5.15, two examples of measured bed level changes for swell (s_{op} of 0.02) and storm (s_{op} of 0.05) wave conditions are presented for six different toe water depths (h_t = 0.06 m; 0.075 m; 0.10 m; 0.15 m; 0.16 m; 0.18 m). The data points correspond to positive values of bed changes, denote accretion whereas negative values indicate scouring at the structure.

Figure 5.15 demonstrates that the maximum accretion or scouring at the structure occurs for the lowest toe water depth for a known wave condition. To cite an example, if we look at the measured data points corresponding to swell waves (s_{op} of 0.02) in Figure 5.15 (a), it is noticeable that the greatest scour depth of 0.098 m occurs at the lowest water depth of 0.06 m.

Furthermore, from the graphs, it is also observed that the storm waves generate scouring while the swell waves provide accretion at the structure for a certain water depth. This may happen due to the two different wave characteristics, which actually dominate the movement or transport of beach materials. Generally, steep storm waves generate scouring at gravel beaches through offshore sediment transport, whereas swell waves (long waves) provide accretion of onshore sediment transport of bed materials (Sherman, 1991). Similar characteristics of accretion and erosion with respect to long and short waves were also observed for the experiments on plain vertical walls with shingle foreshores as noted in Chapter 4.

a.

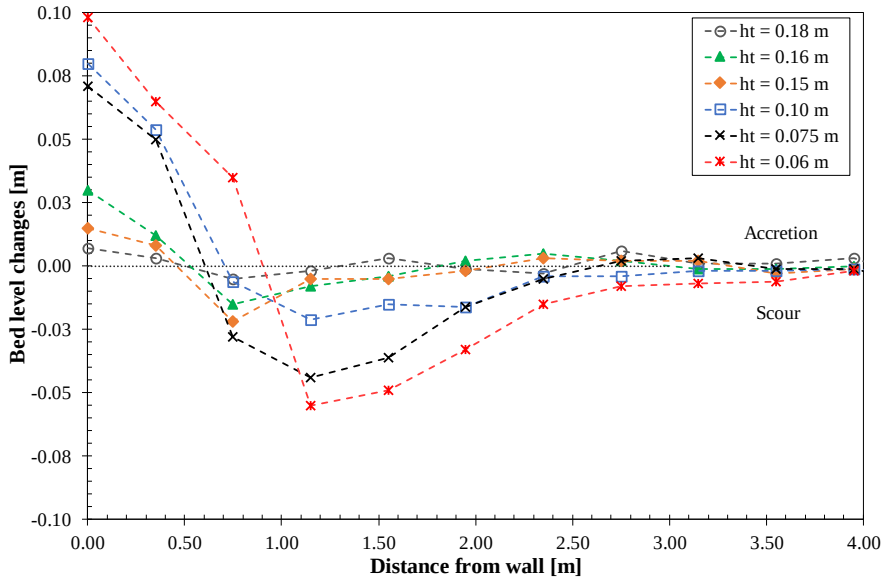

b.

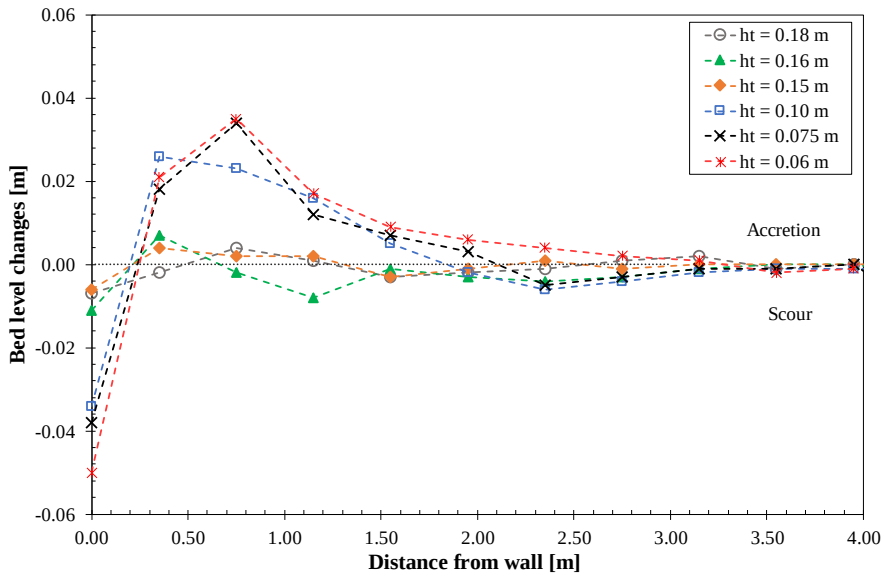

Figure 5.15 Bed level changes after 1000 waves - a) s_{op} = 0.02, H_{m0} = 0.07 m, and b) s_{op} = 0.05, H_{m0} = 0.10 m

5.4.3 Variation of toe scour depth with Iribarren number

To observe the influence of Iribarren number (I_r) on toe scouring, the measured relative scour depths are plotted ($S_t/H_{1/3}$) against Iribarren number (e.g. Equation 2.6) in Figure 5.16. The negative values of relative toe water depth indicate the presence of an extended beach above the still water level prior to the start of the experiment, whereas negative non-dimensional toe scour depths denote the accretion at the structure.

One of the clear conclusions from the graph is that there is a considerable variation in scour depths for similar values of Iribarren number. This may be a result of the variation of toe water depths which has not been fully considered in Figure 5.16.

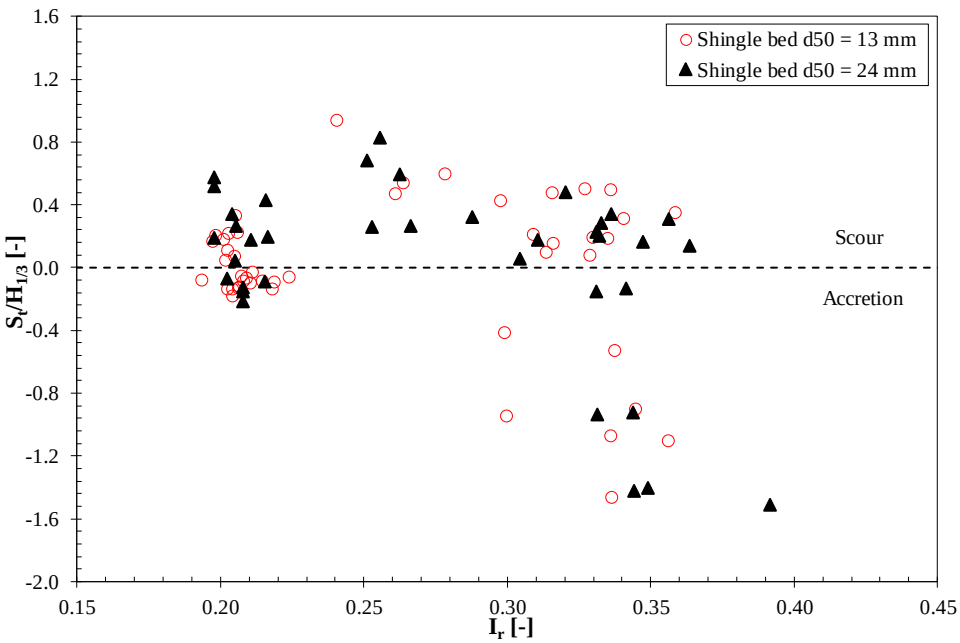

Figure 5.16 Variation of non-dimensional toe scour depth at a sloping structure with Iribarren number

5.4.4 Variation of toe scour depth with local wave height

In Figure 5.17, measured scour depths are plotted against the significant wave height at the toe of the sloping structure adapting the approach followed by Jayaratne et al. (2015), where L_m is the mean wave length based on T_m, S_t is the toe scour depth, $H_{1/3}$ is the significant wave height and h_t is the toe water depth.

The scatter characteristics of data points in the graph demonstrates that there is a noticeable variation in scour depths for similar values of $h_t/H_{1/3}$. This undoubtedly indicate that there is no apparent linear relationship between S_t/L_m and $h_t/H_{1/3}$ for the tested conditions within this study.

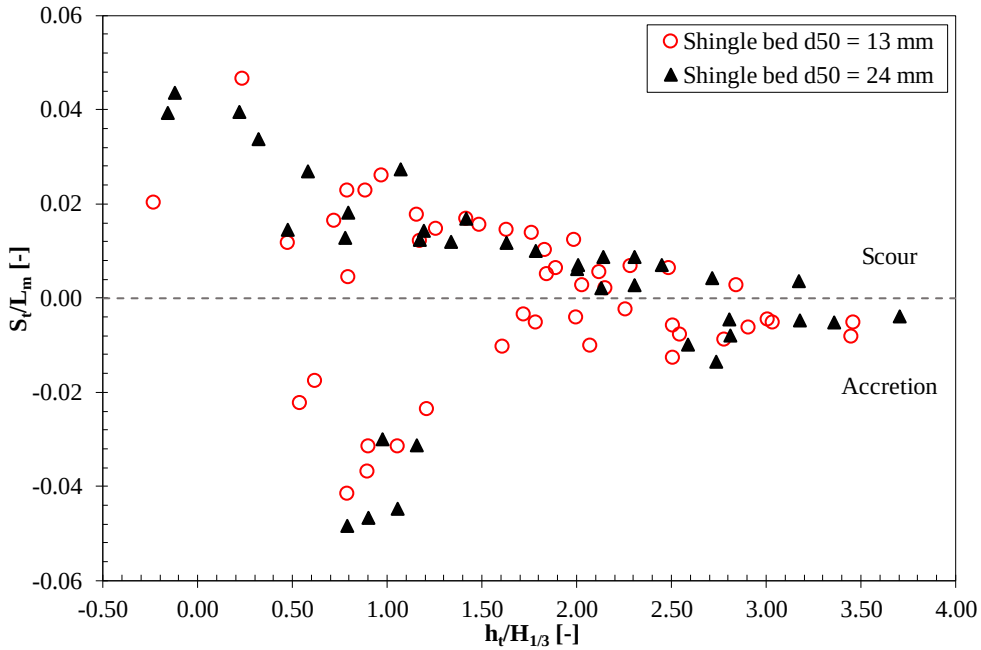

Figure 5.17 Variation of scour depths at a sloping structure with local wave height

5.4.5 Variation of toe scour depth with relative water depth

Figure 5.18 shows the variation of measured relative scour depth with relative water depth at the toe of the structure. The dashed line represents the trend of scour depths at seawalls with sandy foreshores as reported by Wallis et. al. (2009).

The resulting data points show that the maximum scouring at the toe of the structure occurs under spilling and plunging wave conditions ($0.005 \leq h_t/L_m \leq 0.04$). Similar trend of scour depths under spilling and plunging impacts are also noticeable from scouring predictions of Wallis et. al. (2009), see Figure 5.18. For the tested conditions, the maximum erosion at the toe of the structure is observed $S_t/H_{1/3} = 0.93$ at a relative toe water depth (h_t/L_m) of around 0.01 and the maximum accretion is noted $S_t/H_{1/3} = 1.51$ at a relative toe water depth (h_t/L_m) of about 0.03.

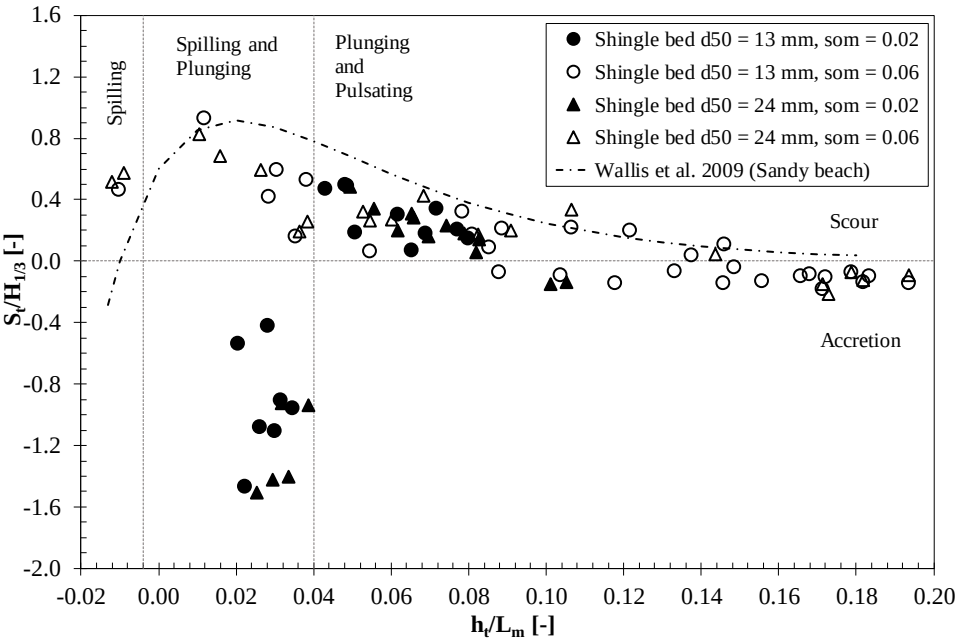

Figure 5.18 Variation of non-dimensional toe scour depth at a sloping structure with relative toe water depth

In Figure 5.18, another clear aspect is that, under plunging and pulsating (surging) breakers ($h_t/L_m > 0.04$), the scour depths continued to decrease with the increase of the relative toe water depth. For the data points corresponding to relatively higher toe water depths ($h_t/L_m > 0.10$), accretion at the toe of the structure is noticeable from the graph. These characteristics were also reported by Sutherland et al. (2006b); Müller et al. (2008) for a plain vertical wall with a sandy foreshore slope.

The results of this study also suggest that there is an influence of wave steepness on the toe scouring at a sloping seawall. For the tested spilling and plunging conditions, accretion mainly occurred for long waves with relatively low wave steepness, whereas scouring was mostly observed for short waves with relatively high wave steepness. In Figure 5.18, if we consider the data points corresponding to average wave steepness of 0.02 under spilling and plunging conditions, the accretion at the structure is observed, while the experiments with relatively high wave steepness of 0.06 give scouring at the structure for a certain relative toe water depth. This can be also related with reality, where accretion at the structure is mostly observed for long waves through the onshore sediment transport of beach materials and toe scouring

phenomenon under storm sea conditions due to the offshore sediment transport.

5.4.6 Variation of toe scour depth with relative water depth and Iribarren number

In Figure 5.19, the measured values of non-dimensional scour depths are plotted against dimensionless toe water depth with the data categorized into two ranges of Iribarren number to investigate the combined influence of relative water depth and Iribarren number on the scour depths, as following:

- $0.20 < I_r < 0.30$ and
- $I_r > 0.30$

The graph demonstrates, that for any known value of relative toe water depth (h_t/L_m), the greatest scour depths occur for the larger Iribarren numbers, see Figure 5.19. Similar trends of scour depths were observed by Sutherland et al. (2006) for a sloping seawall on a sandy beach foreshore.

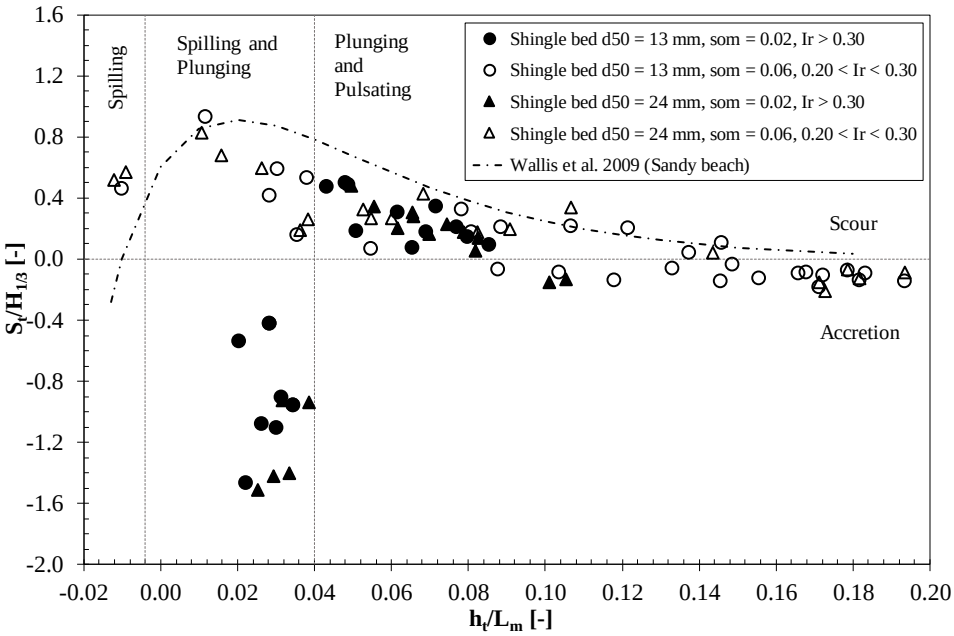

Figure 5.19 Variation of non-dimensional scour depth at a sloping structure with relative toe water depth and Iribarren number

5.4.7 Variation of toe scour depth with wall slope

To investigate the influence of wall slope on the scour depth at coastal structures, the resulting foreshore profiles of this study at 1:2 smooth sloping walls have been compared with the dataset of the plain vertical walls, as reported in Chapter 4, see Figure 5.20.

It is important to note that, for both sloping and vertical structures, the experiments were performed with the same permeable shingle beach materials, but with different structural configurations. As observed in Figure 5.20, the measured scour depths at sloping walls within this study do not remarkably differ from those that were reported at vertical walls in Chapter 4. Similar characteristics of scour depths with respect to wall slope were also observed by Sutherland et al. (2006b) on a sandy slope based on a laboratory study at 1 in 2 sloping wall and a plain vertical wall with sandy foreshore.

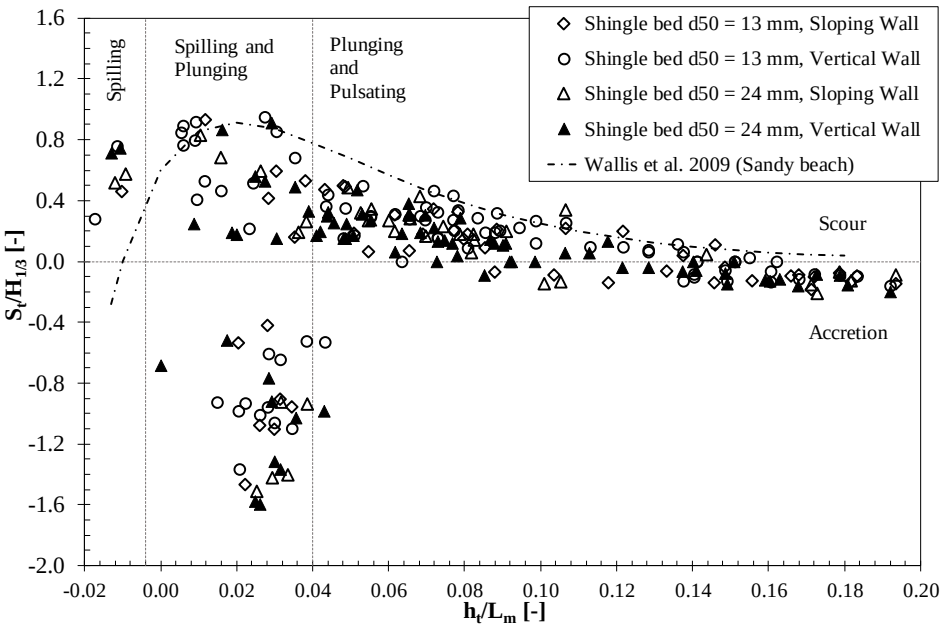

Figure 5.20 Variation of non-dimensional toe scour depth with wall slope

5.5 Relationship between overtopping and scouring

The non-dimensional toe scour depth (S_t / $H_{1/3}$) at sloping structures on shingle beds as a function of Weibull b parameter is shown in Figure 5.20(a) and Figure 5.20(b), for shingle bed d_{50} of 13 mm and 24 mm respectively.

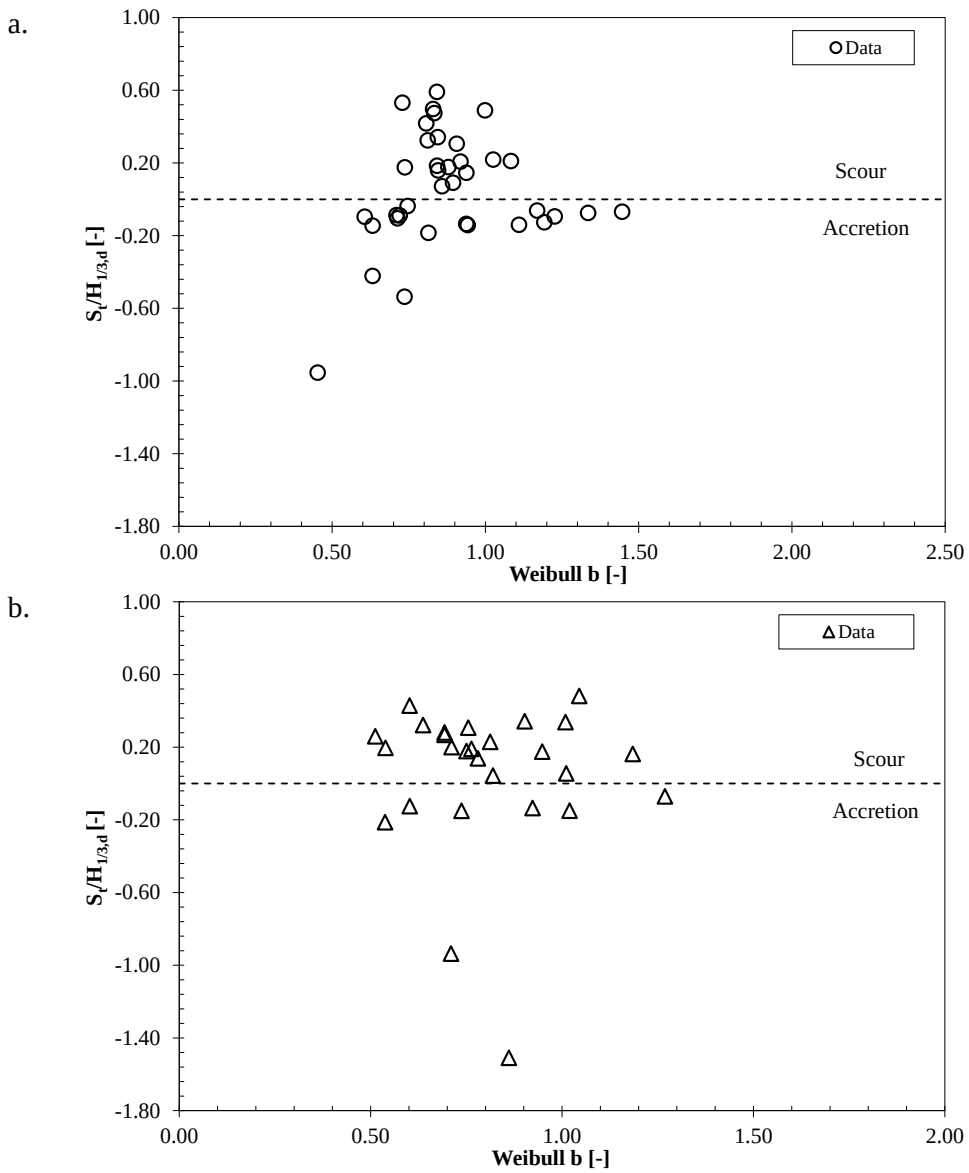

Figure 5.21 Relationship between overtopping and scouring at sloping structures with shingle foreshores - a) d_{50} = 13 mm, and b) d_{50} = 24 mm

The observed non-dimensional scour depths did not vary with the variation of Weibull b values for both shingle bed configurations i.e. d50 of 13 mm (Fig. 5.21a) and 24 mm (Fig. 5.21b). Hence, one can conclude that there is no apparent relationship between the scour depths and Weibull b parameter for the conditions tested within this study.

5.6 Summary

In this chapter, detailed measurements on incident wave conditions, wave overtopping and toe scouring characteristics at sloping structures for both

permeable and impermeable beds have been presented. The results of this study are then compared with existing empirical formulations, which provide a preliminary prediction guidance to estimate these principal coastal processes at sloping structures with permeable foreshores.

For the tested conditions, it was evident that the measured incident wave heights overall followed the prediction of Rayleigh distribution. Also, the test results of the benchmark experiments (impermeable bed) overall exhibited a good relationship with empirical formulations for all the measurements on overtopping. It is therefore anticipated that the outcomes of this work can be applied at prototype situations with minimal 'scale' and 'model' effects.

To estimate the overtopping characteristics at a sloping wall on a gravel foreshore, to date, there are relatively limited prediction tools available in the literature. For a 'traditional' impermeable foreshore slope, the new manual EurOtop (2018) recommended Equation 2.28 for the estimation of average overtopping rates at sloping structures. Within the experimental limitations, the results of this study demonstrate that the average overtopping discharge is reduced noticeably for permeable gravel beaches, when compared to an impermeable slope (reference case). Therefore, a new set of prediction formulae (Equations 5.1-5.2) is proposed in this study for the estimation of average overtopping rates at a 1 in 2 sloping wall with a permeable gravel 1 in 20 foreshore configuration. A conservative method is suggested, i.e. an impermeable slope, see empirical expressions (Equations 2.27-2.28) as described by EurOtop (2018), when there is no other information available.

For the estimation of the average sediment discharges at a sloping structure on a permeable shingle beach, to date, there is no guidance available. Based on an analysis of the measured average sediment discharge, it is recommended to expect up to 1% of the sediment material within the overtopping waves.

Within the experimental limitations it has been found that the scour depths at a sloping wall on a permeable gravel foreshore are strongly correlated with the relative toe water depths and Iribarren numbers.

CHAPTER 6

Distribution of Wave by Wave Overtopping Volumes

6.1 Synopsis

In the previous two chapters, the test outcomes on mean overtopping characteristics at a plain vertical wall and at a 1 in 2 sloping wall with both permeable and impermeable slopes are presented and discussed. This chapter reports the resulting distribution of wave by wave overtopping volumes both at plain vertical wall and at a 1 in 2 sloping wall for the tested impermeable and permeable slopes. Section 6.2 presents the Weibull distribution of the measured individual overtopping volumes at plain vertical walls, along with the estimation of Weibull b values for the distribution. Next, Section 6.3 depicts the Weibull distribution of overtopping volumes at sloping walls for the conditions covered in this study. The next section reports the influence of permeable foreshores on the distribution of individual overtopping volumes for both vertical and sloping structures. Finally, a brief summary of the resulting distribution of both impermeable and permeable foreshores for the tested configurations is given.

6.2 Plain Vertical Walls

6.2.1 Weibull plot of individual overtopping volumes

Generally, the wave-by-wave overtopping volumes in an overtopping sequence adhered to the two-parameter Weibull distribution as reported by many studies, e.g.Van der Meer and Janssen, 1994; Besely, 1999; EurOtop, 2018. Adopting the approach of EurOtop (2018), the measure wave by wave overtopping volumes were plotted on a Weibull scale for each experiment to determine the distribution of these volumes. The straight line on the Weibull plot signifies that the measured data points follow the two parameter Weibull distribution.

Figures 6.1 and 6.2 illustrate the distributions of measured wave-by-wave volumes at plain vertical walls with three tested bed configurations, subjected to the same incident wave condition, where V denotes the individual

overtopping volume, *P(V)* refers to the probability of exceedance, and V_{bar} represents the mean overtopping volume. Figure 6.1 displays the data points that correspond to storm wave condition ($s_{m-1,0}$ = 6%), whereas Figure 6.2 portrays the swell wave attack ($s_{m-1,0}$ = 2%) at plain vertical walls.

Overall, a linear trend of data points can be observed from the graphs given in Figures 6.1 and 6.2 for both low and high wave steepness, indicating that the measured individual overtopping volumes fit the two-parameter Weibull distribution for the tested conditions. The graphs also display no apparent effect of permeable foreshores on the distribution of wave by wave volumes.

In the Weibull distribution of wave by wave volumes, the distributions of small overtopping volumes (lower part) in many cases deviated from the inclination of the upper part of the distribution (Victor et al., 2012; Zanuttigh et al., 2013). Many researchers have reported that higher wave by wave volumes give a good fit to Weibull distribution and offer reliable estimation of extreme individual overtopping wave volumes (Van der Meer and Janssen, 1994; Besley, 1999). Generally, practitioners mainly focus on the largest wave overtopping volumes, wherein Zanuttigh et al., (2013) suggested using the upper part of distribution to get a good fit at the extreme overtopping wave volumes. By adopting the procedure prescribed by Pearson et al., (2002), the best-fit linear trend lines in Figures 6.1 and 6.2 are plotted by considering the upper part of the distribution of wave by wave volumes i.e. considering overtopping volumes greater than the average values ($V > V_{bar}$), as indicated in the graphs.

a.

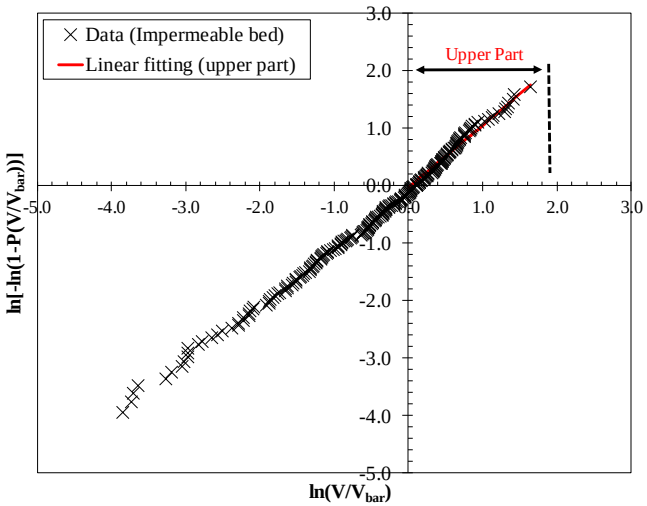

b.

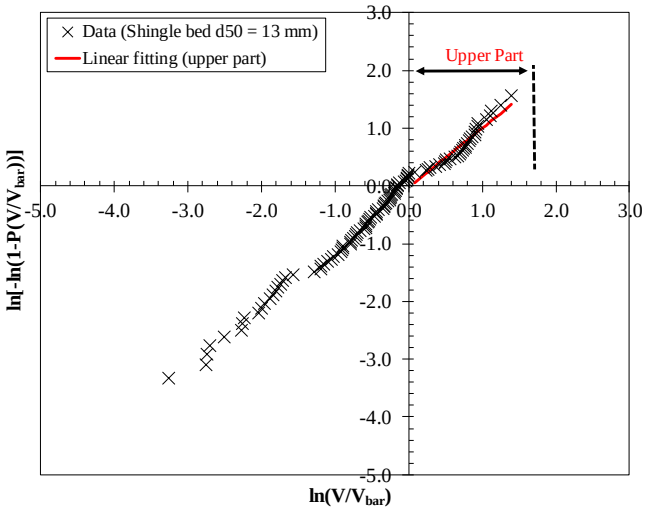

c.

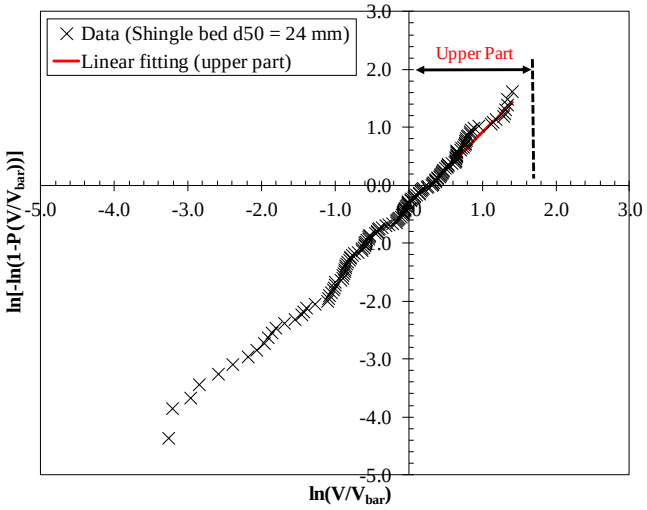

Figure 6.1 Weibull plot of wave by wave overtopping volumes at plain vertical walls for $s_{m-1,0} = 0.06$, $H_{m0} = 0.10$ m - a) Impermeable bed b) Shingle bed $d_{50} = 13$ mm, and c) Shingle bed $d_{50} = 24$ mm

a.

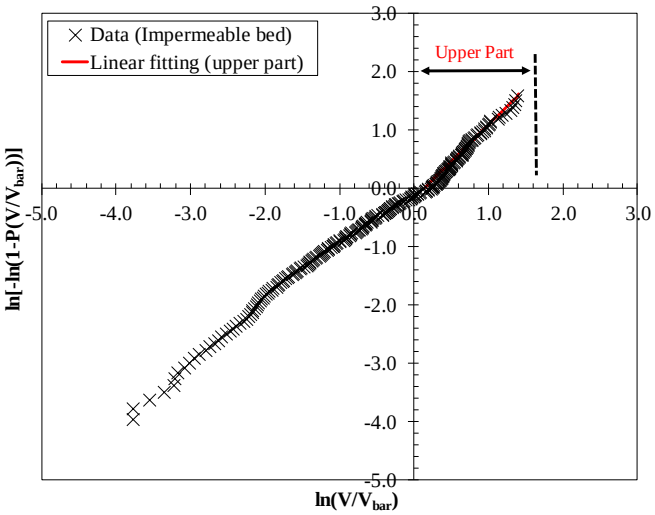

b.

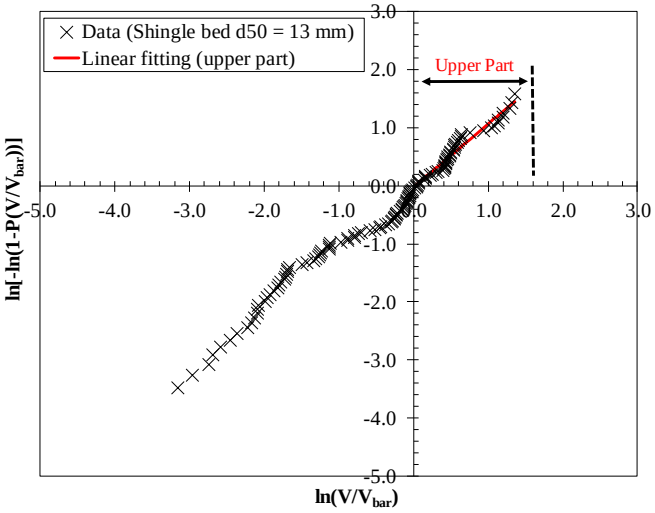

c.

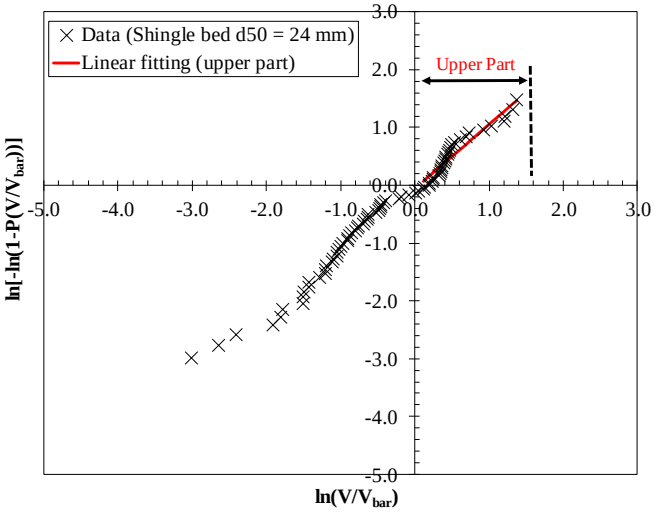

Figure 6.2 Weibull plot of wave by wave overtopping volumes at plain vertical walls for $s_{m-1,0} = 0.02$, $H_{m0} = 0.07$ m - a) Impermeable bed b) Shingle bed d_{50} = 13 mm, and c) Shingle bed d_{50} = 24 mm

The Weibull b parameter can be determined from the inclination of the best-fitting line. From the resulting Weibull distribution of overtopping volumes, the shape factor b of the distribution was determined for each test. Alongside the test results of this study, the measured Weibull b values under VOWS project were analysed in this study. In the VOWS project, specific tests were carried out to assess wave-by-wave overtopping volumes at plain vertical walls (Pearson et al., 2001; 2002). The variations of shape parameter with varied parameters, including percentage of overtopping waves, wave steepness, relative freeboard, relative toe water depth, and relative discharge, are presented in the following sections.

6.2.2 Influence of percentage of overtopping waves on Weibull b

The variation of Weibull shape parameter b with the percentage of overtopping waves is displayed in Figure 6.3, subjected to both impulsive and non-impulsive conditions. The study outcomes showed that the measured Weibull b values fell within the range of 0.65-1.50 for most of the tested conditions. However, in some cases, higher values of (b > 1.5) Weibull shape parameter had been noted, as presented in Figure 6.3.

From the graph illustrated in Figure 6.3, tests with very low overtopping waves resulted in higher Weibull b values (b > 1.5). Similar characteristics of Weibull shape parameter with respect to low overtopping waves (below 5% of overtopping waves) were also reported by Zanuttigh et al., (2013) for rubble mound breakwaters.

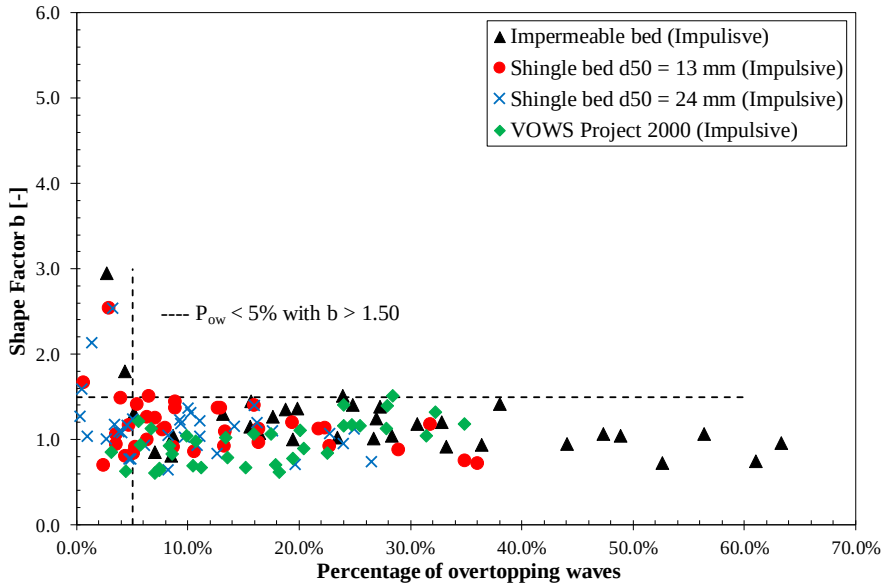

a.

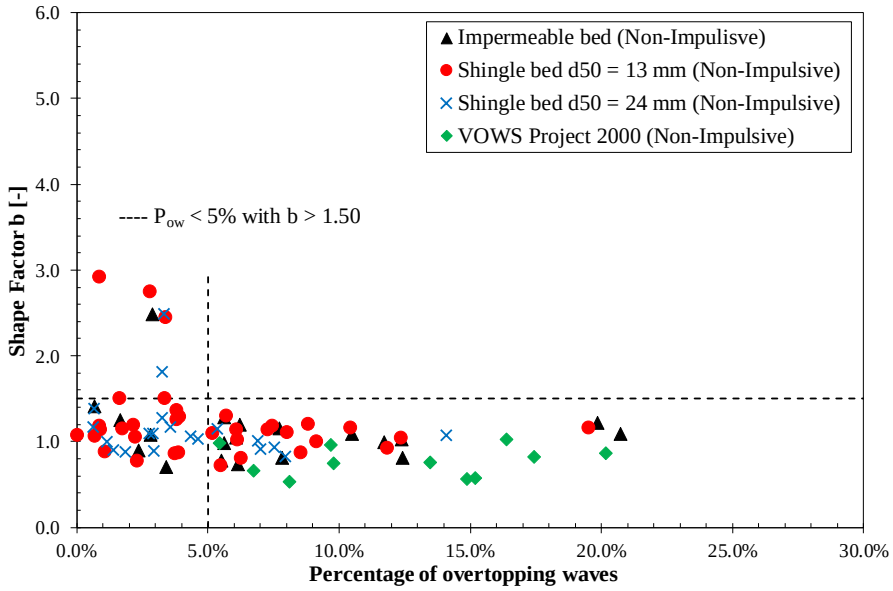

b.

Figure 6.3 Variation of Weibull b with probability of overtopping waves at plain vertical walls – a) Impulsive wave conditions, and b) Non-impulsive wave conditions

6.2.3 Influence of wave steepness on Weibull b

To investigate the influence of wave steepness on the Weibull distribution of the individual volumes, the measured shape factor b was plotted as a function of wave steepness, $s_{m-1,0}$, for both impulsive and non-impulsive conditions (see Figure 6.4). The solid lines in Figure 6.4 represent the b values (b = 0.66 for $s_{m-1,0}$ = 0.02, and b = 0.82 for $s_{m-1,0}$ = 0.04 under non-impulsive conditions, while b = 0.85 for all $s_{m-1,0}$ under impulsive conditions), as recommended by Besley (1999), which have been incorportaed in the new overtopping manual EurOtop (2018).

From Figure 6.4, it is evident that the data points have some scatter, signifying no clear influence of wave steepness on the shape of the Weibull distribution. It was observed that the measured values of the shape parameter were higher than the values suggested by EurOtop (2018) for both impulsive and non-impulsive wave conditions.

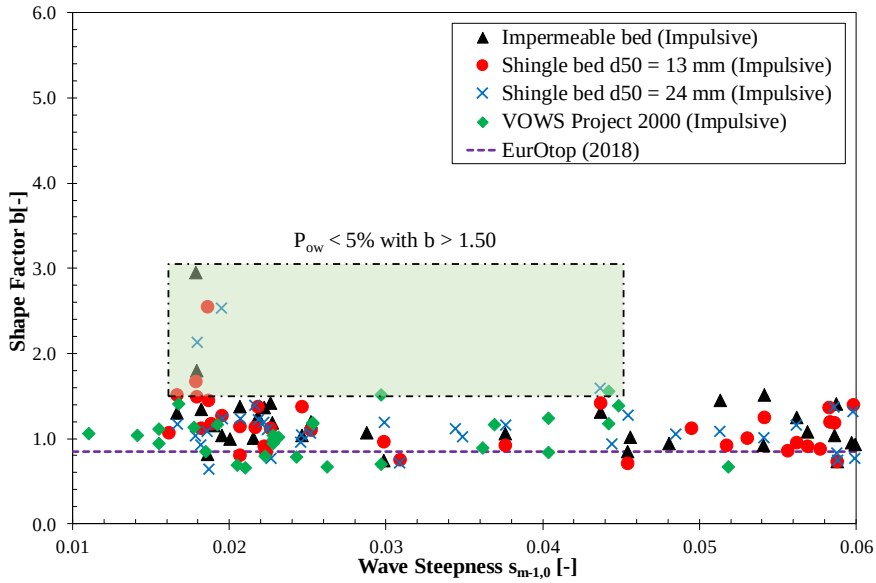

a.

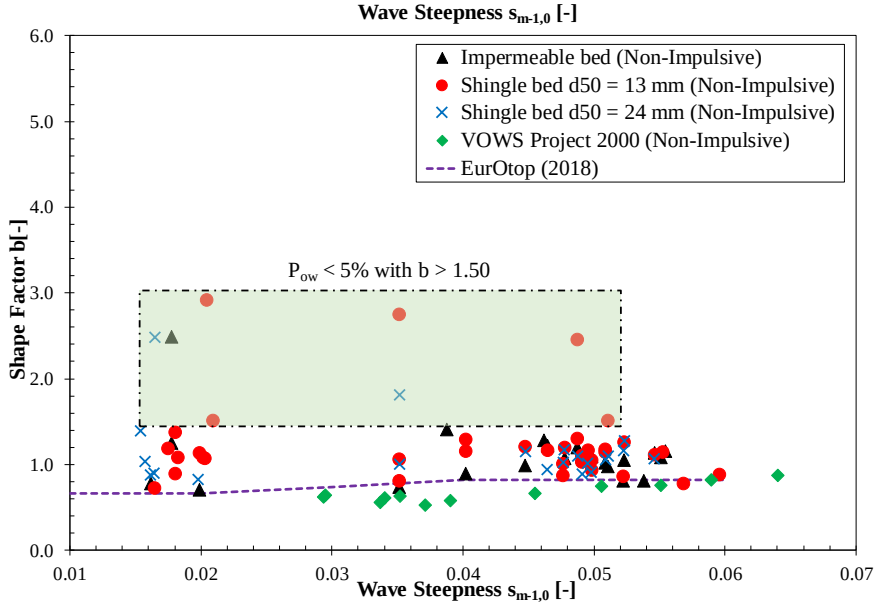

b.

Figure 6.4 Variation of Weibull b with wave steepness at plain vertical walls – a) Impulsive wave conditions, and b) Non-impulsive wave conditions

6.2.4 Influence of impulsive parameter on Weibull b

In Figure 6.5, the Weibull b values are plotted as a function of impulsiveness parameter, ${h_t}^2/(H_{m0}L_{m-1,0})$, where h_t refers to the toe water depth, H_{m0} indicates the significant wave height at the structure, and $L_{m-1,0}$ represents the deep water wave length. The results reflected scattering, thus indicating that the Weibull b values did not vary with the variation of impulsiveness parameter for the tested impulsive and non-impulsive conditions.

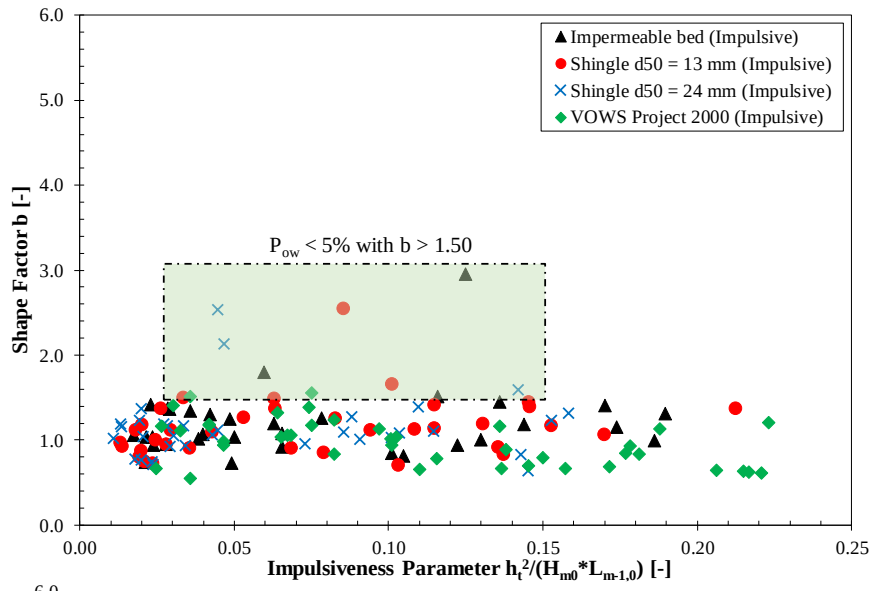

a.

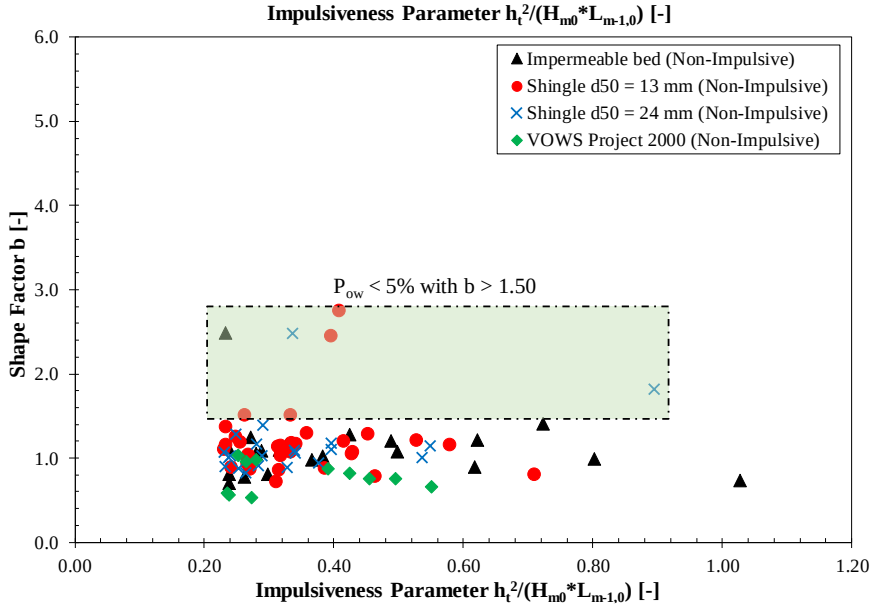

b.

Figure 6.5 Variation of Weibull b with impulsive parameter at plain vertical walls – a) Impulsive wave conditions, and b) Non-impulsive wave conditions

6.2.5 Influence of relative freeboard on Weibull b

The recent advancements on the distribution of wave by wave overtopping volumes revealed an influence of relative crest freeboard on the Weibull shape factor b for rubble mound and smooth sloping structures (see Hughes et al., 2012; Victor et al., 2012). In order to estimate the Weibull b values at smooth sloping structures, Hughes et al., (2012) established a correlation between shape factor b and relative freeboard (see Equation 6.1). For relatively steep low crested sloping structures, Victor et al., (2012) prescribed an empirical formula (see Equation 6.2) to estimate the shape factor as a function of relative freeboard and seaward slope. For vertical walls with relatively high freeboard under non-impulsive conditions, Equation 6.2 gave b = 0.56.

$$\mathrm{b} = \left[\exp\left(-0.6\frac{R_c}{H_{m0}}\right)\right]^{1.8} + 0.64 \tag{6.1}$$

$$\mathrm{b} = \exp\left[-2.0\frac{\mathrm{R_c}}{\mathrm{H_{m0}}}\right] + (0.56 + 0.15\cot\alpha) \tag{6.2}$$

Figure 6.6 portrays the effect of relative crest freeboard on the Weibull shape factor b under both impulsive and non-impulsive conditions. The data retrieved from the VOWS project are also presented in Figure 6.6. The existing empirical formulas for smooth sloping and rubble mound structures are displayed in Figure 6.6 to examine the implications of these formulations for vertical walls.

For both impulsive and non-impulsive wave attack, it is evident from the graphs that the data fairly adhered to the general trend of the prediction line, as reported by Hughes et al., (2012) for smooth sloping structures, particularly given the varied structural configurations. As mentioned previously, the exception is that some data were below 5% of the overtopping waves. The measured Weibull b values for plain vertical walls did not perfectly fit the predictions of Victor et al., (2012), subjected to impulsive and non-impulsive conditions. Nevertheless, based on the predictions reported by Victor et al., (2012), Equation 6.2 seemed inapplicable for impulsive wave attack at plain vertical walls.

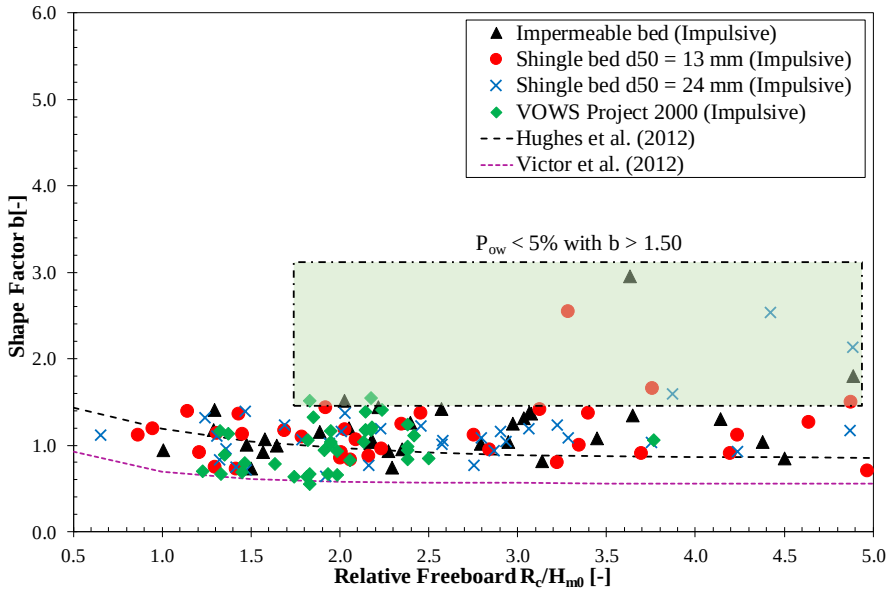

a.

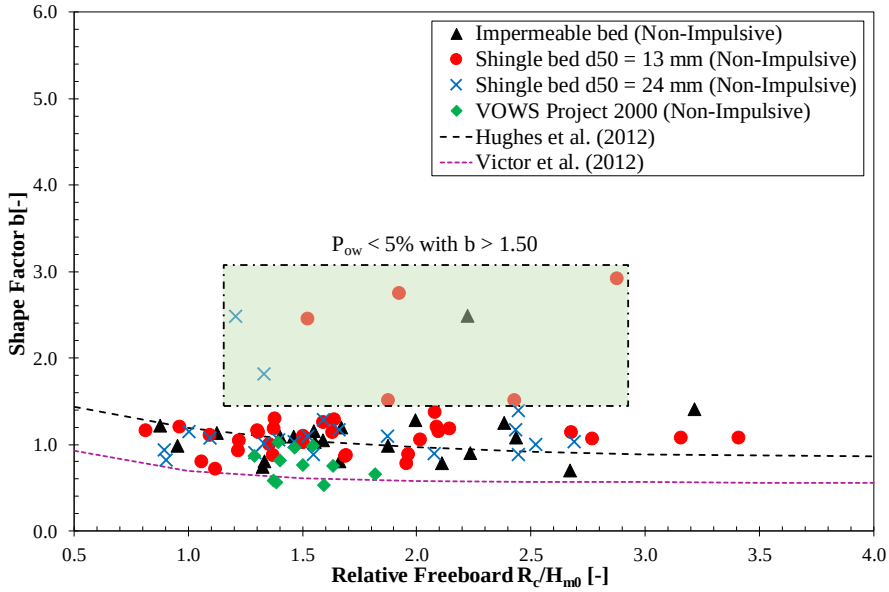

b.

Figure 6.6 Variation of Weibull b with relative freeboard at plain vertical walls – a) Impulsive wave conditions, and b) Non-impulsive wave conditions

6.2.6 Influence of relative toe water depth on Weibull b

Figure 6.7 illustrates the effect of the relative toe water depth (h_t/H_{m0}) on the observed Weibull b values for both impulsive and non-impulsive wave conditions. The observed Weibull b values did not vary with the variation of relative toe water depths for both permeable and impermeable bed configurations. Hence, one can conclude that there is no apparent influence of the relative toe water depths on the measured data points for the conditions tested.

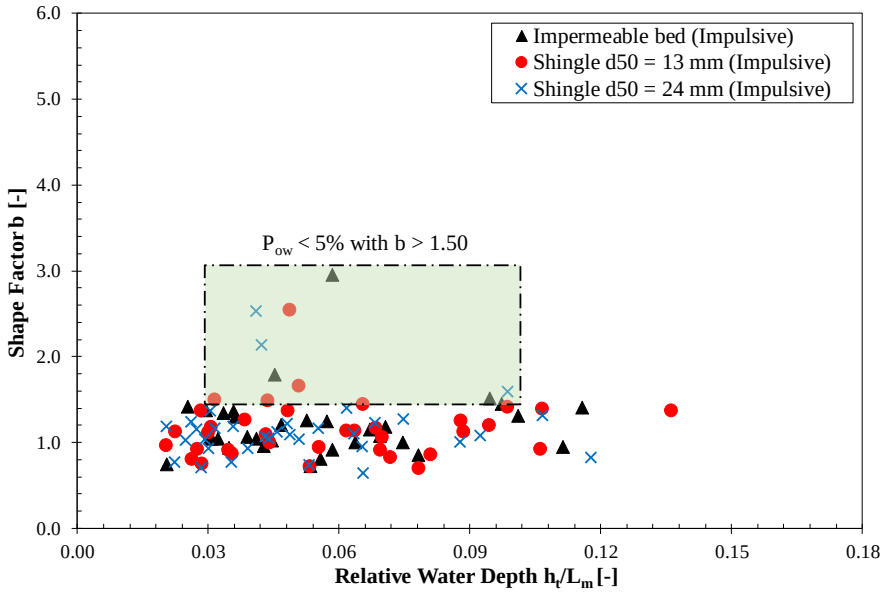

a.

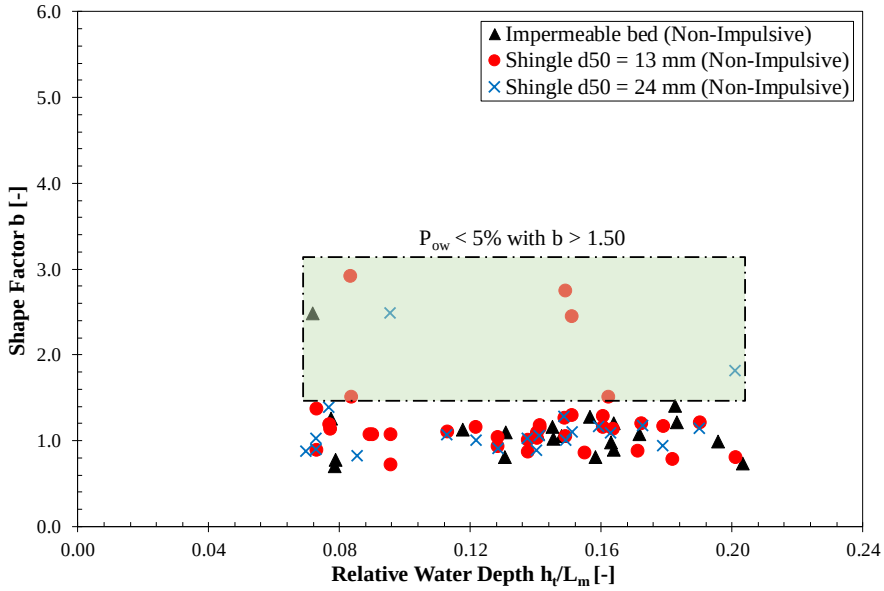

b.

Figure 6.7 Variation of Weibull b with relative toe water depth at plain vertical walls – a) Impulsive wave conditions, and b) Non-impulsive wave conditions

6.2.7 Influence of relative discharge on Weibull b

Zanuttigh et al., (2013) assessed the Weibull distribution of rubble mound and smooth structures, which showed that the shape parameter b can be well predicted by using relative discharge $q/(gH_{m0}T_{m-1,0})$, instead of relative freeboard; Equations 6.3 and 6.4 for smooth structures and rubble mound structures, respectively. These formulations were inserted into the new overtopping manual, EurOtop (2018), in order to estimate the shape factor b for both smooth and armoured structures.

$$b = 0.73 + 55\left(\frac{q}{gH_{m0}T_{m-1,0}}\right)^{0.8} \tag{6.3}$$

$$b = 0.85 + 1500\left(\frac{q}{gH_{m0}T_{m-1,0}}\right)^{1.3} \tag{6.4}$$

In Figure 6.8, the measured Weibull shape parameter b is expressed as a function of relative discharge $q/(gH_{m0}T_{m-1,0})$. The Weibull b values of the vertical walls of VOWS project are presented in Figure 6.8. The dashed lines signify the empirical predictions made by Zanuttigh et al., (2013) for smooth and rubble mound structures.

For impulsive wave conditions, the measured Weibull b values were slightly higher than that in the trend line (see Equation 6.4) reported by Zanuttigh et al. (2013). As observed in Figure 6.8 (a), Equation 6.4 demonstrates a conservative approach to predict the shape parameter for vertical breakwaters. Upon adapting the methodology prescribed by Zanuttigh et al., (2013), a new trend for plain vertical walls is proposed in this study using the data retrieved from measured Weibull b values and VOWS project (see Equation 6.5). The scatter data points that corresponded to low overtopping waves (below 5%) and higher Weibull b values were excluded from Equation 6.5.

For impulsive condition,

$$b = 0.92 + 1500\left(\frac{q}{gH_{m0}T_{m-1,0}}\right)^{1.2} \tag{6.5}$$

The results of non-impulsive wave attack displayed a good agreement with the predictions with relatively small scatter (see Figure 6.8(b)). Hence, the empirical relationship (see Equation 6.4) reported by Zanuttigh et al., (2013) can be applied to predict Weibull b values for plain vertical walls.

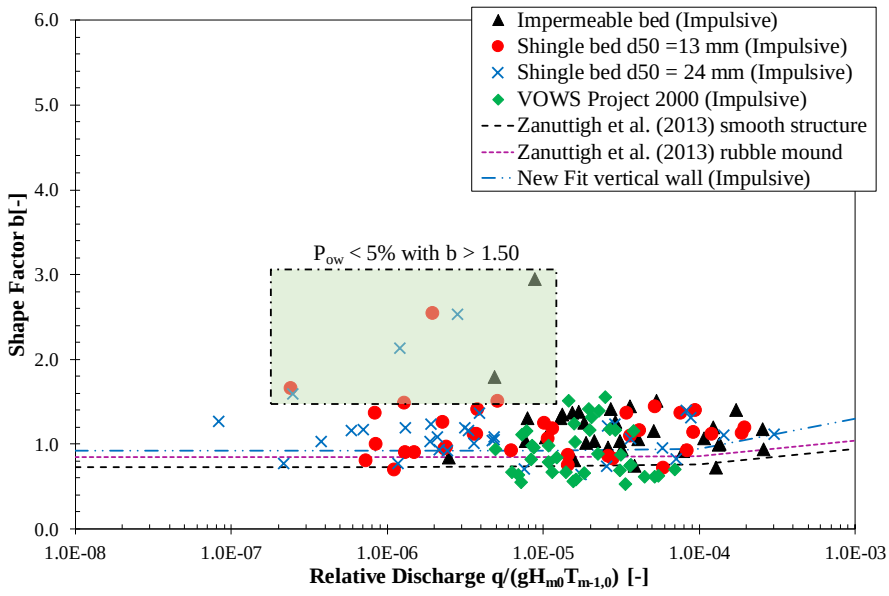

a.

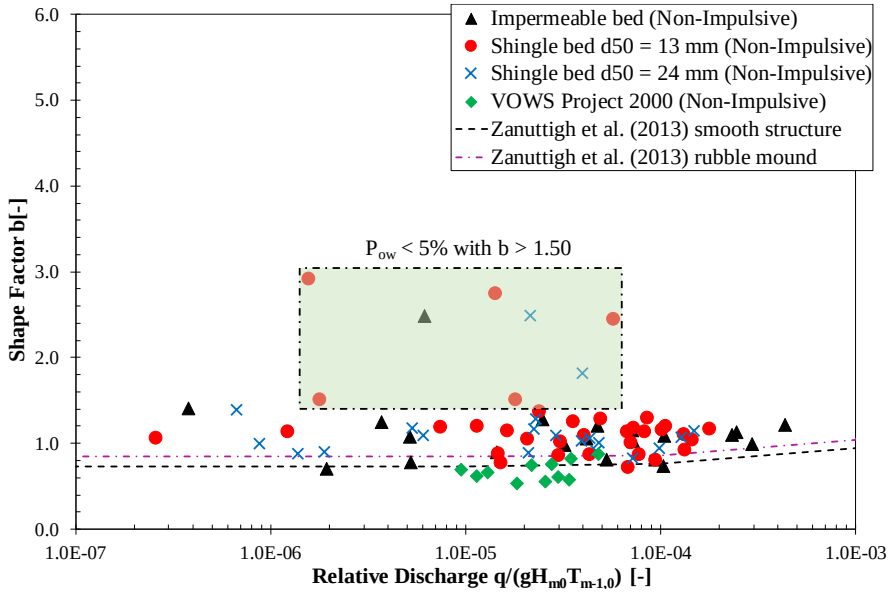

b.

Figure 6.8 Variation of Weibull b with relative discharge at plain vertical walls – a) Impulsive wave conditions, and b) Non-impulsive wave conditions

6.2.8 Implications for prediction of Weibull b at vertical walls

In order to estimate Weibull b at vertical walls with gravel foreshores, to date, there is relatively limited prediction guidance available in the literature. Considering an impermeable foreshore slope, EurOtop (2018) reported b = 0.85 for impulsive conditions, while b = 0.66 for wave steepness ($s_{m-1,0}$) of 0.02, and b = 0.82 for $s_{m-1,0}$ = 0.04 under non-impulsive conditions. As depicted in Section 6.2.3, no influence of wave steepness was noted on the measured Weibull b values for both impulsive and non-impulsive wave conditions.

In revising the prediction tools of Weibull b values at vertical walls, the test results were compared with the appropriate predictions reported in the literature (see Figures 6.4, 6.6, and 6.8). In order to quantify the reliability of the prediction formulae, error statistical indicators, such as scatter index (SI), Bias, and root mean square error (rmse), were calculated using the measured and estimated Weibull b values (see Equations 6.6-6.8). The SI values signified the relative scatter of the measured data points, while the Bias value represented the difference between the measured and estimated mean value, and the rmse values displayed the accuracy of the prediction formulae.

$$SI = \frac{1}{|\bar{X}|}\sqrt{\frac{1}{N_{test}}\sum_{n=1}^{N_{test}}[(b_{estimated})_n - (b_{measured})_n]^2} * 100 \tag{6.6}$$

$$Bias = \frac{1}{N_{test}}\sum_{n=1}^{N_{test}}[(b_{estimated})_n - (b_{measured})_n] \tag{6.7}$$

$$rmse = \sqrt{\frac{1}{N_{test}}\sum_{n=1}^{N_{test}}[(b_{measured})_n - (b_{estimated})_n]^2} \tag{6.8}$$

Where, N_{test} denotes the number of experimental data, $b_{measured}$ and $b_{estimated}$ are the measured and estimated Weibull b values respectively, and $\bar{X}$ denotes the average of $b_{measured}$ values.

For both permeable and impermeable bed configurations, the error measures of the formulae are presented in Table 6.1, subjected to impulsive conditions. As noted earlier in Figures 6.6(a) and Figure 6.8(b), it is evident that the measured data did not adhere to the predictions reported by Victor et al., (2012) (see Equation 6.2) and Zanuttigh et al., (2013) (see Equation 6.3) for sloping structures, thus excluded from being tabulated in Table 6.1.

Table 6.1 The error measures of empirical formulae for the prediction of Weibull b values at plain vertical walls under impulsive conditions

Error Indicator	Foreshore	Hughes et al. (2012) – Eqn. 6.1	Zanuttigh et al. (2013) – Eqn. 6.4	New Formula Eqn. 6.5
SI (%)	Impermeable	21.72	25.02	20.78
	d_{50} = 13 mm	24.50	28.68	22.76
	d_{50} = 24 mm	22.55	25.49	18.99
BIAS	Impermeable	-0.14	-0.22	-0.15
	d_{50} = 13 mm	-0.13	-0.24	-0.15
	d_{50} = 24 mm	-0.10	-0.20	-0.11
RMSE	Impermeable	0.26	0.30	0.25
	d_{50} = 13 mm	0.28	0.33	0.26
	d_{50} = 24 mm	0.26	0.29	0.22

Table 6.1 shows that the SI values of the proposed revised formulation (see Equation 6.5) were lower than those reported by Hughes et al., (2012) and Zanuttigh et al., (2013), indicating that the estimated values of the proposed formula are less scattered than the others. The Bias values tabulated in Table 6.1 show the similarity between the average absolute error by Hughes et al., (2012) and the new formulae, although the latter appear to be relatively lower than those reported by Zanuttigh et al., (2013). The negative Bias values in Table 6.1 certainly indicate that the prediction formulae provided underestimation of Weibull b values. Table 6.1 shows that for all the three bed configurations, the observed rmse values of the proposed equation are relatively lower than those reported in the others; signifying that the proposed formula offers a good fit with the measurements.

For the tested non-impulsive wave conditions, the error measures of the empirical formulae in predicting the Weibull b values at plain vertical walls are shown in Table 6.2. It is evident in Table 6.2 that both the formulae prescribed by Hughes et al., (2012) (see Equation 6.1), and Zanuttigh et al., (2013) (see Equation 6.4) succeeded in giving reliable predictions for shape parameter b values, which had been demonstrated by providing reasonably lower SI, Bias, and rmse values for both permeable and impermeable slopes. Table 6.2 also shows that the measured b values did not follow the predictions of those reported by Victor et al., (2012) (see Equation 6.2) for vertical walls under non-impulsive wave attack.

Table 6.2 The error measures of empirical formulae for the prediction of Weibull b values at plain vertical walls under non-impulsive conditions

Error Indicator	Foreshore	Hughes et al. (2012) – Eqn. 6.1	Victor et al. (2012) – Eqn. 6.2	Zanuttigh et al. (2013) – Eqn. 6.4
SI (%)	Impermeable	24.30	46.49	20.81
	d_{50} = 13 mm	16.69	42.34	23.63
	d_{50} = 24 mm	18.22	43.36	21.75
Bias	Impermeable	0.03	-0.29	-0.14
	d_{50} = 13 mm	-0.03	-0.53	-0.22
	d_{50} = 24 mm	-0.004	-0.28	-0.13
rmse	Impermeable	0.27	0.45	0.23
	d_{50} = 13 mm	0.21	0.52	0.29
	d_{50} = 24 mm	0.21	0.40	0.25

6.3 Sloping Structures

6.3.1 Weibull plot of individual overtopping volumes

In order to investigate the distribution of individual overtopping volumes at sloping walls, the measured wave-by-wave volumes for six test conditions are presented in Figures 6.9 and 6.10. For both impermeable and permeable bed configurations, Figures 6.9 and 6.10 portray the distribution of wave by wave volumes under storm wave attack and swell wave attack, respectively.

Based on Figures 6.9 and 6.10, it is obvious that the observed individual overtopping volumes displayed a linear trend in the Weibull plot, which indicated that the data points adhered to the two-parameter Weibull distribution for the tested conditions. However, for relatively smaller overtopping volumes in some cases, the measured data points revealed a slight deviation from the linear trend line. For example, for the impermeable foreshore slope with swell wave attack (see Figure 6.10a), the measured smaller overtopping volumes displayed some scatter characteristics with the linear trend line. This deviation occurred due to the limitation of overtopping measurement system in the calculation of relatively smaller overtopping volumes, which is beyond the measurement limit in this small-scale investigation. As mentioned earlier in Chapter 5, the sensitivity of the used load-cell in this present study had been limited to the measurement of 5-9 ml of overtopping volume. On this note, it is significant to report that in the distribution of overtopping volumes, the largest wave overtopping volumes are mainly emphasised by practitioners.

a.

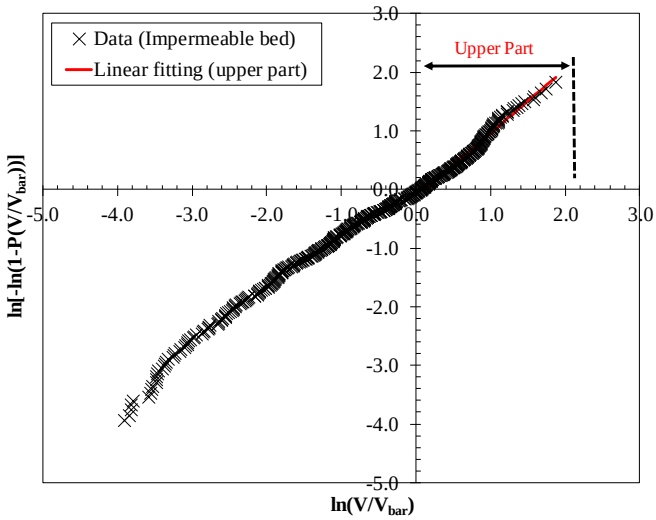

b.

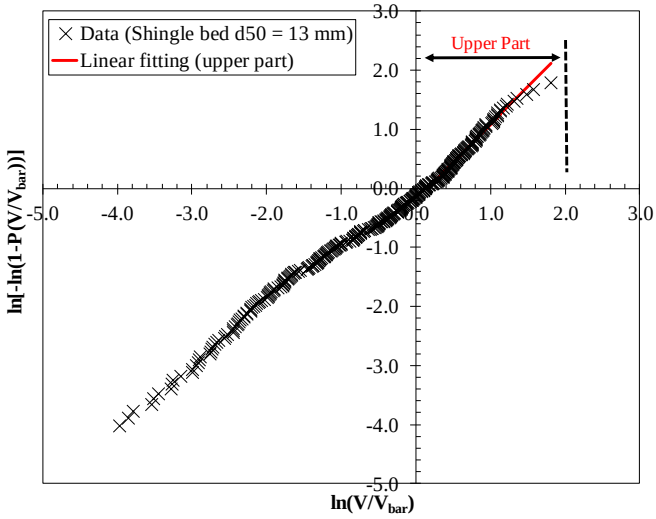

c.

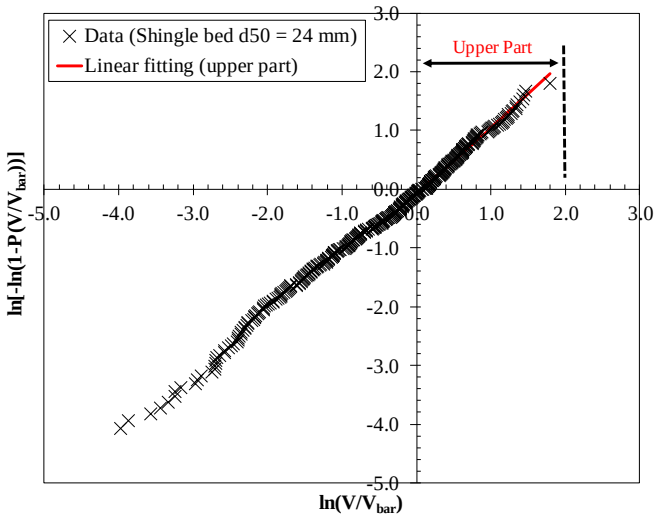

Figure 6.9 Weibull plot of measured wave by wave overtopping volumes at sloping structures for $s_{m-1,0}$ = 0.06, H_{m0} = 0.10 m - a) Impermeable bed b) Shingle bed d_{50} = 13 mm, and c) Shingle bed d_{50} = 24 mm

a.

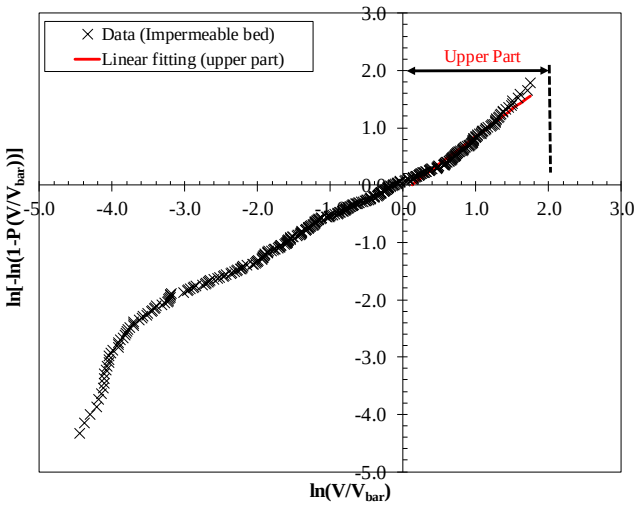

b.

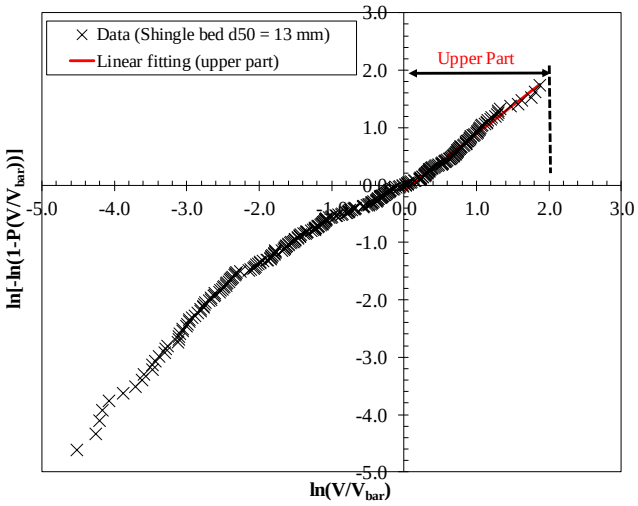

c.

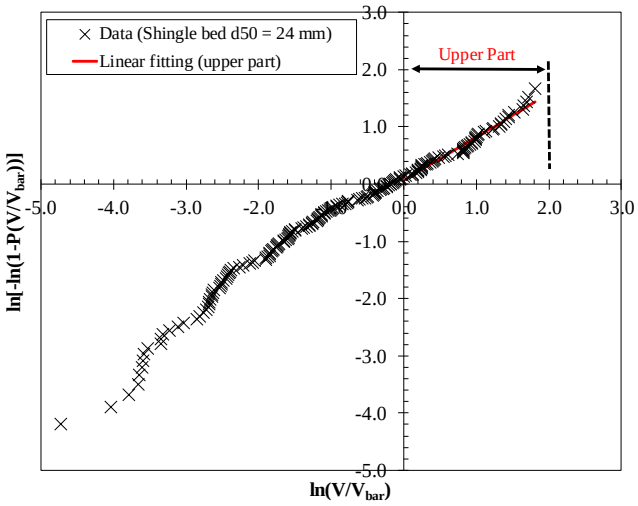

Figure 6.10 Weibull plot of wave by wave overtopping volumes at sloping structures for $s_{m-1,0}$ = 0.02, H_{m0} = 0.07 m - a) Impermeable bed b) Shingle bed d_{50} = 13 mm, and c) Shingle bed d_{50} = 24 mm

6.3.2 Influence of probability of overtopping waves on Weibull b

Figure 6.11 illustrates the correlation between Weibull b parameter and probability of overtopping waves. For the conditions tested in this study, the measured b values were varied from 0.50 to 1.40, except for some cases where higher b values were observed for relatively low overtopping waves (below 5% P_{ow}). Similar trend of Weibull b values with low overtopping waves was noted by Zanuttigh et al., (2013) for rubble mound and smooth sloping structures.

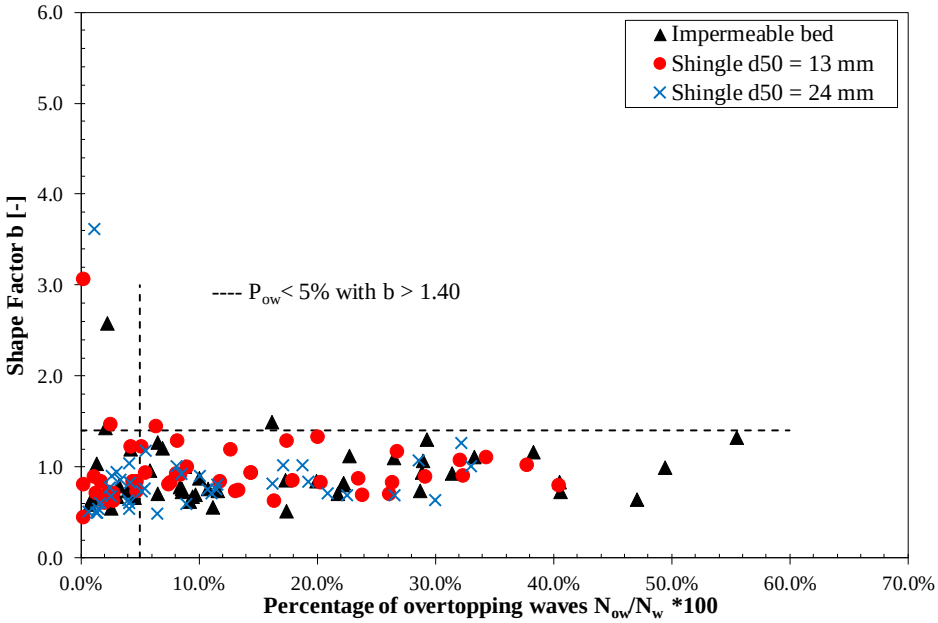

Figure 6.11 Variation of Weibull b values with percentage of overtopping waves at sloping structures

6.3.3 Influence of wave steepness on Weibull b

Besely (1999) asserted the presence of the influence of incident wave steepness on the shape parameter of Weibull distribution of sloping seawalls. The author recommended using Weibull b value of 0.76 for wave steepness of 0.02, while 0.92 for wave steepness of 0.04. On the contrary, based on extensive parametric studies, Bruce et al., (2009) concluded that no relationship is established between shape parameter b and incident wave steepness for armoured rubble mound breakwaters. Similar characteristics of Weibull b values were also reported by Victor et al., (2012) for steep low crested sloping structures.

Figure 6.12 illustrates the variation of shape factor b with incident wave steepness for the conditions tested in this present study. In Figure 6.10, the dashed line represents shape factor b (b = 0.76 for s_{op} = 0.02, and b = 0.92 for s_{op} = 0.04) for sloping seawalls, as prescribed by Besely (1999). One of the main conclusions from the graph is that the measured b values did not vary noticeably with the variation of wave steepness. This suggests that for the tested conditions, there was no apparent influence of incident wave steepness on the shape factor b of the Weibull distribution.

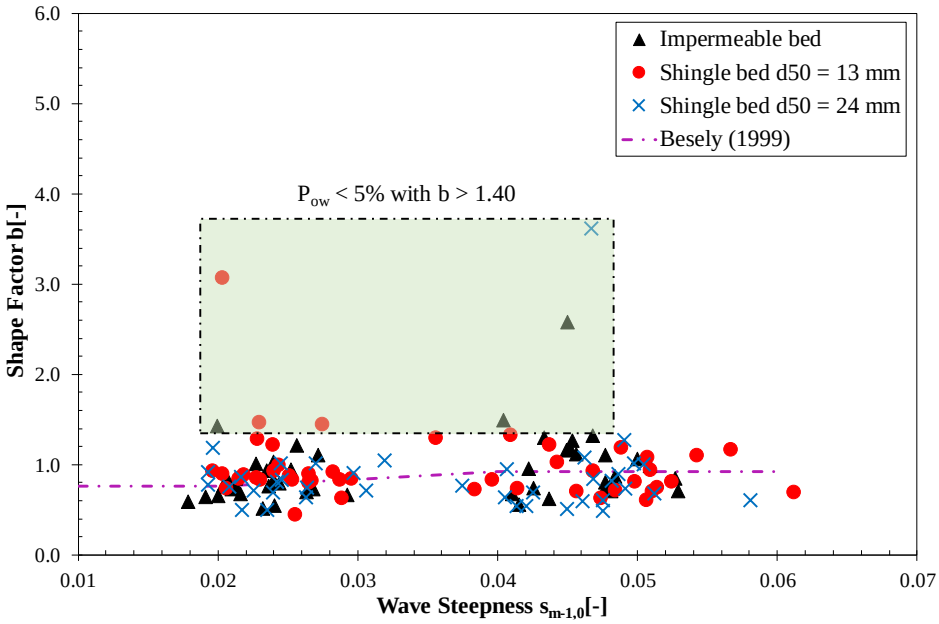

Figure 6.12 Variation of Weibull b with wave steepness at sloping structures

6.3.4 Influence of relative toe water depth on Weibull b

Figure 6.13 portrays the variation of shape factor b with relative toe water depth, h_t/L_m, in which h_t refers to water depth at the toe of the structure, while L_m is deep water wave length based on mean wave period, T_m. The graph reveals no stronger apparent link between Weibull b and relative water depth. For instance, based on the data points that corresponded to impermeable bed configurations, it is evident that the Weibull b values are fairly constant with varying relative toe water depths.

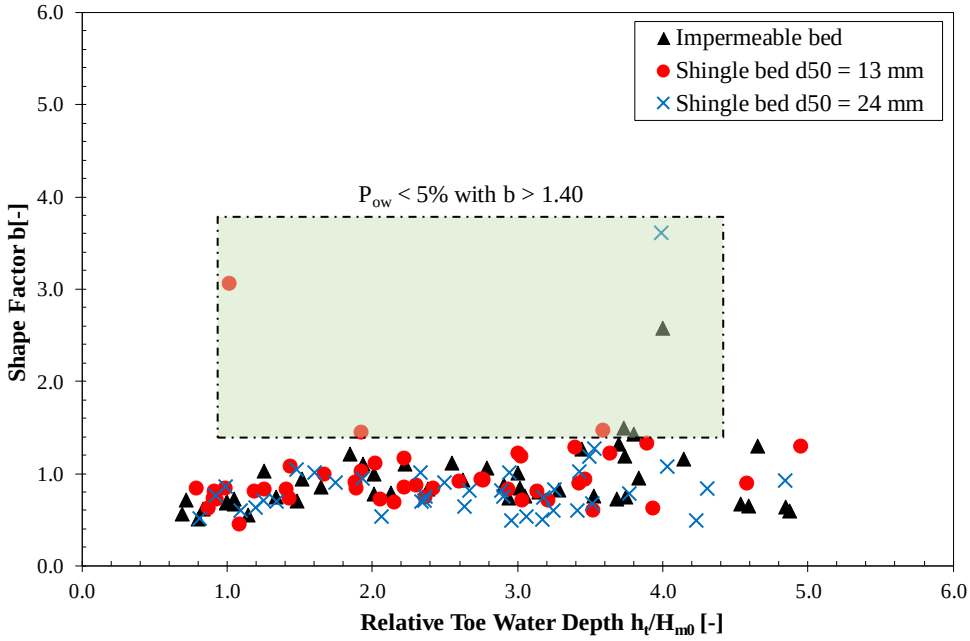

Figure 6.13 Variation of Weibull b with relative toe water depth at sloping structures

6.3.5 Influence of relative freeboard on Weibull b

In order to observe the influence of relative freeboard on the shape parameter of Weibull distribution of the individual volumes, the measured shape factor b values are plotted as a function of relative freeboard in Figure 6.11. The graph compares the resulting Weibull b values with the empirical prediction (see Equations 6.1-6.2) reported by Hughes et al., (2012) and Victor et al., (2012) for the tested conditions. It is certainly noticeable from the graph that the measured b values increased with the decrease of relative freeboard. Similar characteristics of Weibull values with respect to relative freeboard were also reported by Hughes et al., (2012) and Victor et al., (2012). For both impermeable and permeable beach configurations, the measured data points display a good agreement with the empirical predictions reported by Hughes et al., (2012) and Victor et al., (2012).

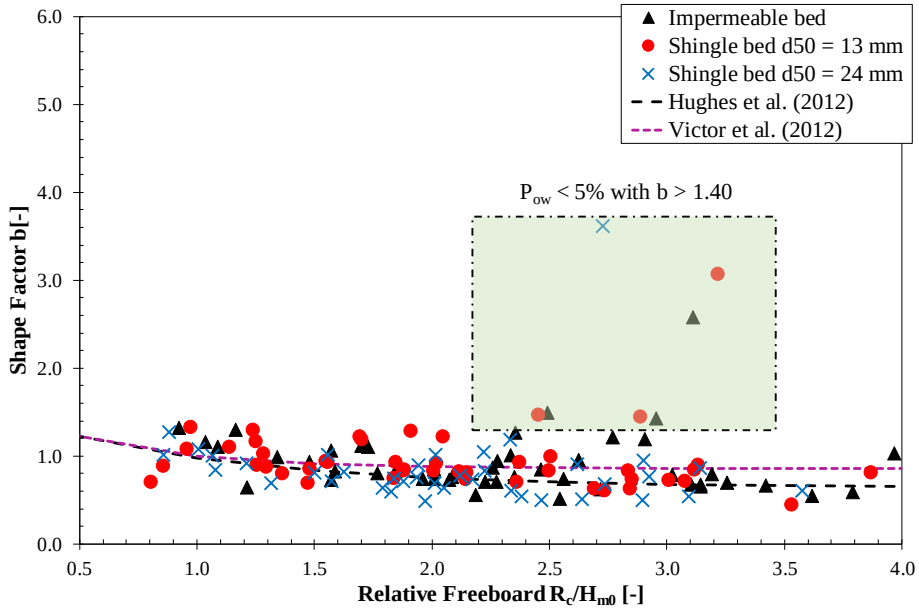

Figure 6. 14 Variation of measured b values with relative freeboard at sloping structures

6.3.6 Influence of relative discharge on Weibull b

Figure 6.15 illustrates the measured shape parameter b as a function of the relative discharge for both impermeable and permeable foreshore configurations. The dashed lines signify the empirical shape parameter predictions reported by Zanuttigh et al., (2013) for smooth and rubble mound structures using Equations 6.3 and 6.4.

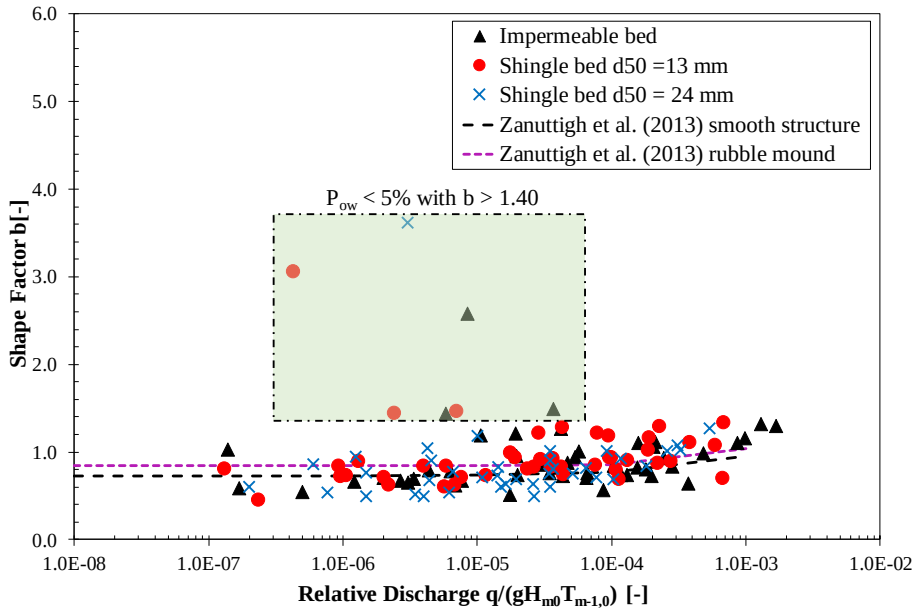

Figure 6.15 Variation of measured b values with relative overtopping discharge at sloping structures

The data in Figure 6.15 present that the measured data are consistent with the findings reported by Zanuttigh et al., (2013) for smooth and rubble mound structures, which certainly validates the findings of the latter. Nonetheless, the predictions given by Zanuttigh et al., (2013) for sloping structures (see Equation 6.3) were mainly based on the measurements at a 1 in 1.5 sloping structure on impermeable bed. As expected, it can be observed in Figure 6.15 that Equation 6.3 performed slightly better for impermeable bed configuration than permeable slopes.

6.3.7 Implications for prediction of Weibull b at sloping walls

In Table 6.3, the error measures of the existing empirical formulae in estimating Weibull b values at smooth sloping walls are presented. It can be seen in Table 6.3 that the overall values of the error indicators were relatively low for the tested conditions in this present study. For instance, the rmse values in Table 6.3 ranged from 0.15 to 0.22, despite the varied structural configurations, thus indicating that the predictions with the use of relative freeboard displayed an encouraging trend with the measurements. Hence, it is evident that the empirical prediction formulae used in this study portrayed an overall good agreement with the measured data points for both permeable and impermeable bed configurations.

The table also shows that the predictions (see Equations 6.3 and 6.4) by Zanuttigh et al., (2013) slightly improved in forecasting the Weibull b values, when compared to those reported by Hughes et al., (2012) and Victor et al., (2012).

Table 6.3 The error statistics of empirical formulae for the prediction of Weibull b values at sloping structures

Error Indicator	Foreshore	Hughes et al. (2012) – Eqn. 6.1	Victor et al. (2012) – Eqn. 6.2	Zanuttigh et al. (2013) – Eqn. 6.3	Zanuttigh et al. (2013) – Eqn. 6.4
SI (%)	Impermeable	25.03	21.72	20.45	20.39
	d_{50} = 13 mm	20.56	18.60	21.85	18.81
	d_{50} = 24 mm	17.90	22.20	19.80	21.52
BIAS	Impermeable	-0.110	0.010	-0.070	0.009
	d_{50} = 13 mm	-0.068	-0.002	-0.089	-0.026
	d_{50} = 24 mm	-0.005	0.093	-0.030	0.060
RMSE	Impermeable	0.22	0.19	0.18	0.18
	d_{50} = 13 mm	0.18	0.17	0.20	0.17
	d_{50} = 24 mm	0.15	0.19	0.17	0.18

6.4 Influence of permeable foreshores on the distribution of wave by wave volumes

6.4.1 Plain vertical walls

In Figure 6.16, the Weibull distributions of measured individual overtopping volumes for both impermeable and permeable foreshores are presented for a certain incident wave condition. The graph (see Figure 6.16) demonstrates no apparent effect of permeable foreshores on the distribution of the largest wave by wave overtopping volumes. For instance, the upper part of the distribution indicated higher overtopping volumes, while no obvious variation in the distribution of overtopping volumes for the tested three foreshores, despite the varying bed configurations. Nevertheless, when comparing the distributions of smaller overtopping volumes (lower part of the distribution) for impermeable and permeable foreshores, the data points that corresponded to impermeable foreshores were somewhat higher than those recorded for permeable ones.

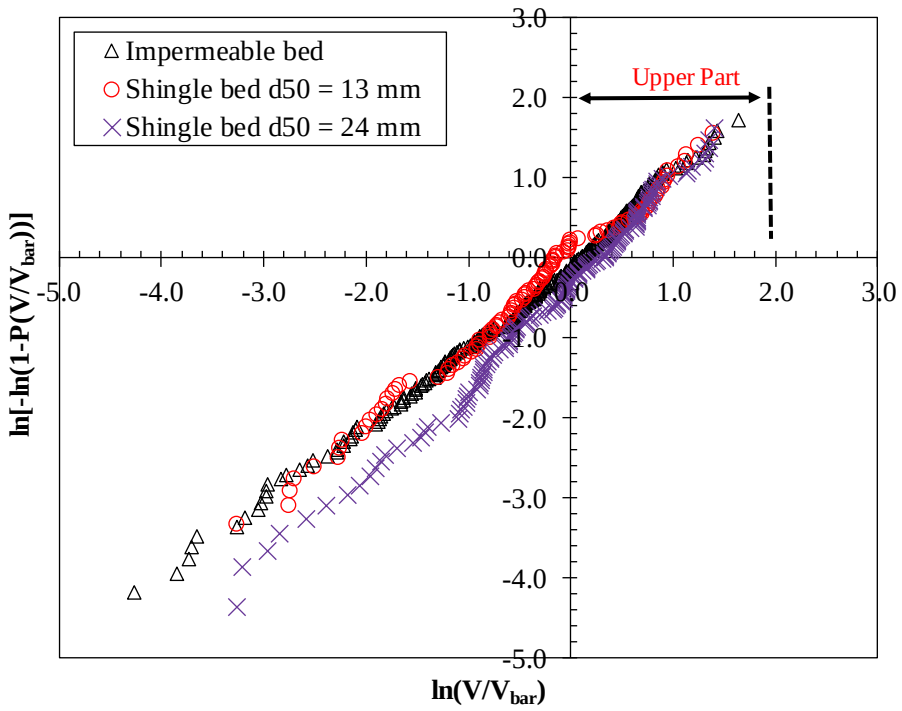

Figure 6.16 Variation of wave by wave volumes at plain vertical walls with different bed configurations for an incident significant wave height (H_{m0}) of 0.10 m with a wave steepness ($s_{m-1,0}$) of 0.06

Next, in observing the influence of permeable foreshores on the maximum wave by wave volumes, the cumulative overtopping volumes for both impermeable and permeable configurations were plotted against the number of overtopping waves, as given in Figures 6.17(a) and 6.17(b) for high and low wave steepness, respectively. Based on Figure 6.16, the impermeable slope clearly gave the largest cumulative overtopping volume, along with the greatest number of overtopping waves. This is especially when comparing the test results for permeable foreshores with those of impermeable foreshore for a certain wave condition. For example, in Figure 6.17(a), it is evident that for the same incident wave condition, the test on impermeable foreshore gave the greatest number of proportion of overtopping waves at 32%, and subsequently, the largest cumulative overtopping volume of 239 (l/m), when compared to those observed for permeable bed configuration.

a.

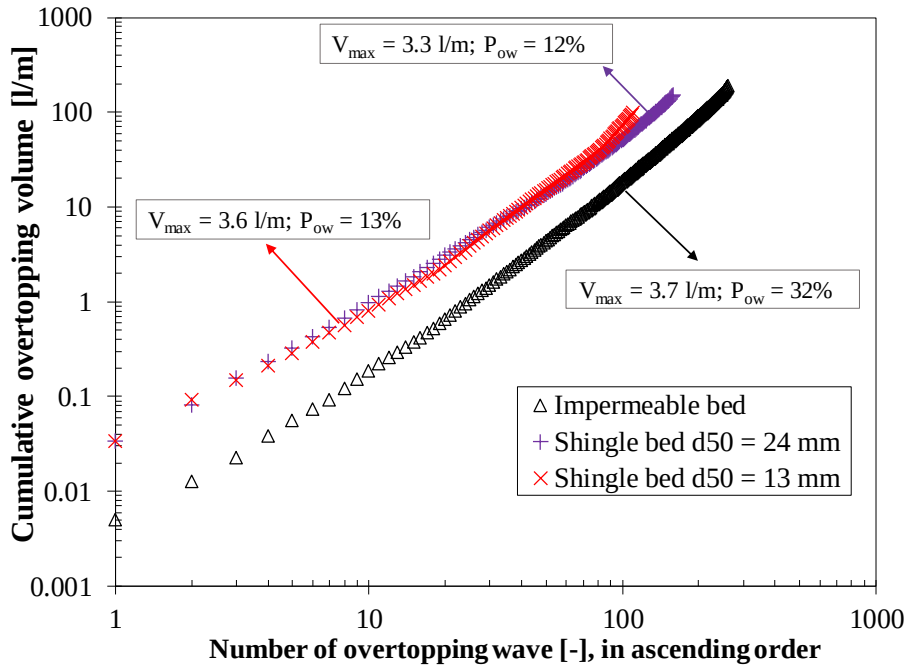

b.

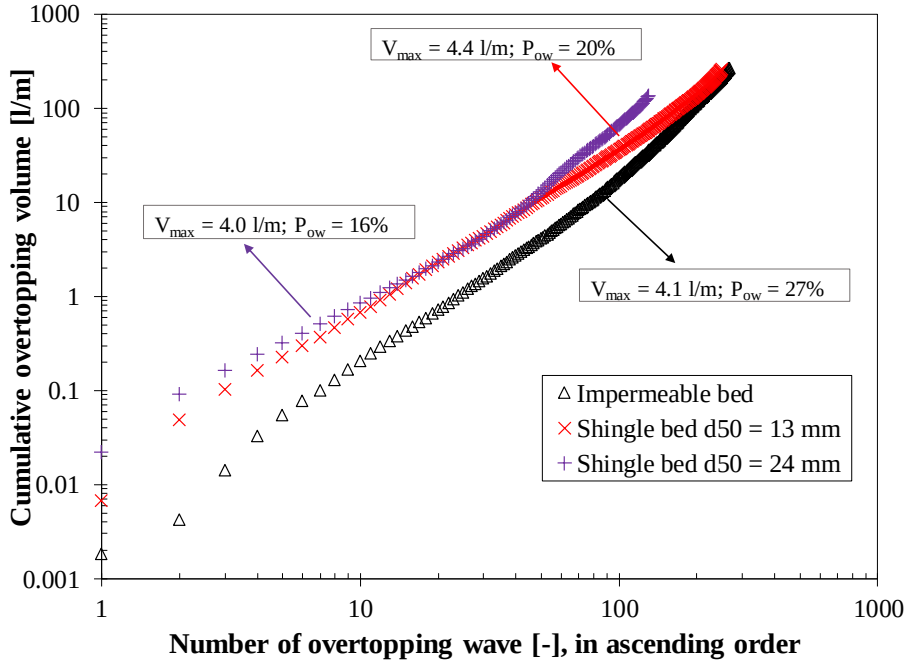

Figure 6.17 Cumulative wave overtopping volumes against number of overtopping waves at plain vertical walls with both impermeable and permeable foreshore configurations a) $s_{m-1,0} = 0.06$, $H_{m0} = 0.10$ m, and b) $s_{m-1,0} = 0.02$, $H_{m0} = 0.07$ m

When comparing the resulting maximum individual overtopping volumes for permeable slopes with impermeable slope for a certain wave condition, the measured V_{max} for shingle foreshores did not differ from those observed for impermeable ones. For instance, Figure 6.17(a) shows that the V_{max} was approximately 3.7 (litre per m) for impermeable foreshore, which is similar to those reported for shingle foreshores, which were about 3.6 (litre per m) and 3.1 (litre per m) for shingle bed d_{50} of 13 mm and 24 mm, respectively. Based on the test results depicted in Figure 6.17, it appears that shingle beaches gave lower wave overtopping events, and subsequently, lower average overtopping volumes, but individual overtopping volumes as big as those of impermeable slopes.

6.4.2 Sloping structures

Figure 6.18 compares the influence of permeable foreshore on the distribution of wave-by-wave overtopping volumes, which demonstrated the Weibull plot for the tested foreshores for a certain incident wave condition.

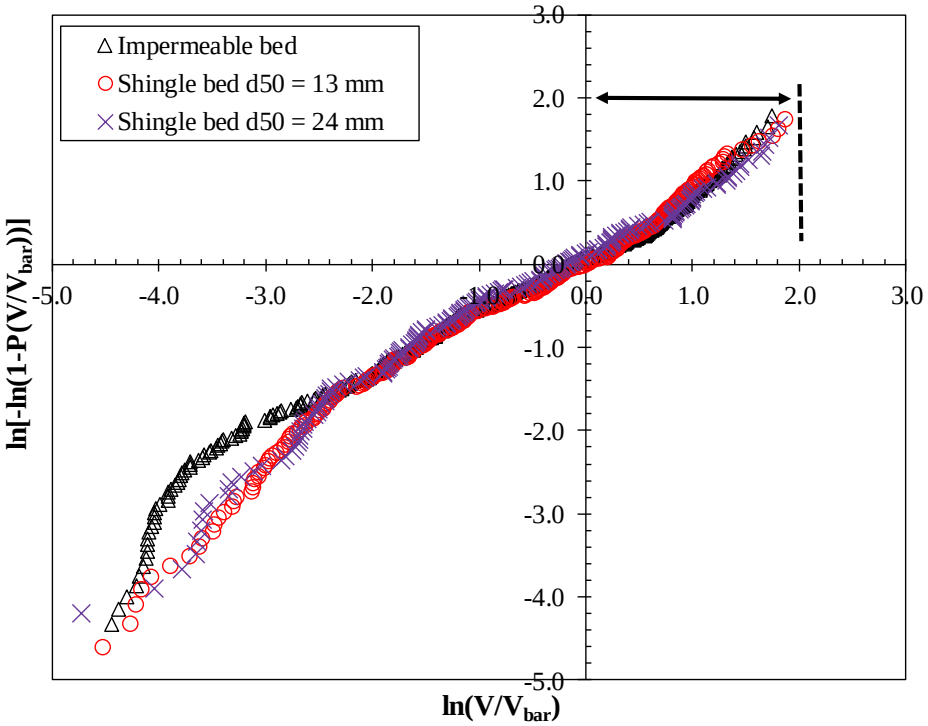

Figure 6.18 Variation of wave by wave volumes at sloping structures with different bed configurations for an incident significant wave height (H_{m0}) of 0.06 m with wave steepness ($s_{m-1,0}$) of 0.02

In Figure 6.18, the distributions of higher overtopping volumes for different bed configurations appear to be very similar to each other, thus signifying no obvious influence of gravel foreshore configurations on the Weibull distribution of overtopping volumes at sloping walls. For example, in the case of extreme tail of the distribution (upper portion of the Weibull plot in Figure 6.18), the data points, which clearly corresponded to both impermeable and permeable slopes, were almost on top of each other, thus indicating very limited influence of the permeable slopes on the distribution of higher wave-by-wave overtopping volumes. However, in Figure 6.18, if we look at the lower part of the distribution that denotes the relatively smaller overtopping volumes, the resulting overtopping volumes of the impermeable foreshore seemed to be slightly higher than those observed for permeable slopes.

In Figure 6.19, correlations between the overtopping wave volumes and the number of overtopping waves for both impermeable and shingle beds are presented. Figure 6.19(a) compares the cumulative overtopping volumes for various foreshore configurations subjected to an incident wave height (H_{m0}) of 0.10 m with relatively high wave steepness ($s_{m-1,0}$) of 0.06, while Figure 6.19(b) represents a comparatively low wave steepness ($s_{m-1,0}$) of 0.02 with an incident wave height (H_{m0}) of 0.08 m. One of the main conclusions from the graphs is that the impermeable foreshore gave a reasonably higher number of overtopping waves, when compared to the shingle foreshores for the same wave condition. For instance, the data points corresponding to impermeable bed in Figure 6.19(a) represent around 49% of the overtopping waves, while shingle bed d_{50} of 13 mm and d_{50} of 24 mm resulted in approximately 33% and 32%, respectively.

Nevertheless, the maximum wave by wave overtopping volumes on gravel beds, overall, did not differ noticeably from those reported on impermeable beach configuration. For instance, Figure 6.19(a) shows the maximum individual overtopping volume of 3.0 litres per m width is for solid impermeable foreshore, whereas 2.9 litres per m width is for shingle bed d_{50} of 13 mm. Similar characteristics of V_{max} can be also noted in Figure 6.19(b) for experiments that involved relatively low wave steepness.

a.

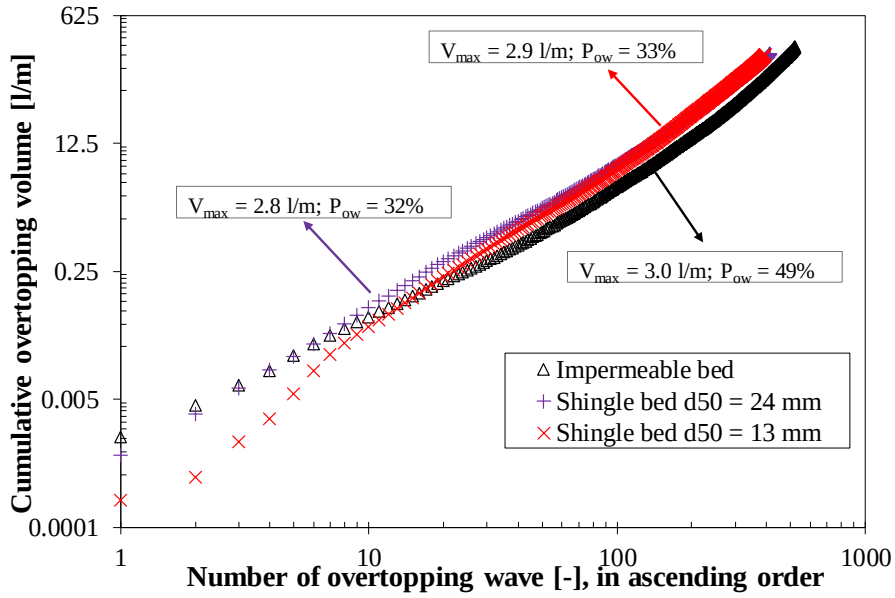

b.

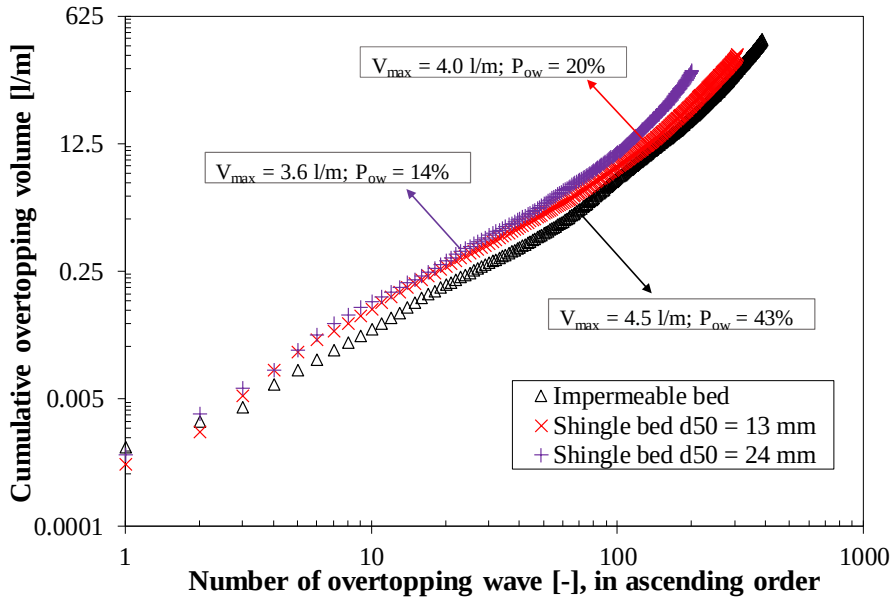

Figure 6.19 Cumulative wave overtopping volumes against number of overtopping waves at sloping structures with both impermeable and permeable foreshore configurations a) $s_{m-1,0} = 0.06$, $H_{m0} = 0.10$ m, and b) $s_{m-1,0} = 0.02$, $H_{m0} = 0.08$ m

This certainly indicates that permeable shingle beaches had less wave overtopping events, hence lower mean overtopping discharges, but wave by wave overtopping volumes as huge as those observed for impermeable beaches. The characteristics of wave-by-wave volumes appeared to be random in nature, thus poses a challenge for prediction in reality. The recently

published EurOtop manual (EurOtop 2018) also emphasised on the influence of individual overtopping volumes on the tolerable overtopping discharges, which prescribed to consider both mean overtopping rate and maximum overtopping volume to identify the tolerable limits for safety and security under extreme wave overtopping events. Thus, a relatively conservative prediction of maximum individual overtopping volumes at sloping walls with permeable shingle beaches is recommended, such as the predictions prescribed by EurOtop (2018) considering a solid foreshore slope.

6.5 Summary

To date, most parametric studies on wave by wave overtopping volumes cited in scientific literature have focused on structures with impermeable foreshores, but leaving investigations on permeable beaches in scarcity. This knowledge gap is addressed in this chapter, which presents the resulting distributions of individual wave by wave overtopping volumes, as well as its comparison with empirical predictions to identify the variances in permeable and impermeable foreshore characteristics.

For both vertical and sloping structures, when comparing the Weibull distribution of permeable slopes with impermeable slopes, no obvious influence was noted for permeable foreshore in the distribution of wave by wave overtopping volumes. Similar characteristics were reported for maximum wave by wave volumes, when the measured data of permeable bed configurations and the impermeable foreshores were compared for the same wave condition.

The variation of the measured Weibull b values in light of various parameters, including percentage of overtopping waves, wave steepness, relative freeboard, relative toe water depth, and relative discharge, had been investigated. It is evident that the predictions of shape parameter b values can be well-described with relative discharge and crest freeboard. For both permeable and impermeable foreshore configurations, the error measures of the existing empirical formulae in predicting Weibull b values at structures (i.e. vertical walls and sloping walls) have been elaborated to determine the reliability of the predictions.

CHAPTER 7

Conclusions and Recommendations

7.1 Synopsis

This chapter presents the main conclusions from the experimental research undertaken in this study, including the scale and model effects on the experiments and the recommendations proposed for further investigation. Section 7.2 discusses the key conclusions drawn from this work, which is then followed by Section 7.3, which reports on the probable scale and model effects on the outputs of the small-scale model tests. Lastly, the chapter concludes by proposing recommendations to extend the nature and scope of this work.

7.2 Conclusions

The purpose of this experimental research was to extend the existing empirical predictions of wave overtopping and toe scouring at sea defences concerning permeable gravel foreshores. The extension that is presented in this research includes a comprehensive study on the overtopping and scouring characteristics at two different sea defences (i.e. a vertical seawall and sloping structure), performed on both impermeable and permeable foreshore slopes.

Detailed measurements were taken to parameterise the mean overtopping rate, mean sediment rate, individual overtopping volume, probability of overtopping and, scour depths on a plain vertical seawall and a 1 in 2 sloping structure, for both impermeable and permeable shingle beach configurations. The resulting overtopping and scouring characteristics at the structures for both impermeable and permeable gravel foreshore configurations were then compared with existing empirical formulations from the literature to determine the differences in permeable and impermeable foreshore characteristics.

Accordingly, based on the analysis and observations of the results of this research, the following conclusions are presented:

7.2.1 Plain vertical walls

— Within the experimental limitations of this study, the resulting overtopping characteristics corresponded to the impermeable bed, showed an overall good agreement with the predictive method of EurOtop (2018) under both impulsive and non-impulsive wave conditions.

— For the impulsive wave conditions tested within this study, it was observed that the dimensionless mean overtopping rate was reduced by factors 3 and 4 for d_{50} of 13 mm and 24 mm respectively when the impermeable and shingle beaches were compared. For non-impulsive waves, the reduction factors were 1.5 for d_{50} of 13 mm and 2 for d_{50} of 24 mm.

— For non-impulsive and impulsive waves with conditions in the range, $(h_t^2/(H_{m0}L_{m-1,0}) > 0.03)$, no sediment was reported to pass the crest of the structure. Under impulsive conditions, in the range of $h_t^2/(H_{m0}L_{m-1,0}) < 0.03$, the measured volume of sediment passing the crest of the seawall was found to be around 0.5% of the total volume of the overtopped water.

— Overall, the maximum individual overtopping wave volumes measured for the shingle foreshores did not noticeably differ from those measured for the impermeable slopes.

— The measured probability of overtopping waves for the gravel beach configurations was also lower compared to the impermeable beach configuration. Here, it was reported that the shingle beach was more ‘efficient’ in reducing the number of overtopping waves, and consequently, resulting in mean overtopping discharge rates.

— When comparing the Weibull distribution of wave by wave overtopping volumes for permeable slopes with the impermeable slopes, it was observed that there was no apparent influence of the permeable foreshore in the distribution of wave by wave overtopping volumes.

— For both the permeable and impermeable slopes, it was apparent that the predictions of Weibull shape parameter b values could be well described with relative discharge and with relative crest freeboard.

— For the tested conditions, it was shown that the relative toe scour depth at a plain vertical wall on a shingle beach, was influenced by the relative toe water depth and Iribarren number. For relative toe water depths in the range of $0.016 \leq h_t/L_m \leq 0.18$, similar characteristics were reported by Sutherland et al. (2006) on sandy beaches.

— Maximum scour depths were reported for spilling and plunging wave conditions ($0.005 \leq h_t/L_m \leq 0.04$). Also, peak accretion was observed $S_t/H_{1/3}$ = 1.60 along with peak erosion reported $S_t/H_{1/3}$ = 0.95 at a relative toe water depth of (h_t/L_m), around 0.025.

7.2.2 Sloping structure

— The measured baseline overtopping characteristics corresponding to the impermeable beach configuration (control condition) correlated well with the existing predictions for the tested conditions.

— The results on the mean overtopping discharge revealed that the overtopping was reduced for the permeable slopes in comparison to the impermeable slopes. A reduction factor of 3.0 and 4.0 was reported for the gravel bed, d_{50} (prototype) of 13 mm and d_{50} of 24 mm respectively.

— The measured volume of the overtopped sediment passed the parapet of the sloping structure was ranged between 0.20 and 1% of the volume of overtopped water for the tested shingle bed configurations.

— For the tested conditions, the measured proportion of waves was reduced by an average of 50% for relative freeboards of 1.0 to 2.0 compared with the empirical predictions whereas an average reduction of 75% was observed for relative freeboards of 2.0 to 3.5.

— The measured values of the wave by wave and maximum overtopping volumes for shingle beaches were to some extent similar (within a factor of 2) to those measured for the impermeable slopes. As such, this indicates that there was no obvious influence of gravel foreshore configurations on the Weibull distribution of overtopping volumes as well as on the maximum individual overtopping volumes for the conditions tested within this study.

— It was also evident that there was no apparent effect of the permeable foreshore on the Weibull distribution of wave by wave overtopping volumes

when the Weibull distribution of permeable bed configurations and the impermeable foreshores were compared for the same wave condition.

— For both the permeable and impermeable bed configurations, the measured Weibull b values overall showed a good agreement with the predictions of Hughes et al. (2012), Victor et al. (2012) and Zanuttigh et al. (2013), indicating that the Weibull b parameter had a strong correlation with the relative crest freeboard along with the relative overtopping discharge.

— The results of this study found that the relative toe scour depth at a sloping structure on a shingle beach was strongly influenced by the relative toe water depth and Iribarren number.

— The peak toe scour depths were observed for the experiments undergoing spilling and plunging wave attack. For the tested conditions, the maximum erosion at the toe of the structure was observed as $S_t/H_{1/3} = 0.93$ at a relative toe water depth (h_t/L_m) of around 0.01, and the maximum accretion was noted as $S_t/H_{1/3} = 1.51$ at a relative toe water depth (h_t/L_m) of about 0.03.

— It was revealed that the scour depths at sloping walls did not differ compared to those reported at vertical walls for same beach configurations and incident wave conditions. As such, this indicates that scour depths are independent of the slope of the structure.

Before conducting this study, limited design guidance was available to predict the mean overtopping discharges and mean sediment rates at vertical seawalls and sloping structures on permeable shingle foreshores. Therefore, a new set of prediction formulae (adapted from EurOtop, 2018) are proposed in this study, based on the new laboratory test results, and a comparison with available prediction methods found in the literature. These are intended for practitioners and researchers in predicting wave overtopping characteristics at sea defence structures having permeable gravel foreshores.

7.3 Scale and Model Effects

A wide range of experiments was conducted in this study to inspect the overtopping and scouring characteristics at a plain vertical wall and a smooth sloping structure on impermeable and permeable gravel foreshores and to provide preliminary guidelines for the prediction of these coastal processes at full-scale. Although the outputs from small scale model tests could be distorted by scale and model effects.

Generally, in the investigation of overtopping processes, Pearson et al. (2002) reported that the 'scale' and 'model' effects in the two-dimensional wave flume physical experiments showed no discernible differences in comparison to large-scale laboratory measurements for impermeable configurations (e.g. vertical walls). Moreover, Victor and Troch (2012) concluded that for smooth impermeable sloping structures, the influence of 'scale' effects is considered to be minimal in the wave overtopping measurements.

Furthermore, to keep the scale effects minimal, the experimental set up was complimented by adapting the well-established guidelines of EurOtop (2018), Powell (1990) and Wolters et al. (2009) for typical two-dimensional experimental investigations. Here, the tested significant wave heights were varied between 50 mm and 160 mm, which were higher compared to the minimum wave heights of 30 mm as suggested by Wolters et al. (2009) to avoid 'scale' effects in the measurements.

To minimise the model effects by mitigating the reflection from the model boundaries, an active wave reflection system was applied. In addition, tests were complemented without the existence of any structure (bare flume) in the wave channel to validate the inshore wave conditions.

Notwithstanding, the measured incident wave conditions within this study overall followed the Rayleigh distribution at deep-water, as discussed in Chapters 4 and 5 of this study. For both structural configurations (e.g. a plain vertical wall and sloping structure), the resulting overtopping characteristics from the benchmark experiments (impermeable foreshore) showed a good agreement with the empirical prediction of EurOtop (2018). Furthermore, it

was also observed that the distribution of wave by wave volumes followed the two-parameter Weibull distribution for the tested conditions covered within this study.

Accordingly, the characteristics of the measurements of this study discussed above indicate that the 'scale' and 'model' effects in small scale physical tests are not significant. Additionally, when combined with all the necessary steps taken, while designing and performing the physical model experiments to avoid the 'scale' and 'model' effects, it is anticipated that the proposed revised prediction methods from this two-dimensional experimental research study, would be applicable at prototype conditions having minimal 'scale' and 'model' effects, even though further validation of the dataset would be desirable.

7.4 Further Work

This research investigated the influence of the permeable foreshore on the wave overtopping and scouring characteristics at sea defences, (e.g. a plain vertical structure and smooth sloping structure through performing comprehensive experimental investigations which were then compared with existing empirical predictions available in the literature). Even though the experimental set up was complimented by adapting the well-established guidelines of EurOtop (2018), Powell (1990) and Wolters et al. (2009) for typical wave flume investigations, to extend the scope of the work several opportunities are proposed for further investigation, as presented below:

— Due to the experimental limitations of this study, only limited experiments were conducted for the cases of small relative freeboards (R_c/H_{m0} < 0.80) for both structural configurations, (e.g. a vertical wall and sloping structure). Therefore, the prediction guidance derived from this study for the wave overtopping at sea defences with permeable foreshores is only valid for those freeboards. As such, further investigations should be undertaken for the cases of small to zero relative freeboards, to extend the dataset of the overtopping characteristics of permeable foreshores.

— For the tested conditions on the smooth sloping structure, the resulting incident wave conditions were predominantly non-breaking or surging waves ($\xi_{m-1,0} > \sim 2$). Accordingly, the derived prediction formulae for overtopping processes at sloping structures are limited to non-breaking wave conditions only. Notably, waves on smooth 1 in 2 impermeable slopes are more likely to be non-breaking waves with extreme overtopping events. Accordingly, further tests could be undertaken by focussing on the breaking wave conditions in order to identify the potential effects of such conditions on overtopping processes.

— Adopting the approach of typical wave flume investigations, all experiments performed within this study were based on the wave attack from one direction only, (i.e. perpendicular to the structure). However, the wave overtopping characteristics at sea defences can be influenced by the presence of bimodal wave conditions with the wave attack from different angles (Van der Werf and Van Gent, 2018; EurOtop, 2018). Therefore, it is recommended to conduct further tests considering a bimodal sea with a wave attack from different angles in order to observe the effect of oblique waves on the wave overtopping at coastal structures with permeable foreshores.

— In this small-scale laboratory work, the influence of wind on overtopping processes was not considered. Even though it is evident that there is the limited influence of wind on relatively larger wave overtopping volumes, for small overtopping discharges, the wind effects are more likely to be prominent (Pearson et al., 2002; EurOtop, 2018). Hence, further experiments could be undertaken on a large scale focussing on the effect of wind on overtopping characteristics.

— Due to the simultaneous measurements of overtopping and scouring characteristics, all the experiments were performed with approximately 1000 random waves. Moreover, the calculated scour depth at around 1,000 waves, was adopted for the tested conditions covered within this study. Although a preliminary investigation on the development time of scour depth showed that the maximum scour depth occurs at approximately 1,000 waves for both structural configurations, additional tests should be performed with a relatively longer storm duration to observe the beach (foreshore) evolution in

response to the different sea states with sophisticated laboratory measurement techniques.

— Only limited tests were performed with shallower water depths, (i.e. spilling wave breakers (h_t/L_m < 0.005) to avoid the scale effects in the measurements). Accordingly, less data (scour depth) was collected for these wave conditions for both vertical and sloping structures. Hence, further investigations focussing on scouring at spilling wave breakers could be performed to collect more data for these conditions.

References

Abolfathi, S., Dong, S., Borzooei, S., Yeganeh-Bakhtiari, A. and Pearson, J.M., 2018. Application of Smoothed Particle Hydrodynamics in Evaluating the Performance of Coastal Retrofits Structures. In: Proceedings of International Conference on Coastal Engineering, ASCE, 1(36): papers.109.

Allsop, N. W. H., Bray, R. N., 1994. Vertical breakwaters in the United Kingdom: historical and recent experience. Paper presented at the Proceedings of the Workshop on Wave Barriers in Deep Waters.

Allsop, N. W. H., Vicinanza, D., Mckenna, J., 1996. Wave forces on vertical and composite breakwaters. Research Report SR 443, HR Wallingford, Wallingford, UK.

Allsop, N. W. H., 2000. Wave forces on vertical and composite walls. In: Handbook of Coastal Enginering. Herbich, J. (ed), McGraw-Hill, New York.

Allsop, N. W. H., 2009. Historical Experience of Vertical Breakwaters in the United Kingdom. In: Proceedings of the 9th international conference on Coasts, marine structures and breakwaters: Adapting to change, ICE, Thomas Telford Ltd, Edinburgh, pp. 14-30.

Altomare, C., Gentile, G.M., 2011. Monitoring phases of the re-naturalization process of the Torre del Porto beach. In: Proceedings of the 5th International Short Conference on Applied Coastal Research. RWTH Aachen University, Germany, pp. 414–421.

Altomare, C., Gentile, G.M., 2013. An innovative methodology for the re-naturalization process of a shingle beach. In: Proceedings of the 12th International Coastal Symposium (Plymouth, England), Journal of Coastal Research, vol.

Altomare, C., Crespo, A. J. C., Domínguez, J. M., Gómez-Gesteira, M., Suzuki, T., Verwaest, T., 2015. Applicability of Smoothed Particle Hydrodynamics for estimation of sea wave impact on coastal structures. Coastal Engineering, 96: pp. 1-12.

BBC, 2018. Storm Callum: Flood defences fail and homes without power. INTERNET: Available from: https://www.bbc.co.uk/news/uk-england-45835824, Accessed date: 10th December 2019.

Besley, P., 1999. Overtopping of Seawalls – Design and Assessment Manual. R&D Technical Report W 178. Environment Agency, UK ISBN 1 85705 069 X.

Bradbury, A., Powell, K., 1992. The short term profile response of shingle spits to storm wave action. In: Proceedings of 23rd International Conference on Coastal Engineering, ASCE, pp. 2694–2707.

Bradbury, A., 2000. Predicting breaching of shingle barrier beaches-recent advances to aid beach management. In: Proceedings of the 35th Annual MAFF Conference on River and Coastal Engineering, 05.3.1-05.3.13.

Bruce, T., Van Der Meer, J.W., 2008. Integrated prediction tools for wave overtopping at vertical structures. Paper presented at the Proceedings of the 31st International Conference on Coastal Engineering, HaMBurg.

Bruce, T., Van der Meer J.W., Franco. L., Pearson, J.M., (2009) Overtopping performance of different armour units for rubble mound breakwaters. Coastal Engineering, 56: pp. 166-179. DOI http://dx.doi.org/10.1016/j.coastaleng.2008.03.015

Bruce, T., Van Der Meer, J.W., Pullen, T., Allsop, N.W.H., 2010. Wave overtopping at vertical and steep structures. In: Kim, Y.C. (Ed.), Chapter 16 in Handbook of Coastal and Ocean Engineering. World Scientific.

Chini, N., Stansby, P., Leake, J., Wolf, J., Roberts-Jones, J., Lowe, J., (2010). The impact of sea level rise and climate change on inshore wave climate: A case study for East Anglia (UK). Coastal Engineering, 57(11-12): pp. 973-984.

Church, J. A., Clark, P. U., Cazenave, A., Gregory, J. M., Jevrejeva, S., Levermann, A., Merrifield, M. A., Milne, G. A., Nerem, R. S., Nunn, P. D., Payne, A. J., Pfeffer, W. T., Stammer, D., Unnikrishnan, A. S., (2013). Sea Level Change in Stocker, T. F., Qin, D., Plattner, G.-K., Tignor, M., Allen, S. K., Boschung, J., Nauels, A., Xia, Y., Bex, V. and Midgley, P. M., (eds.), Climate Change 2013: The Physical Science Basis. Contribution of Working Group I to the Fifth Assessment Report of the Intergovernmental Panel on Climate Change, Cambridge, United

Kingdom and New York, NY, USA. Cambridge University Press: pp. 1137–1216.

CIRIA, CUR, CETMEF, 2007. The Rock Manual. The Use of Rock in Hydraulic Engineering. 2nd Edition, C683, CIRIA, London.

CLASH, 2004. Crest level assessment of coastal structures by full scale monitoring, neural network prediction and hazard analysis on permissible wave overtopping. EC-contract EVK3-CT-2001-00058.

Coates, T.T., Dodd, N., 1994. The response of gravel beaches in the presence of control structures. In: Proceedings of Coastal Engineering, ASCE, Kobe, Japan, pp. 1880–1894.

Dean, R.G., 1973. Heuristic models of sand transport in the surf zone. In: Proceedings of the Conference on Engineering Dynamics in the Surf Zone. Institution of Civil Engineers, Australia, Sydney, pp. 208–214.

De San Román-Blanco, B.L., Coates, T.T., Holmes, P., Chadwick, A.J., Bradbury, A., Baldock, T.E., Pedrozo-Acuna, A., Lawrence, J., Grüne, J., 2006. Large scale experiments on gravel and mixed beaches: experimental procedure, data documentation and initial results. Coastal Engineering, 53 (4): pp. 349–362.

Etemad-Shahidi, A., Jafari, E., 2014. New formulae for prediction of wave overtopping at inclined structures with smooth impermeable surface. Ocean Engineering, 84: pp. 124–132.

EurOtop, 2007. Wave Overtopping of Sea Defences and Related Structures–Assessment Manual. Expertise Network- UK: Allsop, N. W. H., Pullen, T., Bruce, T., NL: Van der Meer, J. W., DE: Schüttrumpf, H., Kortenhaus, A.

EurOtop, 2018. Manual on wave overtopping of sea defences and related structures. 2nd Edition, Available from: www.overtopping-manual.com .

Fowler, J.E., 1992. Scour problems and methods for prediction of maximum scour at vertical seawalls. Technical Report CERC-92-16 In: W E S. (Ed.), Us Army Corps of Engineers. Coastal Engineering Research Center, Vicksburg, MS, USA.

Franco, L., De Gerloni, M., Van der Meer, J. W., 1994. Wave overtopping on vertical and composite breakwaters. In: Proceedings of the 24th ICCE, ASCE, Kobe, Japan.

Geograph, 2012. Sloping Seawall- near to Grain, Medway, Great Britain. INTERNET: Available from : https://www.geograph.org.uk/photo/2996793, Accessed date: 10th December 2019.

Gentile, G.M., Giasi, C., 2003. An example of eco-compatible methodology for coastal remodelling. In: Proceedings of the European Conference on Application of Methodology, Roma.

Goda, Y., 2009. Derivation of unified wave overtopping formulas for seawalls with smooth, impermeable surfaces based on selected CLASH datasets. Coastal Engineering 56 (4): pp. 385–399.

Hasselmann, K., Barnett, E. Bouws, T. P., Carlson, H., Cartwright, D. E., Enke, K., Ewing, J. A., Gienapp, H., Hasselmann, D. E., Kruseman, P., Meerburg, A., Müller, P., Olbers, D. J., Richter, K., Sell, W., Walden, H., 1973. Measurements of wind-wave growth and swell decay during the Joint North Sea Wave Project (JONSWAP). Ergnzungsheft zur Deutschen Hydrographischen Zeitschrift Reihe A8 (12), pp. 1-95.

Holthuijsen, L.H., 2007. Waves in Oceanic and Coastal Waters. Cambridge University Press, Cambridge.

Hughes, S. A., Fowler, J. E., 1991. Wave-induced scour prediction at vertical walls. In: Proceedings of the Coastal Sediments' 91, ASCE, vol. 2, pp. 1886-1900.

Hughes, S. A., 1993. Physical models and laboratory techniques in coastal engineering. In: Advanced Series in Ocean Engineering, vol. 7. World Scientific, Singapore.

Hughes, S, Thornton, C., Van der Meer, J.W., Scholl, B., 2012. Improvements in describing wave overtopping processes. In: Proceedings of International Conference on Coastal Engineering (ICCE), ASCE, Santander, Spain.

IOMTODAY, 2018. New £500,000 sea defence wall to reduce waves overtopping in storms. INTERNET: Available from: http://www.iomtoday.co.im/article.cfm?id=43090&headline=New%20%C2%A3500,000%20sea%20defence%20wall%20to%20reduce%20waves%20overtopping%20in%20storms&sectionIs=news&searchyear=2018, Accessed date: 10th December 2019.

Jayaratne, M. P. R., Abimola, A., Mikami, T., Matsuba, S., Esteban, M., Shibayama, T., 2014. Predictive model for scour depth of coastal structure failures due to tsunamis. Paper presented at the 34th International Conference on Coastal Engineering (ICCE), Seoul.

Jayaratne, M. P. R., Mendoza, E., Silva, R., Gutiérrez, F., 2015. Laboratory Modelling of Scour on Seawalls. Paper presented at the International Conference on Coastal Structures, Boston, MA, USA.

Jayaratne, M. P. R., Premaratne, B., Adewale, A., Mikami, T., Matsuba, S., Shibayama, T., Esteban, M., Nistor, I., 2016. Failure Mechanisms and Local Scour at Coastal Structures Induced by Tsunami. Coastal Engineering Journal, 58(4): pp. 1640017(1)-(38).

Klopman, G., Van der Meer, J.W., 1999. Random wave measurements in front of reflective structures. Journal of Waterway Port, Coastal, and Ocean Engineering, 125 (1): pp. 39–45.

Komer, P.D., Miller, M.C., 1973. The threshold of sediment movement under oscillatory water waves. Journal of Sedimentary Petrology, 43 (4): pp. 1101–1110.

Kraus, N. C., Smith, J. M., 1994. SUPERTANK laboratory data collection project. Volume 1: Main Text Technical Report CERC-94-3. US Army Corps of Engineers Waterways Experiment Station, Coastal Engineering Research Center, Vicksburg. MS, USA, 2191-2204.

Lorang, M.S., 2002. Predicting the crest height of a gravel beach. Geomorphology, 48 (1): pp. 87–101.

Mansard, E.P.D., Funke, E.R., 1980. The measurement of incident and reflected spectra using a least squares method. Coastal Engingeering: pp. 154–172.

Matias, A., Williams, J.J., Masselink, G., Ferreira, O., 2012. Overwash threshold for gravel barriers. Coastal Engingeering: pp. 48–61.

McCall, R.T., Masselink, G., Poate, T.G., Roelvink, J.A., Almeida, L.P., Davidson, M., Russell, P.E., 2014. Modelling storm hydrodynamics on gravel beaches with XBeach- G. Coastal Engingeering, 91: pp. 231–250.

McCall, R.T., Masselink, G., Poate, T.G., Roelvink, J.A., Almeida, L.P., 2015. Modelling the morphodynamics of gravel beaches during storms with XBeach-G. Coastal Engingeering 103: pp. 52–66.

Müller, G., Allsop, N.W.H., Bruce, T., Kortenhaus, A., Pearce, A., Sutherland, J., 2008. The occurrence and effects of wave impacts. In: Proceedings of the ICE Maritime Engineering Conference, pp. 167-173.

Obhrai, C., Powell, K., Bradbury, A., 2008. A laboratory study of overtopping and breaching of shingle barrier beaches. In: Proceedings of the Coastal Engineering Conference, ASCE, Hannover, Germany, pp. 1497–1508.

Oumeraci, H., 1994. Review and analysis of vertical breakwater failures - lessons learned. Coastal Engineering, 22(1): pp. 3-29.

Owen, M. W., 1980. Design of sea walls allowing for wave overtopping. Report EX 924, Hydraulics Research Station of HR Wallingford, Wallingford, UK.

Pearce, A., Sutherland, J., Müller, G., Rycroft, D., Whitehouse, R., 2006. Scour at a seawall-field measurements and physical modelling. In: Proceedings of the 30th International Conference on Coastal Engineering, ASCE, San Diego, USA.

Pearson, J.M., Bruce, T., Allsop, N.W.H., 2001. Prediction of wave overtopping at steep seawalls—variabilities and uncertainties. In: Proceedings of the Conference on Waves '01. ASCE, San Francisco, pp. 1797–1808.

Pearson, J.M., Bruce, T., Allsop, N.W.H., Gironella, X., 2002. Violent wave overtopping measurements at large and small scale. In: Proceedings of the 28th International Coastal Engineering Conference. ASCE, Cardiff, UK, pp. 2227–2238.

Pearson, J. M., 2010. Overtopping and Toe Scour at Vertical Seawalls. In: Proceedings of the 9th international conference on Coasts, marine structures and breakwaters: Adapting to change, Institution of Civil Engineers, Edinburgh, pp. 598–608.

Pierson, W., Moskowitz, L., 1964. A proposed spectral form for fully developed wind seas based on the similarity theory of SA Kitaigorodskii. Journal of geophysical research 69 (24):5181-5190.

Pourzangbar, A., Saber, A., Yeganeh-Bakhtiary, A., Ahari, L.R., 2017. Predicting scour depth at seawalls using GP and ANNs. Journal of Hydroinformatics 19 (2): jh2017125.

Powell, K. A., 1987. Toe scour at sea walls subject to wave action: A literature

review. Report SR 119, HR Wallingford, Wallingford, UK.

Powell, K.A., 1990. Predicting Short Term Profile Response for Shingle Beaches. Report SR 219. HR Wallingford, Wallingford, UK.

Powell, K. A., Lowe, J. P., 1994. The scouring of sediments at the toe of seawalls. In: Proceedings of the Hornafjordor International Coastal Symposium, Iceland, pp. 749-755.

Salauddin, M., Van der Meer, J.W., 2016. An experimental study on wave overtopping of rubble mound breakwater armoured with a new concrete armour unit. In: Proceedings of the 3rd International Conference on Civil Engineering for Sustainable Development (ICCESD), Khulna, Bangladesh, pp. 480-490.

Shao, S., 2010. Incompressible SPH flow model for wave interactions with porous media. Coastal Engineering, 57(3): pp. 304-316.

Sherman, D.J., 1991. Gravel beaches. National Geographic Research and Exploration, 7: pp. 442–452.

Sumer, B.M., Fredsøe, J., 2000. Experimental study of 2D scour and its protection at a rubble-mound breakwater. Coast Engingeering 40: pp. 59–87.

Sumer, B. M. Fredsøe, J., 2002. The mechanics of scour in the marine environment. World Scientific Publishing Co. Pte. Ltd., Singapore.

Sutherland, J., Brampton, A.H., Motyka, G., Blanco, B., Whitehouse, R.J.W., 2003. Beach Lowering in Front of Coastal Structures-Research Scoping Study. Report FD1916/TR London, UK. INTERNET: available from: http://sciencesearch.defra.gov.uk/, Accessed date: 14 February 2019.

Sutherland, J., Brampton, A.H., Whitehouse, R.J.W., 2006a. Toe scour at seawalls: monitoring, prediction and mitigation. Paper presented at the in the 41st Defra Flood and Coastal Management Conference, The Univeristy of York, UK.

Sutherland, J., C. Obhrai, Whitehouse, R.J.W., Pearce, A., 2006b. Laboratory tests of scour at a seawall. In: Proceedings of the 3rd International Conference on Scour and Erosion, Technical University of Denmark, Gouda, The Netherlands.

Sutherland, J., Brampton, A.H., Obrai, C., Dunn, S., Whitehouse, R.J.W., 2008. Understanding the Lowering of Beaches in Front of Coastal

Defence Structures, Stage 2-Research Scoping Study. Report FD1927/TR London, UK. INTERNET: available from: http://sciencesearch.defra.gov.uk/, Accessed date: 20 February 2019.

Tahersima, M., Yeganeh-Bakhtiary, A., Hajivalie, F., 2011. Scour pattern in front of vertical breakwater with wave overtopping. Journal of Coastal Research, (64): 598.

TAW, 2002. Technical report wave run-up and wave overtopping at dikes. In: Van der Meer, J. W. (ed), TAW report (incorporated in the EurOtop manual).

Tofany, N., Ahmad, M., Kartono, A., Mamat, M., Mohd-Lokman, H., 2014. Numerical modeling of the hydrodynamics of standing wave and scouring in front of impermeable breakwaters with different steepnesses. Ocean Engineering 88: pp. 255-270.

Troch, P. E., Mollaert, J., Peelman, S., Victor, L., Van der Meer, J. W., Gallach-Sánchez, D., Kortenhaus, A., 2014. Experimental study of overtopping performance for the cases of very steep slopes and vertical walls with very small freeboards. In: Proceedings of the 34th ICCE, ASCE, Seoul, South Korea.

Tsai, C. P., Chen. H. B., You, S. S., 2009. Toe scour of seawall on a steep seabed by breaking waves. Journal of waterway, port, coastal, and ocean engineering 135(2): pp. 61-68.

Van der Meer, J. W., 1992. Stability of the seaward slope of berm breakwaters. Coastal Engineering 16(2): pp. 205-234.

Van der Meer, J. W., Janssen, J.P.F.M., 1994. Wave run-up and wave overtopping at dikes and revetments. In: Kobayashi, N., Demirbilek, Z. (eds), Wave forces on inclined and vertical wall structures. ASCE, pp. 1 27.

Van der Meer, J. W. , Bruce, T., 2014. New physical insights and design formulas on wave overtopping at sloping and vertical structures. Journal of Waterway, Port, Coastal, and Ocean Engineering 140(6): 04014025.

Van der Werf, I.M., Van Gent, M.R., 2018. Wave Overtopping over Coastal Structures with Oblique Wind and Swell Waves. Journal of Marine Science and Engineering, 6(4): 149.

Van Hijum, E., Pilarczyk, K., 1982. Equilibrium Profile and Longshore

Transport of Coarse Material under Regular and Irregular Wave Attack. Publication No. 174. Delft Hydraulics laboratory, Delft, Netherlands.

Victor, L., Troch, P., 2012. Wave overtopping at smooth impermeable steep slopes with low crest freeboards. Journal of Waterway, Port, Coastal, and Ocean Engineering 138(5): pp. 372-385.

Victor, L., Van der Meer, J.W., Troch, P., 2012. Probability distribution of individual wave overtopping volumes for smooth impermeable steep slopes with low crest freeboards. Coastal Engineering, 64: pp. 87–101.

Wallis, M., Whitehouse, R.J.S., Lyness, N., 2009. Development of guidance for the management of the toe of coastal defence structures. In: Presented in the 44th Defra Flood and Coastal Management Conference, Telford, UK.

Whitehouse, R. J. S., 1998. Scour at Marine Structures: A manual for practical applications. Thomas Telford, London, UK.

Whitehouse, R. J. S., 2006. Scour at coastal structures. Proceedings of the 3rd International Conference on Scour and Erosion, Gouda, The Netherlands.

Williams, J.J., Buscombe, D., Masselink, G., Turner, I., Swinkels, C., 2012a. Barrier Dynamics Experiment (BARDEX): aims, design and procedures. Coastal Engineering 63: pp. 3–12.

Williams, J.J., De Alegría-Arzaburu, A.R., McCall, R.T., Van Dongeren, A., 2012b. Modelling gravel barrier profile response to combined waves and tides using XBeach: laboratory and field results. Coastal Engineering 63: pp. 62–80.

Wolters, G., Van Gent, M.R., Allsop, N.W.H., Hamm, L., Mühlestein, D., 2009. HYDRALAB III: guidelines for physical model testing of rubble mound breakwaters. In: Proceedings of the 9th International Conference on Coasts, Marine Structures and Breakwaters: Adapting to Change, Edinburgh, United Kingdom, pp. 659–670.

Xie, S.L., 1981. Scouring Patterns in Front of Vertical Breakwaters and Their Influences on the Stability of the Foundation of the Breakwaters. Delft University of Technology, Delft, The Netherlands.

Xie, S.L., 1985. Scouring patterns in front of vertical breakwaters. Acta Oceanologica Sinica: 4(1): pp. 153-164.

Yalin, S., 1963. A model shingle beach with permeability and drag forces

reproduced. In: Proceedings of the 10th IAHR Congress 1963. London, pp. 169.

Zanuttigh, B., Van Der Meer, J.W., Bruce, T., Hughes, S., 2013. Statistical characterisation of extreme overtopping wave volumes. In: Proceedings of conference on Coasts, Marine Structures, and Breakwaters, ICE, Edinburgh, UK.

Zhu, X., Linham, M. M., Nicholls, R. J., 2010. Technologies for Climate Change Adaptation - Coastal Erosion and Flooding. Roskilde: Danmarks Tekniske Universitet, Risø Nationallaboratoriet for Bæredygtig Energi. TNA Guidebook Series.

Appendices

Appendix A Load-cell and overtopping detector

The calibration of load-cell was then performed by measuring the change in voltage in the loadcell corresponding to known change in weights in the container, see Fig A.1. As seen in Figure A.1, the observed R^2 value for the calibration tests was close to 1, indicating an overall good linear output behaviour of the loadcell. The observed relationship between the change in voltage and change in load from the calibration of load-cell has been used in the overtopping analysis within this study.

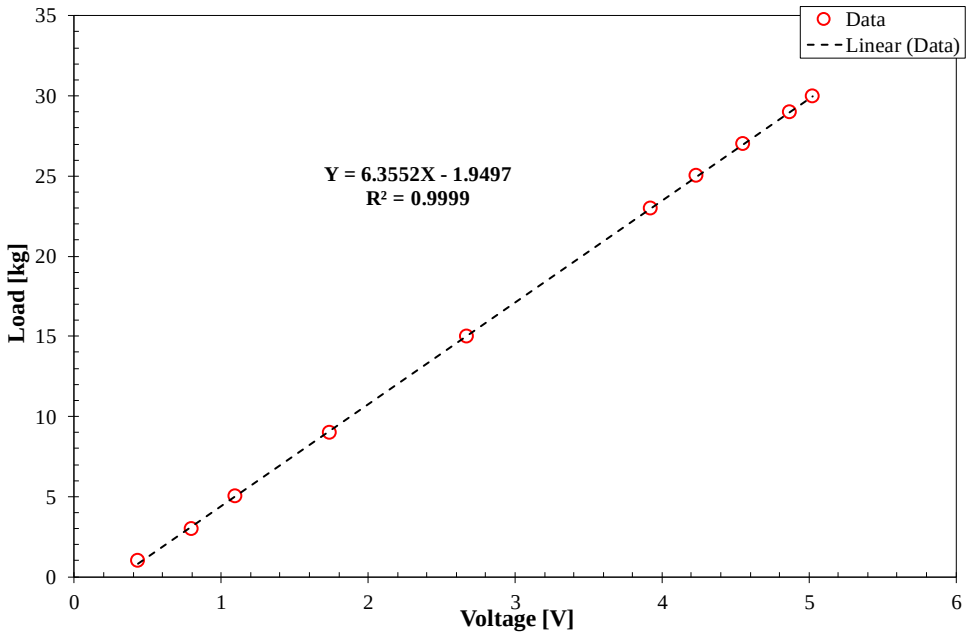

Figure A.1 Calibration of load-cell

In Figure A.2, sample outputs of load-cell and overtopping detector after running through the algorithm are presented. It is noticeable from Figure A.2 that with the use of detector, the wave overtopping events were detected and matched reasonably well with the load-cell observations.

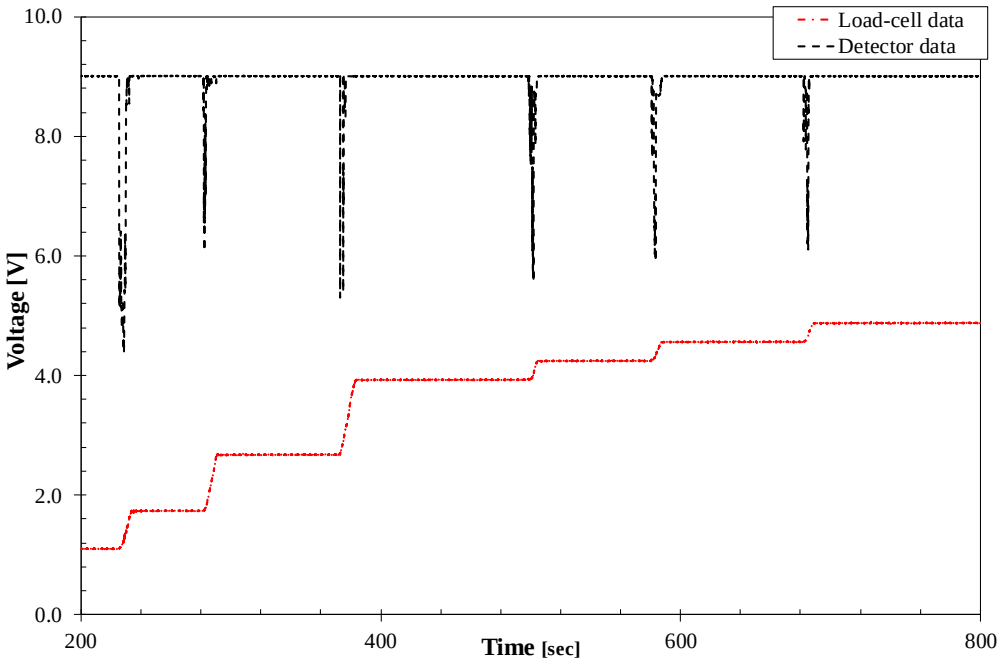

Figure A.2 Sample outputs of load-cell and overtopping detector

Appendix B Accuracy of overtopping measurement system

For both tested structural configurations i.e. vertical wall and sloping wall, the accuracy of the overtopping measurement system was inspected prior to carrying out any experiments, adapting the technique followed by Pearson et al. (2001). The known volumes of water were passed over the crest of the structure into the overtopping measuring container to simulate a known series of overtopping events. Afterwards, the resulting outputs of loadcell and overtopping detector were passed through a MATLAB algorithm to determine the wave by wave overtopping volumes. Finally, the test results achieved from the measurement system were compared with the actual values to determine the accuracy of the system for the particular structural configuration.

Figure A.3 presents a comparison between the actual (or known) and measured overtopping volumes for the experiments at plain vertical seawalls. As it is seen that the results demonstrate that an overall good agreement exists between actual and measured values.

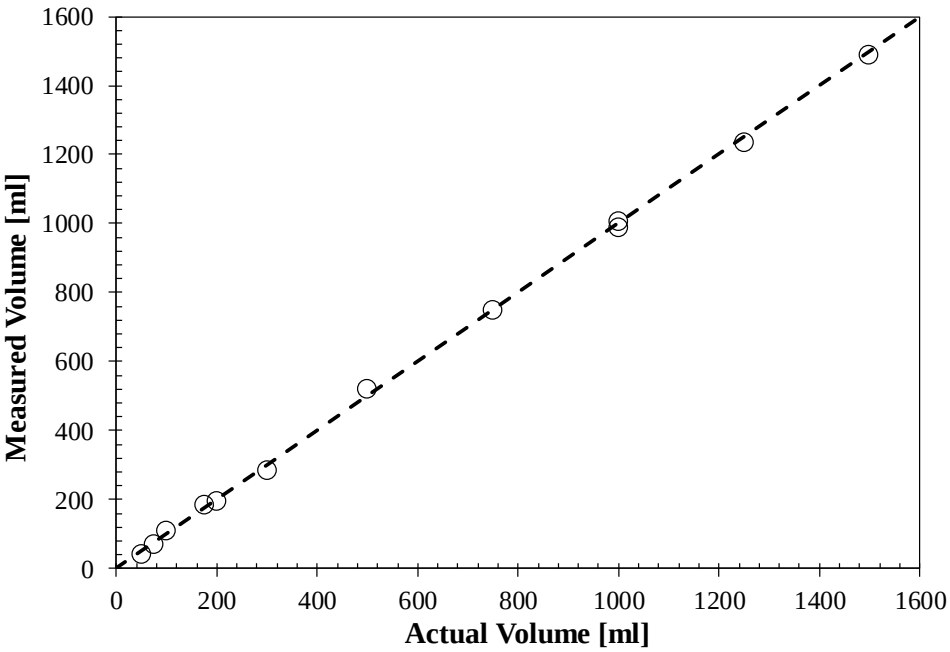

Figure A.3 Actual (known) volume of simulated overtopping events compared with the measured values for plain vertical walls

Further, in Table A.1, pre-measured (actual) volume of each simulated event is compared with measured value by overtopping measurement system, which enables to find the accuracy of the measurement system. The relative error of total measured volumes and actual volumes was found satisfactory around 0.6% and rmse value was observed 10.21 ml indicating that any errors induced by the overtopping measurement technique were minimal. It is to note that the sensitivity of the load-cell was limited to the identification of 5-9 ml of overtopping volume. This is the reason that smaller overtopping volumes showed an overall slightly greater error in the measurements compared to larger values.

Table A.1 The accuracy of the overtopping measurement system for plain vertical walls

No .of event	Actual volume (ml)	Measured volume (ml)	Actual error (ml)	Relative error (%)	RMSE (ml)
1	50	42	-8	-16.0	
2	75	69	-6	-8.0	
3	100	109	9	9.0	
4	175	184	9	5.1	
5	200	193	-7	-3.5	
6	300	284	-16	-5.3	
7	500	519	19	3.8	10.21
8	750	748	-2	-0.3	
9	1000	1006	6	0.6	
10	1250	1234	-16	-1.3	
11	1000	988	-12	-1.2	
12	1500	1486	-14	-0.9	
Total	6900	6862	-38	0.55	10.21

For the tested conditions on sloping structures, a comparison between the actual volume and measured volume through the overtopping measurement system is shown in Figure A.4. The data points in Figure A.4 clearly indicate that measured overtopping volumes were almost identical to actual (given) values.

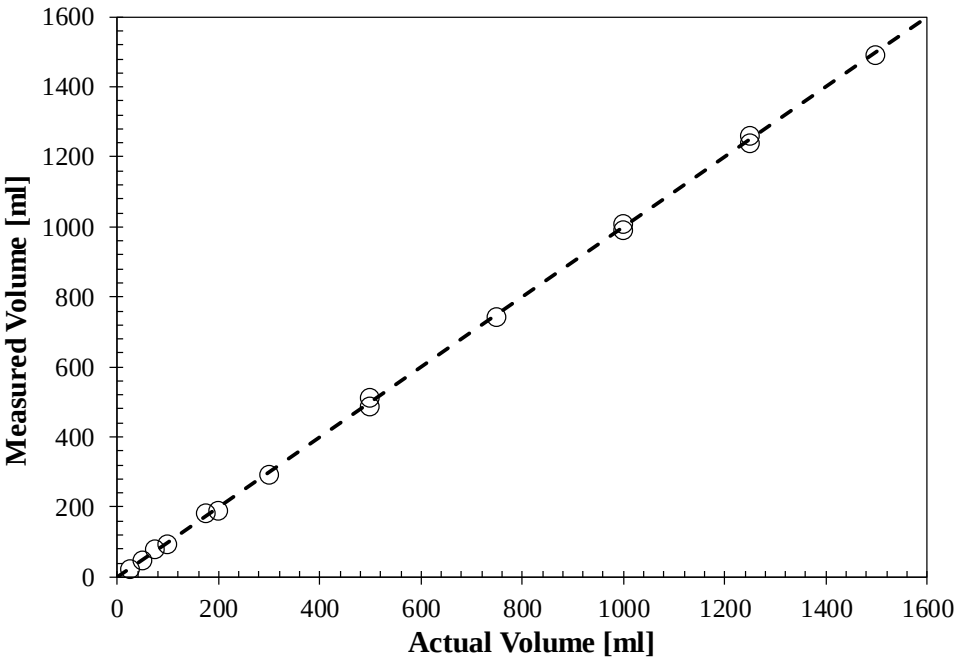

Figure A.4 Actual (known) volume of simulated overtopping events compared with the measured values for sloping structures

The accuracy the overtopping measurement system for the experiments on sloping structures, is presented in Table A.2. The actual volume of each simulated overtopping event was compared with the measured value to determine the relative error in the measurements, see Table A.2.

Table A.2 The accuracy of the overtopping measurement system for sloping structures

No .of event	Actual volume (ml)	Measured volume (ml)	Actual error (ml)	Relative error (%)	RMSE (ml)
1	25	21	-4	-16.0	
2	50	45	-5	-10.0	
3	75	78	3	4.0	
4	100	93	-7	-7.0	
5	175	181	6	3.4	
6	200	189	-11	-5.5	
7	300	289	-11	-3.7	9.38
8	500	511	11	2.2	
9	750	742	-8	-1.1	
10	1000	988	-12	-1.2	
11	1250	1237	-13	-1.0	
12	1500	1489	-11	-0.7	
13	1250	1258	8	0.6	
14	1000	1008	8	0.8	
15	500	486	-14	-2.8	
Total	8675	8615	-60	0.7	9.38

From the results as shown in Table A.2, it is seen that derived total volume slightly varied (0.7%) from the actual total volume with an overall rmse value of 9.38 ml, thus it can be reported that there is no remarkable systematic error induced by overtopping measurement system. It can be noticed that for the experiments with the smaller overtopping volumes, the measurement values overall showed larger variation with the actual values. As already mentioned earlier that this variation for small overtopping volumes was due to the sensitivity of the tested loadcell (5-9 ml) within this study.